UNIVERSITY OF KWAZULU-NATAL

Design, Synthesis and Biological Evaluation of Novel Thiadiazoline-Thiazolone Hybrids as Kinase Inhibitors

MASTERS THESIS
2017

Samukelisiwe Pretty Khathi

Thesis submitted in partial fulfilment of the requirements

For the award of the degree in

MASTER OF MEDICAL SCIENCE

(Pharmaceutical Chemistry)

College of Health Sciences,

University of KwaZulu-Natal

By

Samukelisiwe Pretty Khathi

(B.Sc)

Supervisor

Dr. Rajshekhar Karpoormath **B.Pharm, M.Pharm, Ph.D**

Co- Supervisor

Dr. Balakumar Chandrasekaran **B.Pharm, M.Pharm, Ph.D**

Preface

This study represents original work by the author and has not been submitted in any other form to another university. Where the use of work pertaining to others has been duly acknowledged in the text.

Candidate: Samukelisiwe Pretty Khathi

Signed: **Name:** **Date:**

As the Candidate's supervisor, I have approved this thesis for submission.

Supervisor: Dr. Rajshekhar Karpoormath

Signed:

Name:

Date:

As the Candidate's co-supervisor, I have approved this thesis for submission.

Co-Supervisor: Dr. Balakumar Chandrasekaran

Signed:

Name:

Date:

Declaration – Plagiarism

I, **Samukelisiwe Pretty Khathi,** declare that the experimental work described in this dissertation was carried out at the School of Pharmacy, College of Health Sciences, University of KwaZulu-Natal, Westville campus under the supervision of Dr. Rajshekhar Karpoormath, and Dr. Balakumar Chandrasekaran that:

1. The research reported in this thesis is my original research, except where otherwise indicated.
2. This thesis has not been submitted for any degree or examination at any other university.
3. This thesis does not contain other persons' data, pictures, graphs or other information, unless specifically acknowledged as being sourced from other persons.
4. This thesis does not contain other persons' writing, unless specifically acknowledged as being sourced from other researchers. Where other written sources have been quoted, then:
    a. Their words have been re-written but the general information attributed to them has been referenced.
    b. Where their exact words have been used, then their writing has been placed in italics and inside quotation marks, and referenced.
5. This thesis does not contain text, graphics or tables copied and pasted from the internet, unless specifically acknowledged, and the source being detailed in the thesis and in the references sections.

Signed: **Date:**

List of Publications

1. **Ligand and structure based *in silico* studies to identify kinesin spindle protein (KSP) inhibitors as potential anticancer agents.**

   Balakumar, Chandrasekaran, Muthusamy Ramesh, Chuin Lean Tham, Samukelisiwe Pretty Khathi, Frank Kozielski, Cherukupalli Srinivasulu, Girish A. Hampannavar, Nisar Sayyad, Mahmoud E. Soliman, and Rajshekhar Karpoormath.

   Journal of Biomolecular Structure and Dynamics (2017) 1-77. **DOI:10.1080/07391102.2017.1396255.**

   Contribution: Synthesis of starting material, data collection and spectral characterization.

2. **Design and synthesis of novel thiadiazole-thiazolone hybrids as potential inhibitors of the human mitotic kinesin Eg5.**

   Samukelisiwe Pretty Khathi, Balakumar, Chandrasekaran, Sivanandhan Karunanidhi, Chuin Lean Tham, Frank Kozielski, Girish A. Hampannavar, Nisar Sayyad, and Rajshekhar Karpoormath.

   European Journal of Medicinal Chemistry 2017 (Manuscript to be submitted)

   Contribution: As a principal investigator, I carried out most of the lab work and drafted the experimental part of the manuscript.

3. **Synthesis, anticancer evaluation and molecular docking of some novel fluorinated pyridol[2,3-*d*]pyrimidines.**

   Balakumar, Chandrasekaran, Sivanandhan Karunanidhi Samukelisiwe Pretty Khathi, Girish A. Hampannavar, Afsana Kajee, Koleka P. Mlisana, Vladimir Krystof and Rajshekhar Karpoormath.

   Bioorganic Chemistry (Manuscript under preparation)

   Contribution: synthesized the starting materials and the anti-bacterial screening of the synthesized final compounds.

Acknowledgements

The author wishes to extend her appreciation to the following persons and organizations:

Firstly, I would love to thank God for being my provider, the light in my life. My humble thanks to my master's supervisor Dr. Rajshekhar Karpoormath, Discipline of Pharmaceutical Sciences at University of Kwa-Zulu Natal (UKZN) for his constant supervision, support and valuable advice during my tenure of the research work. I extend my thanks to my co-supervisor Dr. Balakumar Chandrasekaran who consistently assisted with bench work from synthesis, to characterization, and drafting of the manuscript.

I would also like to thank the following experts who were involved (directly/indirectly) in this research project: Without their passionate participation and input, this thesis could not have been successfully conducted: -

I would like to thank the past and the present members of synthetic and medicinal chemistry research group (SMCRG), UKZN, Westville campus for their constant support and encouragement throughout my research work.

I extend my heartfelt thanks to our collaborator Prof. Vladimir Krystof and his team at Laboratory of Growth Regulators, Centre of the Region Hana for Biotechnological and Agricultural Research, Palacky University & Institute of Experimental Botany ASCR, Slechtitelu 27, 78371 Olomouc, Czech Republic for providing the *in vitro* results of the enzyme-based assays (CDK2/ cyclin E, Abl kinase) and cell-based cytotoxicity evaluation against K-562 (chronic myelogeneous leukemia) and MCF-7 (breast adenocarcinoma) cell lines, respectively. We thank for your valuable results and suggestion to improve the anticancer activity profile of the synthesized compounds to generate new anticancer drugs.

I am also very grateful to Prof. Frank Kozielski and Ms. Chuin Lean Tham for conducting the *in vitro* steady state basal- and MT-stimulated KSP ATPase assays of the synthesized compounds at Department of Pharmaceutical and Biological Chemistry, The School of Pharmacy, University College London, 29-39 Brunswick Square, London WC1N 1AX, U.K. Internationally, Prof. Frank is one of the pioneers in the field of KSP research who extended his full support to bring out the research paper and to continue a strong collaboration with us (SMCRG, UKZN, Durban).

I must express my very profound gratitude to my Mom for continuously being a pillar throughout my life. I would love to give a special thanks to Lebogang Khathi for being an inspiration and always motivating me to do the best for him. Another special thanks go to Elton Chiwunze for providing me with unfailing support and continuous encouragement throughout my studies, research till my thesis write up. I am so grateful to my sisters-in-law Hlengiwe, Fikile and Nontobeko and my brothers Senzo, Sandile, Jabulani as well as nephews and niece, this accomplishment would not have been possible without you all. In additional thank you to Ma wase-Folweni and my grandmom mam-Mthembu for being with me in the battle of life.

List of Abbreviations

°C	degrees celsius
^{13}C	NMR Carbon-13 nuclear magnetic resonance spectroscopy
^{1}H	NMR Proton nuclear magnetic resonance spectroscopy
3D-QSAR	three-dimensional quantitative structure activity relationship
3D-QSPR	three-dimensional quantitative structure-property relationship
4ClABT	2-(4- chlorophenylamino)-5-(2,4-dihydroxyphenyl)-1,3,4-thiadiazole
ABC	ATP-binding cassette
Abl	Abelson murine leukemia
ACES	*N*-(2-acetamido)-2-aminoethanesulfonic acid
ADP	adenosine diphosphate
ADME	absorption, distribution, metabolism and excretion
Akt	Akt kinase
Apaf-1	apoptotic protease activating factor 1
Ara-C	cytarabine
ATP	adenosine triphosphate
ATR	attenuated total reflection
ArH	aromatic protons
AZA	acetazolamide
Bcl-2	B-cell lymphoma
BCRP	breast cancer resistance protein
BCG	*Bacillus* Calmette-Guérin
BZA	benzolamide
C	carbon
CA	carbonic anhydrase
CDCl3	deuterated chloroform
CDK	cyclin dependent kinase
CHK1	checkpoint kinase 1
Cl	chloride
CO_2	carbon dioxide
COX-2	cyclooxygenase-2
CYP	cytochrome P_{450}
DNA	deoxyribonucleic acid

DMF	dimethylformamide
DMSO	dimethyl sulfoxide
DMEM	Dulbecco's Modified Eagle Medium
DTT	dithiothreitol
EDTA	ethylenediaminetetraacetic acid
EGTA	ethylene glycol-bis(β-aminoethyl ether)-N,N,N',N'-tetraacetic acid
EtOH	ethanol
ER	estrogen receptor
FABT	2-(4-fluorophenyloamino)-5-(2,4-dihydroxyphenyl)- 1,3,4-thiadiazole
FAK	focal adhesion kinase
FR	folate receptor
FT-IR/IR	fourier-transform infrared spectroscopy
GLIDE	grid-based ligand docking with energetics
GTP	guanosine triphosphate
h	hour
HCV	hepatitis C virus
HDACi	histone deacetylase
HDI	human development index
HepG2	hepatocellular carcinoma cell line
HER2	human epidermal growth factor receptor 2
HRMS	high resolution mass spectra
HSCT	allogeneic hematopoietic stem cell transplantation
IBP	interaction-based pharmacophore
IC50	inhibitory concentration 50
IV	intravenously
JNK	c-Jun N-terminal kinase
JSP-1	JNK stimulating phosphatase-1
KSP/Eg5	kinesin spindle protein
m	multiplet
mp	melting point
MAPK	mitogen activated kinase cascade
MCAK	mitotic centrosome associated kinesin
MCF-7	Michigan cancer foundation-7 (human breast adenocarcinoma cell line)
MDCK	Madin-Darby canine kidney

MDR	multidrug resistance
MeOH	methanol
MGMT	methyltransferase
MKLP	kinesin motor protein
MMPs	matrix metalloproteinases
MMR	mismatch repair
MOPS	morpholinepropanesulfonic acid
MPR	multidrug-associated protein
mRNA	messenger ribonucleic acid
MT	microtubule
MTA	microtubule-targeted antimitotic
MZA	methazolamide
N	nitrogen
NaOEt	sodium ethoxide
NIR	near infrared
O/O_2	oxygen/oxygen atom
OPLS3	optimized potentials for liquid simulations 3
QPPCaco	Caco-2 permeability
QPlogPo/w	partition coefficient
QPlogS	water solubility
PRL-3	phosphatase of a regenerating liver
PCD	programmed cell death
PDB	protein databank
PDT	photodynamic therapy
pH	potential of hydrogen
PI3 K	phosphatidyl-3-phosphate kinase
PK	protein kinase
PLA	peloruside A
PLK	polo-kinase
PTEN	phosphatase and tensin homolog
P-gp	P-glycoprotein
Rb/pRb	retinoblastoma/retinoblastoma protein
RT	room temperature
s	singlet

SAC	spindle assembly checkpoint
SAR	structure-activity relationship
SLC	superfamily of solute carriers
SK	sphingosine kinase
SHP-2	non-membrane protein tyrosine phosphatase
TDT	thiadiazoline-thiazolone
TLC	thin layer chromatography
TNFa	tumour necrosis factor
USA/US$	United State of America/ United State Dollar
UK	United Kingdom
VEGF	vascular endothelial growth factor
WHO	world health organization
XP	extra precision

List of Figures

List of Schemes

List of Tables

Thesis Appendix: List of figures

Abstract

Cancer is a leading cause of death globally, and it was responsible for 8.8 million deaths in 2015. It is predicted that there will be 22 million new cancer cases by 2030 worldwide. Approximately, 70% of deaths from cancer occur in low- and middle-income countries. Furthermore, breast cancer is the second most common cancer among South African women and is reported to affect 1 in every 26 women. The social and economic burdens associated with cancers are severe at national and international levels hence, there is an urgent need for the development of more effective cancer therapeutics. To accomplish this aspect, in this study, thiadiazole-thiazolone (TDT) hybrids were developed as dual inhibitors of cyclin-dependent kinase (CDK) and kinesin spindle protein (KSP), respectively. Twenty-two novel TDT hybrid compounds (**8a-v**) were synthesized using multistep organic synthesis and were characterized using thin layer chromatography (TLC), infrared spectroscopy (FT-IR), nuclear magnetic resonance spectroscopy (^{1}H and ^{13}C NMR), and high-resolution mass spectrometry (HR-MS). All the compounds (**8a-v**) were screened for their potential *in vitro* inhibition of validated anticancer drug targets (CDK, Abl and KSP) and cancer cell lines (MCF-7 and K-562). Results obtained from these evaluations suggested that the synthesized compounds were potent inhibitors of CDK and KSP thus confirming the dual mode of action. Amongst, **8h** was identified as the most potent compound with an IC_{50} value of 3.1 µM against CDK2 enzyme and exhibited good cytotoxicity (GI_{50} = 6.25 µM) against the tested cancer cell lines (MCF-7 and K-562). A brief structure-activity relationship (SAR) analysis indicated that 2-chloro and 4-nitro substituents on the phenyl ring of the thiazolone motif contributed significantly to the inhibition of both of the anticancer drug targets (CDK and KSP). An *in silico* molecular docking study using the crystal structures of the target enzymes (CDK-2 and KSP) further supported the SAR and extrapolated the importance of crucial molecular interactions in influencing the enzyme inhibitory activities.

Table of Contents

Chapter 1
Thesis Overview

1.1. Background and rationale of this study

Cancer, also known as a malignant neoplasm, is a disease that involves abnormal growth of cells with the ability to invade or spread to other parts of the body [1]. There are more than 100 known cancers that can affect different parts of the body. There have been 14.1 million new cancer cases, 8.8 million cancer deaths and 32.6 million people living with cancer that were reported by World Health Organization (WHO 2015) worldwide. The treatment is estimated to cost world economies as much as US$1.16 trillion annually. African countries (including South Africa) have a high risk of dying from cancer than USA and UK. The disease is most common in developing countries (South Africa, sub-Saharan Africa, and Asia) where resources for constant diagnosis and treatment access are limited [2]. Moreover, there is a lot of social and economic burden associated with this dangerous disease nationally and internationally [3]. The current chemotherapy is unable to combat cancer effectively due to multiple factors such as mutation of genes, genetic variation, altered lifestyle and inability to target specific proteins. Though there have been developments in the prevention and treatment of cancer, a successful cancer therapy remains a challenge till date [4]. In general, chemotherapy involves the administration of chemical-based drugs to arrest the growth/kill cancer cells. However, due to these drugs being non-specific, it also destroys the host cells. Furthermore, drug resistance and mutations are a persistent problem during the treatment of cancer with chemotherapeutic drugs [5]. Thus, there is an urgent need to develop new, safe and efficacious anti-cancer agents possessing a broad spectrum of cytotoxicity to tumour cells and which are free of host cell toxicity [6].

Cyclin-dependent kinases (CDKs) and mitotic motor proteins are well-validated checkpoint proteins and the researchers worldwide have focused in developing newer inhibitors of these target enzymes as potential anticancer agents. Hence, the proposed work aims to develop dual inhibitors exhibiting potential and effective anticancer agents with a novel mechanism of action. CDKs are universal eukaryotic cell cycle regulators that promote the passage through the restriction point, mitosis, and initiation of deoxyribonucleic acid (DNA) replication [7]. Given the fact that CDKs have oncogenic potency and are amenable to pharmacological inhibition, their inhibitors have therefore attracted great interest as potential anticancer agents specifically, CDK2 [8]. The CDK enzyme plays an important role in regulating various events of eukaryotic cell division cycle. Accumulated evidence indicated that overexpression of CDK2 causes the abnormal regulation of cell cycle, which is directly associated with hyperproliferation in cancer cells. Therefore, CDK2 is also regarded

as a potential therapeutic target for cancer therapy [9]. Another interesting mitotic target is kinesin spindle protein (KSP; also, known as Eg5), a member of the kinesin superfamily of molecular motor proteins [10]. Inhibition of KSP prevents spindle pole separation, which leads to a prolonged mitotic arrest in prometaphase and subsequent apoptosis [11]. Furthermore, KSP is not expressed in the adult peripheral nervous system and its inhibitors may not cause neuropathic side effects. As evidenced by literature, inhibitors of KSP arrest only cells in mitosis and are not expected to affect non-proliferating cells [12]. Currently, there are many KSP inhibitors under phase-I or II stages of clinical trials [13]. Interestingly, many of the available KSP inhibitors are not adenosine triphosphate (ATP)-competitive inhibitors they are rather allosteric inhibitors. Hence, this research also aimed to consider the enzymes that target KSP to minimize the side effects of cancer chemotherapy.

1.2. Aims of this study

1.2.1. Identification of small organic molecules as potent anticancer agents;

1.2.2. To employ rational drug design approaches through suitable computational techniques (*in silico*);

1.2.3. Design target site-specific inhibitors on the binding-site of CDK and KSP;

1.2.4. Organic syntheses of designed molecules by conventional and/or microwave-assisted organic green chemistry approaches;

1.2.5. Pharmacological evaluation of the final compounds against CDK and KSP using suitable *in vitro* methods; and

1.2.6. Cytotoxicity assays using cancer cell lines (MCF and K-562).

1.3. Objectives of this study

1.3.1. Design of potential anticancer compounds through molecular hybridization approach;

1.3.2. Synthesis of the designed molecules using green chemistry approaches;

1.3.3. Characterization of the synthesized compounds by suitable chromatographic, spectral methods or by single crystal X-ray crystallography;

1.3.4. Pharmacological evaluation for the newly synthesized final compounds by suitable *in vitro* methods (enzyme assays);

1.3.5. Cytotoxicity studies for the synthesized final compounds against cancer cell lines; and

1.3.6. To develop crystal structures of the potent final compounds.

1.4. Novelty and significance of this study

The main aspect of this study is to develop novel anticancer drug-like compounds for cancer chemotherapy with no neuropathic side effects. The research work presented in this thesis involves the design and synthesis of novel thiadiazole-thiazolone (TDT) hybrid compounds as dual inhibitors for CDK and KSP. As per the literature survey, there is no research report so far on TDT compounds as dual inhibitors of CDK and KSP. This work is the first of its kind and all the findings on these novel derivatives are reported in this thesis. Hence, the entire research work is novel and could serve as an ideal alternative path for medicinal and pharmaceutical chemists. The outcome of this research work resulted in one published research paper and two other research articles that are under communications/preparation for high impact journals.

1.5. Outline and structure of this thesis

This thesis is divided into seven different chapters.

Chapter 1: This chapter addresses the overview, aims, objectives, significance of the study, general outline and structure of the thesis;

Chapter 2: This introductory chapter gives a detailed literature survey, background and the design of the present study;

Chapter 3: This chapter describes the synthesis and spectral studies including experimental section);

Chapter 4: This chapter addresses the *in vitro* and *in silico* evaluation of the synthesized compounds against cyclin dependent kinase and cancer cell-lines;

Chapter 5: This chapter describes the *in vitro* and *in silico* evaluation of the compounds against kinesin spindle protein;

Chapter 6: This chapter gives a summary and conclusion of the study as well as future perspectives of the work; and

Chapter 7: Gives all the necessary supporting documents pertaining the spectral studies and pharmacological evaluation.

1.6. References

[1] S.R. Singer, A.G. Creanga, Diagnostic imaging of malignant tumors in the orofacial region, Dental clinics, 60 (2016) 143.

[2] L.A. Torre, F. Bray, R.L. Siegel, J. Ferlay, J. Lortet-Tieulent, A. Jemal, Global cancer statistics, 2012, CA: a cancer journal for clinicians, 65 (2015) 87.

[3] J. Ferlay, I. Soerjomataram, R. Dikshit, S. Eser, C. Mathers, M. Rebelo, D.M. Parkin, D. Forman, F. Bray, Cancer incidence and mortality worldwide: sources, methods and major patterns in GLOBOCAN 2012, International journal of cancer, 136 (2015) e359.

[4] C. Jin, Y.-J. Liang, H. He, L. Fu, Synthesis and antitumor activity of ureas containing pyrimidinyl group, European journal of medicinal chemistry, 46 (2011) 429.

[5] F. Li, R.I. Mahato, MicroRNAs and drug resistance in prostate cancers, Molecular pharmaceutics, 11 (2014) 2539.

[6] S.L. Zhu, Y. Wu, C.J. Liu, C.Y. Wei, J.-C. Tao, H.M. Liu, Design and stereoselective synthesis of novel isosteviol-fused pyrazolines and pyrazoles as potential anticancer agents, European journal of medicinal chemistry, 65 (2013) 70.

[7] M. Malumbres, M. Barbacid, Mammalian cyclin-dependent kinases, Trends in biochemical sciences, 30 (2005) 630.

[8] P.K. Chong, H. Lee, J.W.F. Kong, M.C.S. Loh, C.H. Wong, Y.P. Lim, Phosphoproteomics, oncogenic signaling and cancer research, Proteomics, 8 (2008) 4370.

[9] S. DeBonis, J.P. Simorre, I. Crevel, L. Lebeau, D.A. Skoufias, A. Blangy, C. Ebel, P. Gans, R. Cross, D.D. Hackney, Interaction of the mitotic inhibitor monastrol with human kinesin Eg5, Biochemistry, 42 (2003) 338.

[10] D.A. Compton, Spindle assembly in animal cells, Annual review of biochemistry, 69 (2000) 95-114.

[11] M. Liu, H. Yu, L. Huo, J. Liu, M. Li, J. Zhou, Validating the mitotic kinesin Eg5 as a therapeutic target in pancreatic cancer cells and tumor xenografts using a specific inhibitor, Biochemical pharmacology, 76 (2008) 169.

[12] R. Sakowicz, J.T. Finer, C. Beraud, A. Crompton, E. Lewis, A. Fritsch, Y. Lee, J. Mak, R. Moody, R. Turincio, Antitumor activity of a kinesin inhibitor, Cancer research, 64 (2004) 3276.

[13] J.F. Gerecitano, J.J. Stephenson, N.L. Lewis, A. Osmukhina, J. Li, K. Wu, Z. You, D.

Huszar, J.M. Skolnik, G.K. Schwartz, A phase I trial of the kinesin spindle protein (Eg5) inhibitor AZD4877 in patients with solid and lymphoid malignancies, Investigational new drugs, 31 (2013) 355.

Chapter 2

Introduction

2.1. Cancer

2.1.1. The overview

Cancer is a disease also known as malignant neoplasm or tumour. The uncontrollable division of cells causes this disease. There are two types of cancer including the one classified as malignant that can invade and spread to different body parts [1]. Some tumours are classified as benign, meaning they are localized and do not spread to other body organs [2]. Cancer cells behave differently from normal cells in that, the latter undergo controlled mitotic or meiotic cell divisions creating new daughter cells based on what is needed by the body. The normal cell growth is intended to replace old or damaged cells. However, in cancer cells, this growth gets more and more abnormal and uncontrollable, leading to old, and damaged cells dying and new cells being excessively formed when they not required. Other cancerous cells detach themselves from the tumour and migrate via the circulatory system(s) to different body parts [3]. Cancer cells can "hide" from the immune system, tissues, organs, and other specialized cells essential for homeostasis. Although there have been considerable developments in the prevention and treatment of cancer, successful chemotherapy for numerous types of cancer remains a greater challenge till date [2]. Therefore, it is very imperative to establish new, safe and efficacious chemotherapeutic agents exhibiting a broad spectrum of anticancer properties with devoid of host cell toxicity [4].

2.1.2. Cancer prevalence

Cancer is a leading cause of death globally, and it was responsible for 8.8 million deaths in 2015 [5]. Many cancer deaths are due to liver, lung, colorectal, breast, and stomach cancers. Over 60% of world's total new incidences take place in Africa, Asia, Central and South America [6]. These regions account for 70% of the world's cancer deaths. Predictions suggest that by 2030, 23.6 million new cancer cases would arise worldwide if current drifts in the occurrence of major cancers and population development are seen universally in the future [7]. This is 68% more scenarios compared to 2012, with somewhat larger development in low and medium human development index (HDI) countries (66% raise in 2030 compared to 2012) than in high and extremely high HDI countries (56% raise in 2030 compared to 2012). Cancer tends to affect young people and reduces the work efficiency and quality of life, which has caused an immense damage to the national and the international economy. Thus, the human, social and economic burdens associated with several cancers are severe [8]. Therefore, there is an urgent need for the development of more effective cancer therapeutics and strategies at this point in time.

2.1.3. The hallmarks of cancer

Cancer is a type of disease that is extremely miscellaneous and complex. There are six recognized traits that jointly result to cancer disease (**Fig. 1**). Such traits develop in diverse orders and are said to offer the basis for tumourigenesis [9]. The capacity of cancer cells to develop independency or insusceptibility toward normal growth signals responsible for control of usual tissue propagation is due to the independence of the signals for development and anti-growth insusceptibility. Apoptosis is defined as programmed cell death (PCD) which is a genetically encoded process that leads to cell death [10]. During tumour development apoptosis causes a critical attrition to the population of the cell and the ability to escape PCD forms an additional carcinogenesis phase. These capabilities, for example, deregulation of custom mechanisms of cell development is insufficient for cancer growth since ordinary cells are restricted in terms of replication [11]. Malignant cells divide without stopping, this occurs via the maintenance of telomeres and evasion of senescence, thus enabling continuous expansion. Cancer cells should be nourished to increase their growth as well as to achieve their capacity to trigger and maintain the angiogenesis [12]. The source of death in 90% of cancer patients is because of the invasion of the nearby tissues, and the capacity to spread to other organs which is characteristically the ultimate alteration in the cancer evolution [13].

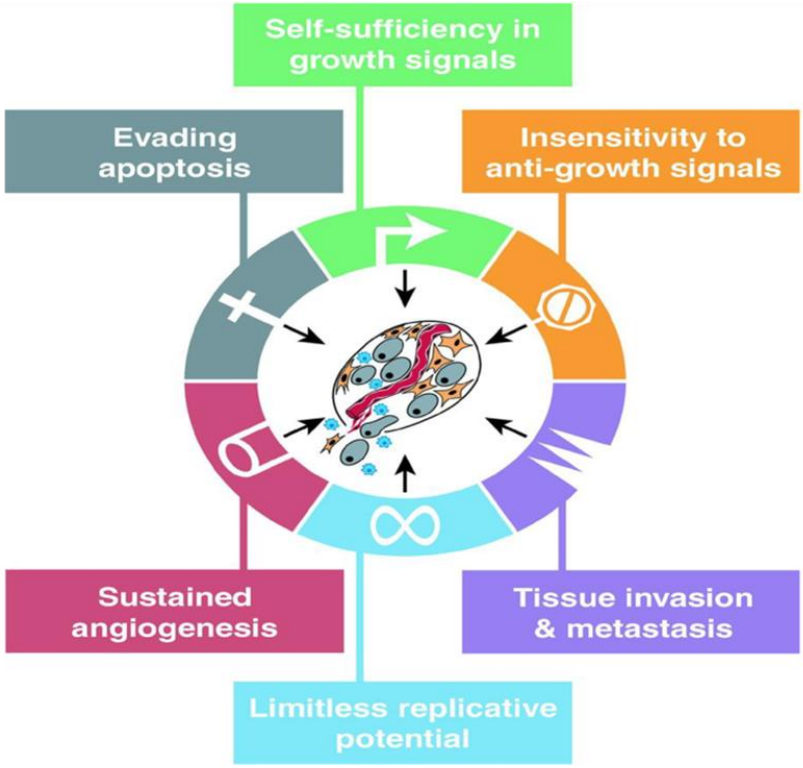

Figure 1: The proposed six assimilated biological abilities gained throughout the entire tumour development [9].

2.1.4. Different types of cancer

Cancer exists in different forms and they are named based on the organs they invaded. The most common type of cancer is the carcinoma, which is formed by the epithelial cells [14]. Another form of cancer is the sarcoma which occurs in the bone and soft tissues, like muscles, fats, and blood vessels. There exist numerous forms of the spinal cord as well as brain tumours, named based on the cell type they develop on [15]. For instance, the astrocytic tumour initiates on the star-structured brain cells known as astrocytes, that aid in keeping nerve cells physically strong. Brain tumours may be malignant or benign. Another type of cancer is leukaemia this cancer activates the blood-forming tissues of the bone marrow. These cancer cells are different from others, in that they do not occur in the form of a solid tumour, instead abnormal white blood cells develop within the blood as well as bone marrow fighting normal blood cells [16]. A decrease in normal blood cells prevents the proper transport of oxygen (O_2) to different parts of the body, control of bleeding or protection against infection. The lymphoma cancer begins in the lymphocytes for example T-cells and B cells. These form an important part in the defence and protection of the body against infections. This type of cancer forms in the lymph nodes and vessels and on other body parts [17]. The multiple myeloma is also known as plasma cell myeloma that forms in the bones and spreads throughout the body. Another type of cancer is melanoma which initiates within the cells that convert to melanocytes and produce melanin. A lot of melanomas occur on the skin; however, they can occur in the pigmented tissues as well, for example, the eye [18].

2.1.5. Treatment options

There are different cancer therapies that have been explored to date. These methods depend on the type of cancer found in a patient's body, and upon how advanced the cancer is in the body [19]. These methods include precision medicine, immunotherapy, hormone therapy, surgery, stem cell transplant, targeted therapy, and chemotherapy [20].

2.1.5.1. Treatment by surgery

Hypothetically non-haematological cancers are cured after complete removal with surgery, however, this is not always doable. When cancerous cells spread to different body parts before the surgery, full removal via surgery is normally difficult [21]. Cancer progression by the model of Halstedian says that the tumour develops in certain area then invade the lymph nodes and finally spreads to the whole body. Small restricted tumours are gradually known as potentially metastatic [22]. Illustrations of surgery for cancer comprise mastectomy,

prostatectomy, and gastrectomy for breast cancer, prostate cancer and, gastric cancer respectively [23]. The purpose of the surgery is to excise an individual tumour or the entire organ. An individual cancer cell is microscopic and may redevelop into a new tumour. Therefore, pathological studies of the sample from surgery are usually performed to find out if an edge of the tissue is healthy or not, hence reducing the possibility that small cancer cells hidden from the eye still exist in the patient [24]. In addition to the removal of a tumour, surgery is frequently vital in investigating how much the disease has extended as well as knowing if it has spread to local lymph nodes [25].

2.1.5.2. Hormonal therapy

Development of other cancers is normally hindered by producing or inhibiting specific hormones secreted in the body. General cases of hormone-sensitive tumours are specific types of breast and prostate cancers [26]. Removal or blockage of the hormone testosterone or estrogen is usually a significant supplementary treatment. In some cancers, hormone agonists administration, for example, progestogens are therapeutically beneficial [27].

2.1.5.3. The immunotherapy

Immunotherapy of cancer is a treatment tactics that encourages the immune system of the patient to attack the tumour [28]. Modern mechanisms of triggering an immune response towards tumours include usage of interferons and some cytokines to generate some response in the immune of patients with renal cell carcinoma in addition to melanoma as well as intravesical *Bacillus* Calmette-Guérin (BCG) immunotherapy for superficial bladder cancer [29]. There has been an intensive exploration of vaccines that can induce specific immune responses in several tumours, particularly malignant melanoma. The sipuleucel-T is a therapy whereby the patient's dendritic cells are loaded with prostatic acid phosphatase peptides that will trigger certain responses from the immune system to work against prostate-derived cells. This vaccine-like approach is applied in the late clinical trials of prostate cancer [30]. The allogeneic hematopoietic stem cell transplantation (HSCT) is measured as a form of immunotherapy, as the donor's immune cells usually attack the tumour known as a graft-vs-tumour outcome. Consequently, this HSCT results in a higher treatment percentage compared to autologous transplant of numerous types of cancer, though it has severe side effects [31].

2.1.5.4. Photodynamic therapy (PDT)

This type of therapy involves stimulation of photosensitizing compounds by near-infrared (NIR) or visible light [32] regions. After excitation, an extremely energetic phase is created

after reacting with O_2 yields a highly reactive singlet O_2 that is able to induce necrosis and PCD within the tumour [33]. The tumour selectivity of porphyrin photosensitizers is due to its distinctive leaky vasculature, made up of lymphatic drainage, as well as the high degrees of recently generated lipids and collagens. The PDT reduces tumours by directly killing the cells, destructing the neo-vasculature tumour, and activating a serious inflammatory response that pulls leukocytes to the tumour [34].

2.1.5.5. Photothermal therapy

The arrival of metal nanoparticles in the 1990's, transformed the photothermal ablation to a new area of slightly aggressive tumour treatment [35]. For instance, gold nanoparticles that heavily absorb light in the NIR area have been established. This has enabled a deep optical penetration into tissues, inducing a dose of heat that is localised and only lethal to the tumour cells [36].

2.1.5.6. Targeted or biologic drug delivery

When a drug is transported to a specific location without exposing other body tissues to the toxicity, this is known as targeted drug delivery system. This is a vital discrepancy from the fundamental targeting concept, where the specific enzyme/receptor is the target and the aim is to improve the affinity and binding to the target which eventually initiate the pharmacological activity [37]. It involves inhibiting specific fragments within cancer cells, thereby slowing down or preventing cancer growth [38]. Other forms of targeted therapies which prevent the natural processes that enable successful growth of tumours are discussed in a review by Johnsen *et al*., [39]. For instance, some targeted therapies stop the supply of blood to the tumour, leading to the death of cancer cells. In comparison to the traditional chemotherapy, targeted agents are precise with reduced side effects that often include infections, weakness, and blood count alterations [40]. Drug targeting occurs via physical, biological, or molecular mechanisms that lead to increased concentrations of the pharmacologically dynamic agent. When it is effectively done, drug targeting can lead to a substantial reduction in the toxicity of the drug, a decrease in the drug dose, as well as improved treatment efficiency [42]. In the study of cancer, the targeted transport of chemotherapeutics has been shown to significantly reduce side effects in comparison to systemic distribution, where tissues in organs such as the liver can accumulate toxic levels of drug. Biological agents as well as targeted therapies are intended to act on specific cellular targets. For example, there are small molecules that block specific protein fragments that are important players in cellular processes that include signal

transduction, PCD, cell cycle among other crucial cellular pathways. Diverse forms of targeted therapies are schematically illustrated in **Fig. 2** [43].

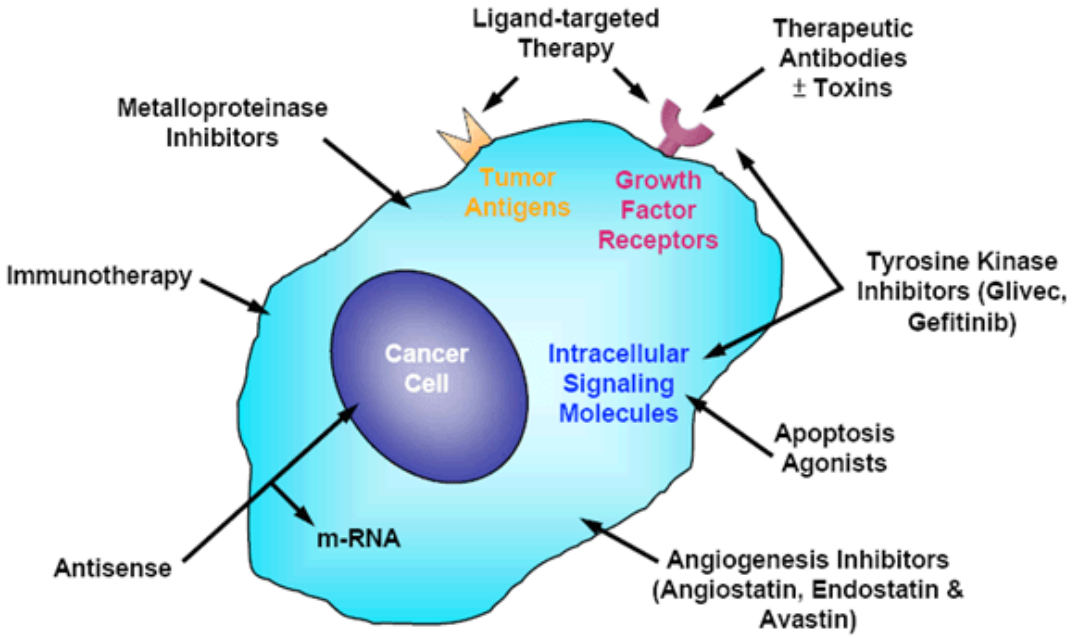

Figure 2: The diverse forms of targeted therapies [41].

2.1.5.7. Radiation

This therapy involves the usage of high-energy radiation such as gamma rays, X-rays, and charged particles to destroy cancer cells. The radiation is either an external beam radiation treatment or internal radiation therapy [44]. Only half of the cancer patients usually receive radiation treatment. This radiation therapy destroys cancer cells by damaging their DNA. The damage can be done directly or via a charged particle in the cell that can result in DNA damage within the cell [45]. However, a disadvantage of radiation therapy is that it is not only specific to cancerous cells but also damages the normal cells. To minimize these negative side effects of radiation treatment, it is sometimes used in combination with other methods such as surgery [46].

2.2. Cancer chemotherapy

Cancer chemotherapy is the use of drugs to destroy a tumour. Currently, chemotherapy refers to cytotoxic agents with an effect on rapidly dividing cells under ordinary circumstances such as bone marrow cells. Chemotherapy has severe side effects [47]. The commonly known side effects include; myelosuppression (production of blood cells decreases), mucositis (the digestive tract's lining becomes inflamed) and alopecia (patient loses hair) [48].

Chemotherapy affect not just a specific part of the body but the whole body. Chemotherapeutic agents among other ways can be administered orally and intravenously (IV). This treatment is either prescribed on its own, or in combination with other cancer therapies [2]. In some cases, prior to the surgery or radiation therapy, a type of chemotherapy known as neo-adjuvant is used to reduce the size of the tumour. When chemotherapy is used to kill cancerous cells that persist after surgery or radiation treatment, it is termed adjuvant chemotherapy [49]. Chemotherapy can also aid the efficacy of radiation and biological therapies by killing recurrent cancer or metastatic cancer. Chemotherapeutic agents have therapeutic guidelines that indicate the dosage levels at which these agents can efficiently affect a tumour and levels at which there is unacceptable toxicity. Hence, more efficient therapies are a consequence of balancing the beneficial as well as antagonistic properties of a combination of different agents, given at different doses throughout the treatment period [32]. Cancer treatment via chemotherapy is classified as either curative (to eradicate tumour) or palliative (when tumour is thought to be incurable with the aim of keeping a reasonable quality of life for as long as possible). Since most anti-cancer agents are extremely toxic, they can affect the whole body through a systemic circulation. In most of the cases, they damage sensitive tissues in different parts of the body [50]. To restrict this damage, toxicity limits should be indicated pertaining the quantity of the drug to be administered at any period [51].

The main purpose of chemotherapy is to elicit a positive effect of the therapeutic objectives without violating the above-stated limitations. There are numerous drugs which are suitable as chemotherapeutic agents, and the selection of a particular drug depends on the nature of cancer to be treated [47]. These drugs are grouped into five main groups such as alkylating drugs, antimetabolites, anthracyclines antibiotics, plant (vinca) alkaloids, and topoisomerase inhibitors[52]. Certain drug examples include cisplatin, doxorubicin, paclitaxel, 5-fluorouracil, adriamycin, irinotecan, etoposide and chlorambucil. These drugs disturb the synthesis and function of DNA or cell division in cancer cells [53]. Based on the chosen drug, chemotherapy affects malignant tumours by damaging the DNA/changing the composition of DNA of the cancer cells thereby arresting their reproduction/replication [4].

Chemotherapeutic agents also inhibit the cell's mitotic processes thus, preventing cancerous cells from dividing into new cells. Development of mitotic spindles which are important in the movement of the original and replicated DNA to opposite ends of the cell (allowing cell division) is also inhibited by some drugs [54]. Clinically, the application of traditional anticancer agents renders patients at high risks as most of these drugs are non-

specific. This causes many cancer patients to endure major side effects including reduced quality of life, and recurring therapy. The inefficiency and side effects of chemotherapy have been mainly related to the formulation and bio-distribution of the drug, normal cell toxicity, and drug-resistance acquisition by the cancer cells. Therefore, scientists are endlessly investigating several ways to overcome these serious problems [50].

2.3. Chemotherapeutic agents

2.3.1. Antimitotic drugs

Antimitotic agents such as paclitaxel as well as vinblastine activate the spindle assembly checkpoint (SAC), this blocks the shift from metaphase to anaphase resulting in polymerization inhibition of the microtubule (MT) dynamics [55]. The cells then experience mitotic arrest and subsequently, the drug interrupts the growth of spindles and orientation of chromosome. This causes the cells to either stay in the prolonged arrest mode resulting in initiation of cell death or in the senescence-like G1 mode [56]. Furthermore, MTs develop in the interphase and are crucial for accurate segregation of chromosome as well as the division of cells in mitosis process. During mitosis, the dynamics of MTs is quicker than during interphase, hence, the MTs are validated targets for anticancer drugs because cancer cells have a hyperproliferative behaviour [57]. There are two categories namely MT-destabilizing agents or MT-stabilizing agents depending on how the agents act on MTs. When the destabilizing agents are administered at high concentrations, these agents inhibit the polymerization of MTs. Numerous destabilizing agents bind to vinca or taxoid-binding domain of mitotic enzymes. In the vinca domain they bind at the vinca site flanked by β- and α-tubulin (known as the vinca alkaloids) these consist of vinflunine, vincristine, vinorelbine, vindesine, and eribulin [58]. While the ones that bind on the colchicine-site consist of cryptophycins, dolastatins, and combretastatin-A4. High dosage of the agents that promote MT polymerization stabilizes MTs. They also inhibit calcium ion- or cold-induced depolymerization, for example, second- and third-generation taxanes, epothilones and ixabepilone. Drugs such as taxanes, attach to the inner surface of the MTs where the taxoid binds to the β-tubulin. The peloruside A (PLA) binding arrests the mitotic cell cycle at the G2/M state triggering apoptosis. Antimitotic drugs are superior to taxanes as well as vinca alkaloids because they are weak substrates of the P-glycoprotein (P-gp) drug efflux pumps [57].

Antimitotic agents are usually administered in combination with an anthracycline (doxorubicin), an antimetabolite (capecitabine), a platinum derivative (carboplatin), or with

human epidermal growth factor receptor 2 (HER2) in targeted therapeutics like trastuzumab [54]. Regardless of the existence of these effective chemotherapeutic drugs, severe side effects (neurotoxicity) and the appearance of mutant tumours, restrict the application of these agents, thus raising the need for novel anticancer drugs with reduced side effects [59]. The severity of the cancer problem can be judged on the basis that, its morbidity and mortality numbers are much greater compared to other diseases [54]. Traditional anticancer drugs (**Fig. 3**) have several undesirable side effects including neurotoxicity and drug-resistance that is acquired over prolonged chemotherapy [60]. Kinesins are specific to mitosis, play a role in the proper execution of mitosis, chromosomal arrangement, separation and centrosome segregation [61].

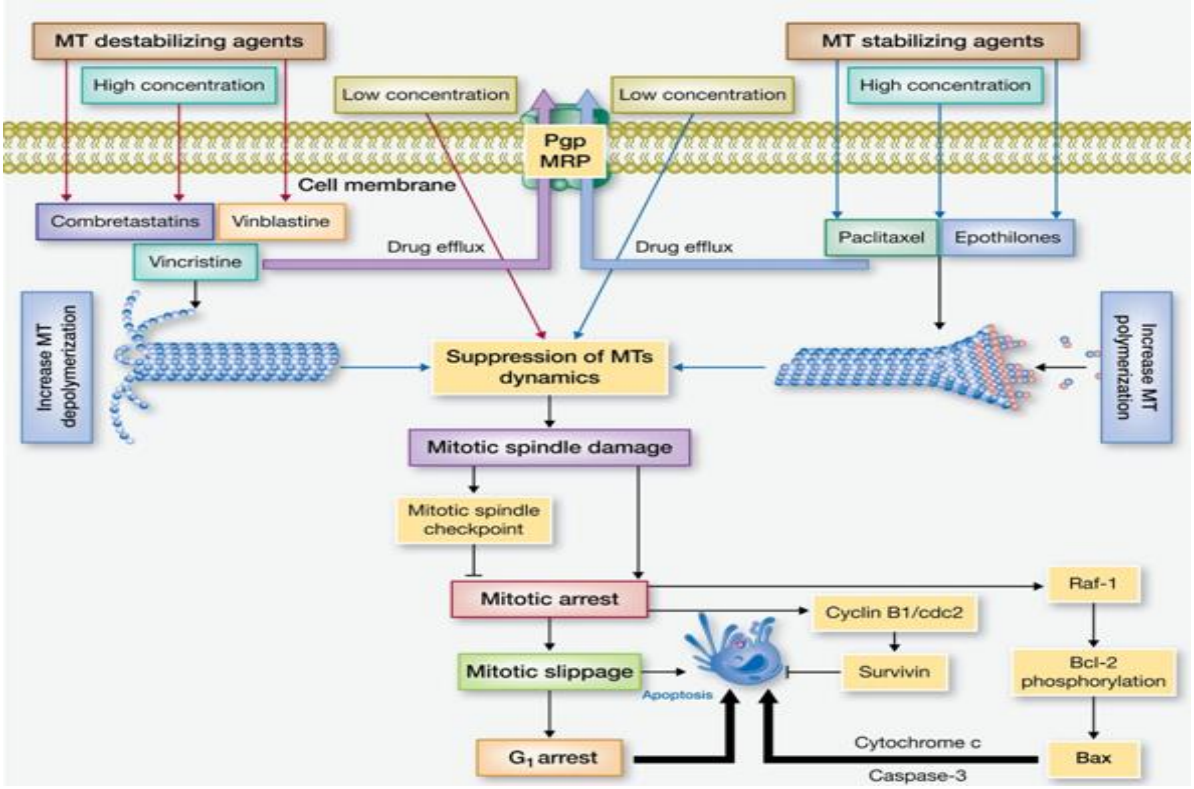

Figure 3: Schematic diagram of putative events involved in MT targeting agents (MTA)-induced apoptosis [60].

2.3.2. Taxanes

Taxanes are widely known chemotherapeutic agents utilized in breast cancer treatment. The combination of the taxane, paclitaxel (taxol), and carboplatin is a mostly used combination routine for lung carcinoma [62]. Paclitaxel binds to β-tubulin and prevent MT

depolymerisation leading to a mitotic arrest followed by stimulation of caspase-dependent apoptosis by B- cell lymphoma (Bcl)-2 proteins. Taxanes often prolong the survival of patients with lung, breast, and ovarian carcinomas [63]. Like any other drugs, taxanes also have side effects these include myelosuppression, skin rash, peripheral neuropathy, and arthralgia. Subsequently adjunctive drugs are essentially used to minimize these side effects [64]. Efficiency of taxanes as adjuvant in the treatment of breast cancer is vivid. HER2 signalling promotes numerous taxane-resistance mechanisms such as drug efflux and the metabolism of drugs [65]. A novel MT-stabilizing taxane called cabazitaxel (Jextana), which is effective on metastatic breast- and metastatic hormone-resistant prostate cancer also acquired paclitaxel and docetaxel resistance mechanism [66]. Cabazitaxel has side effects such as diarrhoea, neurotoxicity, vomiting, and nausea [67].

2.3.3. Epothilones

Mycobacterium *Sorangrum cellulosum* was discovered to have epothilones A and B as cytotoxic metabolites that steady the MTs. Epothilones are more toxic compared to taxanes *in vitro*, for instance, epothilone B is more cytotoxic to human ovarian cancer cells (OV-90) than paclitaxel [68]. Paclitaxel is competitively inhibited by epothilone B, as they both bind at a similar location on the β-tubulin. Taxanes, as well as epothilones, display different modes of resistance. Epothilones are effective against cancer cells that overexpress class III β-tubulin, whereas resistance to taxanes arises when this class is overexpressed [68, 69]. The lactam analogue of epothilone B known as ixabepilone (Ixempra) was accepted in 2007 by USA for metastatic or locally advanced treatment of anthracycline and taxanes resistant breast cancer. This drug was the first amongst all epothilones to be accepted at clinical level [70]. The Ixabepilone is more metabolically stable and more clinically advanced epothilone with respects to its efficiency and tolerability in breast cancer patients. Ixabepilone toxicity is low in cell lines that express P-gp such as Madin-Darby canine kidney (MDCK) cells transfected with the human multidrug resistance (MDR)-1 gene and the kidney epithelial cells from the kidney of a pig transfected with the human MDR1 gene [71]. Ixabepilone is not a substrate of the breast cancer resistance protein (BCRP1), a protein that doxorubicin- and paclitaxel-resistant breast cancer cells (MCF-7 or breast adenocarcinoma /DOX and MCF-7AX) significantly express, this describes the effectiveness of ixabepilone in taxane-resistant breast cancer [68].

2.3.4. Vinca alkaloid

Primary vinca alkaloids were obtained from the *Catharanthus roseus* plant, originally from Madagascar. These alkaloids were discovered to be active against cancer in 1960. In the year 1963, vincristine was approved by USA for chemotherapy of cancer [72]. Such agents bind to the β-tubulin near the guanosine triphosphate (GTP)-binding location (the vinca domain) at the β-α-tubulin heterodimers interface. Attachment at the vinca domain inhibits the straightening of curved tubulin which consequently restricts the growth and assembly of MTs [73]. Vintafolide (EC145) has shown potency in treatment of ovarian and lung cancers in phase II of clinical trials. The vintafolide contains MT-destabilizing molecules, folic acid, desacetylvinblastine hydrazide, hydrophilic peptide spacer, and a disulfide-containing self-immolative linker [68]. Vintafolide transports the MT-destabilizing molecules to the folate receptors (FRs) of FR-tumour cells. In different carcinomas, the FRs are overexpressed and it facilitates the up-take of folic acid-conjugated agents through a process called endocytosis [52]. The disulfide bonds are sliced and active desacetylvinblastine hydrazide diffuses in the endosome to the cytoplasm where they cause MT disturbance upon absorption of the vintafolides by the cell. The FRs are also expressed in small quantities in non-tumourigenic tissues, this makes vintafolide a supreme tumour target [73].

2.3.5. Estrogen derivatives that target the MTs

Estrogen helps during the development, diversity, and maintenance of numerous body tissues by stimulating the nuclear estrogen receptors (ERs), ER-α and ER-β, to trigger the activation of transcription factors [74]. Estrogen promotes proliferation and invasion, in breast and ovarian cancers. The sole purpose of the use of anticancer agents derived from estrogen is to contest with estrogen for the ER binding by antagonistic behaviour. The fulvestrant (ICI182780), is one instance of these compounds and has shown predominant effectiveness compared to the tamoxifen, which is currently a non-steroidal anti-estrogen agent used as standard hormone therapy in breast cancer [75].

2.3.6. The resistance of cancer cell against antimitotic agents

Resistance towards antimitotic agents takes place in different phases of the therapy. An understanding of this resistance mechanism is crucial in the design of new antimitotic drugs [68]. Hereditary variations that occur preceding the cancer therapy are the initial source of therapeutic failure is called intrinsic resistance. Drug treatment leads to a secondary or acquired resistance. Tumour cells have a system of membrane efflux pumps belonging to the

ATP-binding cassette (ABC) family. They have been shown to develop these efflux pumps against chemotherapy involving antimitotic drugs *in vitro* [76]. Production of P-gp is facilitated by MDR1, which effluxes numerous hydrophobic antimitotic agents (vinca alkaloids and taxanes). Vinca alkaloids are transported out of the cell via the multidrug-associated protein-1 (MRP)-1. The MRP2 and MRP7 export the taxanes and epothilone B is solely transported by MRP7 [68]. The expression of these efflux pumps displays some relationship with the poorer reaction toward antimitotic chemotherapy on prime tumours. Therefore, emerging drugs which are not P-gp substrates, for example, epithilones from second- and third-generation as well as taxanes with structural variations enabling them to dodge P-gp, are vital for combating difficulties of cancer resistance [77]. An alternative approach is to utilize molecules with activities that are enhanced by overexpression of P-gp efflux pumps. Reports suggest that when the paclitaxel drug and the P-gp inhibitor verapamil are used in combination, they have a synergistic cytotoxic effect against MDR breast cancer cell line (MCF-7/ADR) by *in vitro*. Within the tumour cells, mutations in the p53 gene, activation of phosphatidyl-3-phosphate kinase (PI3 K) and mutations within Ras/Raf genes, result in increased resistance to antimitotic compounds [68].

The hypomethylation of phosphatase as well as tensin homolog removed from chromosome 10 (PTEN), a tumour suppressor gene, weakens the gene's effect. This results in upregulation of PI3 K or Akt kinase (Akt) pathway. This substantially stimulate Akt, a protein controlling the anti-cell death proteins as well as the entry to the cell cycle. The loss of PI3 K regulation promotes an undesirable phosphorylation, leading to the pro-apoptotic protein deactivation as well as protection of the mitochondrial membrane from any disturbance [76]. This triggers an intrinsic mechanism which further increases the resistance towards apoptosis. When the mitogen-activated protein kinase cascade (MAPK) pathway is overexpressed, MAPK is activated by Ras (a small GTP kinase receptor), which consequentially leads to the Raf stimulation [68]. Mutations in the genes that upregulate this pathway result in survival signalling. The overexpression of class III β-tubulin isotope, an indicator utilised during the diagnosis of solid cancerous tumour for example cancer of ovaries, is assumed to be responsible for resistance against paclitaxel. The class III β-tubulin increases the instability in MT dynamics, in addition, counteracts the taxanes stabilizing action and it influences the vinca alkaloids efficiency [73]. The class III β-tubulin is also expressed in stressed cells and in O_2 as well as nutrient deprived cells. The MT regulating proteins for example tau, stathmin, and mitotic centrosome associated kinesin (MCAK), are

all connected to antimitotic drug resistance. The SAC protein deregulation by gene amplification, for example, deregulation of Aurora kinase protein by the Aurora-A amplification also confers resistance to drugs targeting MTs [78].

2.4. Drug resistance mechanisms

Drug resistance is whereby cells/microbes acquire tolerance against the administered drug. However, comparable mechanisms have transpired in some other diseases such as cancer [65]. Certain mechanisms of drug resistance are specific to a particular disease, whereas others, for instance, drug efflux, witnessed in microorganisms as well as cancers that are resistant to drugs in humans, are evolutionarily well-maintained [53]. Numerous types of cancer were at first sensitive to chemotherapeutic agents. However, after a certain period, they became resistant via these mechanisms in addition to others (**Table 1**), including mutations of DNA and alterations in metabolism promoting drug inhibition as well as degradation (**Fig. 4**) [49].

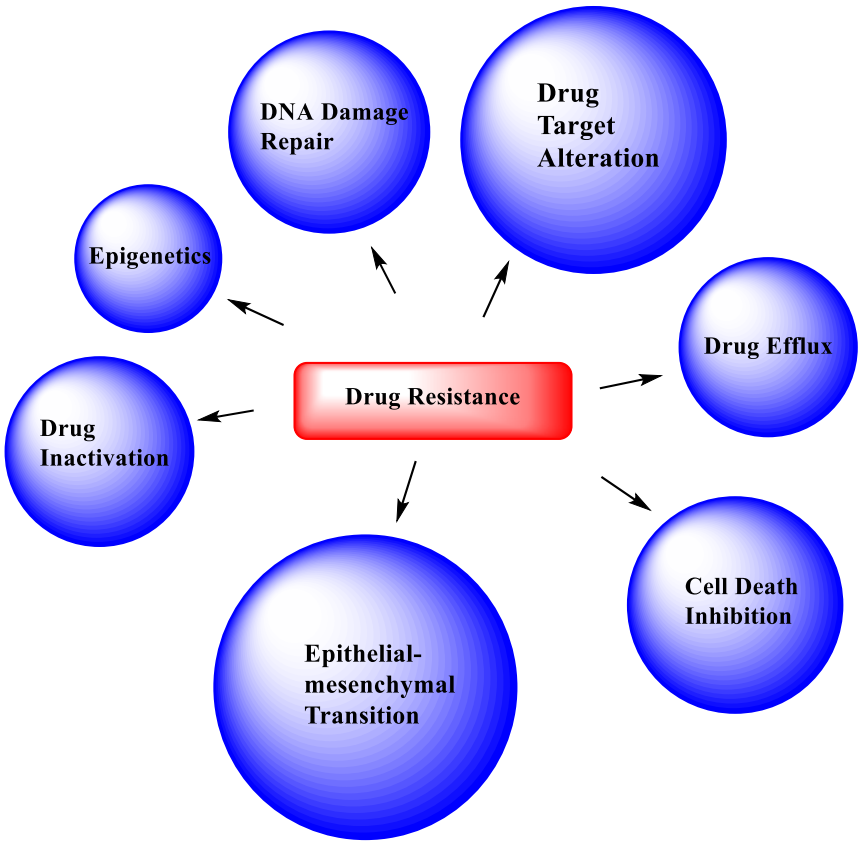

Figure 4: The outline of the methods that enable or stimulate drug resistance in the tumour cells of humans that are either direct or indirect. Such methods can act either individually or in conjunction and via several signal transduction mechanisms [49].

Table 1: The summary of chemo-resistance mechanisms [79].

Mechanism of Chemo-resistance	
The Uptake of Drug	During the administration of cytotoxic agents, the transporters of the superfamily of solute carriers (SLCs) have a crucial role. Alterations in the expression of these transporters, tumour cells are unable to absorb anticancer agents resulting in the development of resistance.
The Export of Drug	Another major cause of resistance occurs when the ABC protein members are overexpressed, for example, the multidrug resistance protein 1(MDR1, ABCB1 gene). It pumps out toxic agents and restricts the intracellular concentration of cytotoxic agents.
Inactivation of Drug or Metabolic Activation of Pro-Drug	Any changes disturbing the metabolism of the drug results in the resistance. Such as tumour cells that overexpress phase I and II detoxifying enzymes having improved capacity to deactivate cytotoxic drugs. Increased activity of CYP3A4, an enzyme belonging to the family of cytochrome P450, deactivates such as paclitaxel in colorectal cancer cells. Moreover, reduced expression of drug activators resulted in decreased drug sensitivity, for example, carboxylesterases, typically involved in intracellular irinotecan stimulation, is reduced in cancerous cells with greater irinotecan resistance.
Molecular Targets Changes	Variations in molecular targets and malfunctioning signalling pathways are changing the sensitivity of a tumour towards the anticancer agents. For instance, the anthracyclines mechanism is based on their capacity to interact with DNA topoisomerases. Mutations in the *TOP1* gene, encoding topoisomerase 1 resulted in a reduced capacity of anthracyclines to interact with their target.
DNA Repair	The capacity of a tumour to mend the DNA damage that was induced by the drug results in resistance for example repair of excised nucleotides caused by alkylating agents use. The mismatch repair (MMR) corrects wrongly matched nucleotides. Loss of MMR capacity results in genetic instability with greater resistance to different anticancer agents.
Modifications in the Pro- and Anti-Apoptotic Balance	Modifications of the programmed cell death key factor, for example, p53 has an important role in chemo-resistance. The *BAX* role is frequently reduced because of the mutation in this gene, resulting in the secretion of shortened proteins and growth of cells resistant to oxaliplatin. Upregulation and abnormal expression of antiapoptotic aspects, for example, Bcl-2 or Bcl-XL (B-cell lymphoma protein extra-large) are linked to enhanced resistance.

One method of drug resistance against cancer includes decreasing the accumulation of drug by promoting the efflux (**Fig. 5**). The family members of ABC transporter protein are vital and allow efflux, these are intensively investigated regulators found in the plasma membranes of a healthy cell. The ABC carriers are trans-membrane proteins found in the cells of humans, exist in all phyla, and they move different molecules across the cell membranes [80]. However, the transporter structure differs amongst proteins and is classified

based on the existence of two different domains known as the extremely conserved nucleotide binding domain and the extremely mutable transmembrane domain. Upon the attachment of a certain substrate to the transmembrane area, on the nucleotide binding domain, ATP hydrolysis initiates an alteration in the structure that thrusts the substrate from the cell [81]. This efflux system has a crucial function in stopping excessive growth of toxins in the cell. The ABC carriers are extremely expressed in the liver as well as intestine epithelium, a site where proteins defend the body by means of pumping drugs and toxic substances into the intestinal lumen as well as bile duct. The ABC transporters also have a huge role in the sustenance of blood-brain barrier. Efflux through ABC carriers is a known method of drug resistance in tumour cells and a regular physiological process [49]. Three transporters such as BCRP, MDR1, and MRP1 are involved in most cancers that are drug resistant. These three carriers have a wide substrate specificity and efflux xenobiotics such as anthracyclines, kinase inhibitors, epipodophyllotoxins, taxanes, and vinca alkaloids from the cells. Therefore, these carriers guard the cancerous cells against several first-line chemo-treatments [65].

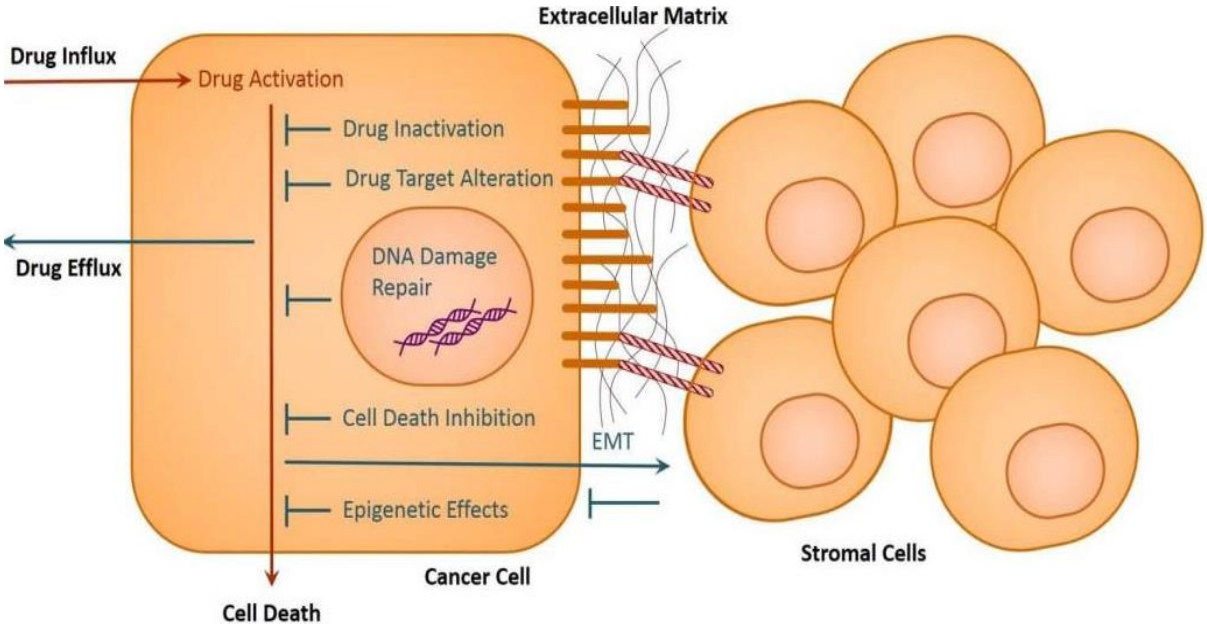

Figure 5: The Illustration of the main pathways leading to the development of drug resistance in the cells of cancer [65].

2.5. Next generation: improvement to existing therapies and novel cellular targets

2.5.1. Protein kinases as potential drug targets for cancer chemotherapy

Protein kinase (PK) defines the process of the enzyme which catalyses the transference of phosphate from the donor to the amino acid residue that is an acceptor in a substrate made up of multiple peptides. The consequential covalently modified structure of this peptide results in the target protein having new pharmacological properties [82]. Following the receptors that were coupled with the G-protein, PKs are currently promising drug targets (**Fig. 6**). Studying the major roles of the PK that contribute to cancer development, made pharmacologists to focus on targeted therapies as an ideal approach in blocking the evolution of cancer. Kinases are recognized as significant intracellular signalling components. For de-phosphorylation and phosphorylation to occur in a cell, protein kinases should be activated and/or inactivated [83]. The kinases can be grouped into two types the serine/threonine kinases and tyrosine kinases. The serine/threonine kinases phosphorylate the substrate on the tyrosine residues, whereas the tyrosine kinase recognizes the substrate molecule via the substrate-recognition site as well as the transfer of a phosphate molecule from ATP to the residues of the bound protein substrate at a nearby site known as ATP-binding or catalytic site [9].

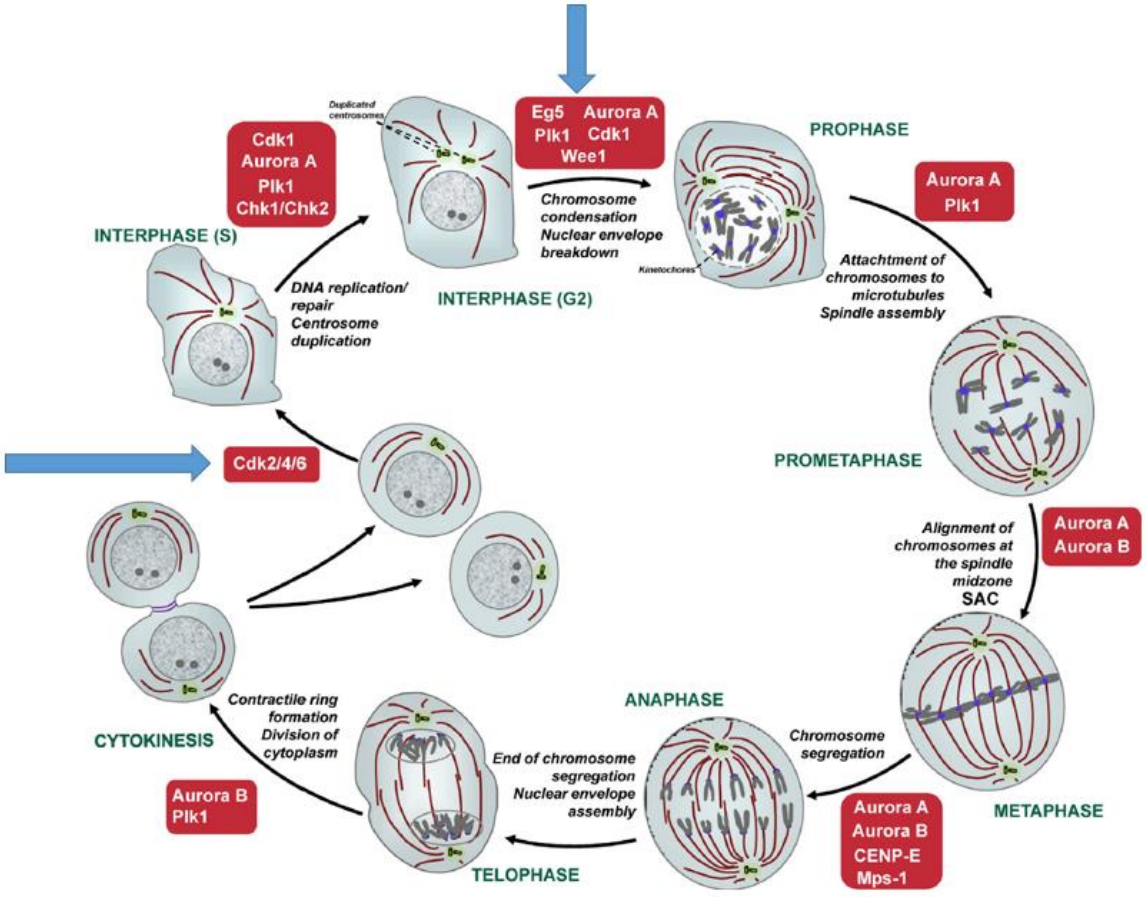

Figure 6: Proteins involved in mitosis as antitumor drug targets [84].

The calmodulin antagonist (Naphthalenesulfonamides) was the first synthesized ATP-competitive inhibitor of the kinase protein. Modification of this calcium binding protein by replacement of naphthalene with isoquinoline exhibited some PK inhibition. However, non-specificity and efficiency of this drug only at high concentration was a serious disadvantage [85]. Staurosporine was then discovered, this drug was capable of inhibiting the PK C, which is a serine/threonine kinase type, which activates the Raf-MAPK as well as the NF-κB signalling system. However, lack of specificity was still a major drawback. More derivatives of staurosporine with some chemical changes and with specificity were synthesized, for example, 7-hydroxy (UCN -01) and N-benzoyl (PKC412) staurosporine, and they both are in clinical trials (**Table 2**) [86]. The UCN-01 blocks G2 from progressing to M in a cell cycle via checkpoint control kinase (CHK1) inhibition. Rapamycin initially discovered as an antifungal drug exhibited promising activity as an anticancer agent and was the first drug to be accepted for clinical trials because it specifically inhibited a single PK. The PKC412 is now used in the treatment of final stage of cancer [84].

Table 2: Kinase inhibitors and their targets [86].

Inhibitor	Targeted kinase
UCN-01, PKC412 (Ser/Thr Kinase)	Analogue of staurosporine and they target the PKC, CHK1, KIT and PDGFR
Rapamycin or Sirolimus (Ser/Thr Kinase)	An immunosuppressant that targets the mTOR or FRAP by binding to the FKBP
CCI-779 or Temsirolimus and RAD001 (Ser/Thr Kinase)	An ATP-competitive small molecule inhibitor that targets the p38 MAPK
PD184352/CI-1040, PD0325901 and ARRY-142886 (Ser/ Thr and Tyr Kinase)	Inhibitors that are not ATP-competitive small molecule targeting the MEKK1/MEK1
Trastuzumab/Herceptin (Tyr Kinase)	A humanized monoclonal antibody targeting HER2/neu/ErbB2

Due to the commercial success and clinical efficiency of the present drugs binding to the MTs, many research studies were conducted to further improve the potency of these drugs [87]. This has been successful with new and altered drugs such as epothilone and ixabepilone. These altered/new drugs are active against βIII-tubulin, which is an isotope that is not subjected to efflux via ABC-encoded P-gp. Whereas, a novel design of paclitaxel with albumin gives lower toxicity. Emphasis points to new routes of intervention in mitosis process that overcome limits involving drugs that target MTs, by having activity against

targets that are more specific. The one possible approach is targeting the kinase and kinesin family members since they are initiators of the phosphotransfer cascades that are essential for the signal transduction [88]. Presently, PKs appear as one of the essential classes of oncological drug targets. The kinases contribute to the biology of cancer via three different mechanisms such as (1) they either occupy the main roles in the oncogenic signalling cascades, (2) aid in development as well as the formation of cancer and (3) through mutationally induced kinases that may themselves trigger oncogenic changes. Interference with the last mechanism is a verified approach for therapeutic intervention. The Aurora kinase, as well as polo-like kinase, are the most studied targets amongst the kinases in the process of mitosis [89].

2.5.2. Aurora kinase

One intensively studied kinases is the Aurora family; with three members that exist in humans, Aurora A, B, and C. Their key role is to accurately align and segregate chromosomes to make sure that the genomic integrity is maintained throughout the mitosis process [90]. Aurora A critically regulates the timing of entrance to mitosis, centrosome maturation, and plays a certain role in spindle assemblage as well as centrosome division via the kinesin motor protein KSP phosphorylation. In the early stages of mitosis, Aurora B regulates proteins that affect dynamics of the MT spindles throughout the spindle development, then encourage proper alignment of chromosomal kinetochore adherence in the mature spindle as well as regulate the spindle checkpoint [89]. In the final phases of mitosis, Aurora B assists in spindle cleavage furrow development, essential for the positive completion of cytokinesis. The role of Aurora C is not as well outlined as Aurora A and B, though it can overlap with Aurora B. Inhibitors with pan-Aurora specificity or selectivity for either Aurora A or Aurora B are currently in clinical trials (phase 2) [91].

2.5.3. Polo-kinase (PLK)

There are five members of polo-kinase (PLK1 to 5) found in humans. In mitosis, PLK1 is extremely expressed and known to be pivotal in the regulation of several important procedures during the cell division, this includes controlling the entrance to mitosis and centrosome maturation, allowing division of duplicated chromatids via phosphorylation of cohesion as well as kinetochore dynamics initiating anaphase [92]. The PLK1 have some roles in the cytokinesis, resulting in mitotic exits, such as regulation of the kinesin motor protein MKLP2 in cytokinesis and phosphorylation of enzyme complexes found in cleavage

furrow formation. Over-expression of PLK1 is also apparent in many tumours and associated with poor diagnosis, and is connected to its capacity to negatively control the significant tumour suppressor p53. Intrinsically, a substantial mitotic controller, PLK1 has appeared to be a significant prognostic and therapeutic oncology target, with quite a few inhibitors currently in stage 2 of clinical trials [89].

2.5.4. CDK and their role in mitosis

There are 21 CDKs that are encoded in a human genome, and only CDK1-4, 6, 10, 11 seem to have some role in the progression of cell cycle. The rest have indirect functions such as activating other CDKs, regulating the transcription process or contain the neuronal responsibilities (CDK3, CDK7-9 and CDK5 respectively) [93]. The expression of CDKs changes during different cell cycle phases. CDK/Cyclin D complexes are active in G1, they also phosphorylate the retinoblastoma (Rb) protein enabling the progress of G1 to S phase. In the G1-S interface, Cyclins A and E accumulate and activate CDK1 and 2 consecutively, allowing further movement to the G2 stage. During this process, the cyclin B members (CDK1, cyclin B1) are the ones driving the cell to the mitosis [94]. In mammalian cells, proliferation becomes independent of growth factors as well as mitogens at the G1 restriction point (R) (**Fig. 7**). The Rb is a tumour suppressor that prevents proliferation via binding to the E2F family of transcription factors, thus suppressing their activities. Hence, the Rb pathway regulates the restriction point that maintains the regulation of cellular proliferation.

During the early G1 phase, under unfavourable conditions for proliferation, cyclin D levels rise via posttranscriptional as well as transcriptional pathways [95]. High levels of D-type cyclin drive the development of active kinase heterodimers with CDK6 and 4 catalytic subunits. Dynamic CDK4 and CDK6 then phosphorylates Rb partially relieving suppression of E2F to allow expression of genes required for the passage through the restriction point. This also involves the expression of E-type cyclin, which triggers CDK2 resulting in Rb hyper-phosphorylation completely freeing the E2F suppression, enabling the cells to exit G1, then initiate replication of DNA [96].

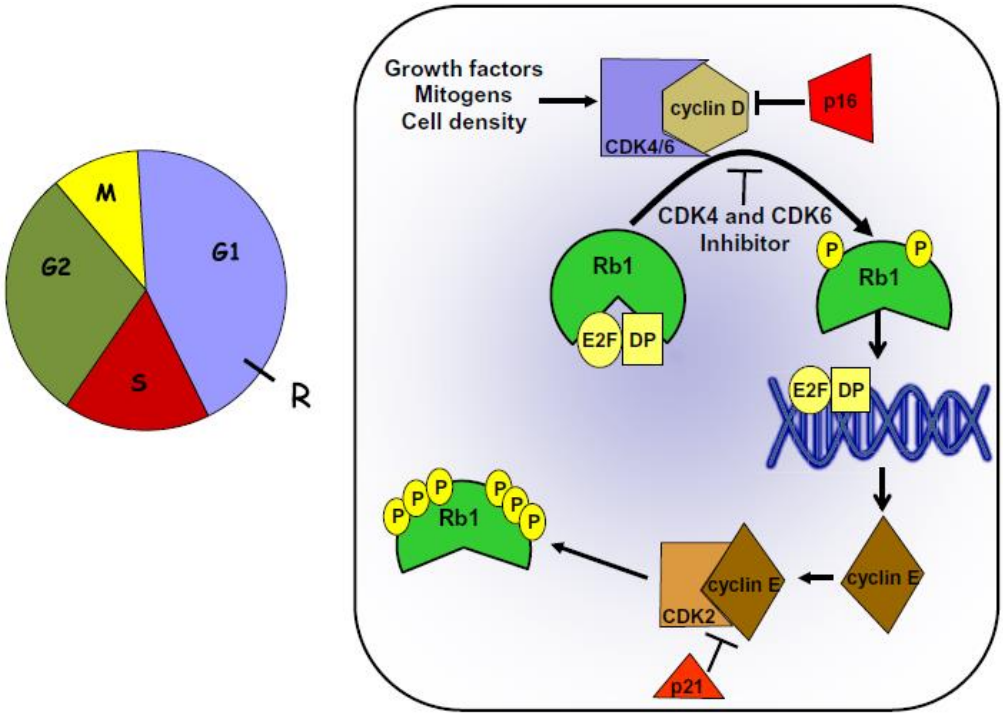

Figure 7: The regulation of mammalian cell cycle via the CDK4 and CDK6-cyclin D1-Rb-p16/ink4a pathway [96].

2.5.5. Small molecule inhibitors of CDK as cancer chemotherapeutic agents

Numerous inhibitors of CDK have been synthesized as potential anticancer agents in the past two decades, and these inhibitors have been evaluated against different types of tumours. [97]. Different chemical groups, characteristically the planar five-membered aromatic moieties such as indolinone, indirubin, thiazole, and flavonoids were characterized as small molecule ATP-competitive (type 1) inhibitors of CDKs. Most were active inhibitors of CDK1/2 because their structures were designed based on studies made on the monomer CDK2 [96]. The first synthesized group of CDK inhibitors were non-selective and are now referred to as pan-CDK inhibitors, these include the flavopiridol (**Fig. 8**). The flavopiridol showed a broad spectrum of activity (inhibited CDK1, 2, 4, 6, 7 and 9). This drug can trigger the cell cycle arrest at G1 and G2 phase; however, it can also trigger a response that is cytotoxic, this may be because of the inhibition of CDK7 and 9 that results in transcriptional suppression [97]. The second group of CDK inhibitors were synthesized with the aim of increasing the selectivity of the drug, these include dinaciclib. This potent inhibitor of CDK1, 2, 5, and 9 had minimal activity against CDK4, 6 and 7 (**Fig. 9**) [96].

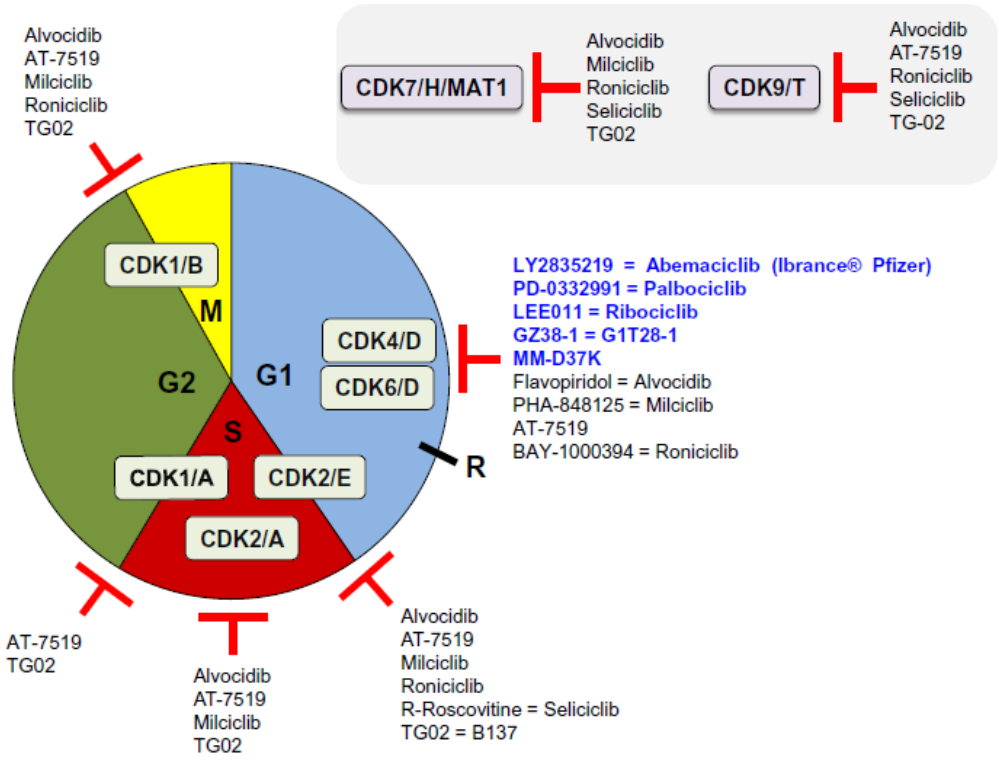

Figure 8: CDK inhibitors targeting different phases of the cell cycle [96].

In a cell-based assay, Dinaciclib inhibited substantially Rb-stimulated phosphorylation process. This drug also inhibited the progression of cell cycle in addition to triggering regression on solid tumours. AT7519, a pyrazole 3-carboxyamide compound inhibited CDK1, 2, 4, 6 and 9 [97].

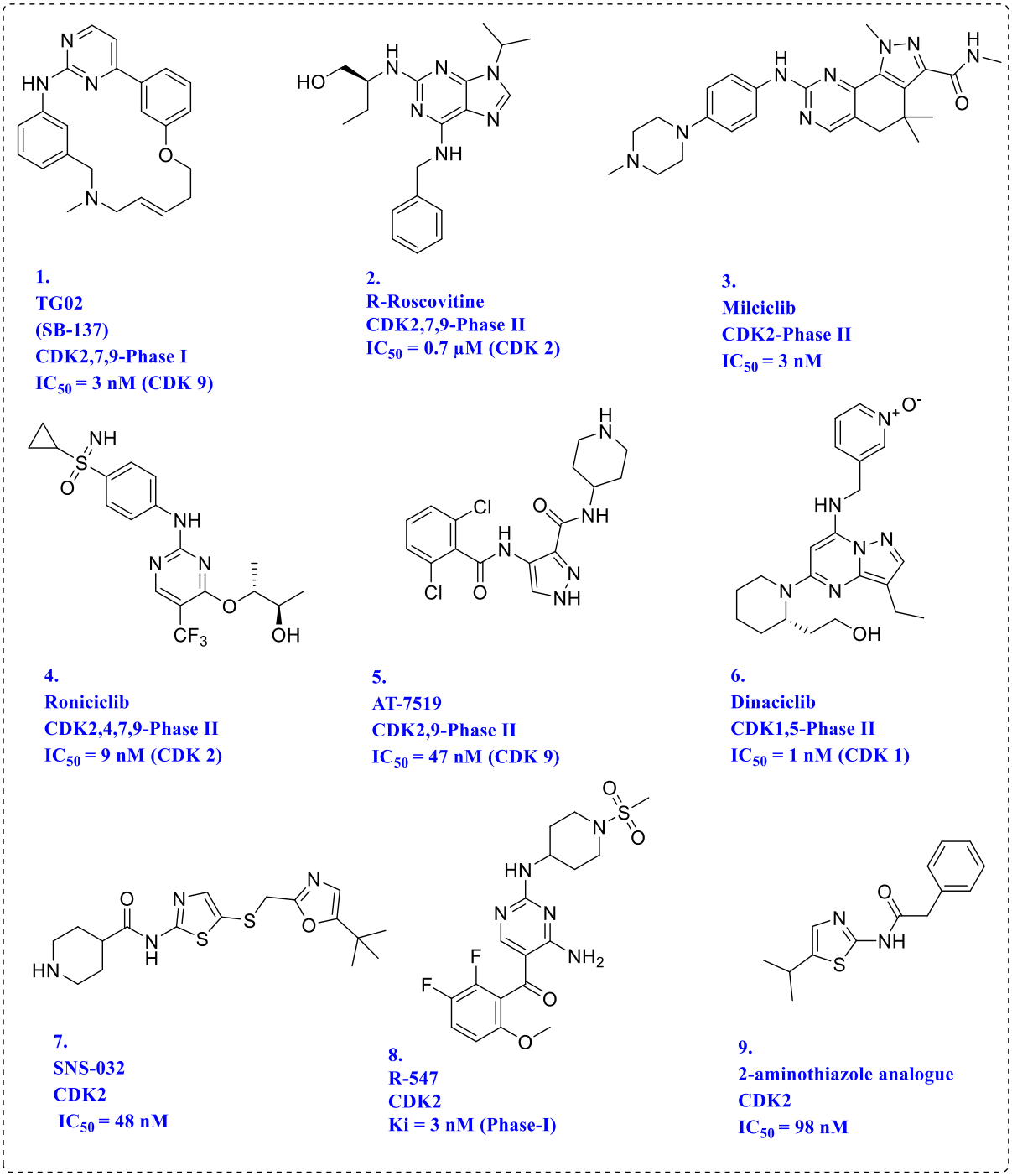

Figure 9: The first and second generation CDK inhibitors [97, 98].

2.5.6. Agents influencing MT dynamics: KSP

Eukaryotic cells have numerous types of molecular machines essential in organising the cellular structure and in the direct intracellular movement. They are grouped into 3 super-families of proteins the dynein, myosin, and kinesin [99]. They all use ATP hydrolysis to yield a coordinated force on MTs to execute their roles. Kinesins are composed of the

superfamily of about 650 distinct MT-dependent motor proteins, up until now found solely in eukaryotes. There are fourteen families under kinesin family grouped based on phylogenetic analyses of their characteristics motor domains of 330– 440 residues in size [89]. They are structurally diverse having minor sequence conservations. The motor domain is located at the C-terminal (C-type kinesins) or N-terminal (N-type kinesins) or inside (kin 1/M-type kinesins). The N-terminal travel to the plus–end of microtubulin (β-tubulin) while C-type kinesins move towards the minus–end (α-tubulin) of the MT. The M-type kinesins move differently because they diffuse toward the end where they display depolymerisation action of MT [100].

The conventional kinesin KHC, Kif5B, Kif5s, kinesin-1 family, were the first kinesin to be discovered. This kinesin is found abundantly as a protein dimer in the human body, containing heavy linkers that are identical and conjoined via a couple of light chains. There are three distinct domains within a prototypical N-type kinesin (**Fig. 10**) [101].

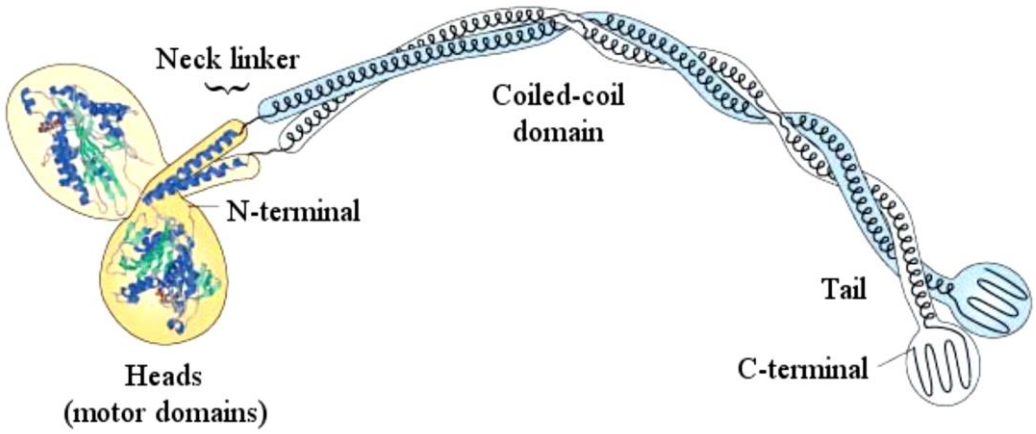

Figure 10: The structure of the N-terminal conventional kinesin [89].

The motor domain contains the pockets where nucleotides bind and regions where MTs interact, and lastly the region that has the neck to neck linker. The linker joins the motor domain to an inner region of the α-helical, thus creating a helical coil responsible for oligomerisation into dimers or complex oligomers. Next is the C-terminal tail domain, direct or indirect cargo interactions occur in this terminal. This site gives kinesins various roles across transport, mitosis, and meiosis [89].

KSP or Eg5 is a kinesin superfamily member of the molecular motor proteins. Inhibition of KSP stops the spindle pole from separating, leading to a lengthy mitotic arrest during the pro-metaphase and consequent cell death. Furthermore, the adult peripheral

nervous system does not express KSP; hence agents that inhibit KSP may not result in side effects that are neuropathic [99]. Agents inhibiting KSP influence the development of cancer cells that are resistant to Taxol. KSP is one of the validated therapeutic targets of choice for many cancers. Inhibitors of kinesin responsible for mitosis can be applied broadly in the treatment of other proliferative illnesses like lymph proliferative disorders found in patients suffered from an autoimmune disease. Moreover, it is found abundantly in the proliferating tissues of humans and over-expressed in the uterus, lung, ovary, breast, and colon [100]. Although KSP is expressed in post-mitotic nerve cells in rats, it was not detected in human nerve cells. Thus, KSP has emerged as an attractive target for new cancer therapies that could avoid the neuropathic side effects caused by taxanes and vinca alkaloids. In addition, KSP inhibitors have demonstrated activity against taxane-resistant tumour cell lines, further supporting their potential value in treating refractory human cancers [88]. Agents with the ability to inhibit KSP can arrest cells undergoing mitotic process only and these agents are expected to be able to distinguish between proliferating and non-proliferating cells. Hence, these inhibitors will not contain severe side effects related to the ones of the antimitotic agents. Efforts have been made in developing agents that are able to inhibit KSP in previous years after monastrol, the first inhibitor of KSP that uses monopolar spindles to arrest mitosis [102].

Many KSP inhibitors have progressed into clinical trials and many others are in preclinical studies. In search of novel KSP inhibitors, ligand-based design strategies (pharmacophore-model and 3D QSAR) and structure-based (docking) or integrated approaches (Interaction based-pharmacophore models) were reported in the literature [103]. The protein data bank (PDB) has the deposit of about 45 X-ray solved crystal structures for the ligand-bound kinesin-like proteins. Among them, recently reported eight PDB structures; 4BXN, 3L9H, 4A5Y, 3CJO, 2Q2Y, 2Q2Z, 2FKY, and 2FL2 carrying different inhibitors bound to the active-site of KSP. The KSP structure is made up of 1057 residues and is separated into three spheres (**Fig. 11**). A short 20-residue-long stretch precedes the motor domain, which ranges from residue Val21 (β1 sheet) to the RAK motif in the α6 helix. The motor domain hydrolyses ATP for energy production and for proteins transport across the fibres of the MT [84]. A short linker (Asn358-Pro363) integrates the motor to the stalk region (Glu364-Val523, Cys684-Lys716, and Gln782-Arg826). The KSP tail domain (residues Tyr829-Leu1057) has a potential site for p34 phosphorylation (Thr927 in human). For dimerization or oligomerization, stalk and tail regions are necessary [104].

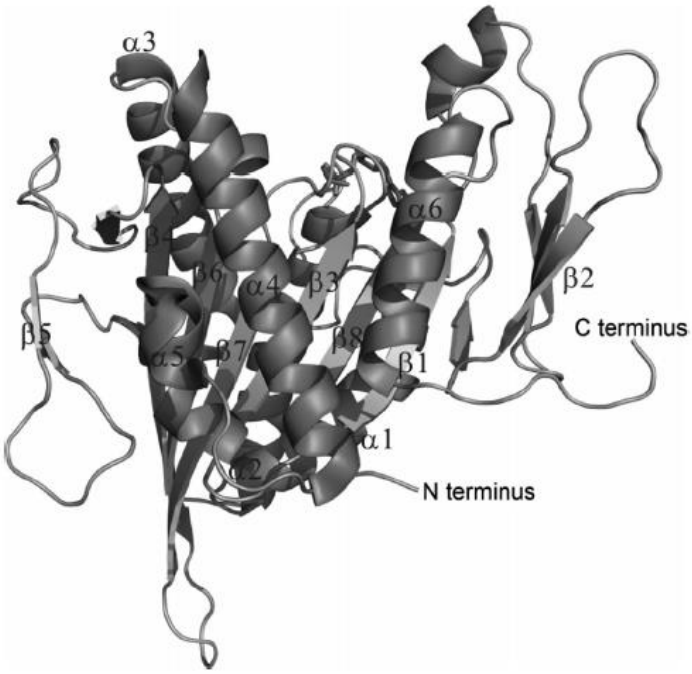

Figure 11: KSP structure solved through X-ray crystallography [104].

In 2007, Liu *et al.*, developed a quantitative three-dimensional pharmacophore model with a correlation coefficient of 0.965 based on 25 inhibitors of KSP [105]. They reported the best hypothesis (Hypo1) bearing four chemical characteristics (one hydrogen-bond acceptor, one hydrogen-bond donor, one aromatic ring and one hydrophobic) which were computed via HypoGen module implemented in Catalyst software package. In the same year, Jiang *et al.*, reported docking (structure-based) studies of 15 KSP inhibitors and proposed the significance of 'minor pocket' at the binding-site other than the existence of 'main pocket'. As per their study, a linear correlation was observed between pIC_{50} values of the compounds and lowest binding free energies computed from the docking simulation which described the role of 'minor binding pocket' in cumulative binding affinity (**Figs. 12, 13**).

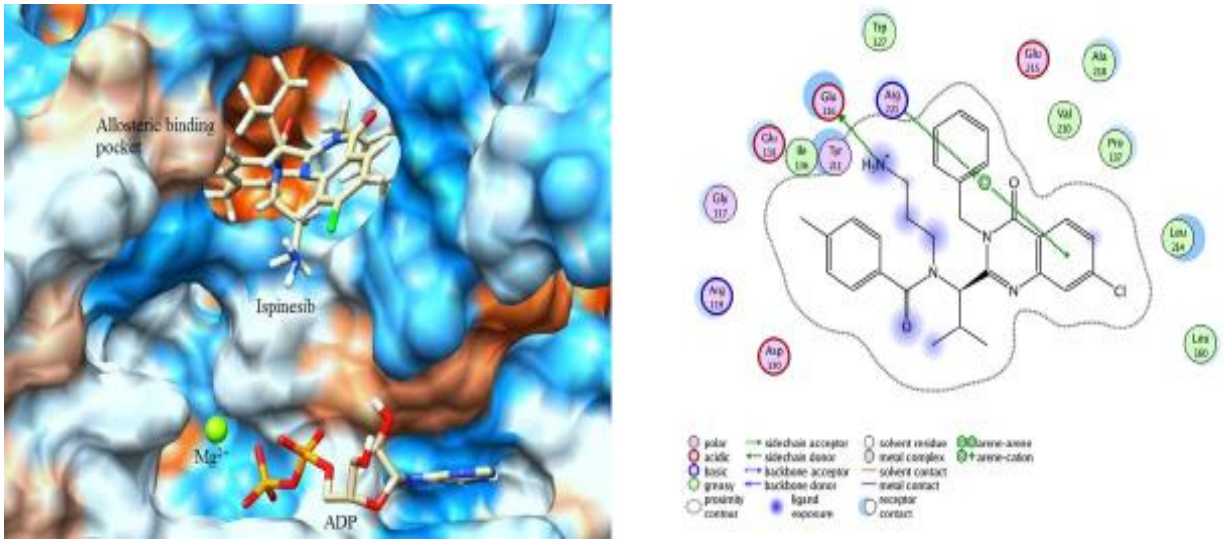

Figure 12: Binding mode of Ispinesib in KSP structure showing allosteric binding [106].

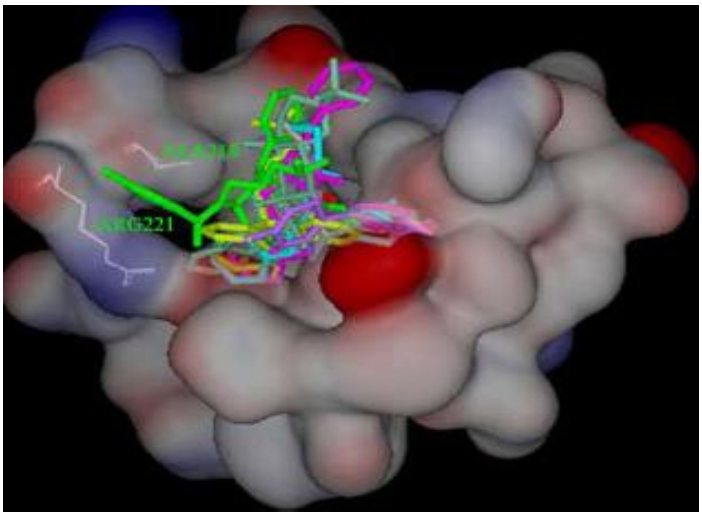

Figure 13: Binding mode of KSP inhibitors at minor binding pocket mainly surrounded by Ala218 and Arg221 [105].

Recently, Nagarajan *et al.*, reported the combined ligand- and structure-based approaches to identify novel KSP inhibitors. In their study, they developed seven interaction-based pharmacophore (IBPs) models using six crystal structures of KSP bound with diversified ligands followed by validation of 16 structures. The developed models were applied to filter the ChemDiv database (0.7 million) with the hits being passed to an *in silico* docking protocol. The IBP-based hits were subjected to docking (GOLD and GLIDE) subsequently compounds sorted based on the Gold fitness or Glide score [100]. Authors

extended the research approach from computational work to biological screening including inhibition of tumour cell proliferation, basal KSP ATPase activity and phenotypic analysis of selected inhibitors. By these integrative approaches, authors identified and developed small molecules as novel KSP inhibitors (**Fig. 14**).

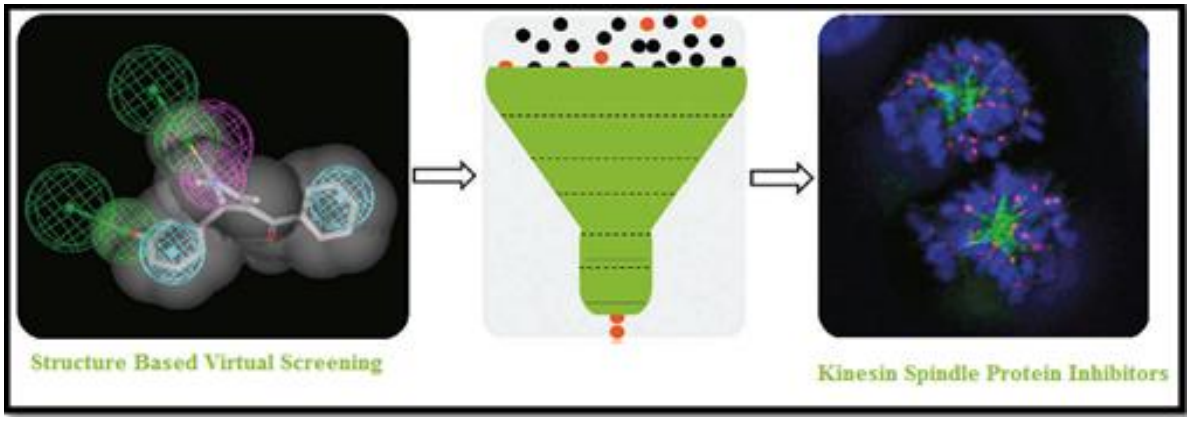

Figure 14: Interaction-based pharmacophore and docking in the identification of novel KSP inhibitors [107].

Carbajales *et al.*, analysed KSP allosteric binding-site, including 24 crystal structures of KSP-allosteric inhibitor and developed planar heterocycle structure based on X-ray crystal structure of the protein (PDB ID: 2GM1). This structure-guided design was followed by multicomponent reaction and functional characterization in enzymatic, cell assays resulted in the detection of novel inhibitors of KSP having anti-proliferative activity [99]. Recently (2015), Yokoyama *et al*. reported for the first time the X-ray crystal structure and biochemical studies on the KSP motor domain in complex with a new type of allosteric inhibitor (PVZB1194). This biphenyl-type inhibitor was proposed to bind with the α4/α6 allosteric pockets 15 Å from the pocket that binds ATP, which varies from traditional allosteric inhibitors which bind to the allosteric L5/ α2/ α3 pocket (**Fig. 15**) [68].

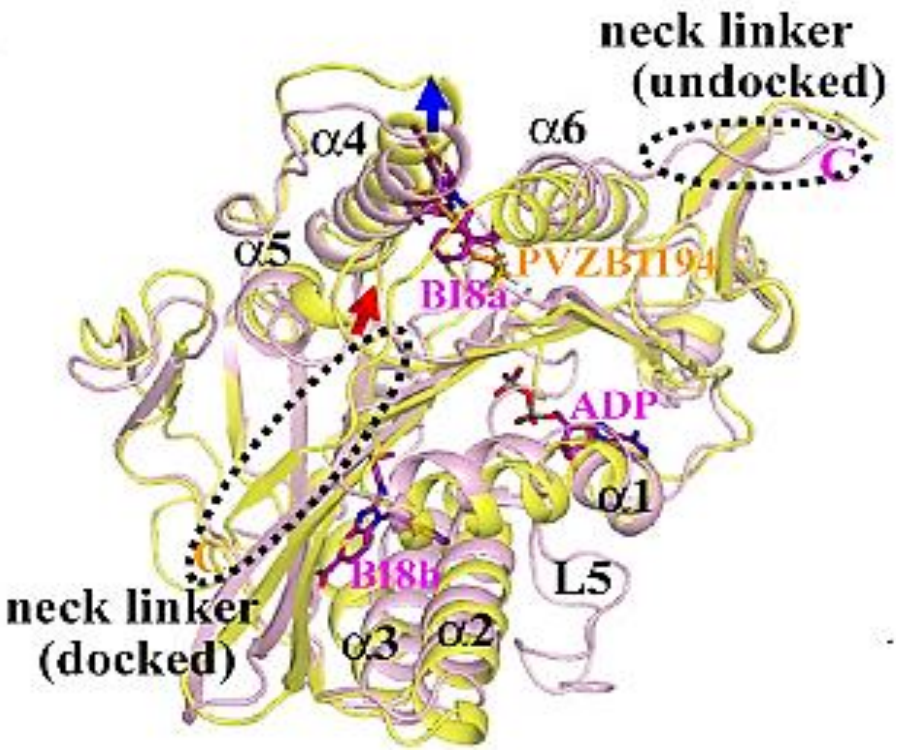

Figure 15: The structure of the KSP-ADP-BI8 complex (pink) was superimposed onto that of the KSP-PVZB1194 complex (yellow). PVZB1194 are shown as orange sticks, and two BI8 (BI8a and BI8b) and ADP are shown as purple sticks. A blue arrow indicates Glu304 Cα displacement from KSP-ADP-BI8 to KSP-PVZB1194. A red arrow indicates Leu324 Cα displacement from KSP-ADP-BI8 to KSP-PVZB1194. Dotted ellipses show neck-linker regions [102].

However, thiazole-containing inhibitors are also reported to compete with ATP but not with MTs, while biaryl compounds antagonize ATP interactions. The major common adverse effect associated with KSP ATPase inhibitors is neutropenia. While, ispinesib resistance was observed in some clinical trials [102]. Preclinical studies indicated that ispinesib is predicted to be a substrate for drug resistance. Mutation in the binding pocket is another origin of drug resistance. An alteration of the L5 pocket of KSP could offset the action of ATP non-competitive inhibitors binding to it. It may probably due to multidrug resistance that is the major barrier for many anticancer drugs. Development of ATP competitive KSP inhibitors binding to ATP binding-site (**Fig. 16**) can overcome mutation-mediated resistance of allosteric inhibitors [108].

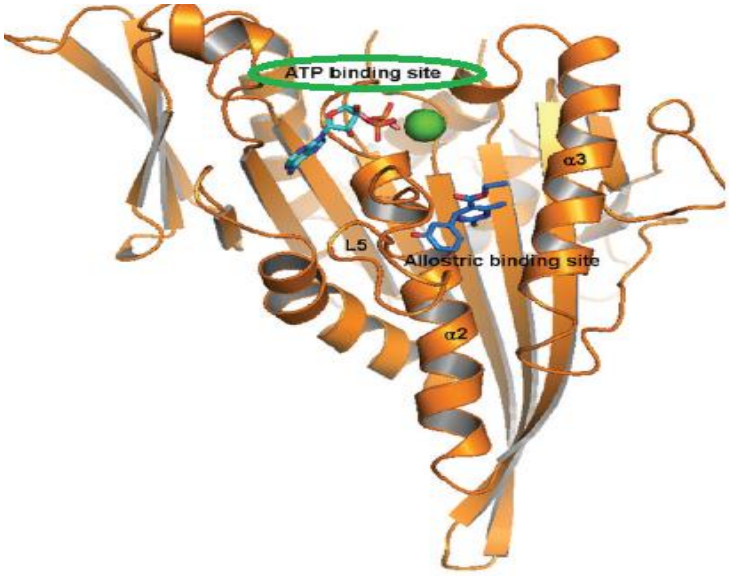

Figure 16: ATP binding-site highlighted in KSP-(*S*)-monastrol complex [105].

Based on these literature reports, it was motivated to take up the proposed investigation involving the development of small organic molecules as KSP inhibitors [109].

2.5.7. KSP inhibitors under clinical evaluations

Ispinesib, a quinazoline-based agent is the most studied KSP inhibitor. (**Table 3**) [54]. Ispinesib was evaluated against different types of solid tumours in combination with other therapeutic agents [110]. Combinations of ispinesib with conventional carboplatin as well as docetaxel have been tried, but, there were no observable synergic effects. Ispinesib has been found to moderately inhibit the cytochrome P_{450} (CYP) metabolic enzyme CYP3A4, which would contraindicate combination with numerous existing drugs [111]. Many KSP inhibitors have progressed into clinical trials and many others are in various stages of preclinical studies. Recently, KSP inhibitors of wide structural diversity have appeared in literature including six-membered heterocycle scaffolds [dihydro-pyrimidine derivative (Monastrol), quinazolinone derivatives (Ispinesib and CK-0106023), flavones, isoflavones, quinazolin-thione derivative (dimethylenastron), isoquinolines, and benzimidazoles], five-membered heterocycles (dihydropyrazoles, dihydropyrroles, thiophenes, dihydrothiadiazoles, thiazoles, and fused pyrroles), biaryl compounds (GSK-1 and GSK-2), natural products (adociasulfate-2), and second-generation KSP inhibitors benzopyranone derivative (SB-743921) [112]. The mechanism of actions of most of the KSP inhibitors include binding to KSP as well as inducing conformational changes that are both local and distal allowing ATP to bind while preventing the release of adenosine diphosphate (ADP). Some of the potent molecules acting

as KSP inhibitors under clinical and preclinical development are presented in **Table 3** and the structures of active compounds are illustrated in (**Fig. 17**) [104].

Table 3: KSP inhibitors under clinical development [104].

S. No.	Compounds	IC_{50} (nM)	Clinical Trial Stage	Type of Cancer	Side effect	Industry
1	Ispinesib	1.7	II	Advanced or metastatic breast cancer, Advanced solid tumours	Neutropenia	Cytokinetics
2	SB743921	0.1	II	Advanced solid tumours or replased/refractory lymphoma	Dose-dependent Neutropenia	Cytokinetics
3	MK-0731	2.2	I	Advanced solid tumours, Taxane-refractory cancer	Myelosuppression	Merck & Co
4	AZD4877	5.0	II	Recurrent or refractory acute myeloid leukemia, Relapsed solid tumours	Dose-dependent Neutropenia	AstraZeneca
5	ARRY-520	6.0	II	Advanced myeloid leukemia	Myelosuppression Neutropenia	Array Bio-Pharma

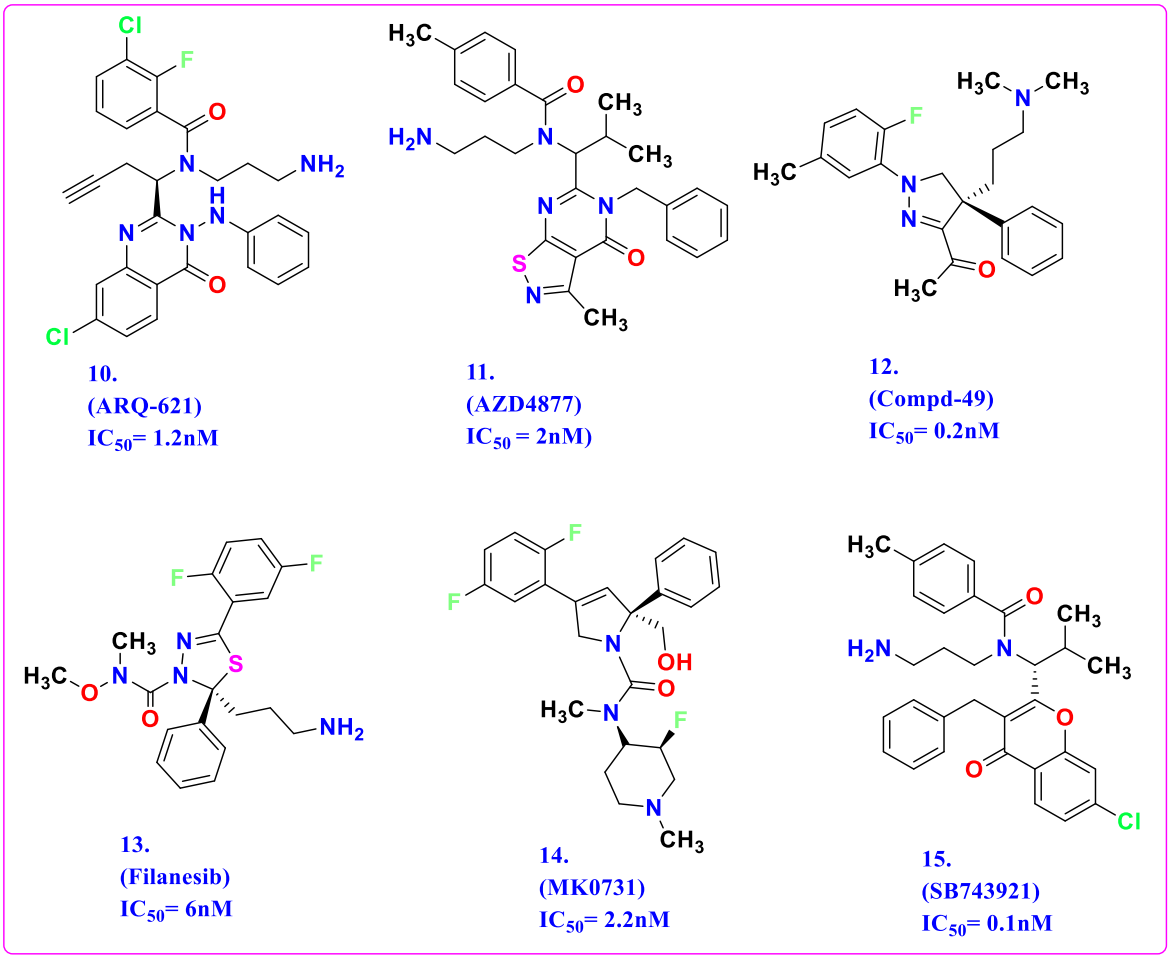

Figure 17: Known potent KSP inhibitors under clinical or preclinical trials [104].

2.6. Chemistry and pharmacological properties of 1,3,4-thiadiazoles

Thiadiazoles are dominant and significant heterocyclic structures that are five-membered ring with sulphur (S) and two nitrogen (N) atoms [113]. Moreover, thiadiazoles are comprised of numerous isomers such as, 1,3,4-thiadiazole, 1,2,5-thiadiazole, 1,2,4-thiadiazole, and 1,2,3-thiadiazole. Amongst the above mentioned thiadiazoles, the 1,3,4-thiadiazole (**Fig. 18**) was extensively studied and well reported in the literature [114].

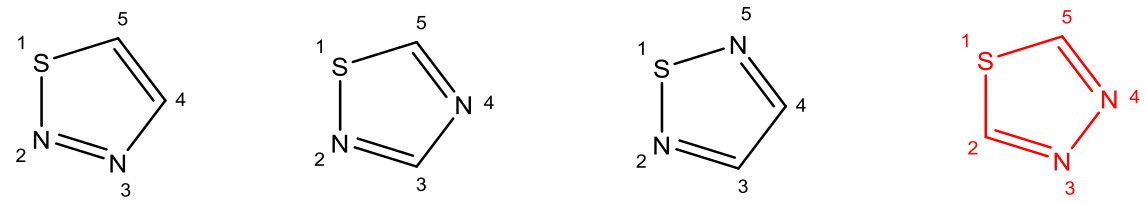

Figure 18: The different isomers of thiadiazoles [115].

Due to the inductive effect of elemental sulphur, 1,3,4-thiadiazole is regarded as a base that is very weak and it displays great aromaticity. The 1,3,4-thiadiazole ring cleaves in the aqueous base but becomes stable in an aqueous acid [116]. The 1,3,4-thiadiazole is comparatively inactive towards electrophilic attack, and seems to be sensitive to the nucleophilic attack. Introduction of substituents at position C2 or C5 makes the ring highly active and to yield compound libraries. Therefore, the above-mentioned properties make the 1,3,4-thiadiazole derivatives ideal candidates for applications in different fields. The 1,3,4-thiadiazole analogues are reported to exhibit versatile applications in the fields of pharmacy, medicinal chemistry, agriculture, and materials chemistry [117]. They have shown potent anticancer [118], antiviral [119], antifungal [120], analgesic [121], anti-inflammatory [122], antiparasitic [123], antitubercular [124], and antioxidant [125] activities. Furthermore, 1,3,4-thiadiazoles are reported to have a role in the management of central nervous system disorders, such as convulsions and mental depression. In addition, they can inhibit mitotic enzymes such as KSP and other kinases. Similarly, these thiadiazoles have shown efficacy against various cancer cell lines such as human hepatocellular carcinoma cell line (HepG2), human breast cancer cells MCF-7 and human lung cancer cells A549 [126].

1,3,4-Thiadiazoles such as methazolamide (MZA), benzolamide (BZA) as well as acetazolamide (AZA) (**Fig. 19**) are well known for their carbonic anhydrase (CA) inhibition devoid of high CA II to CA IX selectivity during cancer therapy [110]. The thiadiazole ring is different when compared to that of the thiadiazoline as well as thiophene in that it partakes in the interaction of H-bonds via the CA active site. 1,3,4-Thiadiazoles hybridized with 1,4-benzodioxan were exhibited good inhibition than the reference drug staurosporine, while few other derivatives showed competitive anticancer potential towards the SW1116, HELA, BGC823 as well as HepG2 cell lines [127]. The molecular docking results showed that the N- of thiadiazole ring formed the H-bond with the Gly505 -NH, this might have contributed to the anticancer capacity of this scaffold [128].

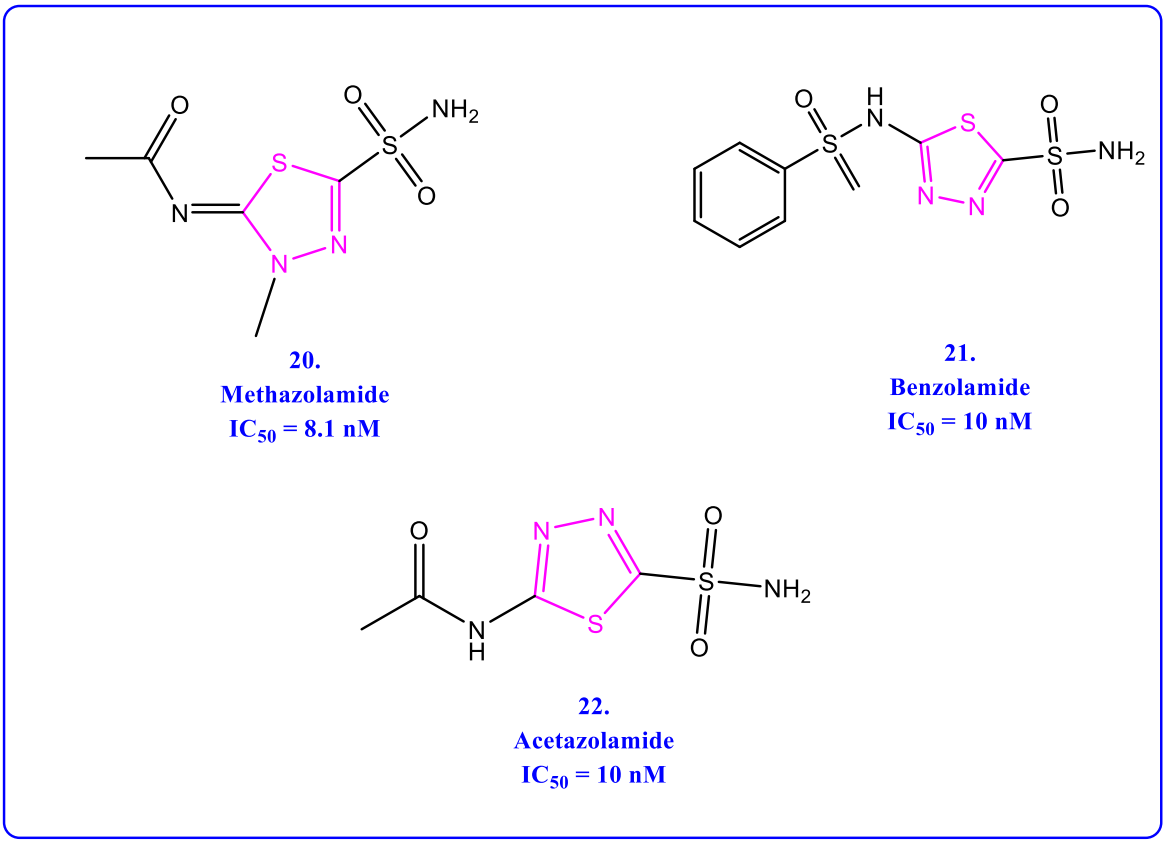

Figure 19: Sulphonamide-1,3,4-thiadiazole hybrids as CA inhibitors [110].

The 1,3,4-thiadiazoles exhibited a wide range of anticancer activities towards human cancer cells in addition to targeted molecular processes involved in proliferation, survival, and metastasis together with the CA, matrix metalloproteinases (MMPs), histone deacetylase (HDACi), Bcl-2, Bcl- XL, Bcl-2-associated X protein, Akt/PKB, tubulin, focal adhesion kinase (FAK) and protein tyrosine kinases [106, 110, 129]. The ring of 1,3,4-thiadiazole is effective against cancer cells because of the two nitrogen atoms having a great electron-donating capacity to chelate with some metal ions or co-enzymes. Moreover, the introduction of different atoms/groups, for example, chloride (Cl) via substitution to the carbon (C) number 2 and 5 in the 1,3,4-thiadiazole increases the anticancer activity of this scaffold. Rizzo *et al.*, computed the binding affinities (MM-GBSA and MM-PBSA) as well as the selectivity of 5-substituted-1,3,4-thiadiazole-2-thiones against two particular MMPs (gelatinase-A and stromelysin-1). It was shown that thiadiazoles selectively inhibit stromelysin-1 more than gelatinase-A [110].

The 2-(4-fluorophenyloamino)-5-(2,4-dihydroxyphenyl)-1,3,4-thiadiazole (FABT) reduced the cell proliferation of the major cell lung cancer A549, this might be because of the inhibition of ERK1/2 kinase pathway. This showed that FABT inhibits the phosphorylation

of the protein without affecting the gene expression. Furthermore, 2-(4- chlorophenylamino)-5-(2,4-dihydroxyphenyl)-1,3,4-thiadiazole (4ClABT) reduced synthesis of DNA, prominent variations in the morphology of a tumour and the decreased motility of cells. The 1,3,4-thiadiazole hybrids containing methoxyphenyl or *p*-hydroxyphenyl have high activity in HDAC inhibition as well as anti-proliferation against carcinoma cells of *Ehrlich ascites* [111].

2.7. Chemistry and pharmacological properties of thiazolones

Thiazolone (**Fig. 20**) has been shown to be another pharmaceutically important scaffold. Thiazolones are well known for their diverse medicinal properties, for example, libraries of 4-Thiazolidinone have continually attracted the interest researchers for years due to their diverse biological activities similar to that of thiadiazoles [130].

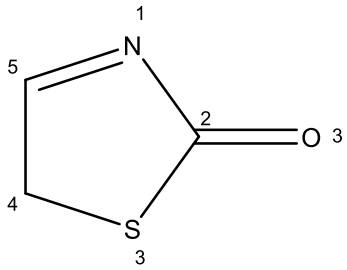

23.
Thiazol-2(5*H*)-one

Figure 20: Structure of a simple thiazolone [130].

Some of the clinically used drugs such as thiazolidomycin, etozoline, ralitoline and pioglitazone (**Fig. 21)** bearing thiazolone pharmacophore in their chemical structures support the versatile applications of thiazolone moiety in therapy [131]. It is possible that the anticancer activity of 4-thiazolidinones correlates with their affinity to antitumor bio-targets, for example, antiapoptotic biocomplex Bcl-XL-BH3, JNK stimulating phosphatase-1 (JSP-1), integrin αvβ3 receptor and tumour necrosis factor (TNFa). For example, 5-arylidene-4-thiazolidinone/ thiazolone is one of the pharmacophores present in many of the reported anticancer compounds, displaying activities against human breast cancer cell line MDA-MB-231, paclitaxel-resistant H460taxR, non-small cell lung cancer cell line H460 and human colon cancer cell line HT29 [131]. These scaffolds have also proven to be potent CDK particularly CDK1 inhibitors. The antagonists of integrin αvβ3 showed to be ideal novel

antitumor drugs amongst three of the substituted 2-arylimino-4-thiazolidinones. The 2-phenylimino-3-alkyl-4-thiazolidinone hybrids inhibited the HT29 cell line, shown by over-expression of cyclooxygenase-2 (COX-2), and inhibited CDK1/cyclin B. These activities were established by blocking G2-to-M progression in the cell cycle and by inducing apoptotic cell death [130, 131]. Derivatives of 5-benzylidene-4-thiazolidinone have antitumor activities containing diverse biotargets such as the non-membrane protein tyrosine phosphatase (SHP-2), JSP-1, sphingosine kinase (SK), and phosphatase of a regenerating liver (PRL-3). Furthermore, these hybrids possess potent anticancer properties against the paclitaxel-resistant H460taxR [132].

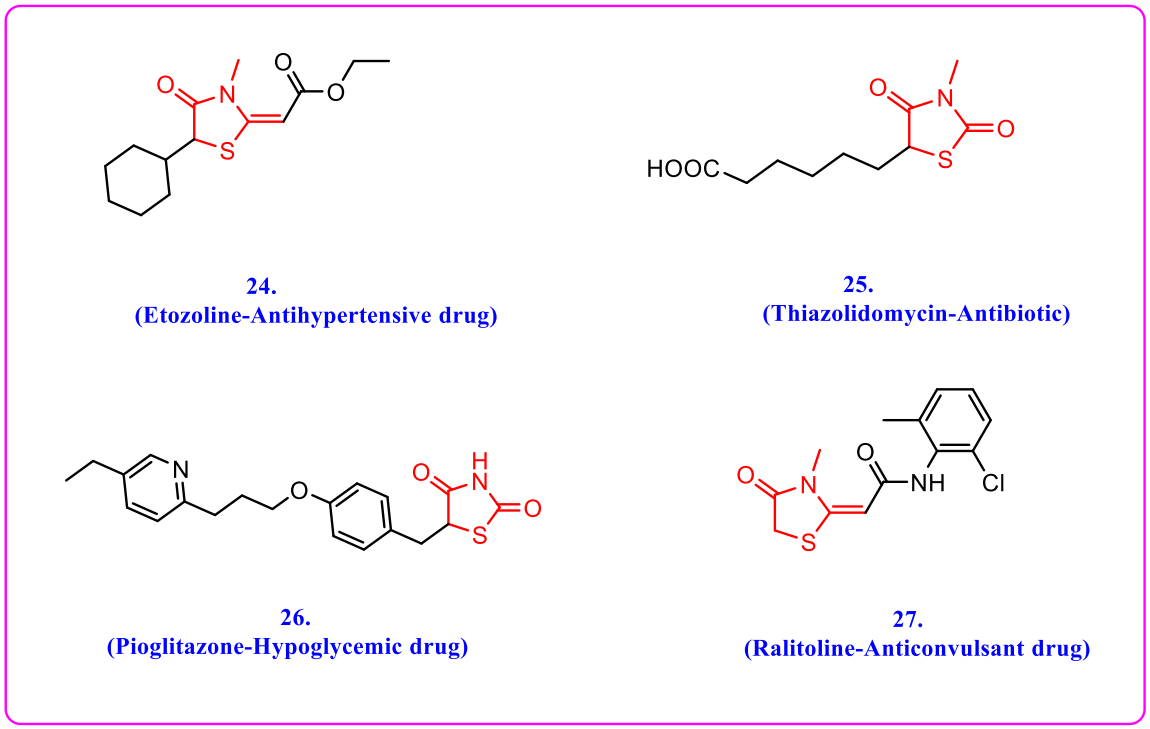

Figure 21: Drugs bearing thiazolone moiety [131].

2.8. Design of the novel anticancer compounds by molecular hybridization

Although there have been considerable developments in preventing and treating cancer by a number of approaches, the successful chemotherapy for many types of cancer remains a greater challenge till date. Therefore, it is very imperative to establish some novel, safe, and efficacious chemotherapeutic agents exhibiting the broad spectrum of anticancer properties to different cancerous tissues with devoid of host cell toxicity. Development of drug-resistance via mutations in amino acid sequence is the major issue commonly observed with the available chemotherapeutic agents during the therapy of cancer.

Rational drug design via molecular hybridization is still a useful and promising approach in synthesis and development of novel pharmaceutically active heterocyclic compounds. The recent continuous emergence of literature reports and patents in the field of pharmaceutical and medicinal chemistry evidenced that this strategy is successfully being adopted.

The thiazolone moiety was proven to be one of the active pharmacophores present in the CDK inhibitors (**Fig. 22**). Similarly, thiadiazole-based compounds are potent inhibitors of KSP (**Fig. 22**). Interestingly, many of the available KSP inhibitors are not ATP-competitive inhibitors, rather allosteric inhibitors. Thus, newer and more selective kinase inhibitors can provide safe and effective treatment for various types of cancer [133]. Hence, we envisaged hybridizing the CDK inhibition moiety (thiazole) with KSP inhibition core (thiadiazole) to obtain a novel library of compounds exhibiting synergistic anticancer activities with dual mode of action. Such analyses may not only reveal the potency but also confirm the pathological events associated with the cancer progression and its control. We herein, report the synthesis and anticancer evaluations of twenty-two novel hybrid molecules bearing 1,3,4-thiadiazole-thiazolone (TDT) (**Fig. 22**).

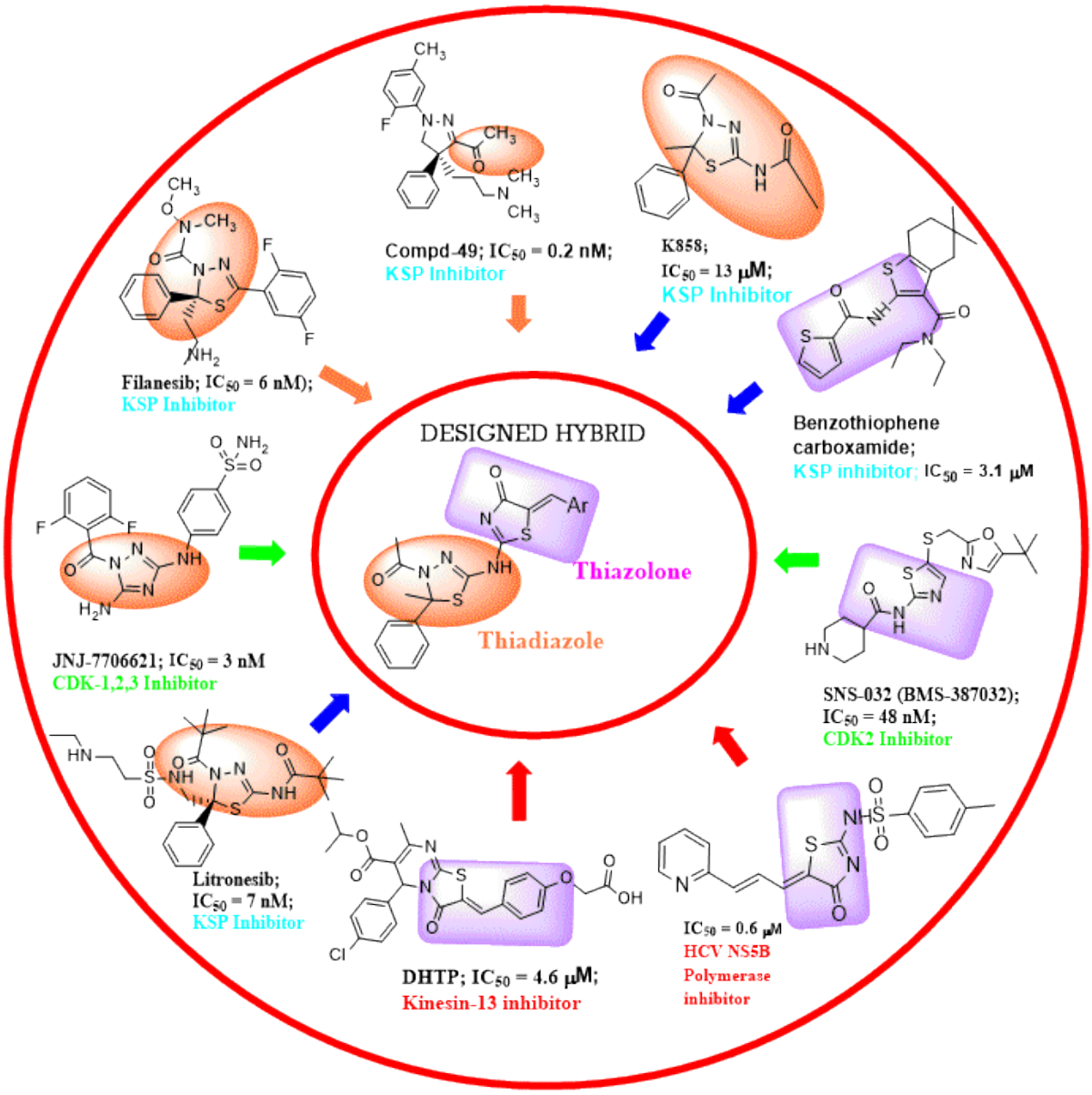

Figure 22: Thiadiazole and thiazolone scaffolds reported as KSP and CDK inhibitors.

2.9. References

[1] S.R. Singer, A.G. Creanga, Diagnostic imaging of malignant tumors in the orofacial region, Dental clinics, 60 (2016) 143.

[2] A. Richards, S. Edwars, Cellular proliferation and cancer, essential pathophysiology for Nursing and healthcare students, McGraw-Hill Education (UK), (2014) 132.

[3] A.G. Clark, D.M. Vignjevic, Modes of cancer cell invasion and the role of the microenvironment, Current opinion in cell biology, 36 (2015) 13.

[4] P. Sharma, J.P. Allison, Immune checkpoint targeting in cancer therapy: toward combination strategies with curative potential, Cell, 161 (2015) 205.

[5] L.A. Torre, F. Bray, R.L. Siegel, J. Ferlay, J. Lortet-Tieulent, A. Jemal, Global cancer statistics, 2012, CA: a cancer journal for clinicians, 65 (2015) 87.

[6] J. Ferlay, I. Soerjomataram, R. Dikshit, S. Eser, C. Mathers, M. Rebelo, D.M. Parkin, D. Forman, F. Bray, Cancer incidence and mortality worldwide: sources, methods and major patterns in GLOBOCAN 2012, International journal of cancer, 136 (2015).

[7] T. Singh, V. Kaur, M. Kumar, P. Kaur, R. Murthy, R.K. Rawal, The critical role of bisphosphonates to target bone cancer metastasis: an overview, Journal of drug targeting, 23 (2015) 1.

[8] A. Linkeviciute, G. Boniolo, L. Chiavari, F.A. Peccatori, Fertility preservation in cancer patients: the global framework, Cancer treatment reviews, 40 (2014) 1019.

[9] D. Hanahan, R.A. Weinberg, Hallmarks of cancer: the next generation, Cell, 144 (2011) 646.

[10] H. Niknejad, M. Khayat-Khoei, H. Peirovi, H. Abolghasemi, Human amniotic epithelial cells induce apoptosis of cancer cells: a new anti-tumor therapeutic strategy, Cytotherapy, 16 (2014) 33.

[11] O. Ammerpohl, K. Hattermann, J. Held-Feindt, Dormancy: an evolutionary key phenomenon in cancer development, Ecology and evolution of cancer, (2017) 235.

[12] L. Viger, F. Denis, M. Rosalie, C. Letellier, A cancer model for the angiogenic switch, Journal of theoretical biology, 360 (2014) 21.

[13] Y. Hu, X. Yu, G. Xu, S. Liu, Metastasis: an early event in cancer progression, Journal of cancer research and clinical oncology, 143 (2017) 745.

[14] B. Vogelstein, N. Papadopoulos, V.E. Velculescu, S. Zhou, L.A. Diaz, K.W. Kinzler, Cancer genome landscapes, Science, 339 (2013) 1546.

[15] Y. Hu, C.Y. Yu, J.L. Wang, J. Guan, H.Y. Chen, J.Y. Fang, MicroRNA sequence polymorphisms and the risk of different types of cancer, Scientific reports, 4 (2014) 3648.

[16] O.I. Aruoma, T. Bahorun, A.K. Agnihotri, Cancer risks and perspectives: molecular mechanisms, Mutation research/fundamental and molecular mechanisms of mutagenesis, 768 (2014) 1.

[17] S.A. Stacker, S.P. Williams, T. Karnezis, R. Shayan, S.B. Fox, M.G. Achen, Lymphangiogenesis and lymphatic vessel remodelling in cancer, Nature reviews cancer, 14 (2014) 159.

[18] D. Schadendorf, D.E. Fisher, C. Garbe, J.E. Gershenwald, J.J. Grob, A. Halpern, M. Herlyn, M.A. Marchetti, G. McArthur, A. Ribas, Melanoma, Nature reviews disease

primers, 1 (2015) 15003.

[19] P. Vader, X.O. Breakefield, M.J. Wood, Extracellular vesicles: emerging targets for cancer therapy, Trends in molecular medicine, 20 (2014) 385.

[20] L. Brannon-Peppas, J.O. Blanchette, Nanoparticle and targeted systems for cancer therapy, Advanced drug delivery reviews, 64 (2012) 206.

[21] X. Zheng, M. Schipper, K. Kidwell, J. Lin, R. Reddy, Y. Ren, A. Chang, F. Lv, M. Orringer, F.M.S. Kong, Survival outcome after stereotactic body radiation therapy and surgery for stage I non-small cell lung cancer: a meta-analysis, International journal of radiation oncology biology physics, 90 (2014) 603.

[22] C.P. Halsted, J.R. Benson, I. Jatoi, A historical account of breast cancer surgery: beware of local recurrence but be not radical, Future oncology, 10 (2014) 1649.

[23] L. Wyld, R.A. Audisio, G.J. Poston, The evolution of cancer surgery and future perspectives, Nature reviews clinical oncology, 12 (2015) 115.

[24] B. Sasu, J. Chaparro-Riggers, T cell redirecting therapies for cancer treatment, Current cancer drug targets, 16 (2016) 22.

[25] A. Mathur, Principles of surgical oncology and pathology, in: Introduction to surgery for students, Springer cham, (2017) 145.

[26] C.E. DeSantis, C.C. Lin, A.B. Mariotto, R.L. Siegel, K.D. Stein, J.L. Kramer, R. Alteri, A.S. Robbins, A. Jemal, Cancer treatment and survivorship statistics, 2014, CA: a cancer journal for clinicians, 64 (2014) 252.

[27] E.A. Wellberg, L.A. Checkley, E.D. Giles, S.J. Johnson, R. Oljira, R. Wahdan-Alaswad, R.M. Foright, G. Dooley, S.M. Edgerton, S. Jindal, The androgen receptor supports tumor progression after the loss of ovarian function in a preclinical model of obesity and breast cancer, Hormones and cancer, (2017) 1.

[28] P. Bhatt, I. Vhora, S. Patil, J. Amrutiya, C. Bhattacharya, A. Misra, R. Mashru, Role of antibodies in diagnosis and treatment of ovarian cancer: Basic approach and clinical status, Journal of controlled release, 226 (2016) 148.

[29] A. El Chediak, A. Shamseddine, L. Bodgi, J.P. Obeid, F. Geara, Y.H. Zeidan, Optimizing tumor immune response through combination of radiation and immunotherapy, Medical oncology, 34 (2017) 165.

[30] L.N. Saligan, Biomarkers for cancer-related fatigue and use thereof, US Patent No. US 8597883 B2 (2013).

[31] D.S. Chen, I. Mellman, Oncology meets immunology: the cancer-immunity cycle, Immunity, 39 (2013) 1.

[32] J.M. Dąbrowski, L.G. Arnaut, Photodynamic therapy (PDT) of cancer: from local to systemic treatment, Photochemical and photobiological sciences, 14 (2015) 1765.

[33] K. Lu, C. He, W. Lin, A chlorin-based nanoscale metal–organic framework for photodynamic therapy of colon cancers, Journal of the american chemical society, 137 (2015) 7600.

[34] D.B. Graves, The emerging role of reactive oxygen and nitrogen species in redox biology and some implications for plasma applications to medicine and biology, Journal of physics D: applied physics, 45 (2012) 263001.

[35] R.G. Smith, Photonic and magnetic nano-and micro-particles for biomedical applications: detection and destruction of bacterial and cancer cells (dissertation), University of Michigan, 2013.

[36] L. Cheng, J. Liu, X. Gu, H. Gong, X. Shi, T. Liu, C. Wang, X. Wang, G. Liu, H. Xing, PEGylated WS2 nanosheets as a multifunctional theranostic agent for in vivo dual-modal CT/photoacoustic imaging guided photothermal therapy, Advanced materials, 26 (2014) 1886.

[37] H. Daraee, A. Etemadi, M. Kouhi, S. Alimirzalu, A. Akbarzadeh, Application of liposomes in medicine and drug delivery, Artificial cells, nanomedicine and biotechnology, 44 (2016) 381.

[38] J. Liang, D. Jiang, P.W. Noble, Hyaluronan as a therapeutic target in human diseases, Advanced drug delivery reviews, 97 (2016) 186.

[39] K.B. Johnsen, J.M. Gudbergsson, M.N. Skov, L. Pilgaard, T. Moos, M. Duroux, A comprehensive overview of exosomes as drug delivery vehicles—endogenous nanocarriers for targeted cancer therapy, Biochimica et biophysica acta (BBA)-reviews on cancer, 1846 (2014) 75.

[40] R. Mazzanti, U. Arena, R. Tassi, Hepatocellular carcinoma: where are we?, World journal of experimental medicine, 6 (2016) 21.

[41] J.F. Chen, H.K. Eltzschig, B.B. Fredholm, Adenosine receptors as drug targets—what are the challenges?, Nature reviews drug discovery, 12 (2013) 265.

[42] V.P. Torchilin, Multifunctional, stimuli-sensitive nanoparticulate systems for drug delivery, Nature reviews drug discovery, 13 (2014) 813.

[43] C.M. Weyand, J.J. Goronzy, L. Shao, Method for improving immune system function by administering agents that inhibit DNA-dependent protein kinase-directed apoptosis, US Patent No. US 9511086 B2 (2016).

[44] G. Yang, J. Wang, Y. Wang, L. Li, X. Guo, S. Zhou, An implantable active-targeting

micelle-in-nanofiber device for efficient and safe cancer therapy, ACS nano, 9 (2015) 1161.

[45] A.C. Wilson, The DNA of cancer centers: an introduction to planning and design, The journal of ambulatory care management, 37 (2014) 51.

[46] T.K.T. Dinh, Circulating micro-RNAs as biomarkers for thoracic radiation therapy in lung cancer (thesis), Harvard medical school, (2016).

[47] J.S. Tobias, D. Hochhauser, J. Tobias, Cancer and its management, John Wiley and sons, 2 (2014).

[48] M.J. Davies, Systemic therapy for non-small cell lung cancer chemotherapy, targeted therapy and immunotherapy, Annals of surgical oncology, 4 (2016) 1008.

[49] G. Housman, S. Byler, S. Heerboth, K. Lapinska, M. Longacre, N. Snyder, S. Sarkar, Drug resistance in cancer: an overview, Cancers, 6 (2014) 1769.

[50] S. Sattar, S.M. Alibhai, M. Fitch, M. Krzyzanowska, N. Leighl, M.T. Puts, Chemotherapy and radiation treatment decision-making experiences of older adults with cancer: a qualitative study, Journal of geriatric oncology, 25 (2017) 879.

[51] R.J. Klement, C.E. Champ, Calories, carbohydrates, and cancer therapy with radiation: exploiting the five R's through dietary manipulation, Cancer and metastasis reviews, 33 (2014) 217.

[52] D. Bates, A. Eastman, Microtubule destabilising agents: far more than just antimitotic anticancer drugs, British journal of clinical pharmacology, 83 (2016) 255.

[53] T. Kuriyama, T. Karasawa, D.W. Williams, Antimicrobial chemotherapy, biofilms in infection prevention and control: a healthcare handbook, Academic press (2014) 209.

[54] N. Vindya, N. Sharma, M. Yadav, K. Ethiraj, Tubulins-the target for anticancer therapy, Current topics in medicinal chemistry, 15 (2015) 73.

[55] E. Di Cesare, A. Verrico, A. Miele, M. Giubettini, P. Rovella, A. Coluccia, V. Famiglini, G. La Regina, E. Cundari, R. Silvestri, Mitotic cell death induction by targeting the mitotic spindle with tubulin-inhibitory indole derivative molecules, Oncotarget, 8 (2017) 19738.

[56] P.R. Coleman, The identification of the novel gene SENEX and its role in endothelial cell senescence and survival (thesis), University of Sidney (2013).

[57] J. Pampalona, E. Roscioli, W.T. Silkworth, B. Bowden, A. Genescà, L. Tusell, D. Cimini, Chromosome bridges maintain kinetochore-microtubule attachment throughout mitosis and rarely break during anaphase, PloS one, 11 (2016) e0147420.

[58] J.J. Field, A. Kanakkanthara, J.H. Miller, Microtubule-targeting agents are clinically

successful due to both mitotic and interphase impairment of microtubule function, Bioorganic and medicinal chemistry, 22 (2014) 5050.

[59] S. Dall'Acqua, Natural products as antimitotic agents, Current topics in medicinal chemistry, 14 (2014) 2272.

[60] E. Mukhtar, V.M. Adhami, H. Mukhtar, Targeting microtubules by natural agents for cancer therapy, Molecular cancer therapeutics, 13 (2014) 275.

[61] I. Shoukat, Elucidating the functions and impact of inhibition of mitotic kinesins in *Candida albicans* (dissertation), Queen's University, (2017).

[62] N. Gupta, H. Hatoum, G.K. Dy, First line treatment of advanced non-small-cell lung cancer–specific focus on albumin bound paclitaxel, International journal of nanomedicine, 9 (2014) 209.

[63] S. Jiang, A.W. Pan, T.Y. Lin, H. Zhang, M. Malfatti, K. Turteltaub, P.T. Henderson, C.X. Pan, Paclitaxel enhances carboplatin-DNA adduct formation and cytotoxicity, Chemical research in toxicology, 28 (2015) 2250.

[64] J. Brett, D. Fenlon, M. Boulton, N.J. Hulbert-Williams, F. Walter, P. Donnelly, B. Lavery, A. Morgan, C. Morris, E. Watson, Factors associated with intentional and unintentional non-adherence to adjuvant endocrine therapy following breast cancer, European journal of cancer care, (2016) 1.

[65] C. Holohan, S. Van Schaeybroeck, D.B. Longley, P.G. Johnston, Cancer drug resistance: an evolving paradigm, Nature reviews cancer, 13 (2013) 714.

[66] Y. Zhao, E.B. Butler, M. Tan, Targeting cellular metabolism to improve cancer therapeutics, Cell death and disease, 4 (2013) e532.

[67] S.C. Tang, A. Kort, K.L. Cheung, H. Rosing, T. Fukami, S. Durmus, E. Wagenaar, J.J. Hendrikx, M. Nakajima, B.J. van Vlijmen, P-glycoprotein, CYP3A, and plasma carboxylesterase determine brain disposition and oral availability of the novel taxane cabazitaxel (Jevtana) in mice, Molecular pharmaceutics, 12 (2015) 3714.

[68] R.J. van Vuuren, M.H. Visagie, A.E. Theron, A.M. Joubert, Antimitotic drugs in the treatment of cancer, Cancer chemotherapy and pharmacology, 76 (2015) 1101.

[69] S. Forli, Epothilones: from discovery to clinical trials, Current topics in medicinal chemistry, 14 (2014) 2312.

[70] C. Marchetti, I. Piacenti, L. Imperiale, F. De Felice, S. Boccia, V. Di Donato, G. Perniola, M. Monti, I. Palaia, L. Muzii, Ixabepilone for the treatment of endometrial cancer, Expert opinion on investigational drugs, 25 (2016) 613.

[71] S. Kaiser, J. John Muller, P. Eduardo Froehlich, S. Cristina Baggio Gnoatto, A. Maria

Bergold, From bacteria to antineoplastic: epothilones a successful history, Formerly current medicinal chemistry-anti-cancer agents, 13 (2013) 1057.

[72] W. Szaflarski, M.M. Fay, N. Kedersha, M. Zabel, P. Anderson, P. Ivanov, Vinca alkaloid drugs promote stress-induced translational repression and stress granule formation, Oncotarget, 7 (2016) 30307.

[73] M. Moudi, R. Go, C.Y.S. Yien, M. Nazre, Vinca alkaloids, International journal of preventive medicine, 4 (2013) 1231.

[74] Z. Madak-Erdogan, S.H. Kim, P. Gong, Y.C. Zhao, H. Zhang, K.L. Chambliss, K.E. Carlson, C.G. Mayne, P.W. Shaul, K.S. Korach, Design of pathway-preferential estrogens that provide beneficial metabolic and vascular effects without stimulating reproductive tissues, Science signaling, 9 (2016) ra53.

[75] A.J. Begam, S. Jubie, M. Nanjan, Estrogen receptor agonists/antagonists in breast cancer therapy: a critical review, Bioorganic chemistry, 71 (2017) 257.

[76] R. Katayama, L. Friboulet, S. Koike, E.L. Lockerman, T.M. Khan, J.F. Gainor, A.J. Iafrate, K. Takeuchi, M. Taiji, Y. Okuno, Two novel ALK mutations mediate acquired resistance to the next-generation ALK inhibitor alectinib, Clinical cancer research, 20 (2014) 5686.

[77] W. Li, H. Zhang, Y.G. Assaraf, K. Zhao, X. Xu, J. Xie, D.H. Yang, Z.S. Chen, Overcoming ABC transporter-mediated multidrug resistance: molecular mechanisms and novel therapeutic drug strategies, Drug resistance updates, 27 (2016) 14.

[78] T. Lu, Synthesis and biological evaluation of novel anti-tumour (E)-styrylsulfonyl methylpyridines (thesis), University of Nottingham, (2014).

[79] K. Hientz, A. Mohr, D. Bhakta-Guha, T. Efferth, The role of p53 in cancer drug resistance and targeted chemotherapy, Oncotarget, 8 (2017) 8921.

[80] Z. Chen, T. Shi, L. Zhang, P. Zhu, M. Deng, C. Huang, T. Hu, L. Jiang, J. Li, Mammalian drug efflux transporters of the ATP binding cassette (ABC) family in multidrug resistance: A review of the past decade, Cancer letters, 370 (2016) 153.

[81] K. Ellis, J.W. Marlin, T.A. Taylor, S. Fitting, K.F. Hauser, G. Rice, M. McRae, The effects of human immunodeficiency virus infection on the expression of the drug efflux proteins P-glycoprotein and breast cancer resistance protein in a human intestine model, Journal of pharmacy and pharmacology, 67 (2015) 178.

[82] L.H. Pearl, A.C. Schierz, S.E. Ward, B. Al-Lazikani, F.M. Pearl, Therapeutic opportunities within the DNA damage response, Nature reviews cancer, 15 (2015) 166.

[83] E.J. Wojcik, R.S. Buckley, J. Richard, L. Liu, T.M. Huckaba, S. Kim, Kinesin-5: cross-bridging mechanism to targeted clinical therapy, Gene, 531 (2013) 133.

[84] I. Marzo, J. Naval, Antimitotic drugs in cancer chemotherapy: promises and pitfalls, Biochemical pharmacology, 86 (2013) 703.

[85] H. Nakano, T. Hasegawa, H. Kojima, T. Okabe, T. Nagano, Design and synthesis of potent and selective pim kinase inhibitors by targeting unique structure of atp-binding pocket, ACS medicinal chemistry letters, 8 (2017) 504.

[86] P.E. Czabotar, G. Lessene, A. Strasser, J.M. Adams, Control of apoptosis by the BCL-2 protein family: implications for physiology and therapy, Nature reviews molecular cell biology, 15 (2014) 49.

[87] T. Sun, Y.S. Zhang, B. Pang, D.C. Hyun, M. Yang, Y. Xia, Engineered nanoparticles for drug delivery in cancer therapy, Angewandte chemie international edition, 53 (2014) 12320.

[88] H. Chen, S. Huang, X. Han, J. Zhang, C. Shan, Y.H. Tsang, H.T. Ma, R.Y.C. Poon, Salt-inducible kinase 3 is a novel mitotic regulator and a target for enhancing antimitotic therapeutic-mediated cell death, Cell death and disease, 5 (2014) e1177.

[89] J.A.D. Good, The development of S-trityl L-cysteine based inhibitors of Eg5 as anticancer chemotherapeutics (thesis), University of Glasgow, (2012).

[90] M. Yan, C. Wang, B. He, M. Yang, M. Tong, Z. Long, B. Liu, F. Peng, L. Xu, Y. Zhang, Aurora-A kinase: a potent oncogene and target for cancer therapy, Medicinal research reviews, 36 (2016) 1036.

[91] H. Hochegger, N. Hégarat, J.B. Pereira-Leal, Aurora at the pole and equator: overlapping functions of Aurora kinases in the mitotic spindle, Open biology, 3 (2013) 120185.

[92] M. Raab, A. Krämer, S. Hehlgans, M. Sanhaji, E. Kurunci-Csacsko, C. Dötsch, G. Bug, O. Ottmann, S. Becker, F. Pachl, Mitotic arrest and slippage induced by pharmacological inhibition of polo-like kinase 1, Molecular oncology, 9 (2015) 140.

[93] C.B. Baltus, R. Jorda, C. Marot, K. Berka, V. Bazgier, V. Kryštof, G. Prié, M.C. Viaud-Massuard, Synthesis, biological evaluation and molecular modeling of a novel series of 7-azaindole based tri-heterocyclic compounds as potent CDK2/Cyclin E inhibitors, European journal of medicinal chemistry, 108 (2016) 701.

[94] T.A. Chohan, H. Qian, Y. Pan, J.Z. Chen, Cyclin-dependent kinase-2 as a target for cancer therapy: progress in the development of CDK2 inhibitors as anti-cancer agents, Current medicinal chemistry, 22 (2015) 237.

[95] A.S. Bhambra, M. Edgar, M.R. Elsegood, L. Horsburgh, V. Kryštof, P.D. Lucas, M. Mojally, S.J. Teat, T.G. Warwick, G.W. Weaver, Novel fluorinated benzimidazole-based scaffolds and their anticancer activity *in vitro*, Journal of fluorine chemistry, 188 (2016) 99.

[96] C. Sánchez-Martínez, L.M. Gelbert, M.J. Lallena, A. de Dios, Cyclin dependent kinase (CDK) inhibitors as anticancer drugs, Bioorganic and medicinal chemistry letters, 25 (2015) 3420.

[97] U. Asghar, A.K. Witkiewicz, N.C. Turner, E.S. Knudsen, The history and future of targeting cyclin-dependent kinases in cancer therapy, Nature reviews drug discovery, 14 (2015) 130.

[98] G. Mariaule, P. Belmont, Cyclin-dependent kinase inhibitors as marketed anticancer drugs: where are we now? a short survey, Molecules, 19 (2014) 14366.

[99] C. Carbajales, M.Á. Prado, H. Gutiérrez-de-Terán, Á. Cores, J. Azuaje, S. Novio, M.J. Nuñez, B. Fernández-García, E. Sotelo, X. García-Mera, Structure-based design of new KSP-Eg5 inhibitors assisted by a targeted multicomponent reaction, ChemBioChem, 15 (2014) 1471.

[100] S. Nagarajan, D.A. Skoufias, F. Kozielski, A.N. Pae, Receptor–ligand interaction-based virtual screening for novel Eg5/kinesin spindle protein inhibitors, Journal of medicinal chemistry, 55 (2012) 2561.

[101] P.D. Campbell, F.L. Marlow, Temporal and tissue specific gene expression patterns of the zebrafish kinesin-1 heavy chain family, KIF5s, during development, Gene expression patterns, 13 (2013) 271.

[102] H. Yokoyama, J.I. Sawada, S. Katoh, K. Matsuno, N. Ogo, Y. Ishikawa, H. Hashimoto, S. Fujii, A. Asai, Structural basis of new allosteric inhibition in kinesin spindle protein Eg5, ACS chemical biology, 10 (2015) 1128.

[103] C. Gao, N.F. Lowndes, L.A. Eriksson, Analysis of biphenyl-type inhibitors targeting the Eg5 α4/α6 allosteric pocket, ACS omega, 2 (2017) 1836.

[104] H. Song, S. Zhou, R. Wang, S. Li, Kinesin spindle protein (KSP) inhibitors in combination with chemotherapeutic agents for cancer therapy, ChemMedChem, 8 (2013) 1736.

[105] H.B. El-Nassan, Advances in the discovery of kinesin spindle protein (Eg5) inhibitors as antitumor agents, European journal of medicinal chemistry, 62 (2013) 614.

[106] V. Ulaganathan, S.K. Talapatra, O. Rath, A. Pannifer, D.D. Hackney, F. Kozielski, Structural insights into a unique inhibitor binding pocket in kinesin spindle protein,

Journal of the american chemical society, 135 (2013) 2263.

[107] Y. Wang, X. Wu, M. Du, X. Chen, X. Ning, H. Chen, S. Wang, J. Liu, Z. Liu, R. Li, Eg5 inhibitor YL001 induces mitotic arrest and inhibits tumor proliferation, Oncotarget, 8 (2017) 42510.

[108] C. Jiang, Q. You, Kinesin spindle protein inhibitors in cancer: a patent review (2008–present), Expert opinion on therapeutic patents, 23 (2013) 1547.

[109] L. Hodson, The synthesis of novel kinase inhibitors using click chemistry (thesis), Stellenbosch: Stellenbosch University, (2014).

[110] Y. Hu, C.Y. Li, X.M. Wang, Y.H. Yang, H.L. Zhu, 1, 3, 4-Thiadiazole: synthesis, reactions, and applications in medicinal, agricultural, and materials chemistry, Chemical reviews, 114 (2014) 5572.

[111] K.M. Dawood, T.A. Farghaly, Thiadiazole inhibitors: a patent review, Expert opinion on therapeutic patents, 27 (2017) 477.

[112] P.T. Parvatkar, P.S. Parameswaran, S.G. Tilve, Recent developments in the synthesis of five-and six-membered heterocycles using molecular iodine, Chemistry-a european journal, 18 (2012) 5460.

[113] A.S. Kostyuchenko, V.L. Yurpalov, A. Kurowska, W. Domagala, A. Pron, A.S. Fisyuk, Synthesis of new, highly luminescent bis (2, 2'-bithiophen-5-yl) substituted 1, 3, 4-oxadiazole, 1, 3, 4-thiadiazole and 1, 2, 4-triazole, Beilstein journal of organic chemistry, 10 (2014) 1596.

[114] Y. Zai, S. Khan, Synthesis, characterization and microbial activity of new thiazole, thiazolidinone, thiadiazole and phenylacrylohydrazide substituted coumarin derivatives (thesis), Universiti Sains Malaysia, (2015).

[115] S. Srivastava, R.K. Prasad, R. Saini, Thiadiazole: a brief review, World journal of pharmacy and pharmaceutical sciences, 3 (2014) 1198.

[116] J. Matysiak, Biological and pharmacological activities of 1, 3, 4-thiadiazole based compounds, Mini reviews in medicinal chemistry, 15 (2015) 762.

[117] Z. Shen, T. Wang, M. Liu, Macroscopic chirality of supramolecular gels formed from achiral tris (ethyl cinnamate) benzene-1, 3, 5-tricarboxamides, Angewandte chemie international edition, 53 (2014) 13424.

[118] H.D. Foda, S. Zucker, Matrix metalloproteinases in cancer invasion, metastasis and angiogenesis, Drug discovery today, 6 (2001) 478.

[119] Y.A. Al-Soud, N.A. Al-Masoudi, R. Loddo, P. La Colla, *In-Vitro* anti-HIV and antitumor

activity of new 3, 6-disubstituted [1, 2, 4] triazolo [3, 4-b][1, 3, 4] thiadiazoles and thiadiazine analogues, Archiv der pharmazie, 341 (2008) 365.

[120] W.S. Alwan, R. Karpoormath, M.B. Palkar, H.M. Patel, R.A. Rane, M.S. Shaikh, A. Kajee, K.P. Mlisana, Novel imidazo [2, 1-b]-1, 3, 4-thiadiazoles as promising antifungal agents against clinical isolate of *Cryptococcus neoformans*, European journal of medicinal chemistry, 95 (2015) 514.

[121] A. Vijesh, A.M. Isloor, P. Shetty, S. Sundershan, H.K. Fun, New pyrazole derivatives containing 1, 2, 4-triazoles and benzoxazoles as potent antimicrobial and analgesic agents, European journal of medicinal chemistry, 62 (2013) 410.

[122] A.K. Gadad, M.B. Palkar, K. Anand, M.N. Noolvi, T.S. Boreddy, J. Wagwade, Synthesis and biological evaluation of 2-trifluoromethyl/sulfonamido-5, 6-diaryl substituted imidazo [2, 1-b]-1, 3, 4-thiadiazoles: a novel class of cyclooxygenase-2 inhibitors, Bioorganic and medicinal chemistry, 16 (2008) 276.

[123] S.A. Carvalho, F.A. Lopes, K. Salomão, N.C. Romeiro, S.M. Wardell, S.L. de Castro, E.F. da Silva, C.A. Fraga, Studies toward the structural optimization of new brazilizone-related trypanocidal 1, 3, 4-thiadiazole-2-arylhydrazone derivatives, Bioorganic and medicinal chemistry, 16 (2008) 413.

[124] A.T. Mavrova, D. Wesselinova, Y.A. Tsenov, P. Denkova, Synthesis, cytotoxicity and effects of some 1, 2, 4-triazole and 1, 3, 4-thiadiazole derivatives on immunocompetent cells, European journal of medicinal chemistry, 44 (2009) 63.

[125] V. Padmavathi, S.N. Reddy, G.D. Reddy, A. Padmaja, Synthesis and bioassay of aminosulfonyl-1, 3, 4-oxadiazoles and their interconversion to 1, 3, 4-thiadiazoles, European journal of medicinal chemistry, 45 (2010) 4246.

[126] K.M. Dawood, T.M. Eldebss, H.S. El-Zahabi, M.H. Yousef, P. Metz, Synthesis of some new pyrazole-based 1, 3-thiazoles and 1, 3, 4-thiadiazoles as anticancer agents, European journal of medicinal chemistry, 70 (2013) 740.

[127] S. Bajaj, V. Asati, J. Singh, P.P. Roy, 1, 3, 4-Oxadiazoles: An emerging scaffold to target growth factors, enzymes and kinases as anticancer agents, European journal of medicinal chemistry, 97 (2015) 124.

[128] S. Haider, M.S. Alam, H. Hamid, 1, 3, 4-Thiadiazoles: A potent multi targeted pharmacological scaffold, European journal of medicinal chemistry, 92 (2015) 156.

[129] R. Kaur, A. Ranjan Dwivedi, B. Kumar, V. Kumar, Recent developments on 1, 2, 4-triazole nucleus in anticancer compounds: a review, Formerly current medicinal chemistry-anti-cancer agents, 16 (2016) 465.

[130] G.H. Al-Ansary, M.A. Ismail, D.A.A. El Ella, S. Eid, K.A. Abouzid, Molecular design and synthesis of HCV inhibitors based on thiazolone scaffold, European journal of medicinal chemistry, 68 (2013) 19.

[131] A.C. Tripathi, S.J. Gupta, G.N. Fatima, P.K. Sonar, A. Verma, S.K. Saraf, 4-Thiazolidinones: the advances continue, European journal of medicinal chemistry, 72 (2014) 52.

[132] M. Lelyukh, D. Havrylyuk, R. Lesyk, Synthesis and anticancer activity of isatin, oxadiazole and 4-thiazolidinone based conjugates, Chemistry and chemical technology, 9 (2015) 29.

[133] B. Chandrasekaran, M. Ramesh, C.L.Tham, S.P. Khathi, F. Kozielski, C. Srinivasulu, G.A. Hampannavar, N. Sayyad, M.E. Soliman, R. Karpoormath, Ligand and structure based *in silico* studies to identify kinesin spindle protein (KSP) inhibitors as potential anticancer agents, Journal of biomolecular structure and dynamics, (2017) 1-77, DOI:10.1080/07391102.2017.1396255.

Chapter 3

Synthesis and Spectral Studies

3.1. Synthesis and spectral studies

The synthesis of a novel series of TDT hybrid compounds (**8a-v**) was accomplished using a multi-step reaction sequence through an efficient synthetic route as illustrated in **scheme 1**.

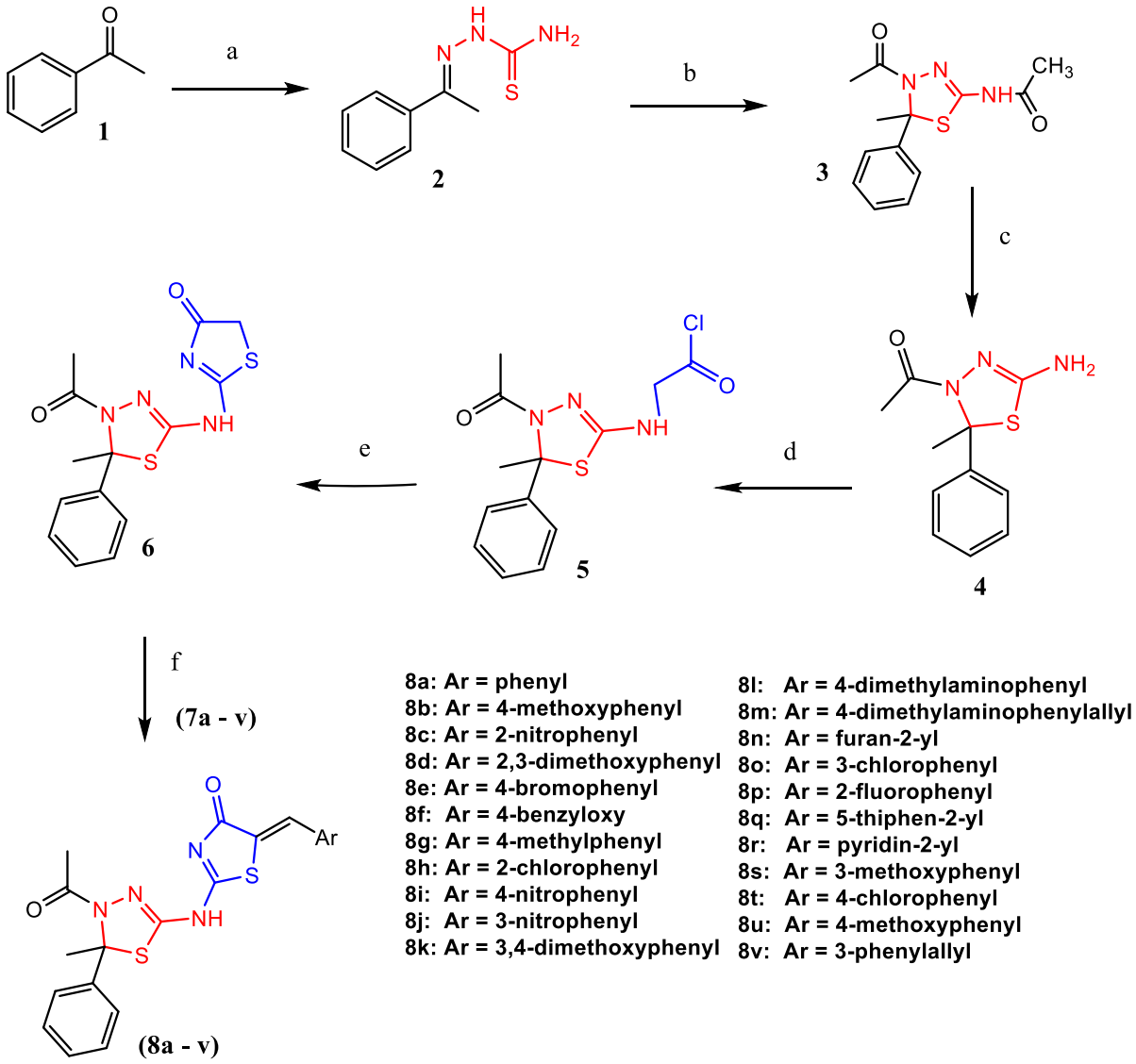

Scheme 1: Synthetic route for novel of TDT hybrids (**8a-v**). (a) $NH_2CSNHNH_2$, MeOH, rt, 15h; (b) $(CH_3CO)_2O$, reflux, 2 h; (c) NH_2NH_2, MeOH, rt, 3 h; (d) $ClCH_2COCl$, *N*,*N*-DMF, rt, 2 h; (e) NH_4SCN, EtOH, reflux, 2h; (f) ArCHO, NaOEt, rt, 1-2 h.

Acetophenone (**1**) reacted with thiosemicarbazide under vigorous stirring conditions afforded (*E*)-2-(1-phenylethylidene)hydrazine-1-carbothioamide (**2**), quantitatively. The

structure of **2** was established based on ^{1}H NMR in which the appearance of a singlet peak at δ 10.27 ppm was attributed to –NH proton. Moreover, the primary amino group (NH_2) demonstrated one singlet at δ 8.26 ppm for one proton, while the other proton was merged with the aromatic region (δ 7.91 – 7.93 ppm). In ^{13}C NMR, we observed a characteristic peak at δ 178.93 ppm which indicated the presence of C=S functionality. Compound **2** undergoes cyclization and subsequent acetylation using acetic anhydride yielded *N*-(4-acetyl-5-methyl-5-phenyl-4,5-dihydro-1,3,4-thiadiazol-2-yl)acetamide (**3**). The formation of compound **3** was confirmed by presence of additional methyl group protons as individual singlets at δ 2.19 ppm and δ 2.28 ppm in ^{1}H NMR and two new carbonyl carbons (C=O) at δ 167 and 169 ppm, respectively in ^{13}C NMR. Nucleophilic displacement of acetyl group of **3** with hydrazine hydrate furnished compound **4** and was confirmed based on ^{1}H NMR, where the amide NH disappeared and the prominent appearance of a new broad singlet at δ 4.11 ppm assigned to the protons of NH_2 group. All these spectral data were corroborated with the literature reported data [1]. Reaction of **4** with chloroacetyl chloride in *N*,*N*-dimethylformamide under the mild basic condition (triethylamine) produced (4-Acetyl-5-methyl-5-phenyl-4,5-dihydro-1,3,4-thiadiazol-2-yl)glycinoyl chloride (**5**) of 91 % yield. The ^{1}H NMR spectrum of **5** revealed the disappearance of broad singlet of the NH_2 proton at δ 4.11 ppm and appearance of two informative singlets at δ 9.29 and 3.91 ppm, which are attributed to NH and methylene protons (CH_2), respectively confirming the formation of **5**. The heterocyclization of **5** in the presence of ammonium thiocyanate and ethanol under reflux conditions, efficiently yielded 2-((4-Acetyl-5-methyl-5-phenyl-4,5-dihydro-1,3,4-thiadiazol-2-yl)amino)thiazol-4(5*H*)-one (**6**), quantitatively. This was confirmed by the ^{1}H NMR spectrum, in which singlet signals corresponding to NH and CH_2 protons appeared at δ 12.18 and 4.06 ppm respectively. This has been further substantiated in ^{13}C NMR which displayed a prominent signal at δ 173.99 ppm accredited to C=O of thiazol-4(5*H*)-one moiety thus confirming the cyclization reaction. The compound **6** possibly exists in different tautomeric states and the theoretical pathway of the tautomers is presented in **scheme 2**.

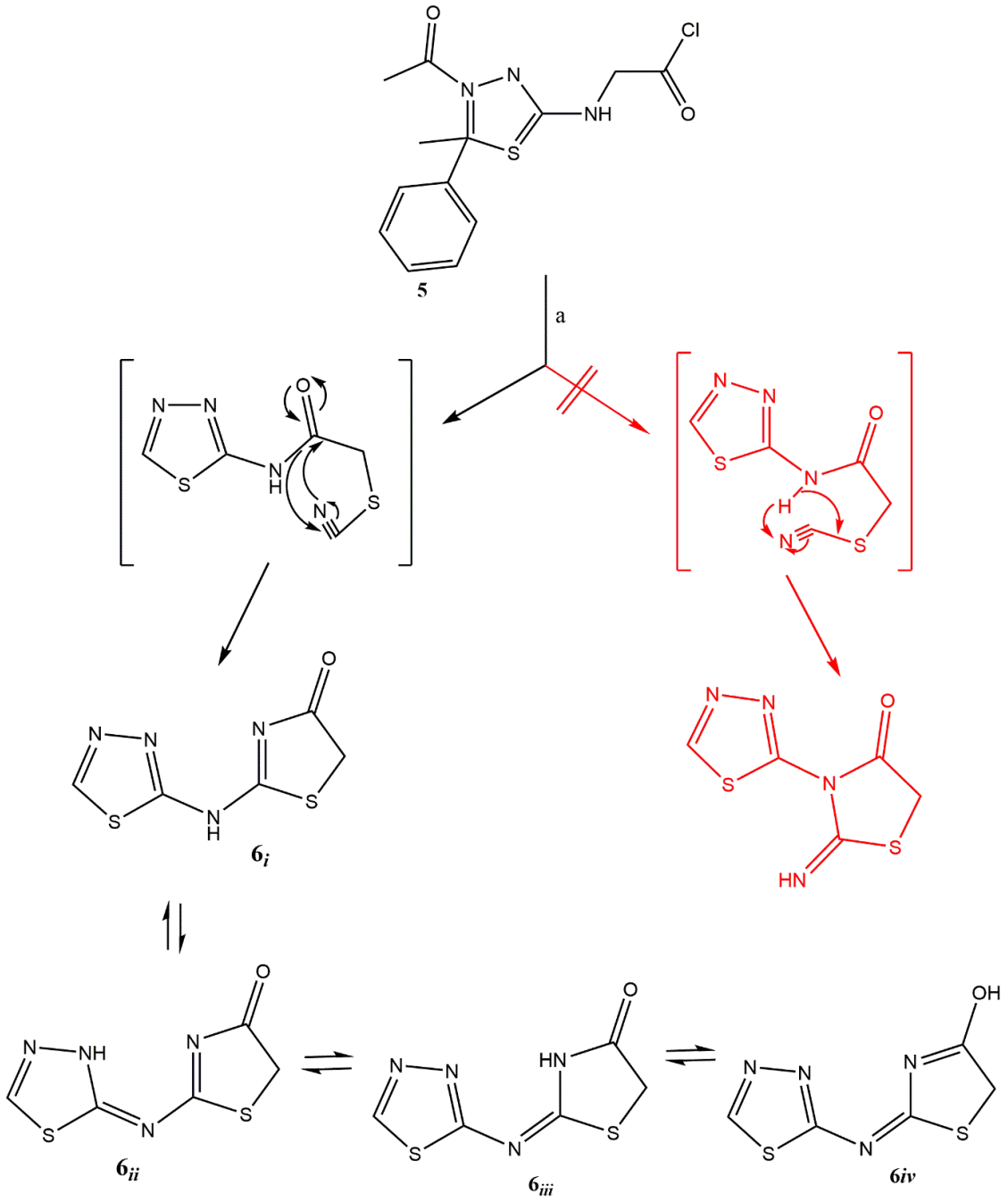

Scheme 2: The tautomeric pathway for compound **6** [2].

To achieve quick access to the final compounds (**8a-v**) for pharmacological evaluation, a facile synthetic strategy was employed consisting of a well-known Knoevenagel reaction of **6** with the appropriate aromatic/heterocyclic aldehydes (**7a-v**). The structures of twenty-two newly synthesized hybrids (**8a-v**) were characterized based on their physicochemical and spectral (FT-IR, ^{1}H NMR, ^{13}C NMR and HR-MS) analysis. The analytical data of all the newly synthesized compounds along with their anticipated structures are summarized in the experimental section.

3.1.1. FT-IR characterization

Infra-red spectroscopy serves as an analytical tool in the identification of different functional groups in all the synthesized novel compounds. There is a consistent and prominent peak around 1663-1716 cm^{-1} indicated the presence of a carbonyl group (C=O) in all synthesized compounds. Similarly, a characteristic peak around 3661 – 3379 cm^{-1} attributed to the presence of NH in all the compounds. All synthesized compounds showed resemblance of the characteristic peaks in the FT-IR, which further confirmed the presence of the expected functional groups. In particular, **8h** showed carbonyl (C=O) stretching bands at 1653 and 1716 cm^{-1} as well as NH bond stretching at 3379 cm^{-1} established its formation (**Fig. 23**).

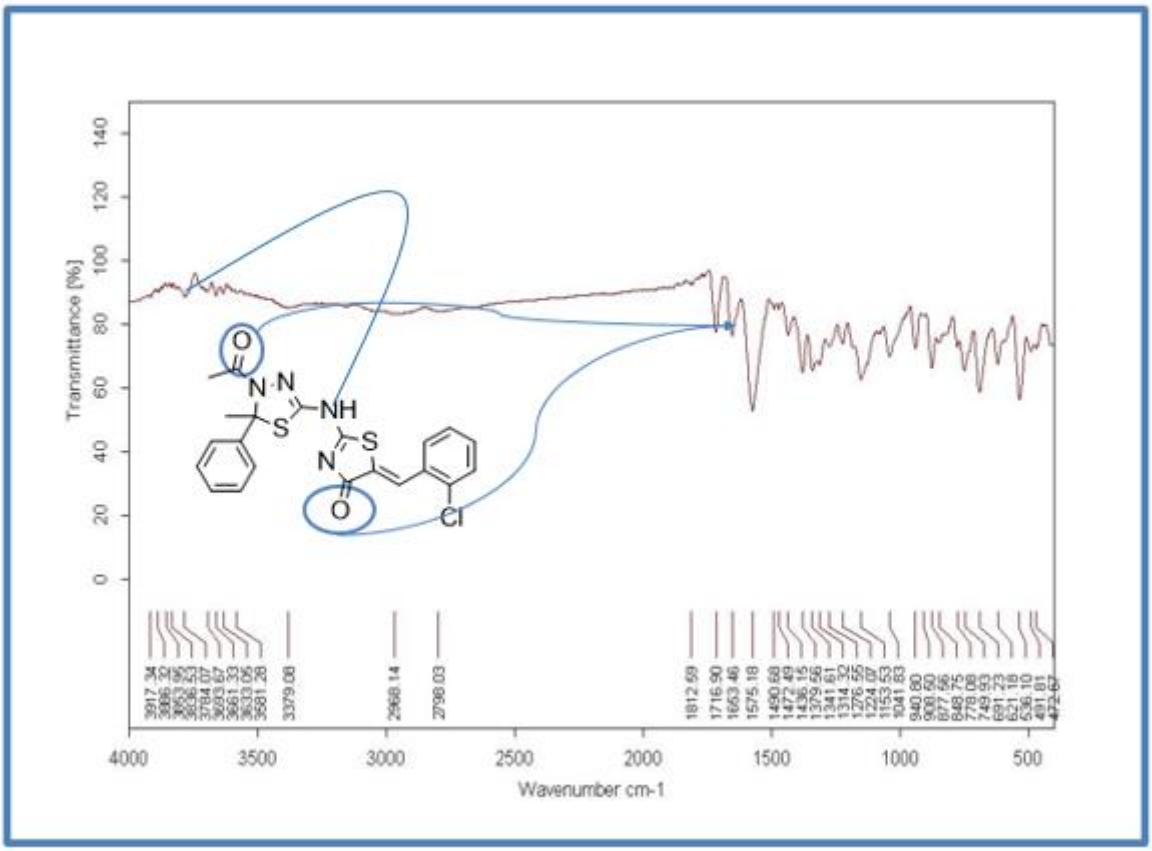

Figure 23: The FT-IR spectrum of compound **8h**.

3.1.2. ^{1}H NMR characterization

In the ^{1}H NMR of **8a-v**, the absence of the singlet signal of methylene protons in thiazolone moiety and appearance of methine proton (=CH-) resonating in the range of δ 7.72 - 7.99 ppm along with aromatic protons confirmed the formation of the final compounds. All the target molecules **8a-v** exists as geometrical isomers (*E* and *Z*). The *Z* conformation of the exocyclic C=C double bond was assigned based on ^{1}H NMR and literature data of reported analogous of 1,2,4-thiazolidinediones and 4-thiazolone [2, 3]. Specifically, the appearance of

methine proton in the deshielded region (> δ 7.72 ppm) adjacent to C=O of thiazolone ring displayed higher chemical shift values than the anticipated values for *E* isomers (< δ 7.5 ppm) which show lower chemical shift values, as they appear mostly in the shielded region [4]. Thus, confirming the *Z* conformation for all the final compounds (**8a-v**). Moreover, in the ^{1}H NMR spectra, the NH proton of **8a-v** was observed at the deshielding position and it displayed higher chemical shift values at δ 13.01-12.56 ppm. This indicated that the substitution is on the 2-position rather than on 3-position, and this pattern correlated with the lactam proton since an imine proton generally get affected by the shielding effect (about δ 9.5 ppm) [5]. The ^{1}H NMR characterization was better explained by illustrating an example of compound **8h**. It is interesting to know that two singlets at δ 2.27 and 2.39 ppm corresponding to two methyl group protons. Also, characteristic broad singlet peak and a sharp singlet appeared at δ 12.9 and 7.88 ppm assigned to NH and arylidine CH, respectively. All this data confirmed the structure of the compound **8h** (**Fig. 24**).

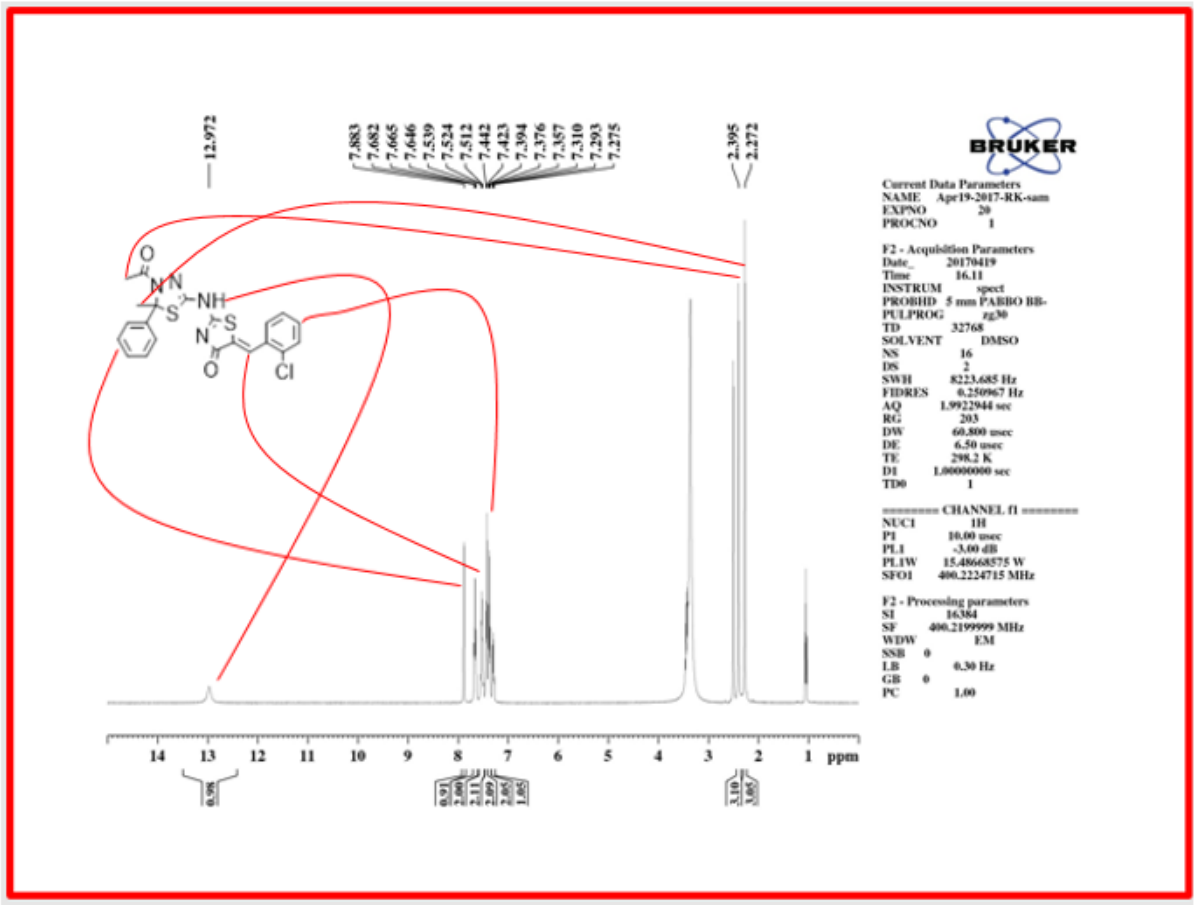

Figure 24: The ^{1}H NMR spectrum of compound **8h**.

3.1.3. ^{13}C NMR characterization

These interpretations were further validated by recording their respective ^{13}C NMR spectra. Where arylidene carbon of the final derivatives resonated in the range of δ 148.9 - 158.5 ppm in addition to the observed aromatic carbons evidently confirmed the formation of desired **8a-v** via Knoevenagel condensation. The ^{13}C NMR of **8g** showed a deshielded peak belonging to the arylidene carbon (δ 148 ppm) and an additional tolyl carbon that belongs to $\underline{C}H_3$ (δ 27 ppm) at shielded region, which substantiated and established the structure of **8g** (**Fig. 25**).

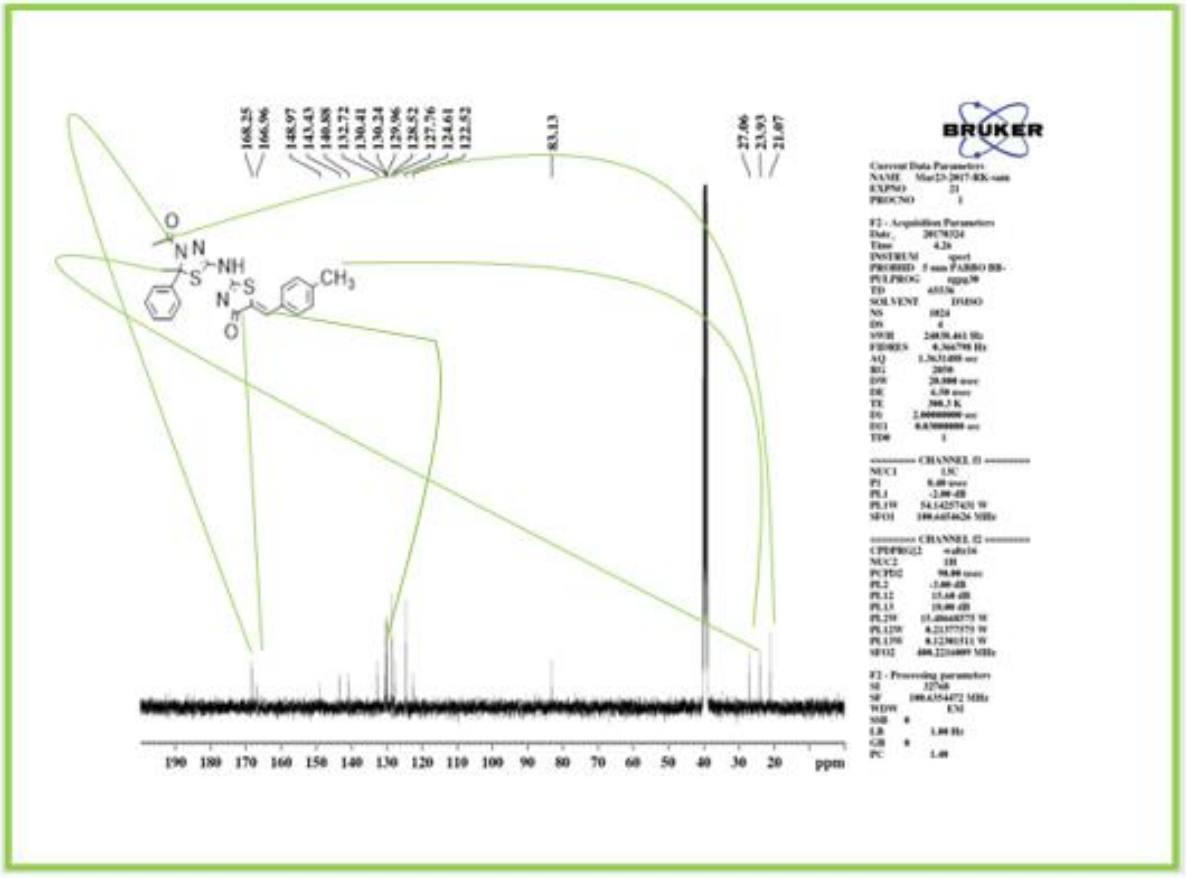

Figure 25: The ^{13}C NMR spectrum of compound **8g**.

3.1.4. HRMS Analysis

Moreover, the formation of final derivatives was confirmed by recording their respective HRMS, which displayed accurate molecular ion peaks that correlated with their expected molecular weights. An illustrative example of HRMS of **8a** is presented in **Fig. 26**.

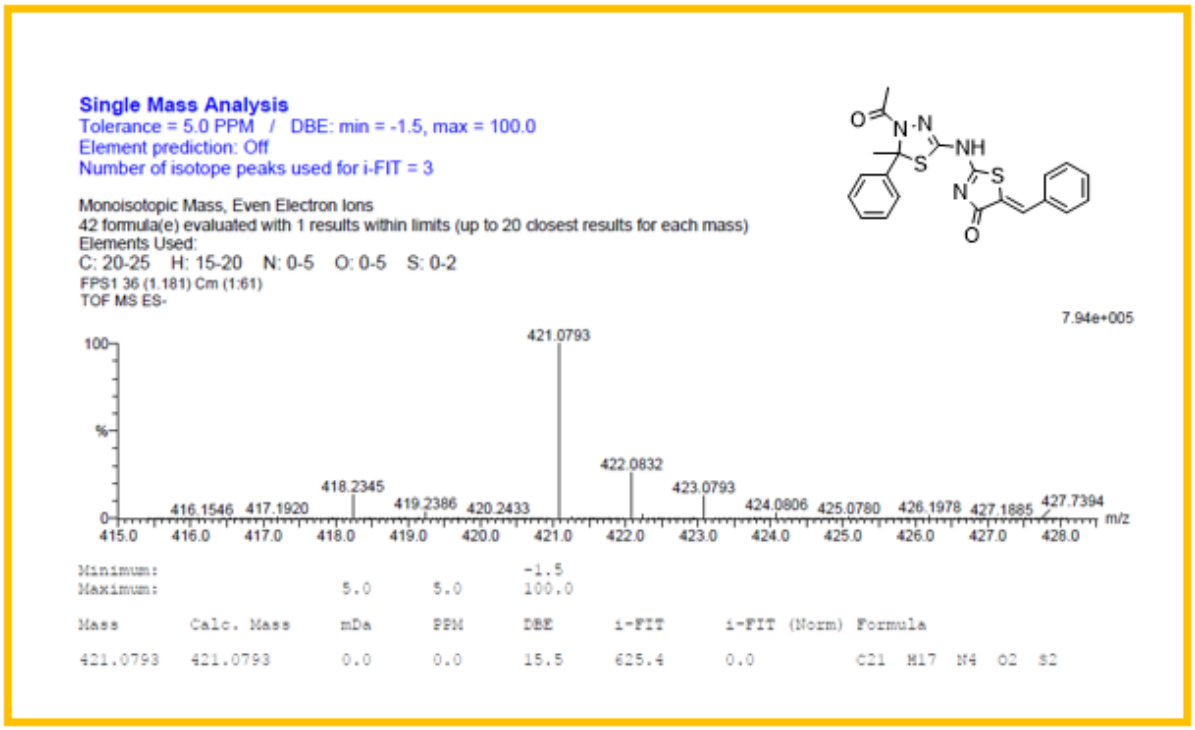

Figure 26: The HRMS spectrum of compound **8a**.

3.2. Experimental (synthesis)

All research chemicals (AR grade) were purchased from Sigma–Aldrich and Merck Millipore, South Africa. Solvents except laboratory reagent grade were dried and purified per the literature when necessary. The progress of reactions and purity of compounds were monitored by thin-layer chromatography (TLC) on pre-coated silica gel plates procured from E. Merck and Co. (Darmstadt, Germany) using methanol (10 %) in chloroform as mobile phase and iodine vapors as a visualizing agent. Compounds were purified by recrystallization technique using ethanol. Melting points of synthesized compounds were determined in Thermo Fisher Scientific (IA9000, Essex, Great Britain) digital melting point apparatus and are uncorrected. IR spectra were recorded on Bruker Alpha FT-IR Spectrometer (Billerica, MA, USA) by using ATR technique. The ^{1}H NMR and ^{13}C NMR were recorded on Bruker AVANCE 400 and 100 MHz (Bruker, Rheinstetten/Karlsruhe, Germany) using DMSO-d_6 or $CDCl_3$. Chemical shifts are reported in δ ppm units with respect to TMS as an internal standard. HRMS were recorded on Autospec Mass Spectrometer under the electron impact at 70 eV.

3.2.1. (E)-2-(1-phenylethylidene)hydrazine-1-carbothioamide (2)

To a solution of acetophenone (33.3 mmol, 4g) and thiosemicarbazide (34.6 mmol, 3.15 g) in 90 ml of methanol, 0.3 ml of concentrated hydrochloric acid was added slowly dropwise and stirred for 15 hours. After completion of the reaction (as monitored by TLC), 30 ml of water was added to the mixture to obtain product **2**. Thus, the obtained solids were filtered and washed with diisopropyl ether to yield white crystals of **2** in pure form (3g, 80 % yield). ^{1}H NMR (400 MHz, $CDCl_3$) δ: 2.29 (s, 3H, CH_3); 7.37 – 7.39 (m, 3H, ArH); 7.91 – 7.93 (m, 2H, ArH, 1H, NH_2); 8.26 (s, 1H, NH_2); 10.2 (s, 1H, NH) ppm; ^{13}C NMR (100 MHz, DMSO-d_6) δ: 13.9 CH_3; 126, 128, 129, 137, 147, 178 ppm.

3.2.2. N-(4-acetyl-5-methyl-5-phenyl-4,5-dihydro-1,3,4-thiadiazol-2-yl)acetamide (3)

Compound **2** (0.889 mmol; 0.3g) in acetic anhydride (11 mmol; 1 ml) was refluxed till it became a homogenous mixture. Then, the solution was cooled to room temperature to obtain compound **3**. Diethyl ether (120 ml) was added to remove non-polar impurities to yield white crystals which was dried under vacuum (0.25 g, 83 %). ^{1}H NMR (400 MHz, $CDCl_3$) δ: 2.01 (s, 3H, CH_3); 2.19 (s, 3H, CH_3); 2.28 (s, 3H, CH_3) ppm; 7.23 – 7.24 (s, 1H, ArH); 7.25 – 7.35 (m, 4H, ArH); 11.6 (s, 1H, NH) ppm; ^{13}C NMR (100 MHz, DMSO-d_6) δ: 22.4, 23.6, 26.5 (3$\underline{C}H_3$); 78.5, 124, 127, 128, 142, 143, 167, 169 (2$\underline{C}$=O) ppm.

3.2.3. 1-(5-amino-2-methyl-2-phenyl-1,3,4-thiadiazol-3(2H)-yl)ethan-1-one (4)

Compound **3** (3 mmol; 1 g) and hydrazine hydrate (13 ml) in 10 ml methanol was stirred for 6 h. After completion, ice was added to yield white precipitates which were filtered and dried (0.83 g, 83 %). ^{1}H NMR (400 MHz, $CDCl_3$) δ: 2.15 (s, 3H, CH_3); 2.34 (s, 3H, CH_3); 7.17 – 7.19 (m, 1H, ArH); 7.20 – 7.28 (m, 2H, ArH); 7.37 – 7.39 (m, 2H, ArH); 4.11 (s, 2H, NH) ppm.

3.2.4. (4-acetyl-5-methyl-5-phenyl-4,5-dihydro-1,3,4-thiadiazol-2-yl)glycinoyl chloride (5)

To a stirred solution of 1-(5-amino-2-methyl-2-phenyl-1,3,4-thiadiazol-3(2*H*)-yl)ethan-1-one **4**, (0.02 mol, 4.7 g) and triethylamine (0.02 mol, 2.78 ml) in *N*,*N*-dimethylformamide (10 ml), a solution of chloroacetyl chloride (0.024 mol, 1.91 ml in 10 ml DMF) was added dropwise. After addition, the mixture was stirred further for 2 h. Then, the mixture was poured onto the crushed ice to obtain a brownish precipitate, which was isolated by filtration, washed with water and dried. Purification of the crude product by 95% ethanol produced a

light-brown product **2** of 91 % yield (4.3 g); mp 188-190 °C; ^{1}H NMR (400 MHz, $CDCl_3$) δ: 2.20 (s, 3H, CH_3), 2.31 (s, 3H, CH_3), 3.91 (s, 2H, CH_2), 7.17 – 7.36 (m, 5H, ArH), 9.29 (s, 1H, NH) ppm.

3.2.5. 2-((4-acetyl-5-methyl-5-phenyl-4,5-dihydro-1,3,4-thiadiazol-2-yl)amino)thiazol-4(5H)-one (6)

A solution of **6** (1 mmol, 0.311g) and ammonium thiocyanate (2 mmol, 0.152g) in 10 ml of 98% ethanol was refluxed for 3 h. Upon completion of the reaction (as monitored by TLC), the solution was kept at room temperature and thus, the precipitates obtained was filtered, washed with water and dried. Recrystallization of the crude product with ethanol produced a grey coloured product **6** (82 % yield). mp 199-200 °C; FT-IR (ATR, cm^{-1}) ν_{max}: 1740 (C=O), 3114 (N-H); ^{1}H NMR (400 MHz, DMSO-d_6) δ: 2.23 (s, 3H, CH_3), 2.37 (s, 3H, CH_3), 4.06 (s, 2H, CH_2), 7.26 – 7.42 (m, 5H, ArH), 12.18 (s, 1H, NH) ppm; ^{13}C NMR (100 MHz, DMSO-d_6) δ: 23.97, 27.01 (2$\underline{C}H_3$), 35.53 ($\underline{C}H_2$), 82.63, 124.50, 127.66, 128.49, 143.57, 149.40, 165.72, 168.10, 173.99 ppm.

3.2.6. General procedure for synthesis of (Z)-2-((4-acetyl-5-methyl-5-phenyl-4,5-dihydro-1,3,4-thiadiazol-2-yl)amino)-5-arylidenethiazol-4(5H)-one (8a-v)

A well-stirred solution of **6** (1 mmol) in 5 ml of ethanol was basified with a catalytic quantity of sodium hydroxide (half-pellet). Appropriate aldehydes (**7a-v**) (1 mmol) were then added to the solution and stirred further for 1-2 h. After completion of the reaction (as monitored by TLC), the solution was buffered with dilute hydrochloric acid dropwise under cold condition. The precipitate thus obtained was filtered, washed with cold ethanol and re-crystallised with absolute ethanol.

*(Z)-2-((4-acetyl-5-methyl-5-phenyl-4,5-dihydro-1,3,4-thiadiazol-2-yl)amino)-5-benzylidenethiazol-4(5H)-one (**8a**)*

Yellow crystals; yield: 70 %; mp 211-212 °C; FT-IR (ATR, cm^{-1}) ν_{max}: 1711 (C=O), 3693 (N-H); ^{1}H NMR (400 MHz, DMSO-d_6) δ: 2.33 (s, 3H, CH_3), 2.40 (s, 3H, CH_3), 7.28 – 7.66 (m, 10H, ArH), 7.77 (s, 1H, arylidene-H), 12.84 (s, 1H, NH) ppm; ^{13}C NMR (100 MHz, DMSO-d_6) δ: 23.97, 27.08 (2$\underline{C}H_3$), 83.22, 123.80, 124.64, 127.80, 128.56, 129.37, 130.18, 130.55, 132.67, 133.20, 143.43, 148.94, 158.57 (arylidene-$\underline{C}$), 166.92, 168.31 (2$\underline{C}$=O) ppm; HR-MS (ES^-) calculated for $C_{21}H_{18}N_4O_2S_2$ $[M-H]^+$: 421.0793; found: 421.0793.

*(Z)-2-((4-acetyl-5-methyl-5-phenyl-4,5-dihydro-1,3,4-thiadiazol-2-yl)amino)-5-(4-methoxybenzylidene)thiazol-4(5H)-one (**8b**)*

Yellow solid; yield: 75 %; mp 223-225 °C; FT-IR (ATR, cm^{-1}) ν_{max}: 1024 (O-C), 1671 (C=O), 3463 (N-H); ^{1}H NMR (400 MHz, DMSO-d_6) δ: 2.35 (s, 3H, CH_3), 2.41 (s, 3H, CH_3), 3.84 (s, 3H, CH_3); 7.11 – 7.63 (m, 9H, ArH), 7.72 (s, 1H, arylidene-H), 12.74 (s, 1H, NH) ppm; ^{13}C NMR (100 MHz, DMSO-d_6) δ: 24.04, 27.05 (2$\underline{C}H_3$), 55.56 (O$\underline{C}H_3$), 83.12, 114.98, 120.45, 124.62, 125.62, 127.77, 128.54, 132.31, 132.76, 143.45, 148.97 (arylidene-$\underline{C}$), 158.63, 161.11, 167.04, 168.28 (2$\underline{C}$=O) ppm.

*(Z)-2-((4-acetyl-5-methyl-5-phenyl-4,5-dihydro-1,3,4-thiadiazol-2-yl)amino)-5-(2-nitrobenzylidene)thiazol-4(5H)-one (**8c**)*

Yellow solid; yield: 85 %; mp 188-190 °C; FT-IR (ATR, cm^{-1}) ν_{max}: 1522 (N-O), 1723 (C=O), 3580 (N-H); ^{1}H NMR (400 MHz, DMSO-d_6) δ: 2.18 (s, 3H, CH_3), 2.37 (s, 3H, CH_3), 7.26 – 7.41 (m, 5H, ArH), 7.72 – 7.92 (m, 3H, ArH), 7.99 (s, 1H, arylidene-H), 8.21 – 8.23 (m, 1H, ArH), 12.99 (s, 1H, NH) ppm; ^{13}C NMR (100 MHz, DMSO-d_6) δ: 23.83, 27.05 (2$\underline{C}H_3$), 83.17, 124.60, 125.51, 127.79, 128.40, 128.52, 128.94, 129.31, 129.58, 131.18, 134.39, 147.89 (arylidene-$\underline{C}$), 168.18 (2$\underline{C}$=O) ppm; HRMS (ES^-) calculated for $C_{21}H_{17}N_5O_4S_2$ $[M-H]^+$: 466.0644; found: 466.0631.

*(Z)-2-((4-acetyl-5-methyl-5-phenyl-4,5-dihydro-1,3,4-thiadiazol-2-yl)amino)-5-(2,3-dimethoxybenzylidene)thiazol-4(5H)-one (**8d**)*

Yellow solid; yield: 80 %; mp 240-241 °C; FT-IR (ATR, cm^{-1}) ν_{max}: 1261 (O-C), 1723 (C=O), 3431 (N-H); ^{1}H NMR (400 MHz, DMSO-d_6) δ: 2.29 (s, 3H, CH_3), 2.39 (s, 3H, CH_3), 3.80 (s, 3H, OCH_3), 3.85 (s, 3H, OCH_3), 7.11 – 7.44 (m, 8H, ArH), 7.87 (s, 1H, arylidene-H), 12.89 (s, 1H, NH) ppm; ^{13}C NMR (100 MHz, DMSO-d_6) δ: 23.92, 27.06 (2$\underline{C}H_3$), 55.97, 61.15 (2O$\underline{C}H_3$), 83.18, 115.57, 120.03, 124.62, 124.73, 124.86, 126.83, 127.22, 127.78, 128.54, 143.43, 148.26, 148.92, 152.82, 158.76, 166.93, 168.25 (2$\underline{C}$=O) ppm.

*(Z)-2-((4-acetyl-5-methyl-5-phenyl-4,5-dihydro-1,3,4-thiadiazol-2-yl)amino)-5-(4-bromobenzylidene)thiazol-4(5H)-one (**8e**)*

Dark yellow solid; yield: 87 %; mp 245-247 °C; FT-IR (ATR, cm^{-1}) ν_{max}: 1711 (C=O), 3581 (N-H); ^{1}H NMR (400 MHz, DMSO-d_6) δ: 2.33 (s, 3H, CH_3), 2.40 (s, 3H, CH_3), 7.28 – 7.61 (m, 7H, ArH), 7.74 – 7.75 (m, 2H, ArH), 7.78 (s, 1H, arylidene-H), 12.89 (s, 1H, NH) ppm; ^{13}C NMR (100 MHz, DMSO-d_6) δ: 24.05, 27.05 (2$\underline{C}H_3$), 83.22, 123.98, 124.62, 127.79,

128.53, 131.90, 132.35, 154.56, 165.73, 167.45 (2C=O) ppm; HR-MS (ES^-) calculated for $C_{21}H_{17}BrN_4O_2S_2$ $[M-H]^+$: 498.9898; found: 498.9888.

*(Z)-2-((4-acetyl-5-methyl-5-phenyl-4,5-dihydro-1,3,4-thiadiazol-2-yl)amino)-5-(4-(benzyloxy)benzylidene)thiazol-4(5H)-one (**8f**)*

Yellow solid; yield: 79 %; mp 196-197 °C; FT-IR (ATR, cm^{-1}) ν_{max}: 1249 (O-C), 1700 (C=O), 3581 (N-H); ^1H NMR (400 MHz, DMSO-d_6) δ: 2.34 (s, 3H, CH_3), 2.40 (s, 3H, CH_3), 5.19 (s, 2H, CH_2), 7.18 – 7.47 (m, 12H, ArH), 7.60 – 7.62 (m, 2H, ArH), 7.72 (s, 1H, arylidene-H), 12.75 (s, 1H, NH) ppm; ^{13}C NMR (100 MHz, DMSO-d_6) δ: 24.02, 27.04 (2$\underline{C}H_3$), 69.53 ($\underline{C}H_2$), 83.12, 115.74, 120.63, 124.62, 125.83, 127.80, 128.01, 128.48, 128.52, 132.27, 132.68, 136.47, 143.44, 148.96, 158.64, 160.17, 167.02, 168.26 (2$\underline{C}$=O) ppm.

*(Z)-2-((4-acetyl-5-methyl-5-phenyl-4,5-dihydro-1,3,4-thiadiazol-2-yl)amino)-5-(4-methyl benzylidene)thiazol-4(5H)-one (**8g**)*

Yellow solid; yield: 72 %; mp 246-248 °C; FT-IR (ATR, cm^{-1}) ν_{max}: 1714 (C=O), 3386 (N-H); ^1H NMR (400 MHz, DMSO-d_6) δ: 2.33 (s, 3H, CH_3), 2.36 (s, 3H, CH_3), 2.40 (s, 3H, CH_3), 7.27 – 7.45 (m, 7H, ArH), 7.53-7.55 (m, 2H, ArH), 7.72 (s, 1H, arylidene-H), 12.83 (s, 1H, NH) ppm; ^{13}C NMR (100 MHz, DMSO-d_6) δ: 21.07, 23.93, 27.06 (3$\underline{C}H_3$), 83.13, 122.52, 124.61, 127.76, 128.52, 129.96, 130.24, 130.41, 132.72, 140.88, 143.43, 148.97, 166.96, 168.25 (2$\underline{C}$=O) ppm.

*(Z)-2-((4-acetyl-5-methyl-5-phenyl-4,5-dihydro-1,3,4-thiadiazol-2-yl)amino)-5-(2-chloro benzylidene)thiazol-4(5H)-one (**8h**)*

Yellow crystals; yield: 88 %; mp 185-186 °C; FT-IR (ATR, cm^{-1}) ν_{max}: 1716 (C=O), 3379 (N-H); ^1H NMR (400 MHz, DMSO-d_6) δ: 2.27 (s, 3H, CH_3), 2.39 (s, 3H, CH_3), 7.27 – 7.53 (m, 7H, ArH), 7.64 – 7.68 (m, 2H, ArH), 7.88 (s, 1H, arylidene-H), 12.97 (s, 1H, NH) ppm; ^{13}C NMR (100 MHz, DMSO-d_6) δ: 23.93, 27.07 (2$\underline{C}H_3$), 83.27, 124.63, 127.45, 127.56, 127.81, 128.03, 128.55, 129.16, 130.45, 131.16, 131.99, 134.49, 143.37, 148.85, 158.19, 166.54, 168.29 (2$\underline{C}$=O) ppm.

*(Z)-2-((4-acetyl-5-methyl-5-phenyl-4,5-dihydro-1,3,4-thiadiazol-2-yl)amino)-5-(4-nitro-benzylidene)thiazol-4(5H)-one (**8i**)*

Orange solid; yield: 78 %; mp 154-156 °C; FT-IR (ATR, cm^{-1}) ν_{max}: 1514 (N-O), 1719 (C=O), 3405 (N-H); ^1H NMR (400 MHz, DMSO-d_6) δ: 2.34 (s, 3H, CH_3), 2.41 (s, 3H, CH_3), 7.28 – 7.46 (m, 5H, ArH), 7.85 (s, 1H, arylidene-H), 7.88-7.90 (m, 2H, ArH), 8.35-8.37 (m,

2H, ArH), 13.02 (s, 1H, NH) ppm; ^{13}C NMR (100 MHz, DMSO-d_6) δ: 24.11, 27.07 (2<u>C</u>H$_3$), 83.33, 124.31, 124.62, 127.80, 128.13, 128.53, 129.80, 131.00, 139.52, 143.35, 147.45, 148.79, 157.69, 166.58, 168.44 (2<u>C</u>=O) ppm.

*(Z)-2-((4-acetyl-5-methyl-5-phenyl-4,5-dihydro-1,3,4-thiadiazol-2-yl)amino)-5-(3-nitro-benzylidene)thiazol-4(5H)-one (**8j**)*

Light orange solid; yield: 72 %; mp 180-182 °C; FT-IR (ATR, cm^{-1}) ν_{max}: 1526 (N-O), 1718 (C=O), 3430 (N-H); ^{1}H NMR (400 MHz, $CDCl_3$) δ: 2.46 (s, 3H, CH_3), 2.48 (s, 3H, CH_3), 7.27 – 7.51 (m, 5H, ArH), 7.66 – 7.70 (m, 1H, ArH), 7.83 – 7.85 (m, 2H, ArH), 8.28 – 8.31 (m, 1H, ArH), 8.47 (s, 1H, arylidene-H) ppm, ^{13}C NMR (100 MHz, $CDCl_3$) δ: 24.34, 27.46 (2<u>C</u>H$_3$), 84.04, 123.71, 124.82, 125.12, 128.17, 128.56, 130.43, 131.29, 134.72, 136.41, 148.74, 149.15, 154.78, 165.50 (2<u>C</u>=O) ppm.

*(Z)-2-((4-acetyl-5-methyl-5-phenyl-4,5-dihydro-1,3,4-thiadiazol-2-yl)amino)-5-(3,4-dimethoxybenzylidene)thiazol-4(5H)-one (**8k**)*

Yellow solid; yield: 78 %; mp 186-187 °C; FT-IR (ATR, cm^{-1}) ν_{max}: 1267 (O-C), 1692 (C=O), 3430 (N-H); ^{1}H NMR (400 MHz, $CDCl_3$) δ: 2.38 (s, 3H, CH_3), 2.47 (s, 3H, CH_3), 3.91 (s, 3H, OCH_3), 3.95 (s, 3H, OCH_3), 6.95 – 6.97 (m, 1H, ArH), 7.04 (s, 1H, ArH), 7.17-7.19 (m, 1H, ArH), 7.27 – 7.37 (m, 3H, ArH), 7.49 – 7.51 (m, 2H, ArH), 7.79 (s, 1H, arylidene-H) ppm; ^{13}C NMR (100 MHz, $CDCl_3$) δ: 24.31, 27.34 (2<u>C</u>H$_3$), 55.86, 56.11 (2O<u>C</u>H$_3$), 83.65, 111.44, 112.31, 119.53, 125.13, 125.46, 125.90, 128.10, 128.50, 135.38, 142.85, 149.45, 149.56, 151.65, 156.79, 166.54, 168.87 (2<u>C</u>=O) ppm.

*(Z)-2-((4-acetyl-5-methyl-5-phenyl-4,5-dihydro-1,3,4-thiadiazol-2-yl)amino)-5-(4-(dimethylamino)benzylidene)thiazol-4(5H)-one (**8l**)*

Orange solid; yield: 71 %; mp 229-231 °C; FT-IR (ATR, cm^{-1}) ν_{max}: 1713 (C=O), 3581 (N-H); ^{1}H NMR (400 MHz, DMSO-d_6) δ: 2.35 (s, 3H, CH_3), 2.40 (s, 3H, CH_3), 3.02 (s, 6H, N-2CH_3), 6.81 – 6.83 (m, 2H, ArH), 7.27 – 7.40 (m, 3H, ArH), 7.43 – 7.48 (m, 4H, ArH), 7.62 (s, 1H, arylidene-H), 12.60 (s, 1H, NH) ppm; ^{13}C NMR (100 MHz, DMSO-d_6) δ: 24.08, 27.06 (2<u>C</u>H$_3$), 82.93, 112.09, 115.70, 119.87, 124.62, 127.73, 128.53, 132.48, 133.96, 134.36, 143.54, 149.10, 151.57, 167.17, 168.19 (2<u>C</u>=O) ppm.

*(Z)-2-((4-acetyl-5-methyl-5-phenyl-4,5-dihydro-1,3,4-thiadiazol-2-yl)amino)-5-((E)-3-(4-(dimethylamino)phenyl)allylidene)thiazol-4(5H)-one (**8m**)*

Brown solid; yield: 73 %; mp 232-234 °C; FT-IR (ATR, cm^{-1}) ν_{max}: 1715 (C=O), 3405 (N-H); ^{1}H NMR (400 MHz, DMSO-d_6) δ: 2.35 (s, 3H, CH_3), 2.39 (s, 3H, CH_3), 2.99 (s, 6H, N-2CH_3), 6.74 – 6.83 (m, 3H, ArH), 7.19 – 7.23 (m, 1H, ArH), 7.99 – 7.31 (m, 1H, ArH), 7.36 – 7.42 (m, 4H, ArH), 7.45 (s, 1H, alkene-H), 7.53 (s, 1H, alkene-H), 7.55 (s, 1H, alkene-H), 12.56 (s, 1H, NH) ppm; ^{13}C NMR (100 MHz, DMSO-d_6) δ: 23.97, 26.75 (2$\underline{C}H_3$), 82.50, 124.28, 127.40, 128.20, 129.42, 134.10, 143.24, 145.01, 148.75, 158.11, 16612,168.06 (2$\underline{C}$=O) ppm.

*(Z)-2-((4-acetyl-5-methyl-5-phenyl-4,5-dihydro-1,3,4-thiadiazol-2-yl)amino)-5-(furan-2-ylmethylene)thiazol-4(5H)-one (**8n**)*

Yellow solid; yield: 76 %; mp 219-221 °C; FT-IR (ATR, cm^{-1}) ν_{max}: 1701 (C=O), 3581 (N-H); ^{1}H NMR (400 MHz, DMSO-d_6) δ: 2.34 (s, 3H, CH_3), 2.40 (s, 3H, CH_3), 6.75 – 6.77 (m, 1H, furyl-H), 7.11 – 7.12 (d, 1H, furyl-H), 7.27 – 7.44 (m, 5H, ArH),7.58 (s, 1H, arylidene-H), 8.06 (d, 1H, furyl-H), 12.72 (s, 1H, NH) ppm; ^{13}C NMR (100 MHz, DMSO-d_6) δ: 24.00, 27.05 (2$\underline{C}H_3$), 83.08, 113.70, 118.98, 120.67, 124.61, 127.76, 128.54, 143.47, 147.68, 149.04, 149.49, 159.65, 166.73, 168.25 (2$\underline{C}$=O) ppm.

*(Z)-2-((4-acetyl-5-methyl-5-phenyl-4,5-dihydro-1,3,4-thiadiazol-2-yl)amino)-5-(3-chloro-benzylidene)thiazol-4(5H)-one (**8o**)*

Orange solid; yield: 85 %; mp 212-214 °C; FT-IR (ATR, cm^{-1}) ν_{max}: 1726 (C=O), 3581 (N-H); ^{1}H NMR (400 MHz, DMSO-d_6) δ: 2.33 (s, 3H, CH_3), 2.40 (s, 3H, CH_3), 7.27 – 7.45 (m, 5H, ArH), 7.56 – 7.63 (m, 3H, ArH), 7.71 (s, 1H, ArH), 7.75 (s, 1H, arylidene-H), 12.95 (s, 1H, NH) ppm; ^{13}C NMR (100 MHz, DMSO-d_6) δ: 23.96, 27.06 (2$\underline{C}H_3$), 83.21, 124.63, 125.78, 127.81, 128.55, 128.70, 129.44, 130.03, 130.91, 131.18, 133.94, 135.41, 143.39, 148.98, 166.73, 168.21 (2$\underline{C}$=O) ppm.

*(Z)-2-((4-acetyl-5-methyl-5-phenyl-4,5-dihydro-1,3,4-thiadiazol-2-yl)amino)-5-(2-fluoro-benzylidene)thiazol-4(5H)-one (**8p**)*

Yellow crystals; yield: 81 %; mp 185-186 °C; FT-IR (ATR, cm^{-1}) ν_{max}: 1697 (C=O), 3491 (N-H); ^{1}H NMR (400 MHz, DMSO-d_6) δ: 2.30 (s, 3H, CH_3), 2.40 (s, 3H, CH_3), 7.27 – 7.31 (m, 1H, ArH), 7.36 – 7.45 (m, 6H, ArH), 7.54 – 7.64 (m, 2H, ArH), 7.75 (s, 1H, arylidene-H), 12.93 (s, 1H, NH) ppm; ^{13}C NMR (100 MHz, DMSO-d_6) δ: 23.62, 26.75 (2$\underline{C}H_3$), 82.93,

116.13, 120.80, 123.24, 124.31, 125.07, 126.17, 127.48, 128.22, 128.86, 132.52, 132.61, 143.07, 148.54, 157.81, 158.94, 161.45, 166.31, 167.97 (2C=O) ppm.

*(Z)-2-((4-acetyl-5-methyl-5-phenyl-4,5-dihydro-1,3,4-thiadiazol-2-yl)amino)-5-(thiophen -2-ylmethylene)thiazol-4(5H)-one (**8q**)*

Yellow solid; yield: 89 %; mp 222-225 °C; FT-IR (ATR, cm^{-1}) ν_{max}: 1701 C=O, 3489 NH; ^1H NMR (400 MHz, DMSO-d_6) δ: 2.38 (s, 3H, CH_3), 2.41 (s, 3H, CH_3), 7.28 – 7.46 (m, 5H, ArH, 1H, thienyl-H), 7.72 – 7.73 (d, 1H, thienyl-H), 8.05 (m, 1H, thienyl-H), 8.06 (s, 1H, arylidene-H), 12.79 (s, 1H, NH) ppm; ^{13}C NMR (100 MHz, DMSO-d_6) δ: 24.07, 27.07 (2CH_3), 83.04, 121.01, 124.62, 125.99, 127.79, 128.56, 129.02, 133.64, 135.33, 137.37, 143.46, 149.09, 157.94, 166.70, 168.23 (2C=O) ppm.

*(Z)-2-((4-acetyl-5-methyl-5-phenyl-4,5-dihydro-1,3,4-thiadiazol-2-yl)amino)-5-(pyridin-2-ylmethylene)thiazol-4(5H)-one (**8r**)*

Orange solid; yield: 68 %; mp 213-215 °C; FT-IR (ATR, cm^{-1}) ν_{max}: 1716 (C=O), 3406 (N-H); ^1H NMR (400 MHz, DMSO-d_6) δ: 2.33 (s, 3H, CH_3), 2.41 (s, 3H, CH_3), 7.28 – 7.45 (m, 5H, ArH), 7.58 – 7.59 (m, 2H, ArH); 7.72 (s, 1H, arylidene-H), 8.74 – 8.75 (m, 2H, ArH) 12.94 (s, 1H, NH) ppm; ^{13}C NMR (100 MHz, DMSO-d_6) δ: 24.04, 27.07 (2CH_3), 83.38, 123.58, 124.63, 127.82, 128.56, 129.03, 129.33, 140.54, 143.36, 148.79, 150.39, 157.74, 166.56, 168.39 (2C=O) ppm.

*(Z)-2-((4-acetyl-5-methyl-5-phenyl-4,5-dihydro-1,3,4-thiadiazol-2-yl)amino)-5-(3-methoxybenzylidene)thiazol-4(5H)-one (**8s**)*

Yellow solid; yield: 71 %; mp 180-182 °C; FT-IR (ATR, cm^{-1}) ν_{max}: 1229 (O-C), 1721 (C=O), 3430 (N-H); ^1H NMR (400 MHz, DMSO-d_6) δ: 2.31 (s, 3H, CH_3), 2.40 (s, 3H, CH_3), 3.80 (s, 3H, OCH_3), 7.06 – 7.08 (m, 1H, ArH), 7.20 – 7.31 (m, 3H, ArH), 7.36 – 7.46 (m, 5H, ArH), 7.74 (s, 1H, arylidene-H), 12.84 (s, 1H, NH) ppm; ^{13}C NMR (100 MHz, DMSO-d_6) δ: 23.95, 27.08 (2CH_3), 55.25 (OCH_3), 83.07, 114.64, 116.84, 122.74, 123.99, 124.62, 127.79, 128.55, 130.44, 132.71, 134.49, 143.44, 148.96, 158.43, 159.69, 166.87, 168.18 (2C=O) ppm.

*(Z)-2-((4-acetyl-5-methyl-5-phenyl-4,5-dihydro-1,3,4-thiadiazol-2-yl)amino)-5-(4-chloro-benzylidene)thiazol-4(5H)-one (**8t**)*

Yellow solid; yield: 89 %; mp 203-206 °C; FT-IR (ATR, cm^{-1}) ν_{max}: 1715 (C=O), 3392 (N-H); ^1H NMR (400 MHz, DMSO-d_6) δ: 2.33 (s, 3H, CH_3); 2.40 (s, 3H, CH_3); 7.28 – 7.45 (m,

5H, ArH); 7.60 – 7.67 (m, 4H, ArH); 7.75 (s, 1H, arylidene-H), 12.87 (s, 1H, NH) ppm; ^{13}C NMR (100 MHz, DMSO-d_6) δ: 24.05, 27.07 (2<u>C</u>H$_3$), 83.24, 124.56, 124.64, 127.81, 128.55, 129.42, 131.26, 131.76, 132.12, 135.09, 143.41, 148.88, 158.16, 166.79, 168.36 (2<u>C</u>=O) ppm.

*(Z)-2-((4-acetyl-5-methyl-5-phenyl-4,5-dihydro-1,3,4-thiadiazol-2-yl)amino)-5-((E)-3-(4-methoxyphenyl)allylidene)thiazol-4(5H)-one (**8u**)*

Orange solid; yield: 86 %; mp 232-234 °C; FT-IR (ATR, cm^{-1}) ν_{max}: 1241 (O-C), 1701 (C=O), 3581 (N-H); ^{1}H NMR (400 MHz, DMSO-d_6) δ: 2.35 (s, 3H, CH$_3$), 2.39 (s, 3H, CH$_3$), 3.80 (s, 3H, OCH$_3$), 6.87 (m, 1H, alkene-H), 6.97– 6.99 (m, 2H, ArH), 7.24 – 7.31 (m, 2H, ArH), 7.36 – 7.46 (m, 5H, ArH), 7.63 (d, 1H, alkene-H), 7.65 (d, 1H, alkene-H), 12.61 (s, 1H, NH) ppm; ^{13}C NMR (100 MHz, DMSO-d_6) δ: 24.31, 27.08 (2<u>C</u>H$_3$), 55.35 (O<u>C</u>H$_3$), 82.92, 114.49, 120.76, 122.84, 124.61, 127.74, 128.34, 128.53, 129.75, 133.61, 143.52, 144.12, 149.01, 158.30, 160.78, 166.47, 168.43 (2<u>C</u>=O) ppm.

*(Z)-2-((4-acetyl-5-methyl-5-phenyl-4,5-dihydro-1,3,4-thiadiazol-2-yl)amino)-5-((E)-3-phenylallylidene)thiazol-4(5H)-one (**8v**)*

Orange solid; yield: 86 %; mp 229-231 °C; FT-IR (ATR, cm^{-1}) ν_{max}: 1717 (C=O), 3581 (N-H); ^{1}H NMR (400 MHz, DMSO-d_6) δ: 2.35 (s, 3H, CH$_3$), 2.39 (s, 3H, CH$_3$), 7.03 – 7.09 (m, 1H, alkene-H), 7.26 – 7.40 (m, 5H, ArH), 7.42 – 7.48 (m, 5H, ArH), 7.67 (d, 1H, alkene-H), 7.69 (d, 1H, alkene-H), 12.69 (s, 1H, NH) ppm; ^{13}C NMR (100 MHz, DMSO-d_6) δ: 24.3, 27.0 (2<u>C</u>H$_3$), 82.99, 123.08, 124.60, 127.75, 127.91, 128.53, 128.95, 129.81, 132.90, 135.58, 143.49, 143.96, 148.97, 158.16, 166.45, 168.44 (2<u>C</u>=O) ppm.

3.3. References

[1] W. Hunter, D. Herndon, Mobile terminals for supplementing game module resources and methods and computer program products for operating the same, US Patent No. US 20070015580 A1 (2005).

[2] P. Vicini, A. Geronikaki, K. Anastasia, M. Incerti, F. Zani, Synthesis and antimicrobial activity of novel 2-thiazolylimino-5-arylidene-4-thiazolidinones, Bioorganic and medicinal chemistry, 14 (2006) 3859.

[3] A.A. Geronikaki, A.A. Lagunin, D.I. Hadjipavlou-Litina, P.T. Eleftheriou, D.A. Filimonov, V.V. Poroikov, I. Alam, A.K. Saxena, Computer-aided discovery of anti-inflammatory thiazolidinones with dual cyclooxygenase/lipoxygenase inhibition, Journal of medicinal chemistry, 51 (2008) 1601.

[4] Y. Momose, K. Meguro, H. Ikeda, C. Hatanaka, S. Oi, T. SOHDA, Studies on antidiabetic agents. X. Synthesis and biological activities of pioglitazone and related compounds, Chemical and pharmaceutical bulletin, 39 (1991) 1440.

[5] G. Bruno, L. Costantino, C. Curinga, R. Maccari, F. Monforte, F. Nicolo, R. Ottana, M. Vigorita, Synthesis and aldose reductase inhibitory activity of 5-arylidene-2, 4-thiazolidinediones, Bioorganic and medicinal chemistry, 10 (2002) 1077.

Chapter 4
Screening against kinases and cancer cell-lines

4.1. *In vitro* evaluation against kinase targets (CDK and Abl)

All the synthesized final compounds (**8a-v**) were evaluated for *in vitro* CDK2/ cyclin E and Abelson murine leukaemia (Abl) kinase inhibitory activity as well as anti-proliferative activity against K-562 (chronic myelogeneous leukaemia), and MCF-7 cell lines. The data obtained are shown in **Table 4**.

Table 4: Kinase (CDK2/E and Abl) inhibition and anti-proliferative activity data of the final compounds (**8a-v**).

Compounds	IC_{50} (μM)[a]		Cytotoxicity in cancer cell lines GI_{50} (μM)[a]	
	CDK2/E	Abl	K-562	MCF-7
8a	5.1	>25	>6.25	>6.25
8b	3.2	>25	>6.25	>6.25
8c	6.0	>25	>6.25	>6.25
8d	3.8	>25	>6.25	>6.25
8e	6.3	>25	>6.25	>6.25
8f	4.4	>25	>6.25	>6.25
8g	5.8	>25	>6.25	>6.25
8h	3.1	>25	>6.25	>6.25
8i	3.2	>25	>6.25	>6.25
8j	10.4	>12.5	>6.25	>6.25
8k	3.6	>12.5	>6.25	>6.25
8l	4.6	>25	>6.25	>6.25
8m	8.6	>25	>6.25	>6.25
8n	17.2	>25	>6.25	>6.25
8o	3.9	>25	>6.25	>6.25
8p	5.8	>25	>6.25	>6.25
8q	4.1	>25	>6.25	>6.25
8r	9.7	>25	>6.25	>6.25
8s	3.3	>25	>6.25	>6.25
8t	3.4	>25	>6.25	>6.25
8u	3.5	>25	>6.25	>6.25
8v	4.5	>25	>6.25	>6.25
Roscovitine	**0.1**	**>100**	**42**	**11**
Imatinib	**>100**	**0.2**	**0.5**	**>10**

[a]IC_{50} values were determined in triplicate in the range of 0.05 to 100 μM. IC_{50} value indicates concentration (μM) that inhibits activity of tested enzyme to 50% or for cytotoxic assays, concentration (μM) that reduces 50% of cells during a three-day cultivation.

Most of the synthesized compounds displayed good inhibitory effect against CDK2 at the micromolar level. These derivatives could be ideal starting point molecules toward the development of novel anticancer agents. As the total number of evaluated compounds is quite appreciable, a meaningful structure-activity relationship (SAR) was established and potent active members in the series were identified. A positive correlation was observed between the effect of diversified substituents on aromatic ring/bioisosteric replacement and inhibitory

potential of CDK2/E. Of the 22 evaluated derivatives, 10 compounds showed potent CDK2/E inhibition with IC_{50} ranging from 3.1 to 4.1 µM. Compounds bearing electron-withdrawing halogens (Cl) and weak electron donating groups (OCH_3) bound on their aromatic ring showed more potency. Among the halogenated derivatives, chlorine in the *ortho* position of the aromatic ring (**8h**) demonstrated higher potency (IC_{50} = 3.1 µM) followed the same chlorine on the *para*- (**8t**) and *meta* (**8o**) position resulted IC_{50} values 3.4 µM and 3.9 µM, respectively.

Substitution using other halogens such as fluorine or bromine showed a moderate inhibition (IC_{50}) at 5.8 µM (**8p**) and 6.3 µM (**8e**), respectively. In comparison with chlorine, the methoxy substituent also equally contributed to the inhibitory potential of the final compounds. Remarkably, compound **8b** and **8s** bearing OCH_3 at *para* and *meta* position of the aromatic ring showed higher inhibition at 3.2 and 3.3 µM, respectively. Elongation of the linker by two carbon distance (**8u**) did not exhibit a substantial improvement in the activity against CDK2 (IC_{50} = 3.5 µM) even when the methoxy substituent was retained at the para position. Similarly, dimethoxy substitution on different positions of the ring (**8k** and **8d**) did not show any significance effect. The introduction of an additional aromatic ring (**8f**), and an extended conjugation with two carbon distance on the thiazolone moiety (**8v**) resulted in moderate inhibition of CDK2 (IC_{50} = 4.5 µM). However, for unsubstituted derivative **8a** there was a low potency (IC_{50} = 5.1 µM). Compounds substituted with weak electron donating groups (CH_3 and N-$(CH_3)_2$) on para position of the aromatic ring (**8g** and **8l**) displayed moderate inhibition. Exocyclic conjugation with additional two carbons (**8l**) resulted in the formation of **8m** which demonstrated lower inhibition (IC_{50} = 8.6 µM).

As shown in **Table 4**, **8i** the compound bearing a nitro (strong electron withdrawing) group on para position of the aromatic ring exhibited potent inhibitory effect with an impressive IC_{50} value of 3.2 µM. Surprisingly, the nitro substituent at *meta* position of the aromatic ring (**8j**) showed lower CDK2 inhibition (IC_{50} = 10.4 µM). Bioisosteric replacement of phenyl ring (**8a**) with thiophene (**8q**) retained its inhibitory potential with an IC_{50} of 4.1 µM. Whereas, replacing a phenyl group with other heterocycles such as 2-pyridyl (**8r**) and furan (**8n**) resulted in lower activity compared to other synthesized compounds. Conversely, when comparing the inhibitory profiles of the synthesized compounds **8a-v** against the standard imatinib, they were all highly active CDK2 inhibitors.

4.1.1. SAR Analysis

The SAR of the synthesized compounds **8a-v** and their *in vitro* CDK2/ cyclin E profiles are presented in **Fig. 27**.

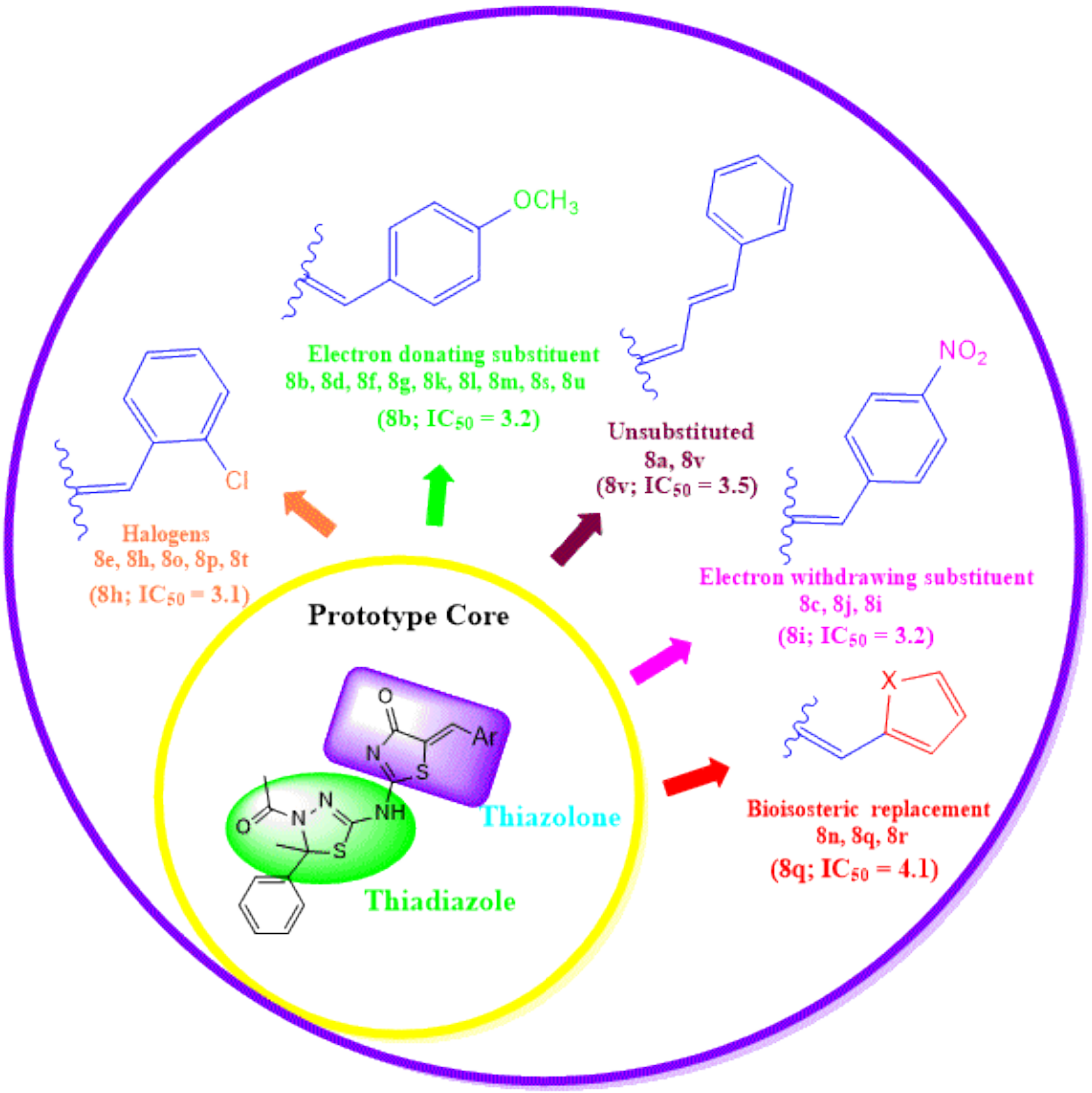

Figure 27: SAR of **8a-v** against CDK2.

Surprisingly, a couple of compounds (**8j** and **8k**) exhibited moderate inhibition (IC_{50} >12.5 µM) against the Abl kinase compared with the standard imatinib (IC_{50} = 0.2 µM). However, these compounds can be considered as potent compounds when compared with standard roscovitine (IC_{50} >100 µM). All other derivatives in this series exhibited poor inhibition of Abl kinase (IC_{50} >25 µM). Interestingly, all the synthesized compounds **8a-v** exhibited good anti-proliferative activity (IC_{50} >6.25 µM) against both the K-562 and MCF-7 cell lines. When compared to the standard drugs (roscovitine and imatinib), the compounds **8a-v** showed great inhibitory profiles. When they were further evaluated against MCF-7 cell line they showed an impressive inhibitory effect suggesting that they can be potential anti-

breast cancer hit compounds. It was also observed that the inhibitory profiles of the **8a-v** were higher (IC_{50} >6.25 µM) against K-562 when compared to the standard roscovitine (IC_{50} = 42 µM).

4.2. Experimental (*in vitro*)

4.2.1. *In vitro* evaluation against CDK2 and Abl kinase

Kinase assays were performed using a 96-well plate setup with recombinant CDK-cyclin complexes generated on the Cyclacel. CDK2 and Abl assays were performed using an assay buffer consisting of 25 mM *b*-glycerolphosphate, 20 mM MOPS, 5 mM EGTA, 1 mM DTT, and 1 mM NaVO3 at pH 7.4. To this buffer, 2–4 µg of active enzyme was added with an appropriate substrate (purified histone H1 for CDK2/cyclin, Abl). Ice was used to stop the reaction, then 50 mg avidin was added to each well and incubated for 10 min, the solution was filtered through p81 or GF/C filter plates (WhatmanPolyfiltronics). Then the plate was washed three times with 75 mM aqueous orthophosphoric acid, and dried. The scintillant (Microscint 40) was then added, and incorporated radioactivity measured with a scintillation counter (TopCount; Packard Instruments). CDK2 and Abelson murine leukemia viral oncogene homolog-1 (Abl-1) were assayed using commercial assay kits (AmershamBiotrak CDK2 and Abl1 assay kits). Data was analyzed using curve-fitting software (GraphPad Prism version 3.00 for Windows) to determine IC_{50} values (concentrations inhibiting kinase activity by 50%) [1].

4.2.2. Anti-proliferative activity against K-562 and MCF-7 cell lines

The tumour cells (purchased from the American Type Culture Collection and the German Collection of Microorganisms and Cell Cultures) were grown in DMEM medium (Gibco BRL) supplemented with 10% (v/v) fetal bovine serum and L-glutamine (0.3 g/L). The tumour cells were then maintained at 37°C in a humidified atmosphere with 5% CO_2. For anticancer cytotoxicity estimations, 104 cells were seeded into each well of a 96-well plate, and they were allowed to stabilize for atleast 4 h. Test inhibitors were then added at different concentrations (ranging from 0.1 to 100 µM) in triplicate. Three days after addition of the inhibitors, calcein AM solution (Molecular Probes) was added. An hour later, fluorescence of cells was quantified using a Fluoroskan Ascent (Labsystems) reader. Cytotoxic effective concentrations were calculated and expressed as IC_{50} values deduced from the dose-response curves. The p53 status of the cell lines was considered to be wild-type or mutant (including

deletions) according to the literature [2, 3]. Roscovitine and imatinib were used as reference drugs.

4.3. *In silico* evaluation against CDK

To get an insight into the binding motif of the active compounds with the CDK2 protein, a molecular docking was performed. Glide program of Schrodinger-Maestro 11.2 was employed for validation of the docking protocols and to reproduce the orientation of *R*-roscovitine reported in the PDB structure (ID: 2A4L). The pose of *R*-roscovitine obtained from the docking results revealed similar molecular interactions as reported in the literature [3]. The docked complex presented characteristic hydrogen bonding (H-bond) interactions with crucial active-site residues. A strong H-bond (1.91 Å) was observed between benzylamino NH- of *R*-roscovitine with a hinge residue (Leu83), whereas a weak H-bond (2.39 Å) was demonstrated by C=O (*R*-roscovitine) with a ring N of the same residue (Leu83). Similarly, Asp86 interacted with OH group of *R*-roscovitine via a strong H-bond (1.67 Å), whereas Lys89 exhibited π–cation interaction with a phenyl ring of the ligand. **Fig. 28** represents the reproduced 3D molecular interactions of the docked pose.

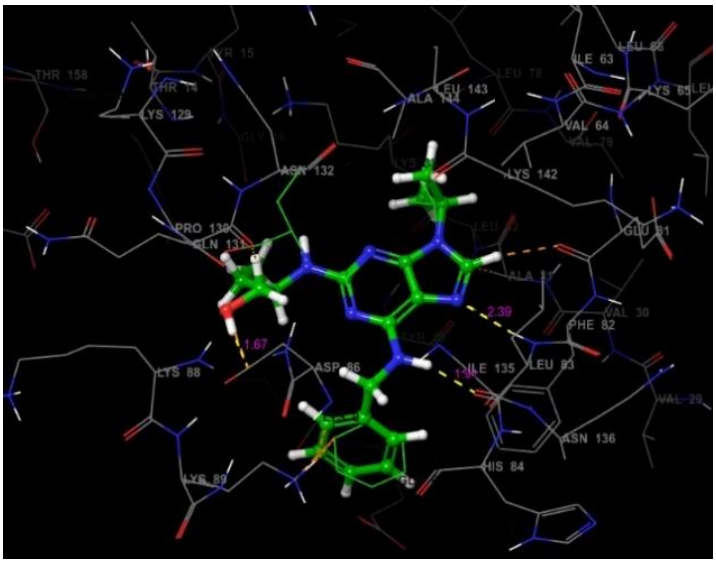

Figure 28: Reported pose (wire-frame model) and docked pose (thick tube model; green coloured) into the active-site showing similar interactions (docking validation).

The docking of the synthesized compounds with CDK2 protein revealed that they docked well into the binding-site and displayed favourable interactions with the crucial amino acid residues. The docked pose of the active compound **8u** demonstrated a strong H-bond between the carbonyl oxygen (C=O) of thiazolone motif and –HN- of Asn132 at a distance of

2.08 Å. The thiadiazole moiety settled well in the binding-site surrounded by the residues of Asp127, Gly131, Glu162, Val164, and Thr165 showing hydrophobic interactions. The extended conjugation from the thiazolone moiety guided the phenolic ring to orient towards aromatic amino acid residues Phe80, Phe82, and His84. There were no significant H-bond interactions identified with the other H-bond donors, for example, the phenolic hydroxyl and secondary amino groups.

In the case of the moderately active compound **8m**, the C=O of thiazolone displayed two H-bond interactions with Asn132 (1.96 Å) and Lys129 (2.53 Å), respectively. The hydrophobic interactions were observed for the thiadiazole moiety with the residues of Thr14, Thr158, Glu162, Val163 and Val164. The extended conjugation in the thiazolone directed the *N*,*N*-dimethylamino to orient towards aromatic amino acid residues Phe80, Phe82, and His84. The compound **8n** (least active) showed an orientation of docked pose that is different from **8u** (active) and **8m** (moderately active). The C=O of thiazolone motif and H-bond donating secondary amine (NH-) of **8n** displayed H-bond interactions toward Lys33 (NH-) and Gln131 (C=O), respectively. The furyl ring exhibited a π–π interaction with an aromatic residue Phe80. From the docking results, it was deduced that the molecular interaction of the synthesized compounds with the basic residue Asn132 is very crucial in influencing the *in vivo* CDK2 inhibition of the compounds. **Fig. 29** presents the different molecular interactions of **8u**, **8m** and **8n** with the active site residues of CDK-2 protein (PDB ID: 2A4L).

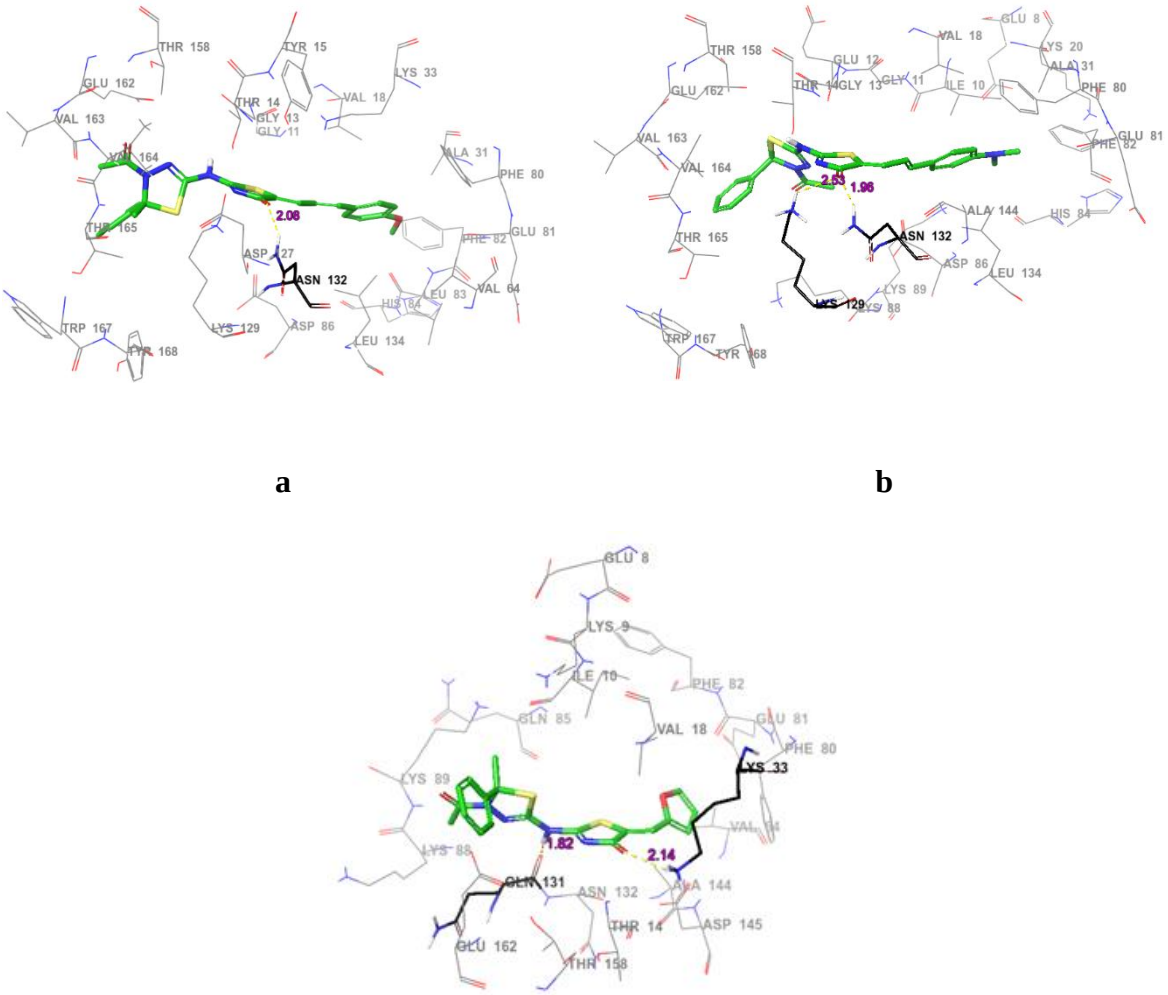

a **b**

c

Figure 29: Molecular interactions of a) active compound **8u** b) moderately active compound **8m** c) less active compound **8n** into the binding site of CDK2/cyclin E protein. Nonpolar hydrogens were hidden for clarity and yellow dashed line indicate H bond.

4.4. Experimental (*in silico*)

4.4.1. Molecular docking simulation

Molecular docking was performed using Glide software package [4] implemented in Schrodinger Suite (2017-2) (Schrödinger, Inc., USA) running on Intel CORE i7 based hpZ230 workstation with the Microsoft Windows 10 OS. In this protocol, the protein structure was kept rigid, while the ligands were allowed to flex throughout the simulation.

4.4.2. Protein preparation

The X-ray solved protein crystal structure of CDK2 bound with *R*-roscovitine was retrieved from PDB bearing ID 2A4L [5, 6]. The protein was automatically prepared by Protein Preparation Wizard of Glide via the Optimized Potentials for Liquid Simulations 3 (OPLS3) forcefield. During the pre-processing stage, crystallographic water molecules were removed and missing hydrogen atoms were added to the protein structure corresponding to pH 7.0. The protein's metal ions and cofactors were also viewed and removed from the protein structure. This tool neutralized the side chains that were far from the binding cavity and that did not participate in salt bridges. The pre-processed protein structure was initially refined by optimizing the sample-water orientation followed by restrained minimization of co-crystallized complex using OPLS3. This process reoriented the side chain hydroxyl groups and alleviated potential steric clashes. Thus, the complex obtained was minimized until it reached the convergent of heavy atom to RMSD 0.3 Å and finally taken in .mae format.

4.4.3. Grid file generation

Receptor-grid generation protocol of Maestro 11.2 was used to define the binding-site of the protein for docking simulation. This was done by excluding any co-crystallized metals, co-factors, water molecules that might have crystallized during experimental crystallization of the CDK-2 protein. A grid box was generated around the centroid of the cognate ligand (*R*-roscovitine) specifying the size for the docking ligands (20 Å) with default settings.

4.4.4. Ligand preparation

Structures of the synthesized ligands and standard *R*-roscovitine were sketched using built panel of Maestro and taken in .mae format. LigPrep is a utility of Schrodinger software suit that combines tools for generating 3D structures from 1D (Smiles) and 2D (SDF) representation, searching for tautomers, steric isomers and perform a geometry minimization of the ligands. By employing Ligprep protocol, all the ligands were prepared using OPLS3 with default settings and the output file was automatically saved in .maegz format.

4.4.5. Docking simulation

For the precision and accuracy of the docking protocols, the co-crystallized ligand was extracted from the crystal structure and re-docked using Glide docking algorithm (Schrodinger Inc) in its extra precision (XP) mode with default settings without applying any constraints. A good agreement of the obtained docked pose of *R*-roscovitine with cognate ligand indicated the reliability of the selected docking parameters. Hence, by specifying the

ligands against the receptor grid, molecular docking was performed using default settings in Glide XP mode.

4.4.6. Binding mode analysis

The protein-ligand complexes were analysed to investigate various types of interactions using the XP visualizer protocol. For the best-scored ligands, the 2D and 3D plots of molecular ligand-receptor interactions were analysed for H-bond, halogen bond, salt bridges, π-π stacking, and π-cation interactions.

4.5. References

[1] V. Kryštof, I. McNae, M. Walkinshaw, P. Fischer, P. Müller, B. Vojtěšek, M. Orsag, L. Havlíček, M. Strnad, Antiproliferative activity of olomoucine II, a novel 2, 6, 9-trisubstituted purine cyclin-dependent kinase inhibitor, Cellular and molecular life sciences, 62 (2005) 1763.

[2] P.M. O'Connor, J. Jackman, I. Bae, T.G. Myers, S. Fan, M. Mutoh, D.A. Scudiero, A. Monks, E.A. Sausville, J.N. Weinstein, Characterization of the p53 tumor suppressor pathway in cell lines of the National Cancer Institute anticancer drug screen and correlations with the growth-inhibitory potency of 123 anticancer agents, Cancer research, 57 (1997) 4285.

[3] M. Olivier, R. Eeles, M. Hollstein, M.A. Khan, C.C. Harris, P. Hainaut, The IARC TP53 database: new online mutation analysis and recommendations to users, Human mutation, 19 (2002) 607.

[4] R.A. Friesner, R.B. Murphy, M.P. Repasky, L.L. Frye, J.R. Greenwood, T.A. Halgren, P.C. Sanschagrin, D.T. Mainz, Extra precision glide: Docking and scoring incorporating a model of hydrophobic enclosure for protein− ligand complexes, Journal of medicinal chemistry, 49 (2006) 6177.

[5] L. Prabhu, L. Chen, H. Wei, O. Demir, A. Safa, L.-F. Zeng, R. Amaro, B.H. O'Neil, Z.-Y. Zhang, T. Lu, Development of AlphaLISA high throughput technique to screen for small molecule inhibitors targeting protein arginine methyltransferases, Molecular biosystems, 13 (2017) 2509.

[6] W.F. Azevedo, S. Leclerc, L. Meijer, L. Havlicek, M. Strnad, S.H. Kim, Inhibition of cyclin-dependent kinases by purine analogues, The FEBS journal, 243 (1997) 518.

Chapter 5
Screening against KSP

5.1. *In vitro* evaluation against KSP

All the synthesized final compounds **8a-v** were evaluated for their potential inhibition of MT-stimulated KSP ATPase activity using established *in vitro* assay protocols [1, 2]. The data obtained for **8a-v** and K-858 (reference standard) are shown in **Table 5**.

Table 5: Inhibition of the MT-stimulated ATPase activity of KSP by the final compounds **8a-v** and K-858.

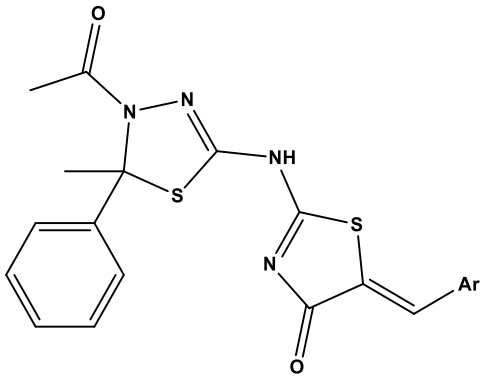

Compound	Ar	IC_{50} (µM) MIA [%]*
8a	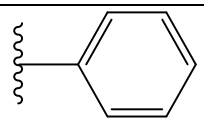	62.1 ± 17.3 (84)
8b	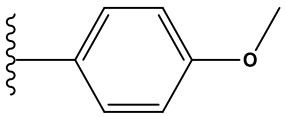	42.7 ± 14.6 (90)
8c	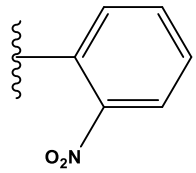	NT
8d	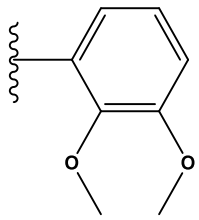	71.9 ± 19.1 (98)

8e	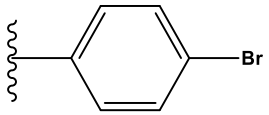	39.2 ± 13.2 **(**100)
8f	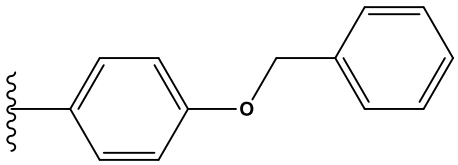	17.2 ± 5.9 (95)
8g	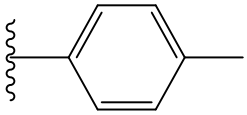	63.3 ± 19.3 (85)
8h	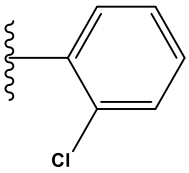	13.2 ± 2.3 (90)
8i	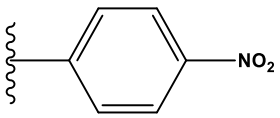	20.2 ± 3.1 **(**100)
8j	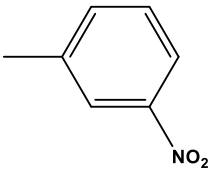	27.5 ± 7.3 (90)
8k	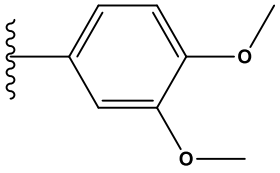	111.9 ± 16.1** 60 ^ (90)
8l	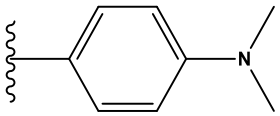	252.2 ± 159.5** 90 ^ (80)
8m	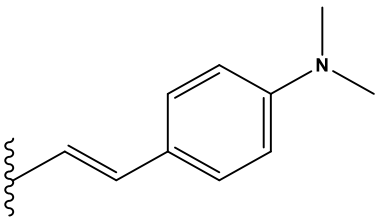	128.7 ± 73.0 **(**100)

8n	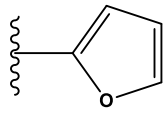	330.6 ± 217.8** 120 ^ (70)
8o	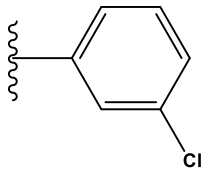	47.8 ± 14.5 (90)
8p	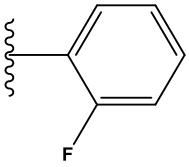	132.9 ± 77.8** 70 ^ (80)
8q	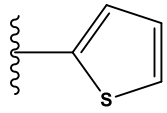	133.5 ± 129.0 (100)
8r	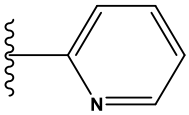	NT
8s	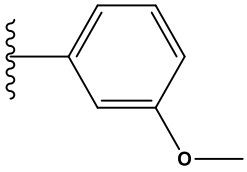	NT
8t	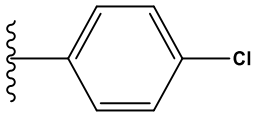	106.2 ± 47.7 (92)
8u	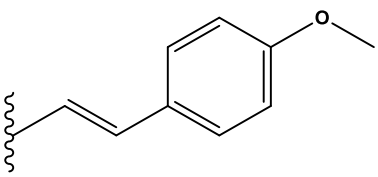	414.5 ± 101.0** 90 ^ (85)
8v	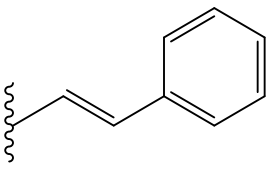	247.6 ± 61.1** 75 ^ (97)

K-858	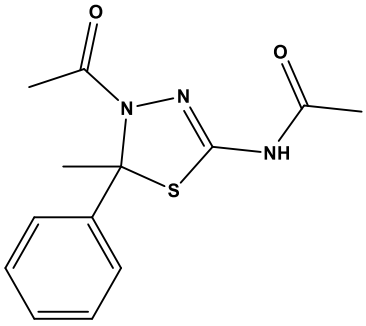	0.80 ± 0.04 (100)

*: Maximum inhibition attained in percentage.
**: IC_{50} values calculated by Kaleidagraph.
^: IC_{50} values extracted manually.
NT: not tested.

Most of the compounds displayed good to moderate inhibition (micro molar ranges) of the MT-stimulated KSP ATPase activity when compared to the standard K-858. As the total number of evaluated compounds is quite appreciable, a meaningful SAR was established. A positive correlation was recognized between the presence of diversified substituents on the aromatic ring of the thiazolone and their inhibitory potential on KSP ATPase activity.

Ten of the tested compounds showed considerable inhibition of the MT-stimulated KSP ATPase activity with IC_{50} values ranging from 13.2 to 62.1 µM. Compounds bearing electron-withdrawing groups such as halogen (Cl), nitro (NO_2), and weak electron donating groups (OCH_3, OBz) on the aromatic ring demonstrated higher inhibition activity. Within the halogenated derivatives, chlorine at the 2nd position of the aromatic ring (**8h**) showed the most significant inhibition with an IC_{50} of 13.2 µM. However, moderate (IC_{50} = 47.8 µM), and poor (IC_{50} = 106.2 µM) inhibitions were observed when the chlorine was substituted at the 3rd (**8o**) and 4th (**8t**) positions, respectively. The 4-bromo substituted analogue **8e** displayed a moderate (39.2 µM) inhibition, while a three-fold decrease (132.9 µM) in the activity was observed for fluorine at the 2nd position (**8p**). The benzyloxy substituted compound **8f** also displayed a significantly higher inhibition of the MT-stimulated KSP ATPase activity with an IC_{50} of 17.2 µM.

Compared to other electron-withdrawing substituents (e.g. chlorine), nitro-bearing compounds also showed relatively good inhibitory potential. Remarkably, compounds bearing the nitro group at 4th (**8i**) and 3rd position (**8j**) of the phenyl ring exhibited almost the same inhibition (20.2 µM and 27.5 µM, respectively). This observation indicated that there is no significant difference between these two substitutions in terms of enzyme inhibition.

Methoxy substitution (**8b**) gave a moderate inhibition with IC_{50} of 42.7 µM, while dimethoxy substitution (**8d**) (IC_{50} = 71.9 µM) did not improve the activity, rather a one-fold decrease was observed. Compounds that were unsubstituted (**8a**) or 4-methyl substituted (**8g**) presented similar IC_{50} values (~ 62 µM). Extending the exocyclic unsaturation of **8a** yielded **8v** which resulted in a decrease in potency by four-fold (IC_{50} = 247.6 µM). The latter revealed that extending the conjugation does not substantially increase the potency of a compound.

Presence of two methoxy groups at the 3rd and 4th positions of phenyl ring in **8k** displayed a weaker inhibitory effect (IC_{50} = 111.9 µM). An extended unsaturation on thiazolone with a methoxy substituent (**8u**) at position 4 showed weaker inhibition. The *N*,*N*-dimethylamino substituent on the phenyl in **8l** demonstrated poor inhibition (IC_{50} = 252.2 µM), whereas, exocyclic conjugation with additional two carbons (**8m**) resulted in one-fold increase in the potency (IC_{50} = 128.7 µM) when compared to **8l**. Bioisosteric replacement of phenyl ring of **8a** with pyridine (**8r**) or thiophene (**8q**) resulted in reduced inhibition with IC_{50} values 120 µM and 133.5 µM, respectively. Bioisosteric replacement using furan (**8n**) showed very poor or no inhibition (IC_{50} = 330.6 µM) of MT-stimulated KSP ATPase activity.

5.1.1. SAR Analysis

A brief SAR analysis revealed that the chloro substituent at 2nd position of the phenyl ring (**8h**) of the thiazolone motif exhibited higher potency followed by a highly electron-withdrawing nitro group at the 4th position (**8i**) (**Fig. 30**). The presence of an electron donating functionalities on the aromatic ring yielded relatively moderate potency. In addition, the unsubstituted compounds and analogues bearing bioisosterically-replaced moieties displayed poor inhibition of MT-stimulated ATPase activity of KSP.

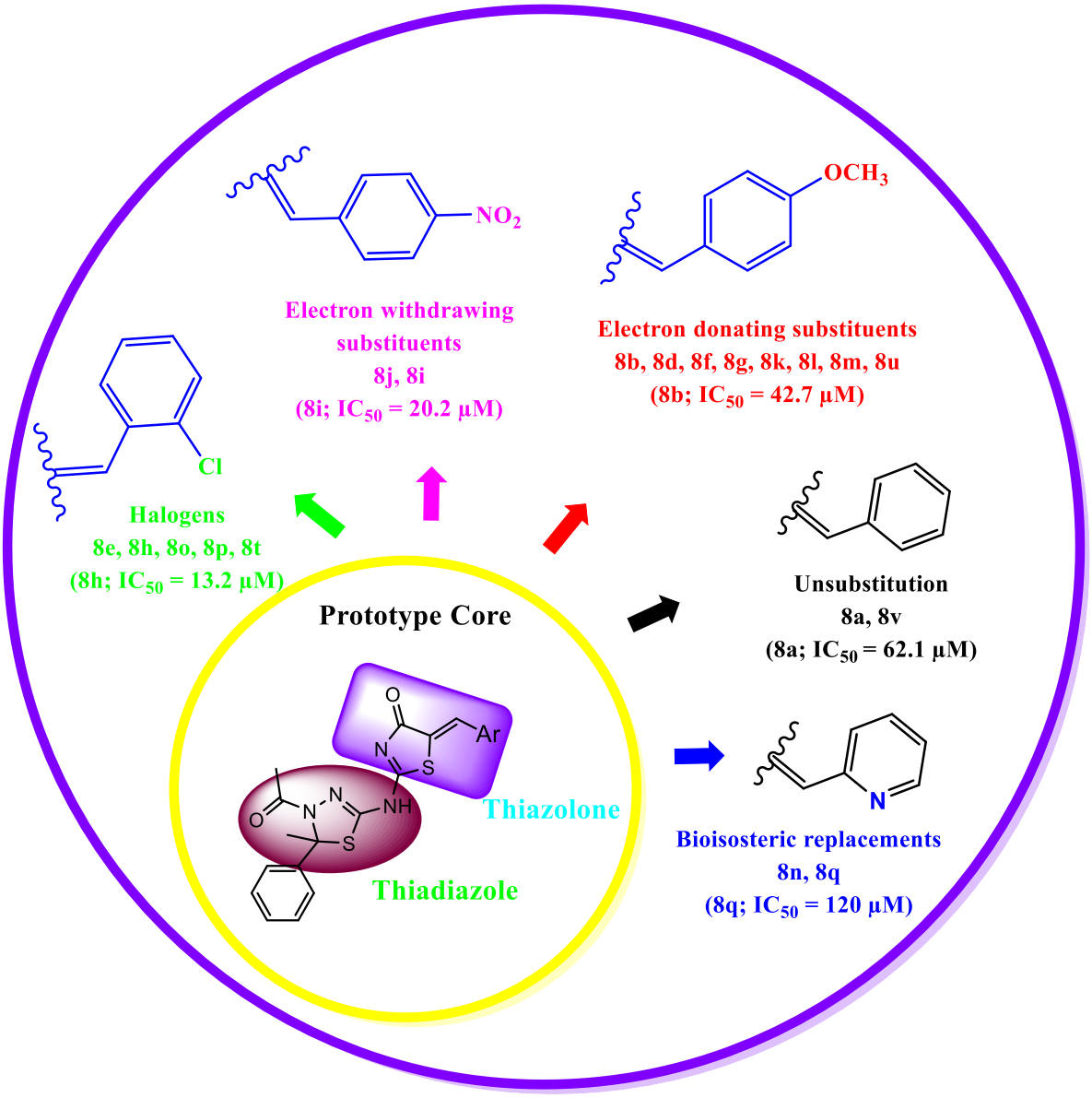

Figure 30: SAR of **8a-v** against KSP

5.2. Experimental (*in vitro*)

5.2.1. Inhibition of the MT-stimulated KSP ATPase activity

The experiments were performed at 25 °C using a 96-well Sunrise photometer (Tecan, Mannesdorf, Switzerland) with a final volume of 100 μL per well. The MT-stimulated KSP ATPase rates were measured using the pyruvate kinase/lactate dehydrogenase linked assay in the buffer A25 [25 mmol/L potassium ACES (pH 6.9), 2 mmol/L magnesium acetate, 2 mmol/L potassium EGTA, 0.1 mmol/L potassium EDTA, 1 mmol/L β-mercaptoethanol]. The amounts of KSP was optimized at 5 nM for the assay. The IC_{50} values for the inhibition of the MT-stimulated ATPase activities of KSP were measured between 1 and 200 μM for positive control (K-858). The ATP concentration was fixed at 1 mM, whilst the MT concentration was kept at 1 μM. The data was analyzed using Kaleidagraph 3.0 (Synergy Software Reading, PA) and Microsoft Excel to obtain IC_{50} values [1, 2].

5.3. *In silico* evaluation of TDT against KSP

5.3.1. Molecular docking simulation

Molecular docking simulations were performed in order to gain more insight into the binding mode of the synthesized compounds **8a-v** in the active-site of KSP and to further support the SAR study. This molecular docking was performed using X-ray crystal structure of KSP complexed with a thiophene containing inhibitor K-03 [PDB ID: 2UYM] [3]. Prior to the docking of the synthesized ligands, the protocol was validated by docking a cognate ligand (K03) into the pre-defined binding site of KSP using Glide module [4] of Schrodinger-Maestro 11.2 [5] with default settings. The docked pose of K-03 revealed a similar type of binding orientation and molecular interactions with crucial amino acid residues of KSP as that of the cognate ligand in PDB structure. Apart from exhibiting essential molecular interactions, the secondary amino NH of K03 showed a weak hydrogen bonding (2.56 Å) specifically with the carbonyl oxygen of Glu116 of KSP (**Fig. 31**).

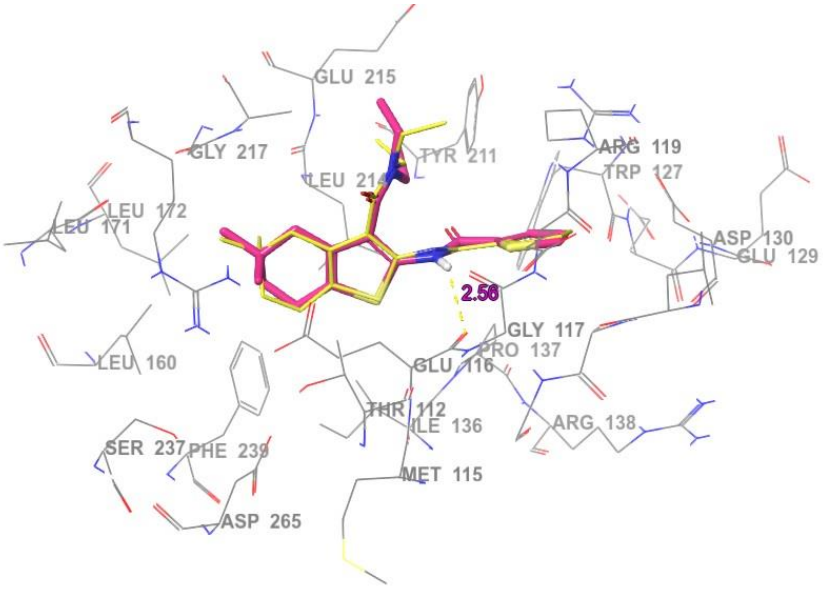

Figure 31: The docked pose of the ligand (pink coloured ball-stick model) with the pose of the native K-03 extracted from PDB (yellow coloured ball-stick model) in the active-site residues of KSP (wire-frame). Nonpolar hydrogens were hidden for clarity and the yellow dashed line indicates a hydrogen bond.

The most active compound **8h** docked well into the active site of KSP (PDB ID: 2UYM) and exhibited molecular interactions with crucial amino acid residues (**Fig. 32a**). The secondary amino NH- of **8h** demonstrated a strong H-bonding (1.75 Å) interaction with -O=C of Glu116. Furthermore, 2-chloro phenyl ring of **8h** exhibited a remarkable π-cation interaction with the basic residue Arg119 and showed hydrophobic interactions with the residues Trp127, Tyr211, and Leu132. The phenyl ring at the chiral center of thiadiazole core moiety settled well in the binding pocket surrounded by the residues of Arg221, Glu162, Tyr231, and Ser237. As expected, there is no hydrogen bonding interaction was observed for the carbonyl oxygens of **8h** towards any of the active-site residues of KSP (**Fig. 32a**).

The docked pose of weakly active compound **8u** disclosed a weak H-bonding interaction between NH- of the ligand and –O=C of Gly117 at a distance of 1.94 Å (**Fig. 32b**). Also, a π-cation interaction between the methoxy phenyl ring of **8u** and the basic residue Arg221 was observed in the docked pose. The phenyl ring on the chiral carbon of **8u** was encompassed by the active-site residues of Tyr211, Leu214, and Phe239. The methoxy phenyl substitution of **8u** was buried in the cavity formed by amino acid residues such as Thr112, Ser232, Phe239, and Asp265 (**Fig. 32b**).

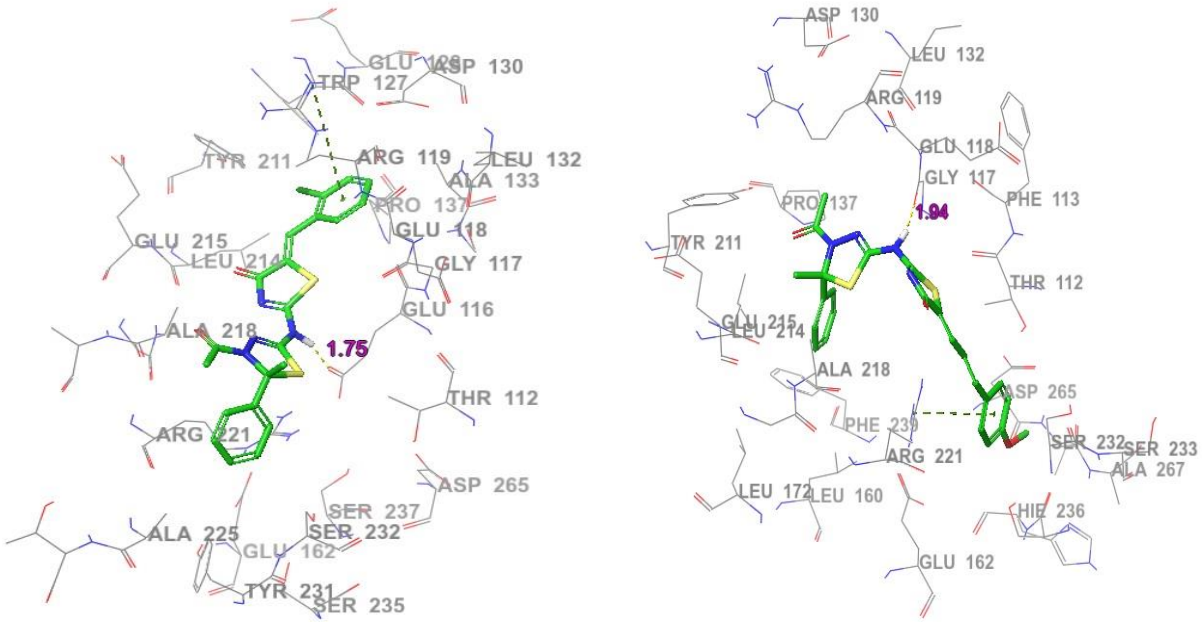

a **b**

Figure 32: 3D-molecular interactions of **a**) **8h** (more active); **b**) **8u** (weakly active) in the binding site of KSP. Nonpolar hydrogens were hidden for clarity and yellow dashed line indicates H-bond, whereas green coloured dashed lines indicate π-cation interactions.

From the docking simulations, it was deduced that H-bonding interaction of secondary amino NH- with –O=C of Glu116 is crucial for the enzyme inhibition which had a positive impact on the *in vitro* assay outcome, accordingly. Highly active compounds such as **8h** could retain this crucial H-bond interaction with the Glu116, whereas the less active compound (**8u)** could not. It is also interesting to note that a flipped orientation of the side chain phenyl ring of **8u** was observed due to the presence of an extended conjugation from thiazolone moiety (**Fig. 32b**). This flipping pattern in **8u** guided the orientation of the methoxy phenyl ring more towards the acidic amino acid residues displaying a π-cation interaction with Arg221 instead of Arg119 which was observed for the most active compound **8h**. Hence, deviation from these essential molecular interactions with specific amino acids could be a contributing factor for the weaker inhibition that **8u** exhibited in the *in vitro* assay.

5.3.2. *In silico* prediction of drug likeliness and pharmacokinetic (ADME) parameters

In order to recognize the synthesized compounds **8a-v** to be drug-like molecules, we have evaluated them against Lipinski's rule of five in which molecular properties are correlated with the oral bioavailability of a drug/drug-like compound. The QikProp of Schrodinger Maestro-11.2 [6] was used to determine the drug likeliness (Lipinski's rule of rive) and *in silico* ADME (absorption, distribution, metabolism, and excretion) parameters. The results (**Table 6**) demonstrated that all the synthesized compounds complied with the rule except **8e**, **8f** and **8m.** These compounds did not comply with a couple of the properties (molecular weight and QPlogP O/W) as they violated 1 or 2 out of 5 properties (Lipinski's rule of five). In addition, numerous drug candidates that failed during clinical trials were because of issues related to the ADME pharmacokinetic properties being violated. Human intestinal absorption (HIA) and Caco-2 permeability (QPPCaco) parameters are good indicators of drug absorbance in the intestine and Caco-2 monolayer penetration, respectively. HIA data is a sum of bioavailability and absorption obtained from the ratio of excretion or cumulative excretion in urine, bile, and feces [7]. Similarly, QPPCaco parameter is a key feature that regulates the drug metabolism and its access through the biological membranes [8]. The predicted percentages of human oral absorption for **8a-v** were 80.84% to 100% in all cases and permeability values (QPPCaco) ranged from 92.946 to 968.211 clearly indicating that all the synthesized compounds theoretically have good oral absorption.

The partition coefficient (QPlogPo/w) and water solubility (QPlogS) are thecrucial factors with regards to the absorption and distribution of the drugs in a human body. For the synthesized molecules **8a-v**, QPlogPo/w, and QPlogS values ranged from 3.188 to 5.759 and -8.093 to -4.981, respectively. Furthermore, we predicted the number of violations of Jorgensen's rule of three with the recommended parameters (QPlogS > -5.7, QPPCaco > 22 nm/s, primary metabolites < 7) [9]. Except **8n** and **8r**, most of the compounds deviated by one parameter out of three. Thus, the QikProp predicted the physico-chemically significant descriptors and pharmaceutically relevant properties, and all established that compounds **8a-v** acquire subsequent applicability as drug-like compounds for human use (**Table 6** and footnote).

Table 6: The drug likeliness and *in silico* ADME properties of synthesized compounds **8a-v** by QikProp.

Entry	Drug likeliness (Lipinski's rule of five)					*In silico* ADME by QikProp						
	Molecular weight	**QPlogPO/W[a]**	**H-bond donor**	**H-bond acceptor**	**Violation of Lipinski's rule**	**QPlogS[b]**	**QPlogHERG[c]**	**QPPCaco[d]**	**QPPMDCK[e]**	**QPlogKhsa[f]**	**% human oral absorption[g]**	**Violation of rule of three**
8a	422.519	3.891	1	7.50	0	-5.864	-6.623	916.992	992.873	0.342	100	1
8b	452.545	3.927	1	8.25	0	-5.978	-6.465	905.090	981.113	0.322	100	1
8c	467.516	3.270	1	8.50	0	-5.937	-6.501	125.105	115.654	0.298	83.632	1
8d	482.571	4.011	1	9.00	0	-5.948	-6.255	968.211	1032.439	0.308	100	1
8e	501.415	4.459	1	7.50	1	-6.720	-6.560	905.090	2602.580	0.480	93.013	1
8f	528.643	5.759	1	8.25	2	-8.093	-8.118	914.792	1000.235	0.901	87.749	1
8g	436.546	4.191	1	7.50	0	-6.425	-6.525	905.090	981.105	0.495	100	1
8h	456.964	4.319	1	7.50	0	-6.749	-6.518	905.833	2142.073	0.442	100	1
8i	467.516	3.188	1	8.50	0	-6.553	-6.591	92.946	83.865	0.305	80.838	1
8j	467.516	3.195	1	8.50	0	-6.075	-6.575	97.448	86.006	0.305	81.247	1
8k	482.571	3.908	1	9.00	0	-5.944	-6.283	916.992	921.033	0.282	100	1
8l	465.587	4.223	1	8.50	0	-6.650	-6.701	770.211	592.801	0.503	100	1
8m	491.625	5.134	1	8.50	1	-7.587	-7.188	926.505	1102.894	0.705	100	1
8n	412.480	3.200	1	8.00	0	-4.981	-6.112	926.505	1027.827	0.062	100	0
8o	456.964	4.376	1	7.50	0	-6.574	-6.521	926.505	2442.855	0.453	100	1

8p	440.509	4.091	1	7.50	0	-6.163	-6.508	905.090	1611.434	0.379	100	1
8q	428.541	3.832	1	7.50	0	-5.841	-6.251	916.992	1880.843	0.268	100	1
8r	423.507	3.321	1	8.50	0	-5.422	-6.534	728.176	796.853	0.110	100	0
8s	452.545	3.924	1	8.25	0	-5.958	-6.457	926.505	1004.805	0.318	100	1
8t	456.964	4.383	1	7.50	0	-6.607	-6.534	905.090	2420.576	0.457	100	1
8u	448.557	4.609	1	7.50	0	-6.596	-7.141	926.505	1102.894	0.523	100	1
8v	478.583	4.643	1	8.25	0	-6.707	-6.975	916.992	1089.749	0.502	100	1

[a]Predicted octanol/water partition co-efficient log p (acceptable range from -2.0 to 6.5).
[b]Predicted aqueous solubility in mol/L (acceptable range: -6.5 to 0.5).
[c]Predicted IC_{50} value for blockage of HERG K+ channels (concern below -5.0).
[d]Predicted Caco-2 cell permeability in nm/s (acceptable range: <25 is poor and >500 is great).
[e]Predicted apparent MDCK cell permeability in nm/s (acceptable range: <25 is poor and >500 is great).
[f]Prediction of binding to human serum albumin (acceptable range: -1.5 to 1.5).
[g]Percentage of human oral absorption (<25% is poor and >80% is high)

5.4. Experimental (*in silico*)

5.4.1. Molecular docking simulation

Molecular docking experiments were performed using Glide software package [4] implemented in Schrodinger Suite (2017_2) (Schrödinger, Inc., USA) unning on Intel CORE i7 based hpZ230 workstation with the Microsoft Windows 10 OS. The X-ray crystal structure of the protein was kept rigid, while the ligands were flexible throughout the simulation.

5.4.2. Protein preparation

The X-ray determined crystal structure of KSP complexed with a thiophene-containing inhibitor K-03 was retrieved from the PDB bearing ID 2UYM [3]. The protein was prepared using automatic preparation in the 'Protein Preparation Wizard' of Glide via the Optimized Potentials for Liquid Simulations 3 (OPLS3) forcefield. During the pre-processing stage, crystallographic water molecules, ADP (cofactor), and magnesium (metal ion) were removed and missing hydrogens were added to the protein structure. The tool neutralized the side chains that were far from the binding cavity and did not participate in the formation of salt bridges. The pre-processed protein structure was refined initially by optimizing the sample-water orientation followed by a restrained minimization of the co-crystallized complex using OPLS3, which reoriented the side chain hydroxyl groups and alleviated potential steric clashes. Thus, the complex obtained was minimized until it reached the convergent of a heavy atom RMSD to 0.3 Å and finally taken in a .mae format.

5.4.3. Grid file generation

Receptor-grid generation protocol of Maestro 11.2 was used to define the binding site of the protein (2UYM) for the docking simulation by excluding any co-crystallized metals, co-factors, and water molecules that may have crystallized during an experimental crystallization of KSP protein. A grid box was generated around the centroid of the cognate ligand (K-03) specifying the size (20 Å) for the docking with default settings and the output files were saved as a grid folder in .zip format.

5.4.4. Ligand preparation

Structures of the synthesized ligands and K-03 were sketched using 2D built panel of Maestro and taken in .mae format. LigPrep is a utility of Schrodinger software suit that combines tools for generating 3D structures from 1D (Smiles) and 2D (SDF) representation, searching for tautomers, steric isomers and perform a geometry minimization of the ligands. By employing

Ligprep protocol, all the ligands were prepared using OPLS3 with default settings and the output file were automatically saved in .maegz format.

5.4.5. Docking simulation

For the precision and accuracy of the docking protocols, the co-crystallized ligand (K-03) was extracted from the PDB structure (PDB ID: 2UYM) and docked using the Glide-docking algorithm (Schrodinger Inc.) in its extra precision (XP) mode without employing any specific constraints. A good correlation between the docked pose of K-08 and the cognate ligand in PDB structure was achieved in terms of binding orientation and molecular interactions with crucial amino acid residues of KSP that validated the default docking protocol for the subsequent docking of the synthesized ligands (**8a-v**). Hence, by specifying the ligands against the receptor grid, molecular docking was performed under Glide XP mode.

5.4.6. Binding mode analysis

The generated pose viewer files were imported to the Maestro interface and then all the protein-ligand complexes were investigated for various types of intermolecular (H-bond, halogen bond, salt bridges, π-π stacking, and π-cation) interactions and binding orientation, respectively by employing the XP visualizer module of Schrodinger software.

5.5. References

[1] S. Nagarajan, D.A. Skoufias, F. Kozielski, A.N. Pae, Receptor-ligand interaction-based virtual screening for novel Eg5/kinesin spindle protein inhibitors. Journal of medicinal chemistry, 55 (2012) 2561.

[2] S. K. Talapatra, N. G. Anthony, S. P. Mackay, F. Kozielski, Mitotic kinesin Eg5 overcomes inhibition to the phase I/II clinical candidate SB743921 by an allosteric resistance mechanism, Journal of medicinal chemistry, 56 (2013) 6317.

[3] A. B. Pinkerton, T. T. Lee, T. Z. Hoffman, Y. Wang, M. Kahraman, T. G. Cook, D. Severance, T.C. Gahman, S.A. Noble, A.K. Shiau R.L. Davis, Synthesis and SAR of thiophene containing kinesin spindle protein (KSP) inhibitors, Bioorganic and medicinal chemistry letters, 17 (2007), 3562.

[4] R.A. Friesner, R.B. Murphy, M.P. Repasky, L.L. Frye, J.R. Greenwood, T.A. Halgren, P.C. Sanschagrin, D.T. Mainz, Extra precision glide: docking and scoring incorporating a model of hydrophobic enclosure for protein - ligand complexes, Journal of medicinal chemistry, 49 (2006) 6177.

[5] L. Prabhu, L. Chen, H. Wei, O. Demir, A. Safa, L.F. Zeng, R. Amaro, B.H. O'Neil, Z.Y. Zhang, T. Lu, Development of AlphaLISA high throughput technique to screen for small molecule inhibitors targeting protein arginine methyltransferases, Molecular biosystems, 13 (2017) 2509.

[6] J. Bhat, S. Mondal, P. Sengupta, S. Chatterjee, *In Silico* screening and binding characterization of small molecules toward a g-quadruplex structure formed in the promoter region of c-myc oncogene, ACS omega, 2 (2017) 4382.

[7] Y.H. Zhao, J. Le, M.H. Abraham, A. Hersey, P.J. Eddershaw, C.N. Luscombe, D. Boutina, G. Beck, B. Sherborne, I. Cooper, J.A. Platts, Evaluation of human intestinal absorption data and subsequent derivation of a quantitative structure–activity relationship (QSAR) with the Abraham descriptors, Journal of pharmaceutical sciences, 90 (2001) 749.

[8] H.M. Patel, B. Sing, V. Bhardwaj, M. Palkar, M.S. Shaikh, R. Rane, W.S. Alwan, A.K. Gadad, M.N. Noolvi, R. Karpoormath, Design, synthesis and evaluation of small molecule imidazo [2, 1-b][1, 3, 4] thiadiazoles as inhibitors of transforming growth factor-β type-I receptor kinase (ALK5). European journal of medicinal chemistry, 93 (2015) 599.

[9] F. Ntie-Kang, An in silico evaluation of the ADMET profile of the StreptomeDB database. Springerplus, 2 (2013) 353.

Chapter 6
Summary and Conclusion

6.1. Summary and conclusion

Cancer is one of the dreaded diseases in mankind accounting more than 8.8 million deaths in 2015. Approximately, 70% of deaths from cancer occur in low- and middle-income countries. It is predicted that there will be 23 million new cancer cases by 2030 worldwide. Breast cancer is the second most common cancer among South African women population accounting 1 in every 26 women. Thus, social and economic burdens associated with cancers are severe at national and international levels. Hence, there is an urgent need for the development of more effective cancer therapeutics at this point of time. To accomplish this aspect, novel TDT hybrids were designed and synthesized as dual inhibitors of CDK and KSP, respectively for the cancer chemotherapy.

1,3,4-Thiadiazole analogs are reported for versatile applications in the field of pharmaceuticals, medicinal chemistry, agricultural and material chemistry. They are also reported as anticancer agents acting through the profound inhibition of different kinases (KSP and ALK5). Similarly, thiazolone is one of the pharmaceutically important scaffolds known for their diverse medicinal properties for example, they are potent inhibitors of CDK. Hence, the aim of this study was to hybridize these potential anticancer scaffolds in one molecular platform to obtain potent anticancer compounds with dual mode of action conferring minimal/no side effects.

Twenty-two novel TDT hybrid compounds (**8a-v**) were synthesized using multistep organic synthesis and well characterized by TLC, FT-IR, ^{1}H NMR, ^{13}C NMR, and HR-MS. All the title compounds (**8a-v**) were screened for their potential *in vitro* inhibition against the validated anticancer drug targets (CDK, Abl and KSP). Results obtained from these evaluations suggested that the synthesized compounds are indeed potent inhibitors of CDK and KSP confirming dual mode of action.

In chapter 2, we have performed comprehensive literature survey and presented a glimpse on different aspects such as cancer, statistics, therapy, chemotherapeutic agents, kinase targets, CDKs, KSP and molecular modelling studies. The inspiring literature reports encouraged us to design novel TDT hybrids as potential chemotherapeutic agents. In the chapter 3, we have described the synthetic strategy adopted for the synthesis of novel hybrids (**8a-v**). The designed scheme was very facile which resulted the desired compounds **8a-v** with good yields (70-89%). The title compounds (**8a-v**) were obtained by treating different aldehydes (**7a-v**) with an intermediate compound **6** (1,3,4-thiadiazol-2-yl)amino)thiazol-

4(5*H*)-one) *via* a Knoevenagel condensation reaction. Structures of all the synthesized compounds were characterized using the IR, ^{1}H NMR, ^{13}C NMR, and HR-MS spectra.

Chapter 4 describes the *in vitro* kinase inhibition and cytotoxicity evaluation of the synthesized compounds **8a-v**. The synthesized derivatives were screened for their potential inhibition of two kinase targets (CDK2/ cyclin E, Abl kinase) together with cytotoxicity evaluation against K-562 and MCF-7 cell lines. From the *in vitro* kinase inhibition data, one of the final compounds **8h** was identified as lead compound with IC_{50} value of 3.1 µM against CDK2 enzyme. The promising cytotoxicity (GI_{50} = 6.25 µM) evaluation of the compounds further supported the anticancer potential of the lead compound **8h**. From the SAR analysis (CDK-2), an electron-withdrawing halogen (Cl) at the *ortho* position of the aromatic ring (**8h**) demonstrated higher potency (IC_{50} = 3.1 µM) followed by the substitutions at *para*- and *meta* position displaying IC_{50} of 3.4 µM and 3.9 µM for **8t** and **8o**, respectively. Surprisingly, a couple of compounds (**8j** and **8k**) exhibited higher inhibition (IC_{50} >12.5 µM) against the Abl kinase when compared with the standard roscovitine (IC_{50} >100 µM). In comparison to the standard drugs (roscovitine and imatinib), the inhibitory profiles of all the final compounds **8a-v** against MCF-7 were good indicating that **8a-v** can be considered as potential anti-breast cancer hit compounds. Molecular docking studies against the CDK2 protein (PDB ID: 2A4L) revealed crucial molecular interactions required for *in vitro* inhibition of the synthesized compounds supporting our SAR analysis.

In the chapter 4, we discussed the *in vitro* evaluation **8a-v** against the steady state basal- and MT-stimulated KSP ATPase activities. The *in vitro* screening results presented no characteristic inhibition of state basal KSP ATPase, while good inhibition was observed against MT-stimulated KSP ATPase activity. From the evaluated derivatives, **8h** displayed the highest inhibition with an IC_{50} value of 13.2 µM against the MT-stimulated KSP ATPase activity. Similarly, compounds **8f** and **8i** also showed promising inhibition with IC_{50} of 17.2 µM and 20.2 µM, respectively. A brief SAR analysis (KSP), indicated that 2-chloro and 4-nitro substituents on the phenyl ring of the thiazolone motif contributed significantly to the enzyme inhibition. An *in silico* molecular docking study using the crystal structure of KSP (PDB ID: 2UYM) further supported the SAR and extrapolated the importance of crucial molecular ligand-protein interactions in influencing the *in vitro* enzyme inhibition. The magnitude of the electron-withdrawing functionalities over the hybrids and the critical molecular interactions with the enzyme imparted the compounds toward higher *in vitro* potency. The drug-like properties of the synthesized final compounds **8a-v** were also

calculated based on the Lipinski's rule of five and *in silico* computation of key pharmacokinetic parameters (ADME).

Thus, the research work finally concluded that the hybrid molecules (**8a-v**) are novel and potential dual inhibitors of CDK2 and KSP with promising drug-like properties for future development as anti-breast cancer agents.

6.2. Future studies

As most of the synthesized compounds exhibited promising anticancer activity through the inhibition of potential drug targets (CDK2 and KSP), the generated *in vitro* results can be effectively used as a preliminary data for further lead optimization using three-dimensional quantitative structure activity relationship (3D-QSAR) models. Using the 3D-QSAR models, the IC_{50} values of the compounds that are not synthesized will be predicted and can be further optimized structurally to improve the pharmaceutical properties (solubility, cell permeability and efficiency) through the development of 3D Quantitative Structure-Property Relationship (3D-QSPR) models. Thus, potential lead compounds identified by above mentioned computer-aided design techniques will be synthesized and evaluated by *in vitro* enzyme inhibition (CDK2 and KSP). Moreover, in depth mechanistic studies will be conducted to deduce mode of action of compounds with biological systems. From the *in vitro* cytotoxicity results of the compounds against K-562 and MCF-7 cell lines, it was observed that all the synthesized final compounds can be further developed as anti-breast cancer compounds. To accomplish this task, ligand (3D-QSAR and pharmacophore modeling) and structure-based drug design techniques (molecular docking and molecular dynamics) will be employed integrating molecular hybridization/ bioisosteric replacement strategies. Thus, the research work will be extended potentially through a combination of effective computer-aided drug design tools and modern synthetic medicinal chemistry approaches to develop novel thiadiazole-based anticancer drugs.

Chapter 7
Thesis Appendix

7.1. Spectral images

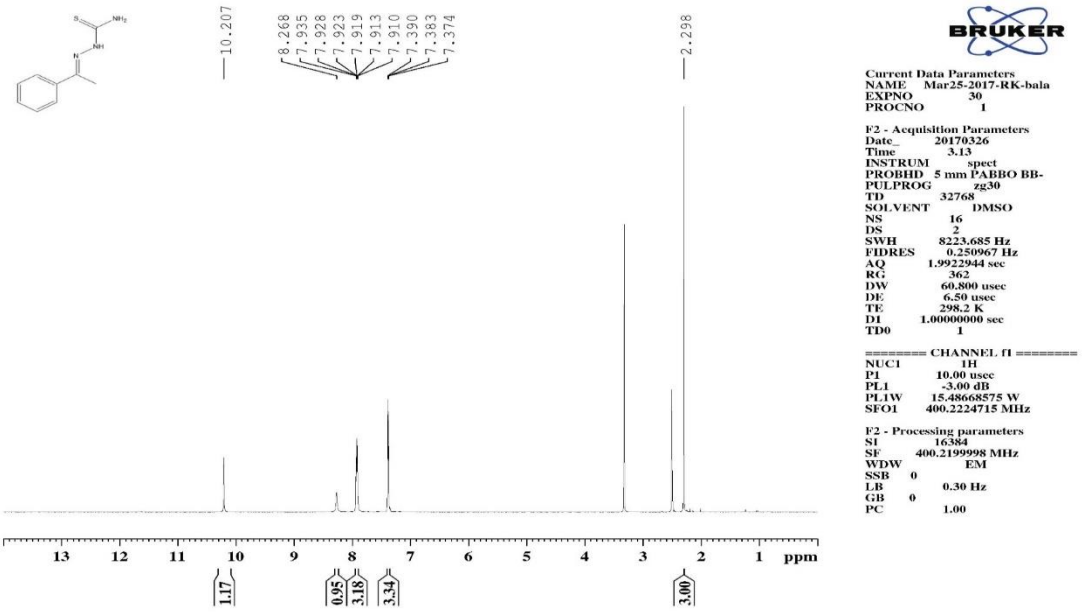

Figure S1: ^{1}H NMR of compound **2**

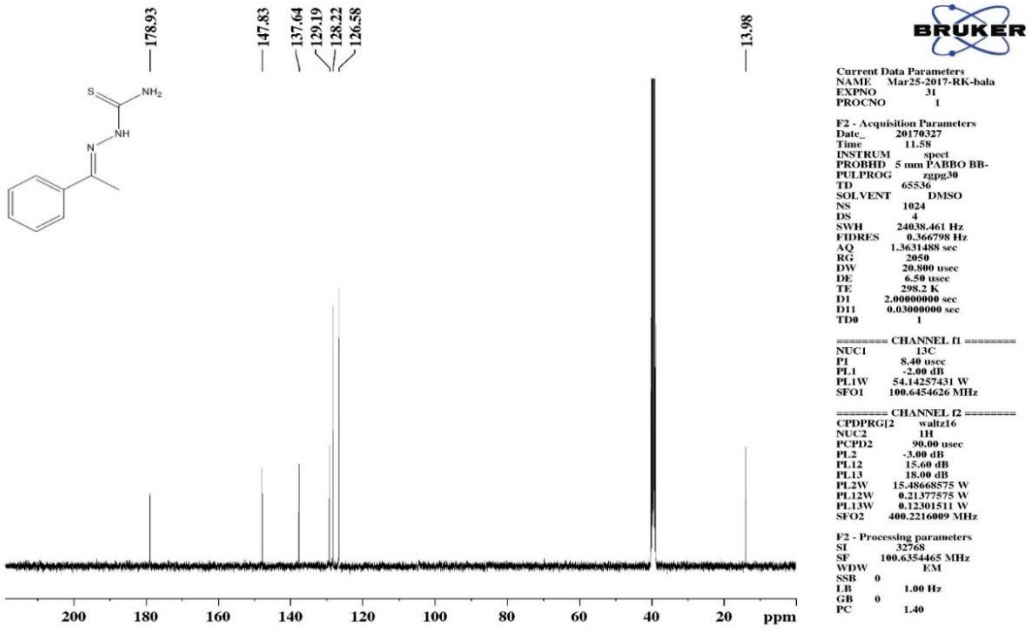

Figure S2: ^{13}C NMR of compound **2**

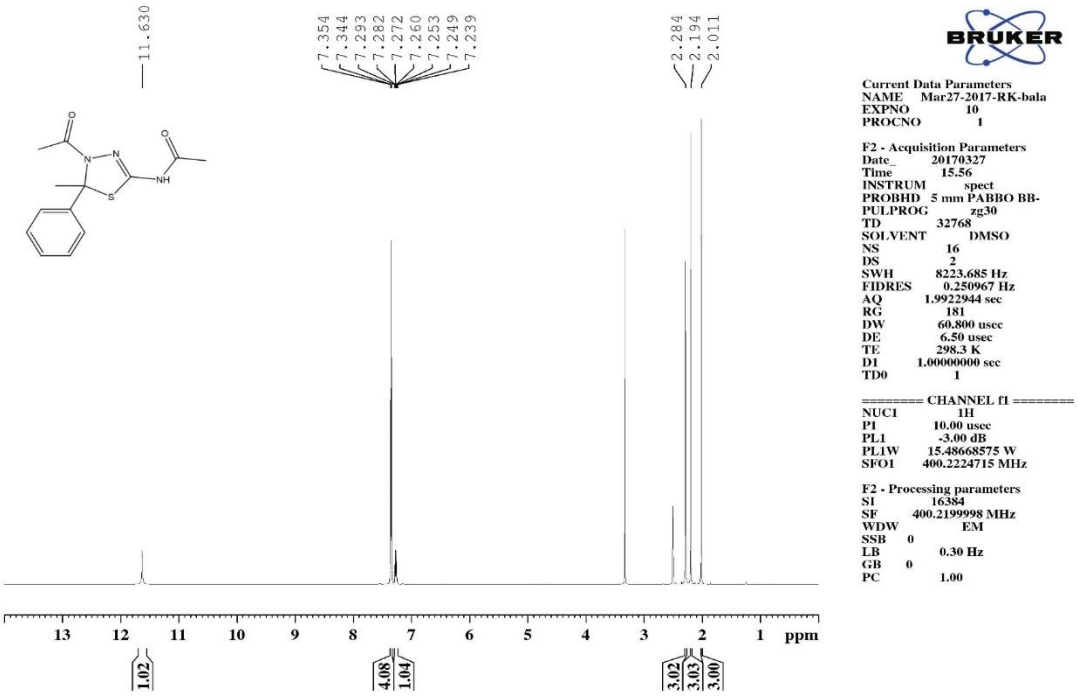

Figure S3: ^{1}H NMR of compound **3**

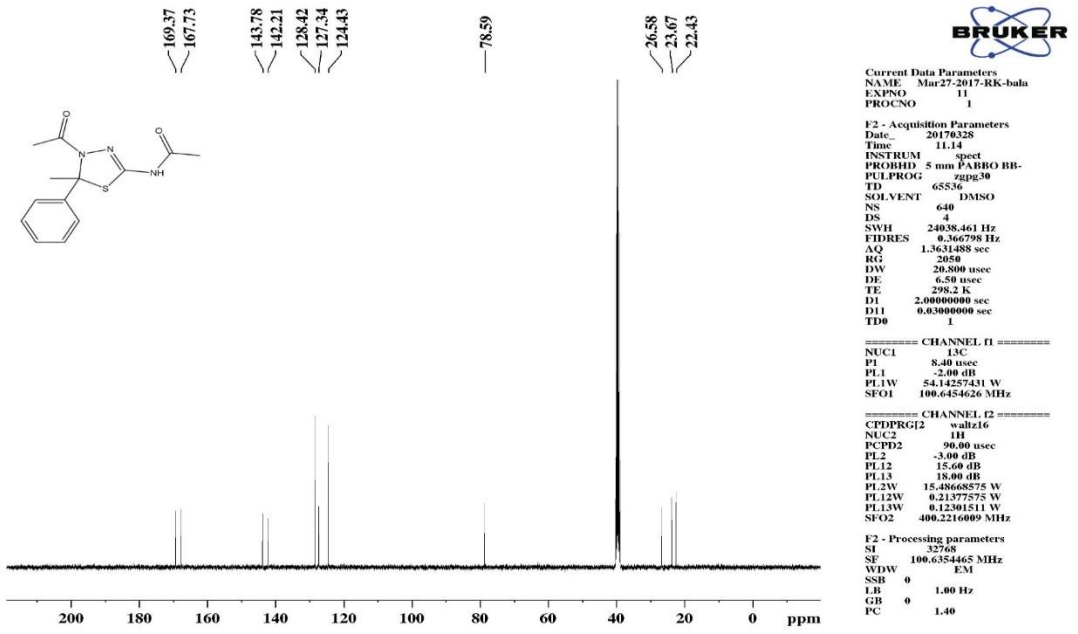

Figure S4: ^{13}C NMR of compound **3**

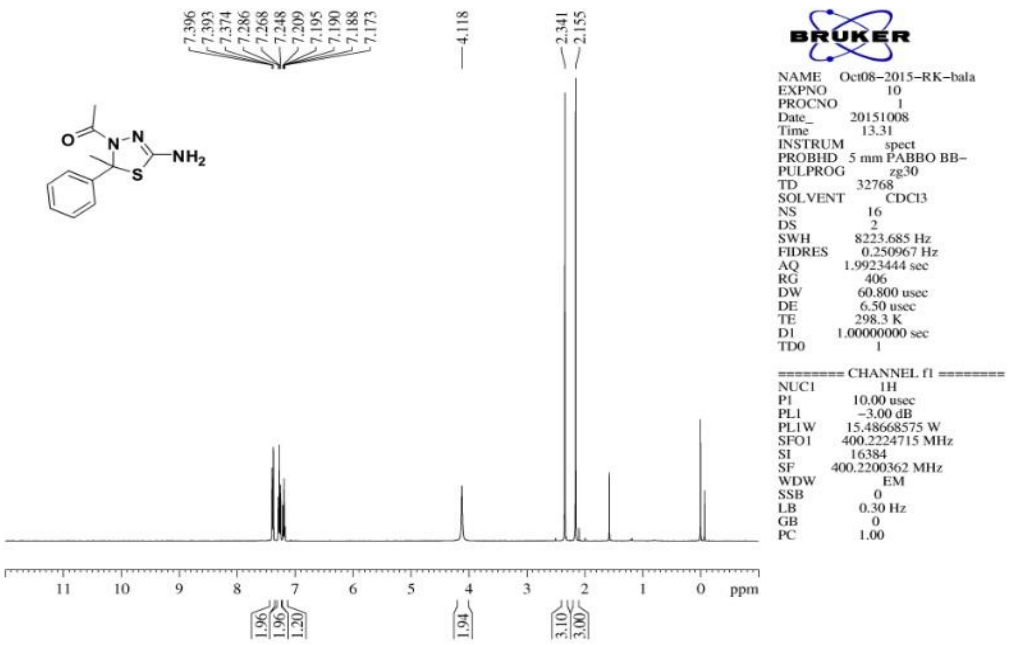

Figure S5: ^{1}H NMR of compound **4**

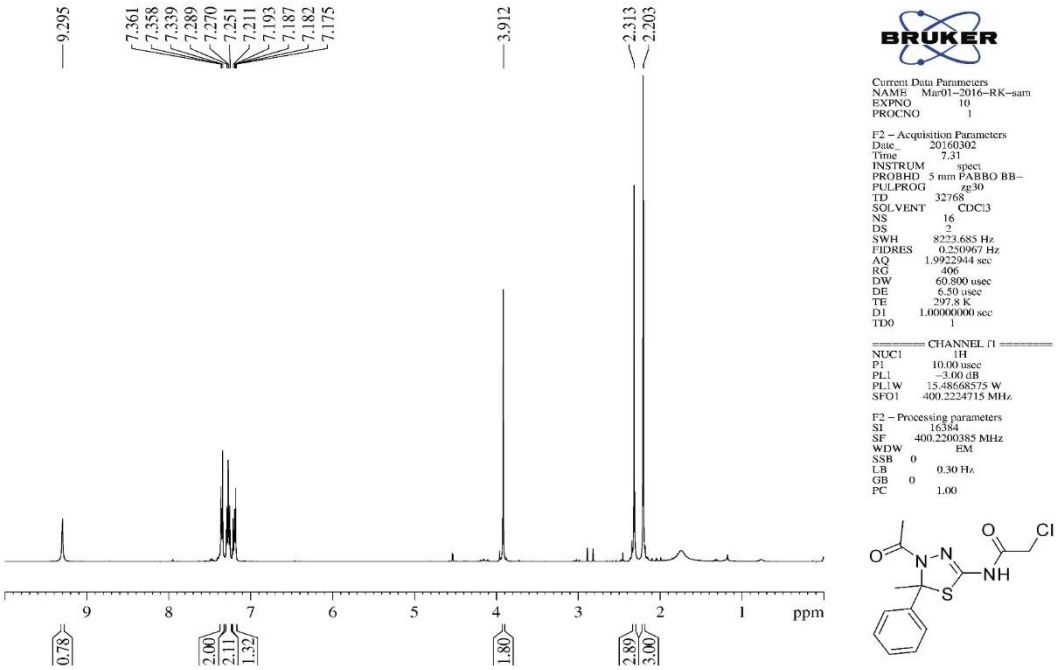

Figure S6: ^{1}H NMR of compound **5**

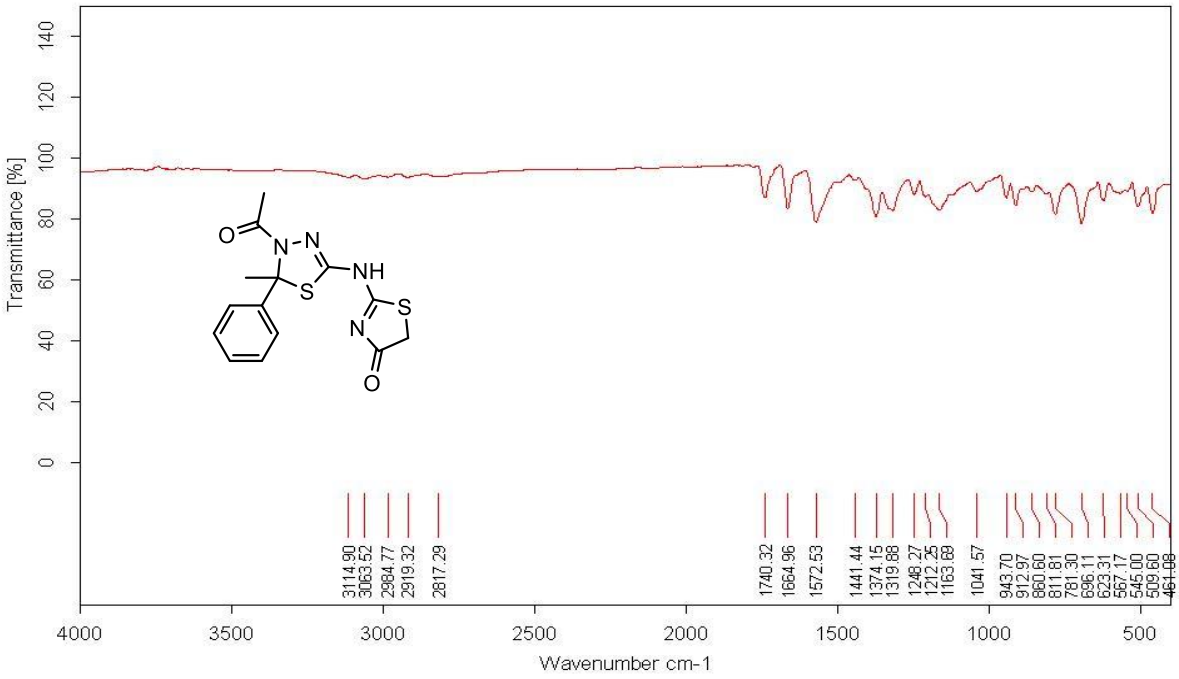

Figure S7: FT-IR of compound **6**

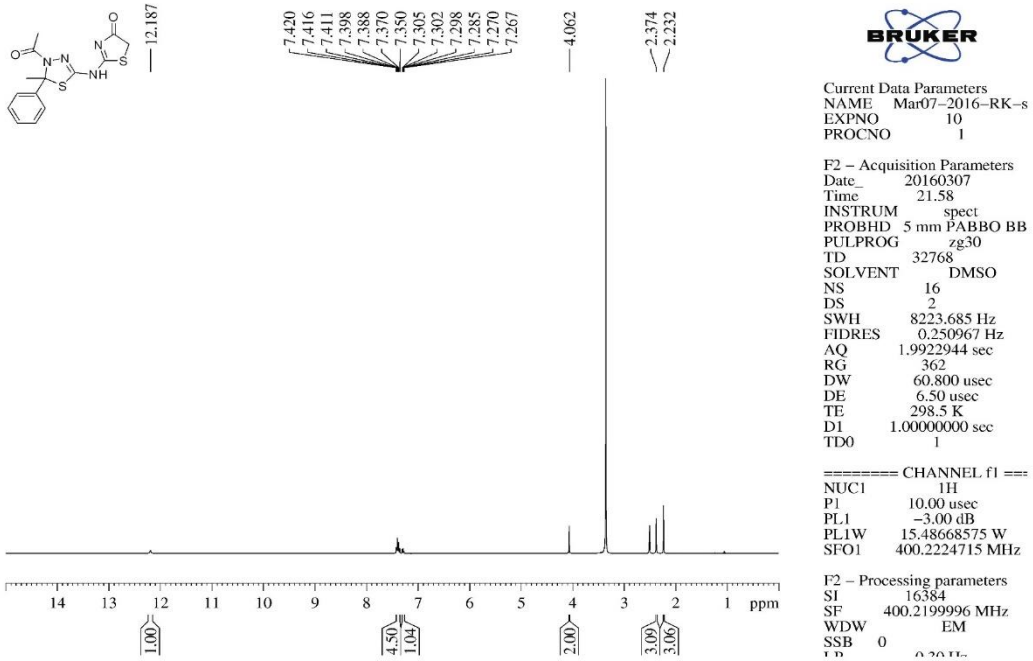

Figure S8: ^{1}H NMR of compound **6**

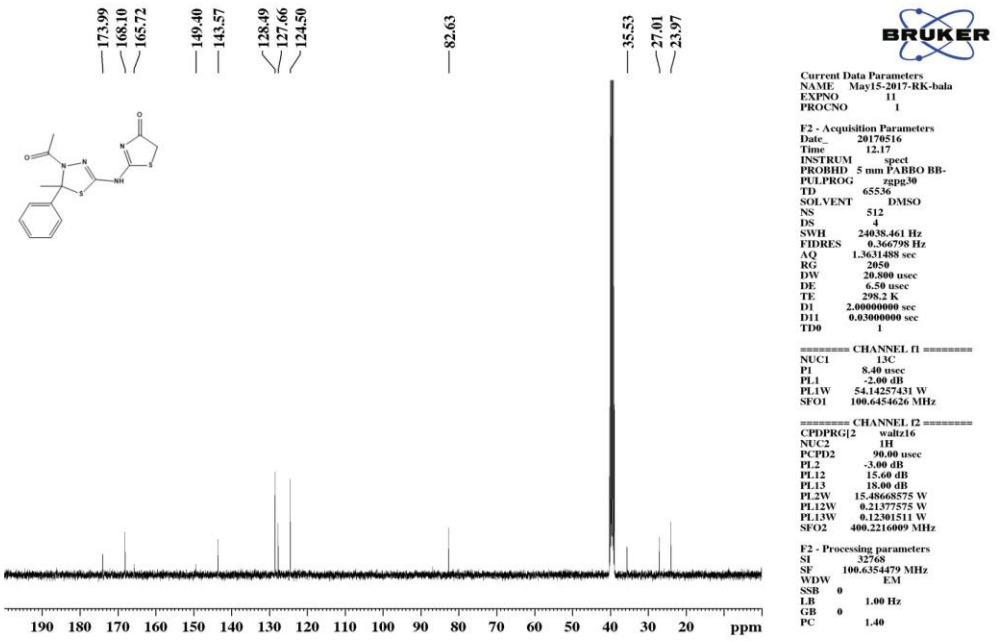

Figure S9: ^{13}C NMR of compound **6**

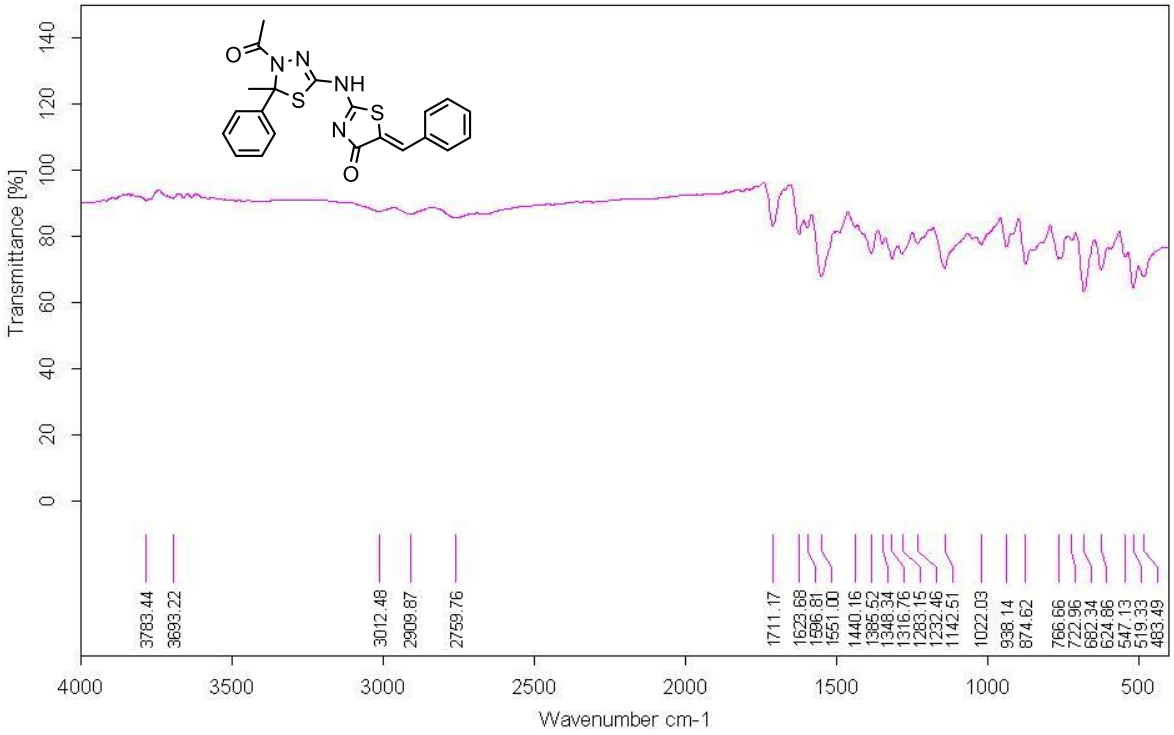

Figure S10: FT-IR of compound **8a**

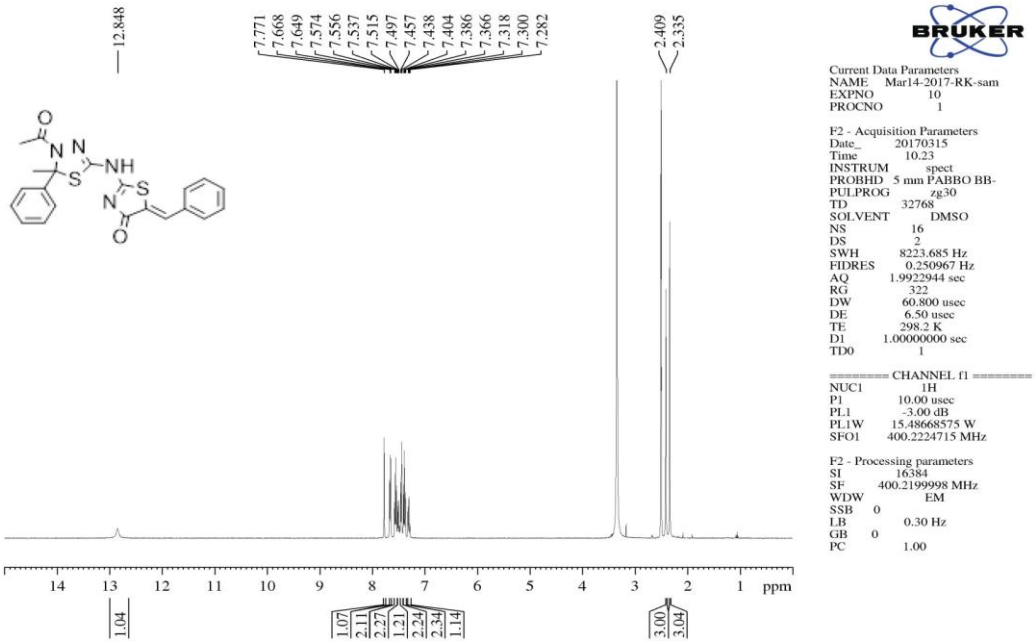

Figure S11: ^{1}H NMR of compound **8a**

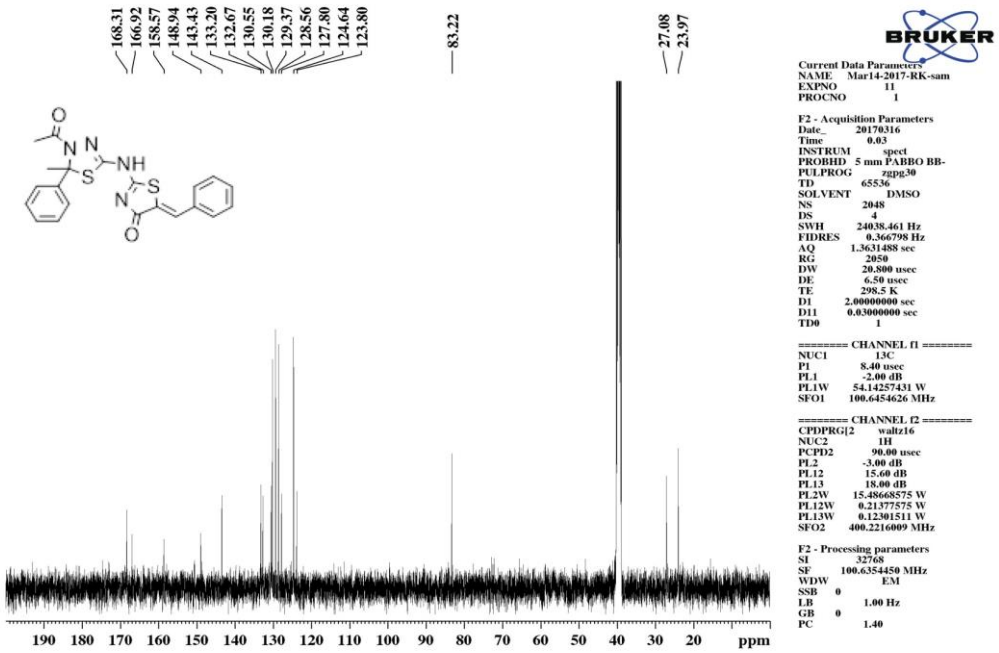

Figure S12: ^{13}C NMR of compound **8a**

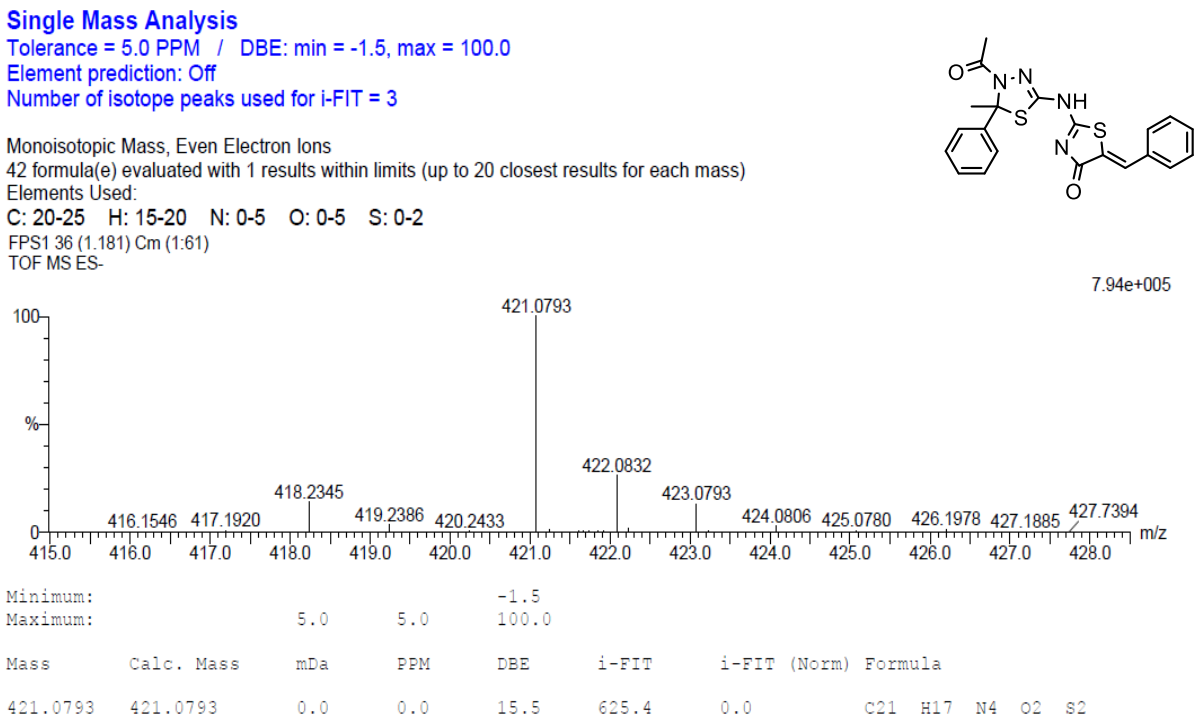

Figure S13: HR-MS of compound **8a**

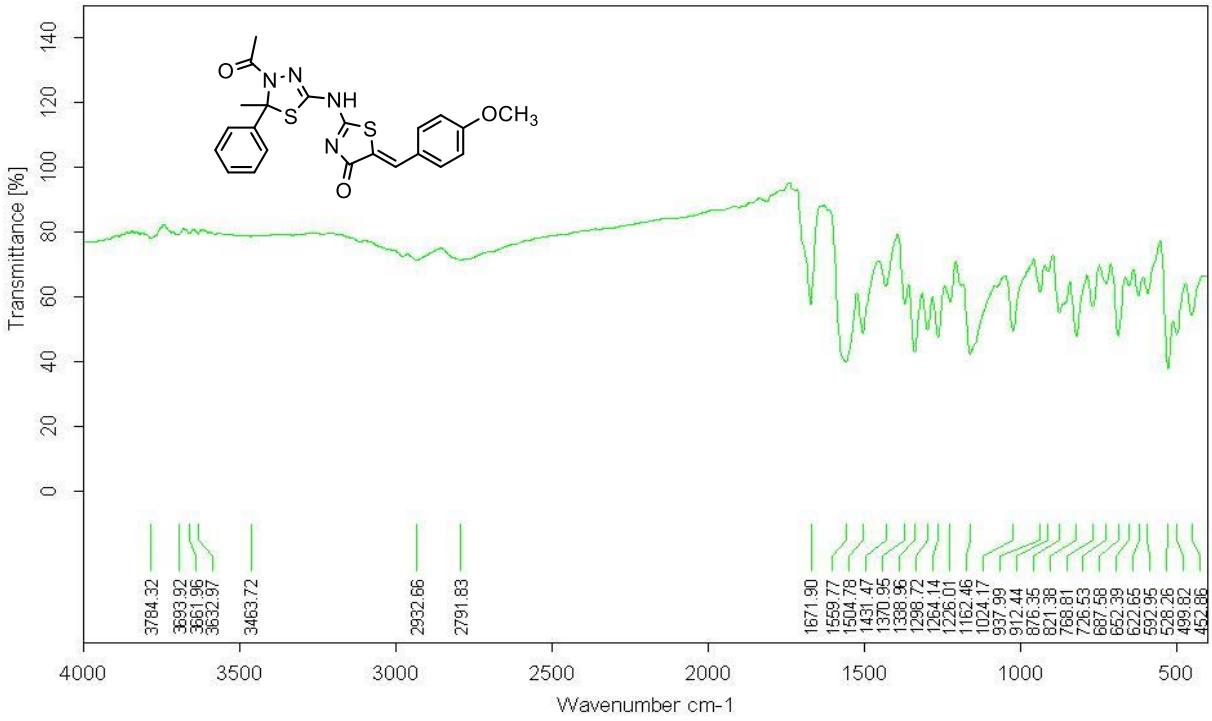

Figure S14: FT-IR of compound **8b**

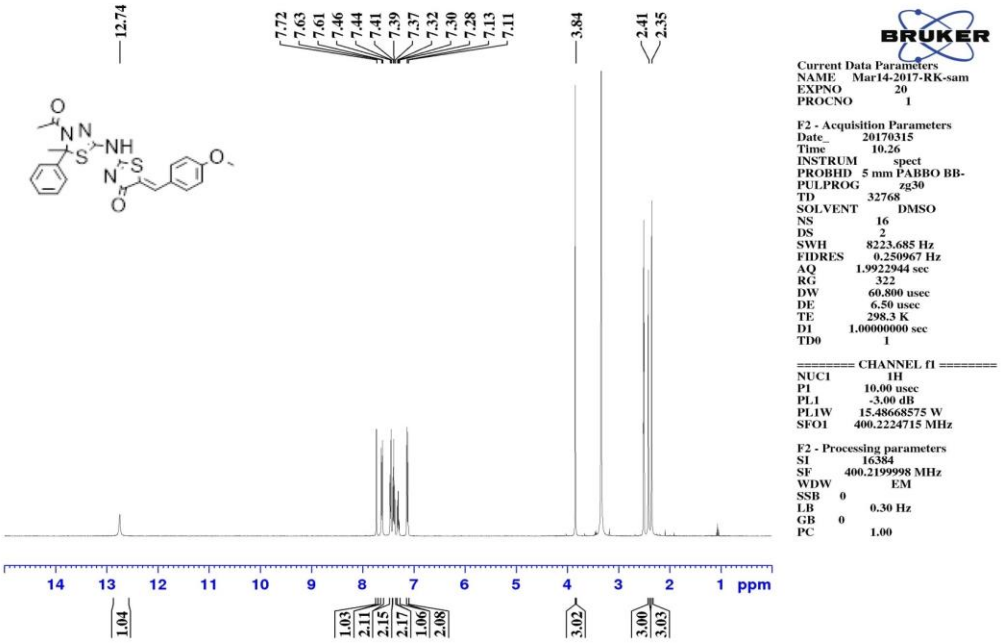

Figure S15: ^{1}H NMR of compound **8b**

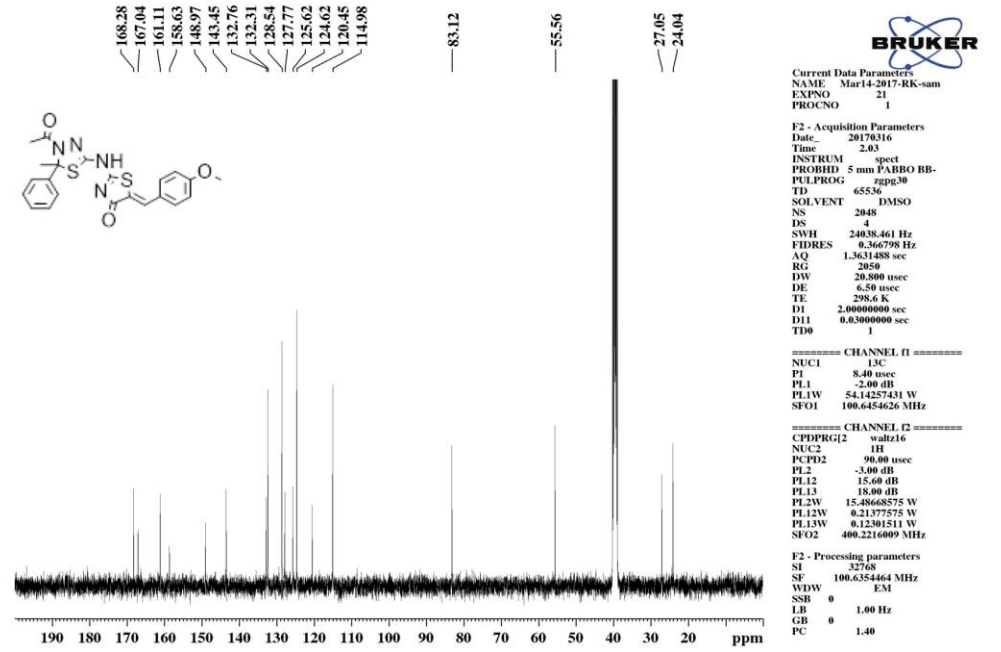

Figure S16: ^{13}C NMR of compound **8b**

Elemental Composition Report **Page 1**

Single Mass Analysis
Tolerance = 5.0 PPM / DBE: min = -1.5, max = 100.0
Element prediction: Off
Number of isotope peaks used for i-FIT = 2

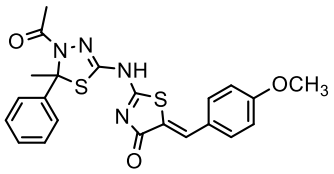

Monoisotopic Mass, Even Electron Ions
47 formula(e) evaluated with 1 results within limits (up to 20 best isotopic matches for each mass)
Elements Used:
C: 20-25 H: 15-20 N: 0-5 O: 0-5 S: 0-2
FSP2 37 (1.214) Cm (1:61)
TOF MS ES-

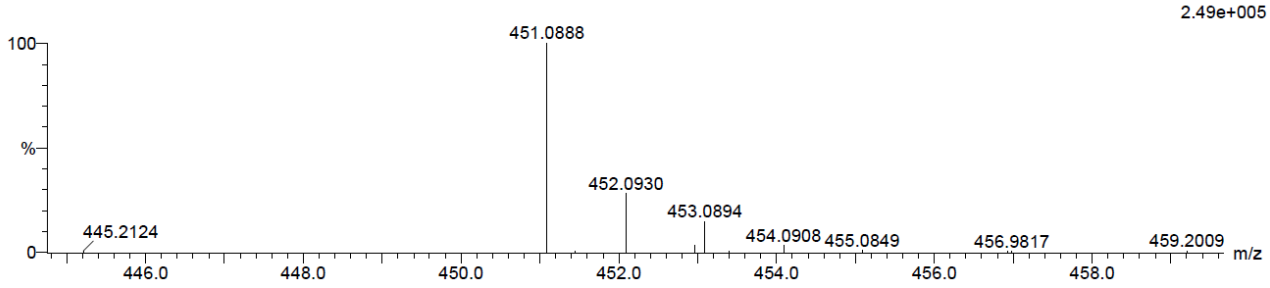

Minimum:				-1.5			
Maximum:		5.0	5.0	100.0			
Mass	Calc. Mass	mDa	PPM	DBE	i-FIT	i-FIT (Norm)	Formula
451.0888	451.0899	-1.1	-2.4	15.5	25.0	0.0	C22 H19 N4 O3 S2

Figure S17: HR-MS of compound **8b**

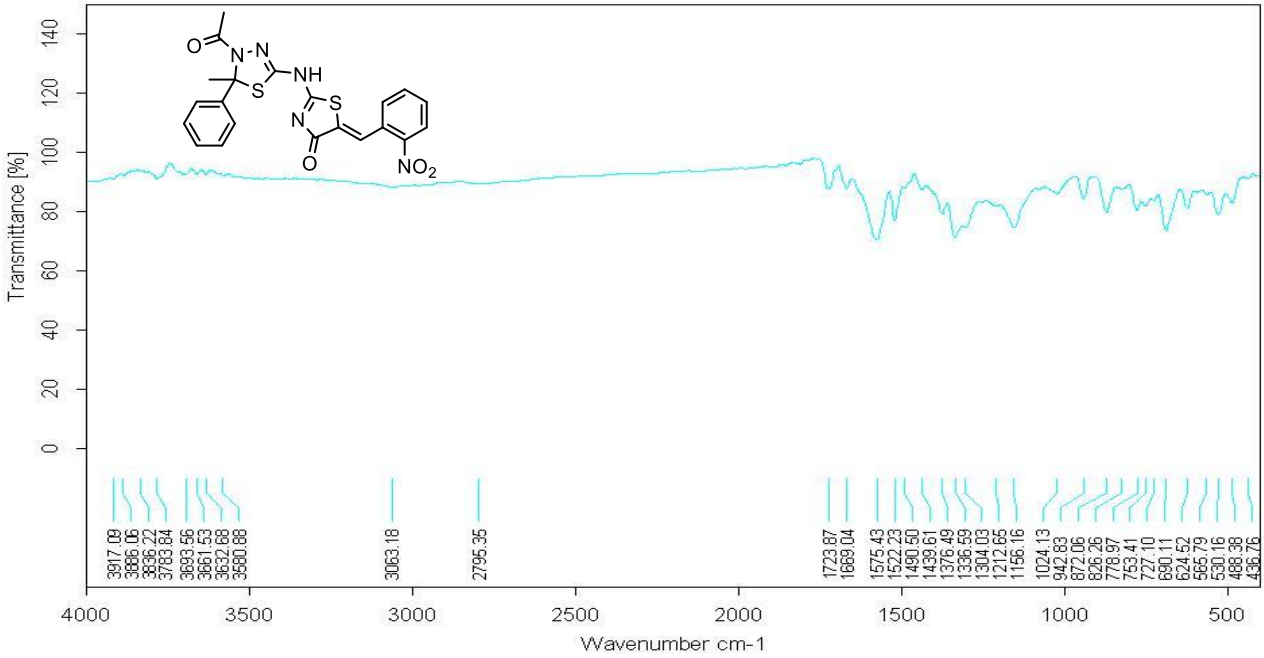

Figure S18: FT-IR of compound **8c**

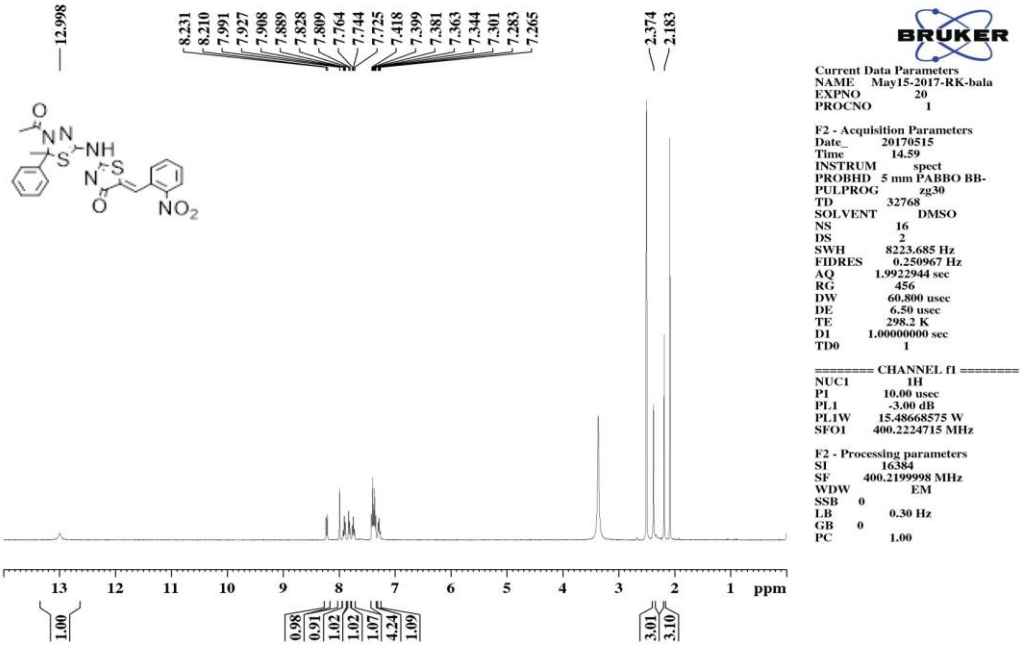

Figure S19: ^{1}H NMR of compound **8c**

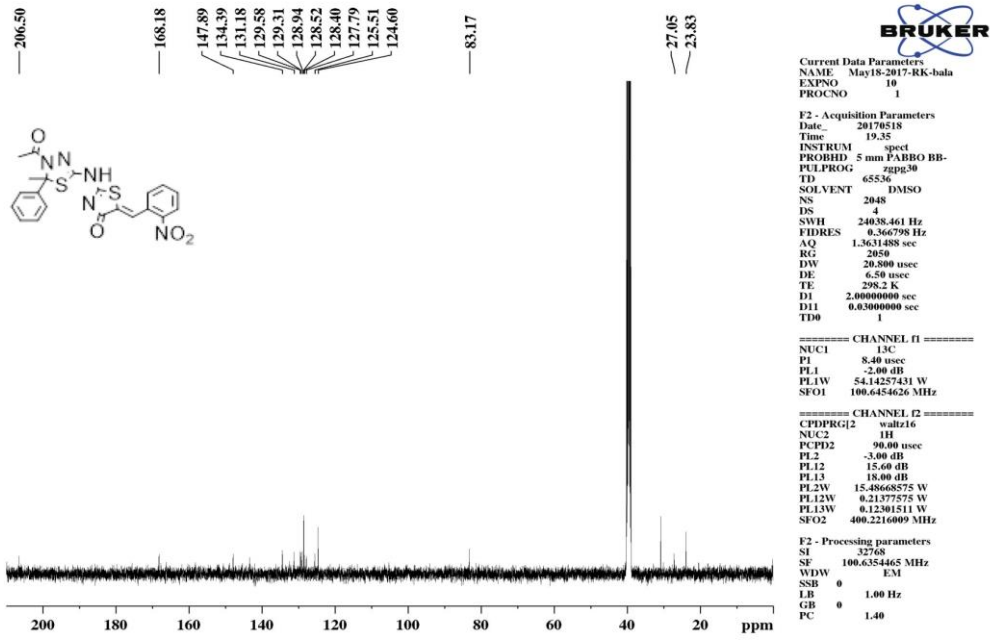

Figure S20: ^{13}C NMR of compound **8c**

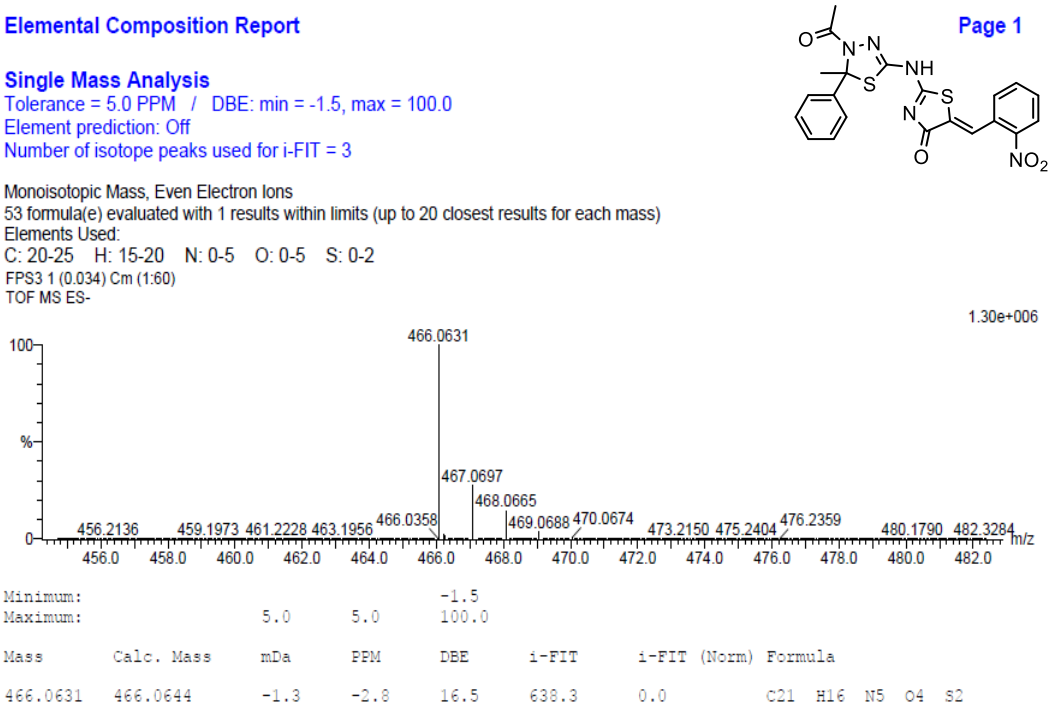

Figure S21: HR-MS of compound **8c**

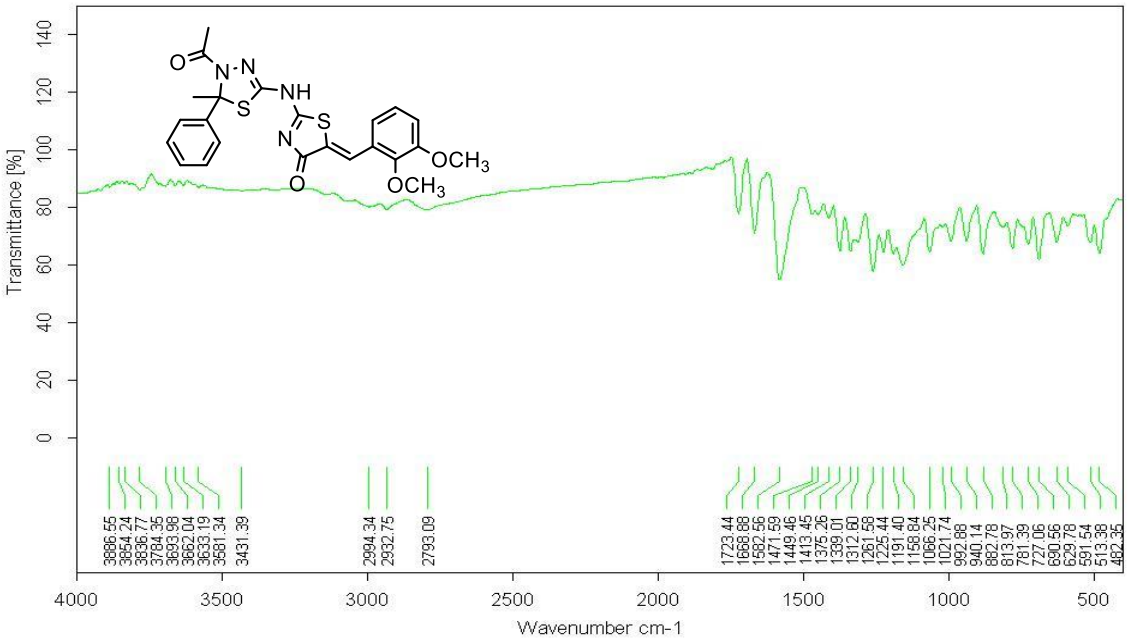

Figure S22: FT-IR of compound **8d**

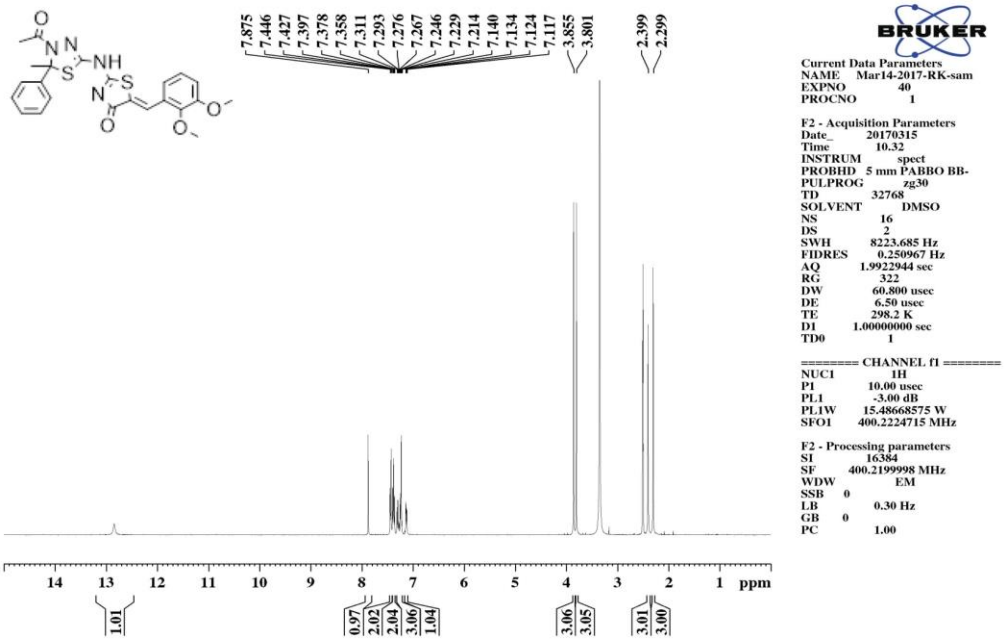

Figure S23: ^{1}H NMR of compound **8d**

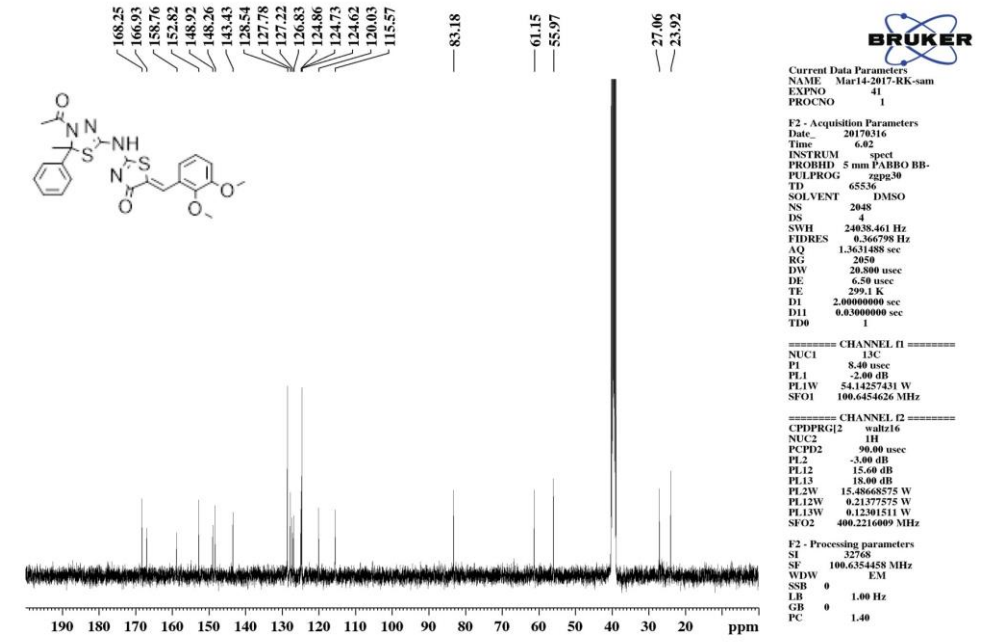

Figure S24: ^{13}C NMR of compound **8d**

Elemental Composition Report **Page 1**

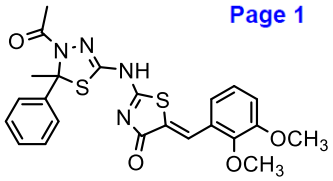

Single Mass Analysis
Tolerance = 5.0 PPM / DBE: min = -1.5, max = 100.0
Element prediction: Off
Number of isotope peaks used for i-FIT = 2

Monoisotopic Mass, Even Electron Ions
58 formula(e) evaluated with 1 results within limits (up to 20 best isotopic matches for each mass)
Elements Used:
C: 20-25 H: 20-25 N: 0-5 O: 0-5 S: 0-2
FSP5 7 (0.202) Cm (1:61)
TOF MS ES-

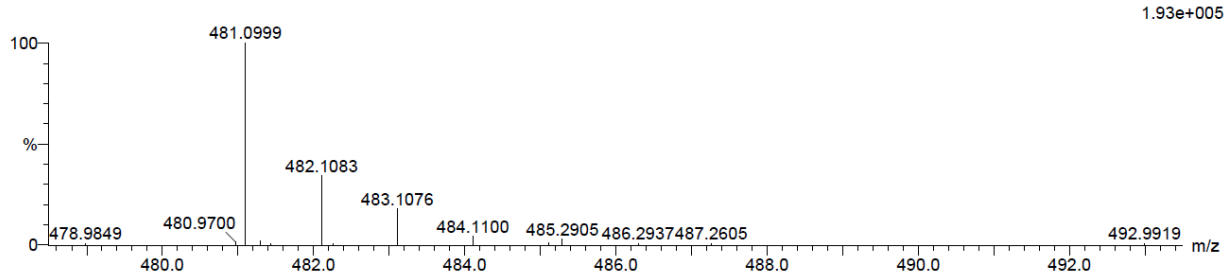

Minimum:				-1.5			
Maximum:		5.0	5.0	100.0			
Mass	Calc. Mass	mDa	PPM	DBE	i-FIT	i-FIT (Norm)	Formula
481.0999	481.1004	-0.5	-1.0	15.5	66.1	0.0	C23 H21 N4 O4 S2

Figure S25: HR-MS of compound **8d**

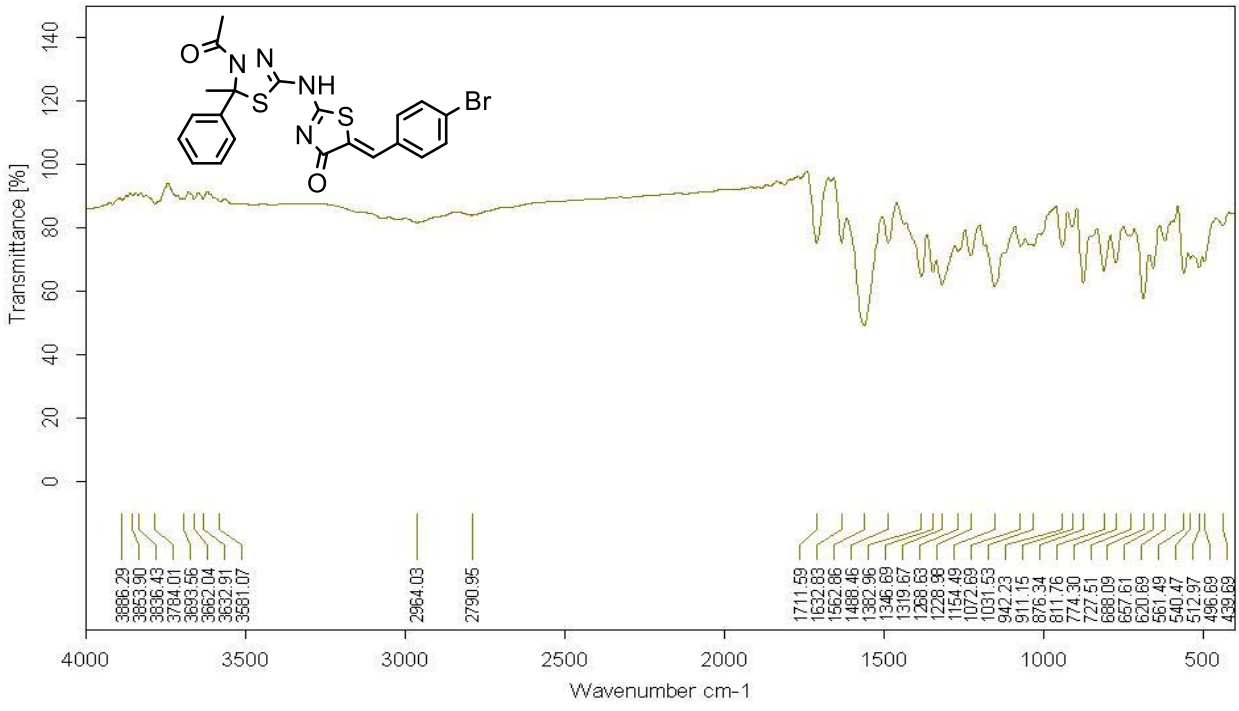

Figure S26: FT-IR of compound **8e**

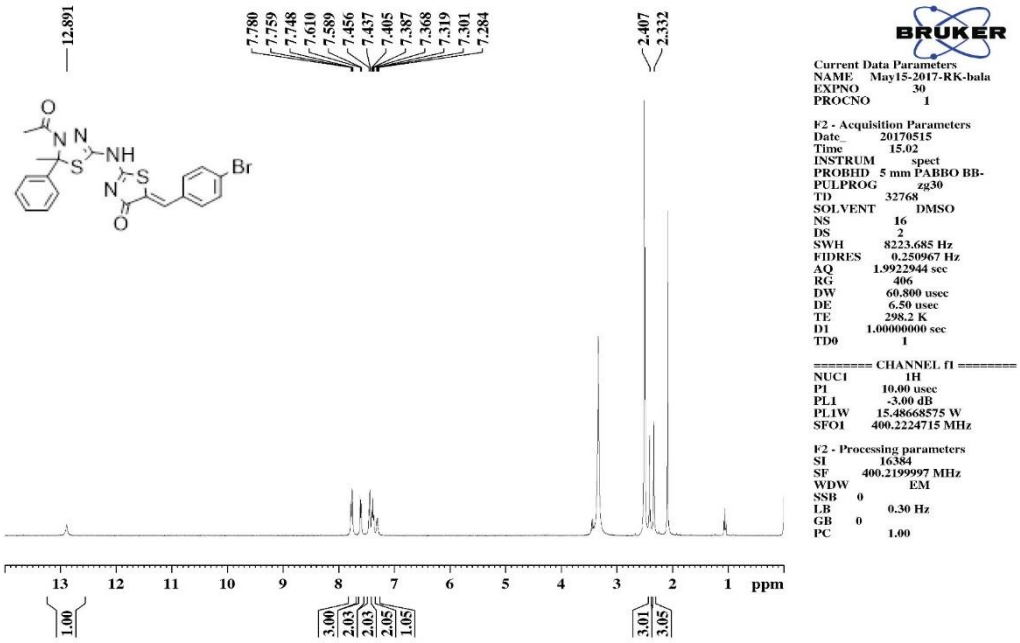

Figure S27: ^{1}H NMR of compound **8e**

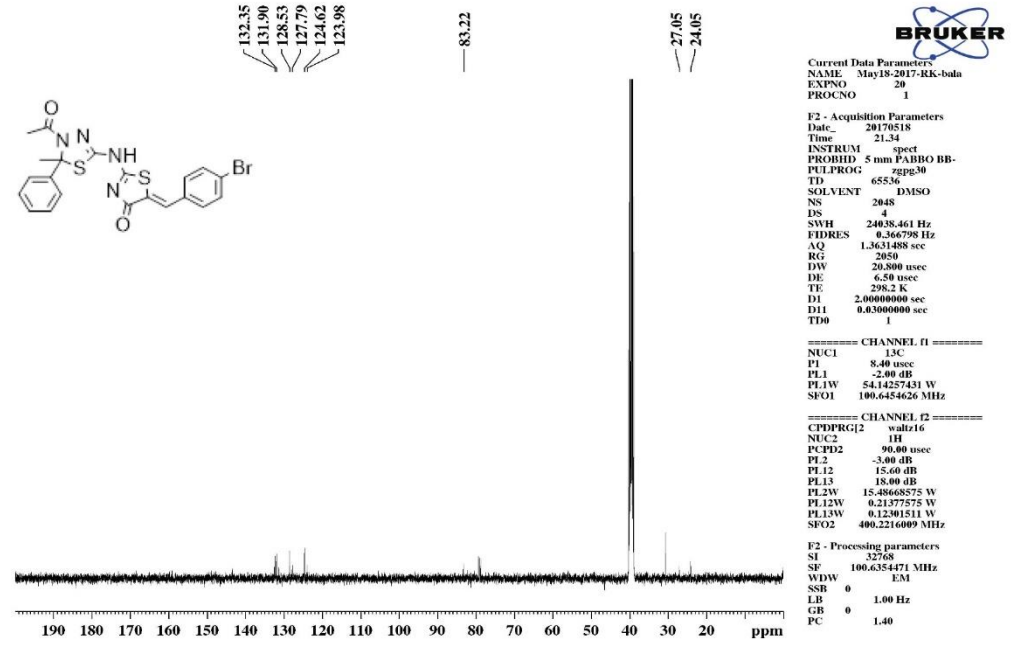

Figure S28: ^{13}C NMR of compound **8e**

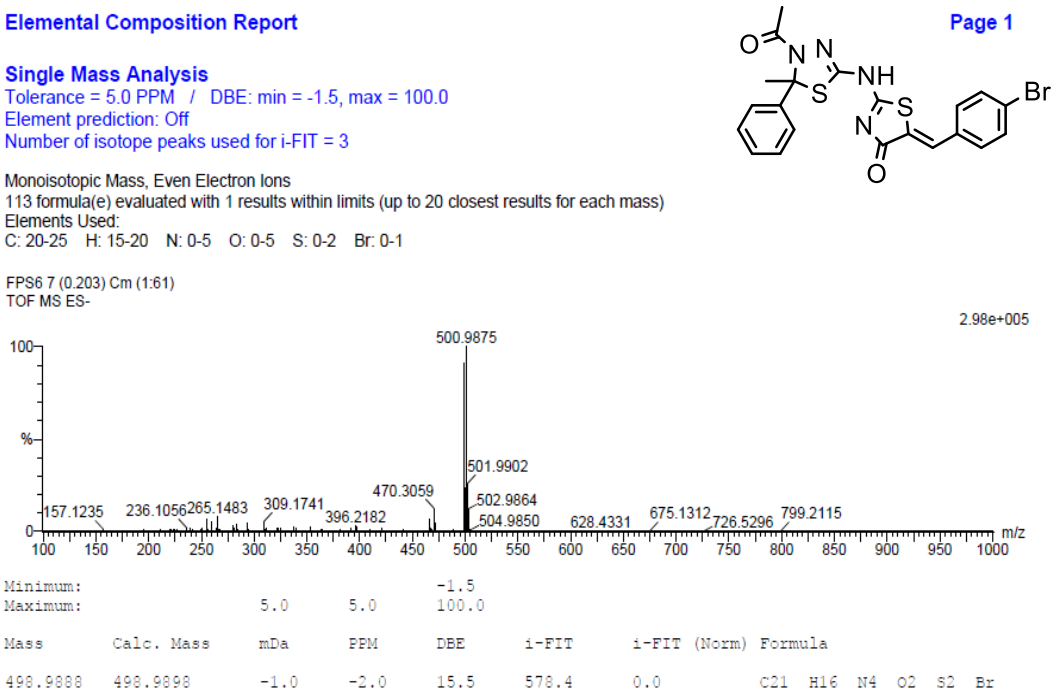

Figure S29: HR-MS of compound **8e**

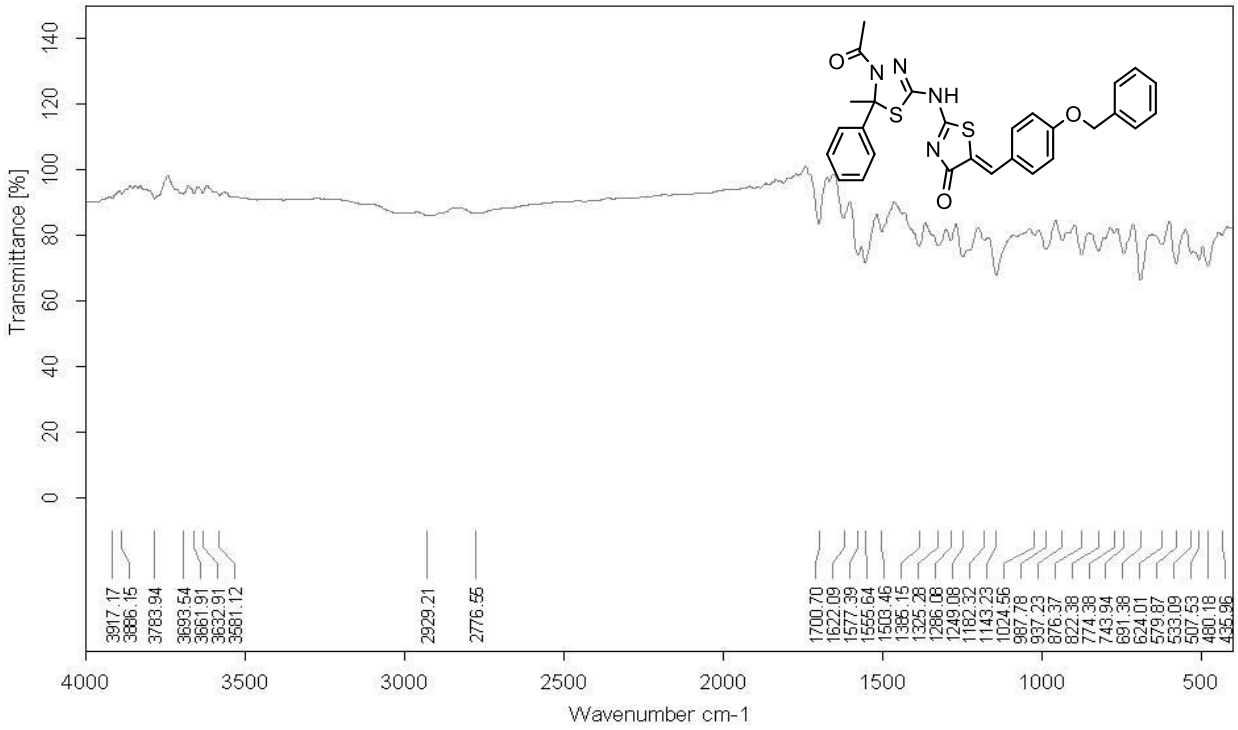

Figure S30: FT-IR of compound **8f**

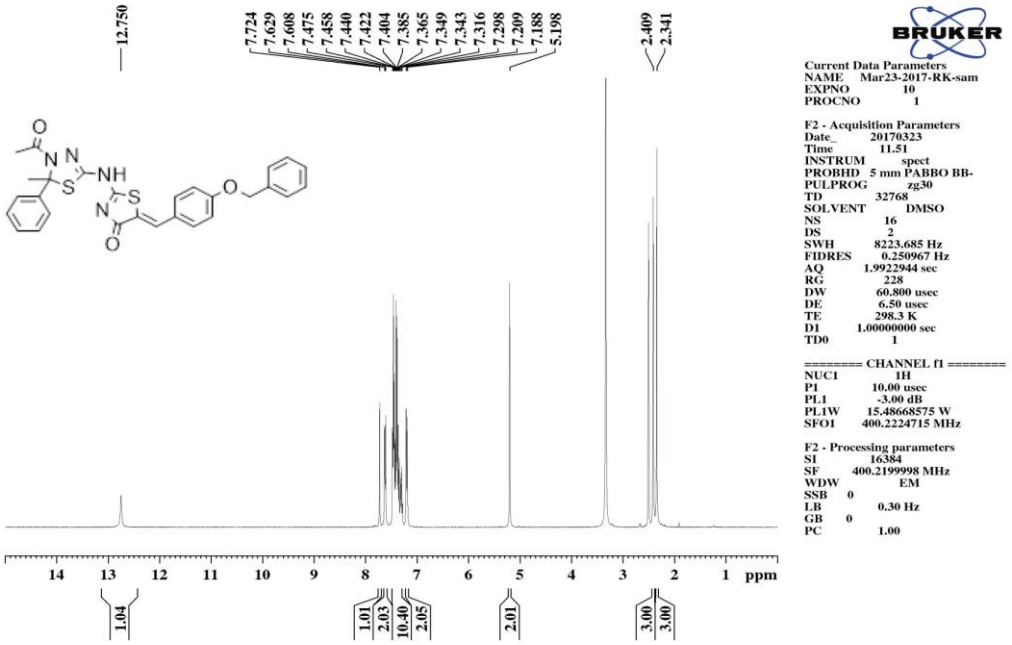

Figure S31: ^{1}H NMR of compound **8f**

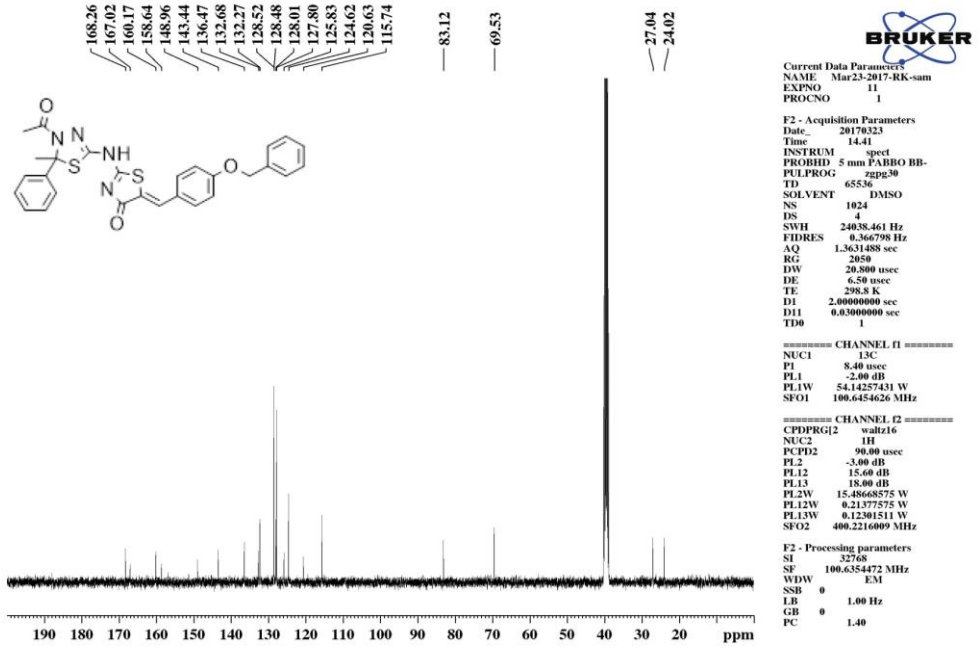

Figure S32: ^{13}C NMR of compound **8f**

Elemental Composition Report

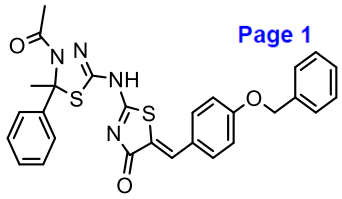

Single Mass Analysis
Tolerance = 5.0 PPM / DBE: min = -1.5, max = 100.0
Element prediction: Off
Number of isotope peaks used for i-FIT = 2

Monoisotopic Mass, Even Electron Ions
44 formula(e) evaluated with 1 results within limits (up to 20 best isotopic matches for each mass)
Elements Used:
C: 25-30 H: 20-25 N: 0-5 O: 0-5 S: 0-2
FSP7 39 (1.282) Cm (1:61)
TOF MS ES-

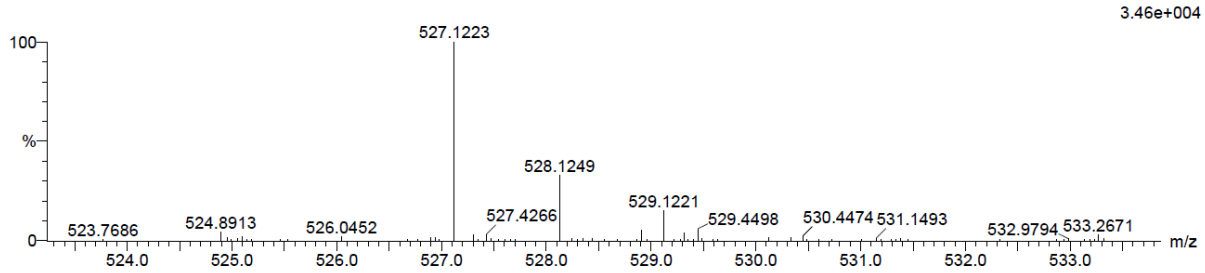

Minimum:				-1.5			
Maximum:		5.0	5.0	100.0			
Mass	Calc. Mass	mDa	PPM	DBE	i-FIT	i-FIT (Norm)	Formula
527.1223	527.1212	1.1	2.1	19.5	154.9	0.0	C28 H23 N4 O3 S2

Figure S33: HR-MS of compound **8f**

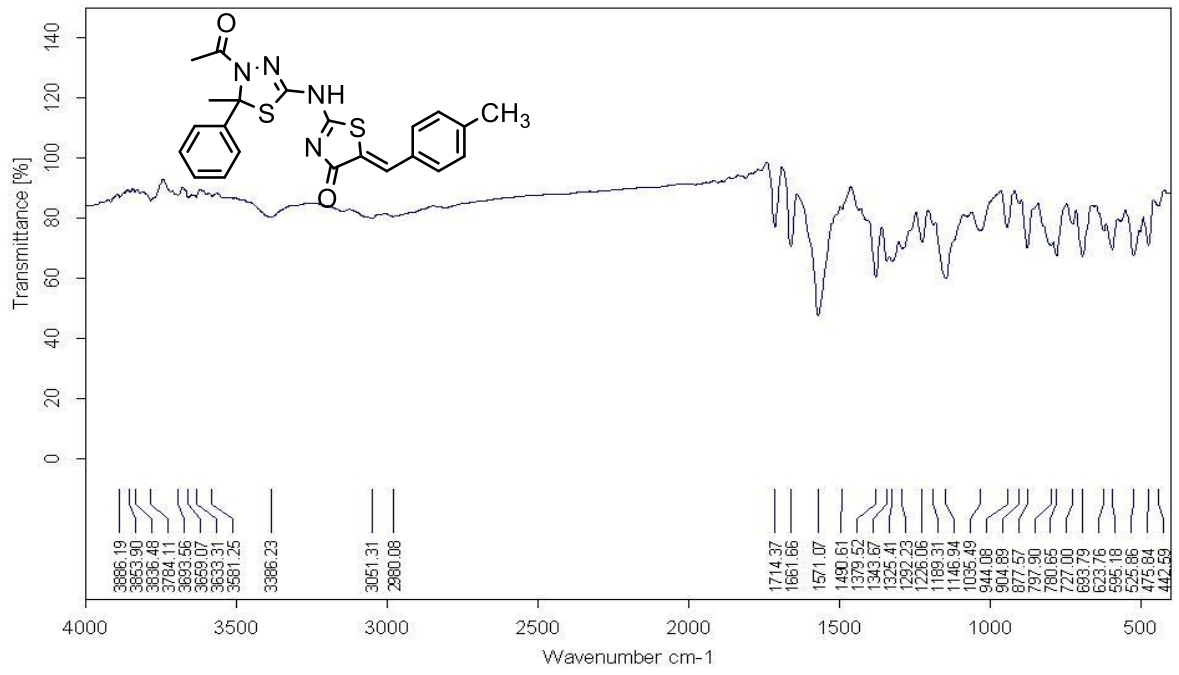

Figure S34: FT-IR of compound **8g**

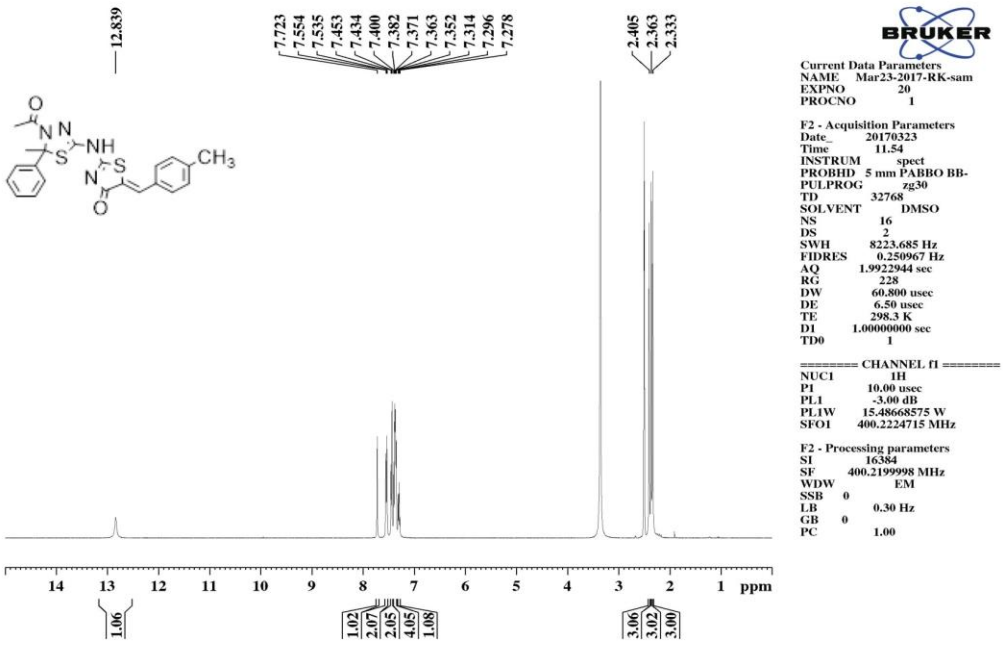

Figure S35: ^{1}H NMR of compound **8g**

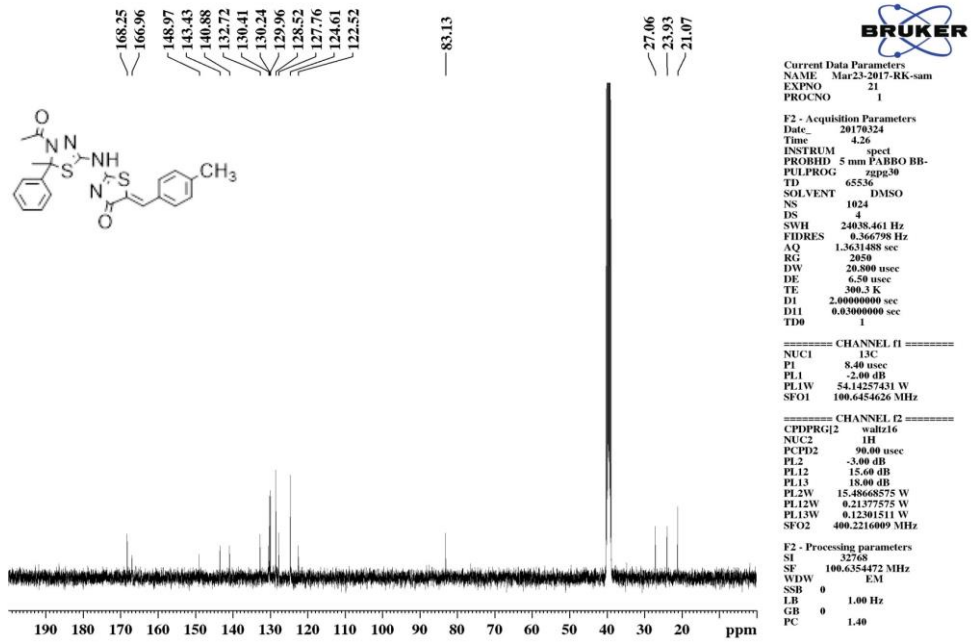

Figure S36: ^{13}C NMR of compound **8g**

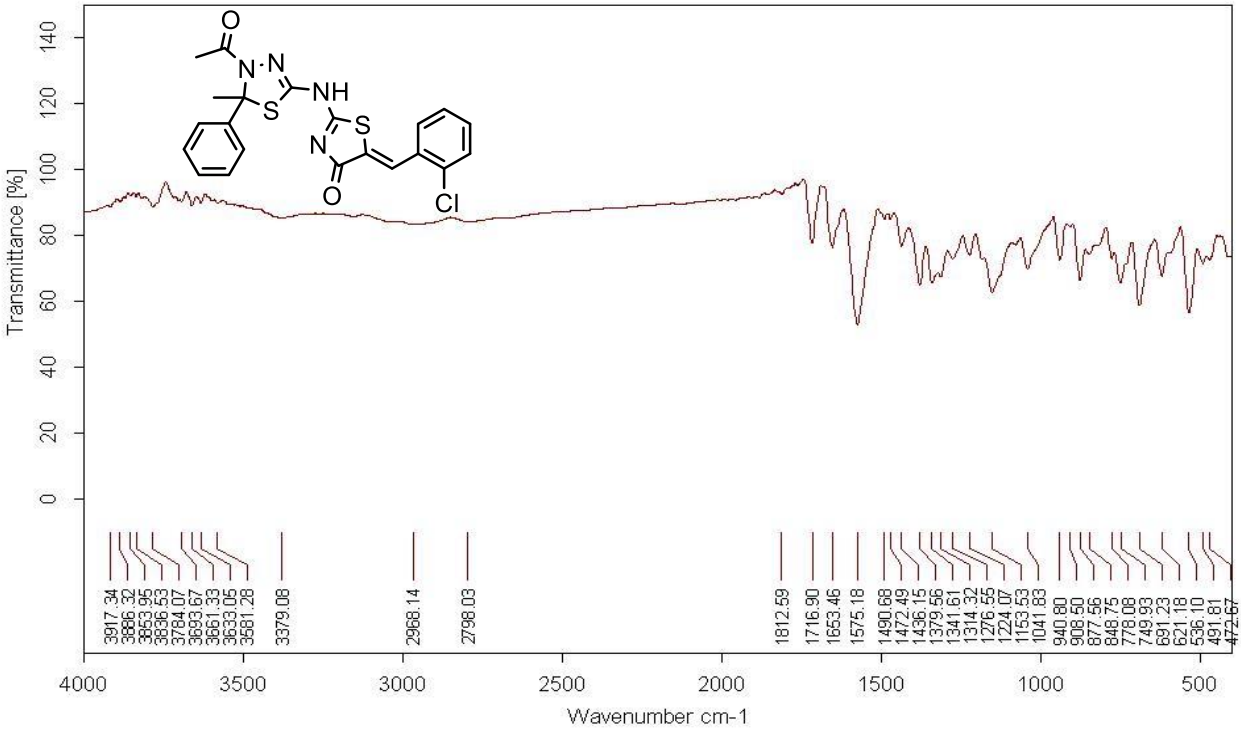

Figure S37: FT-IR of compound **8h**

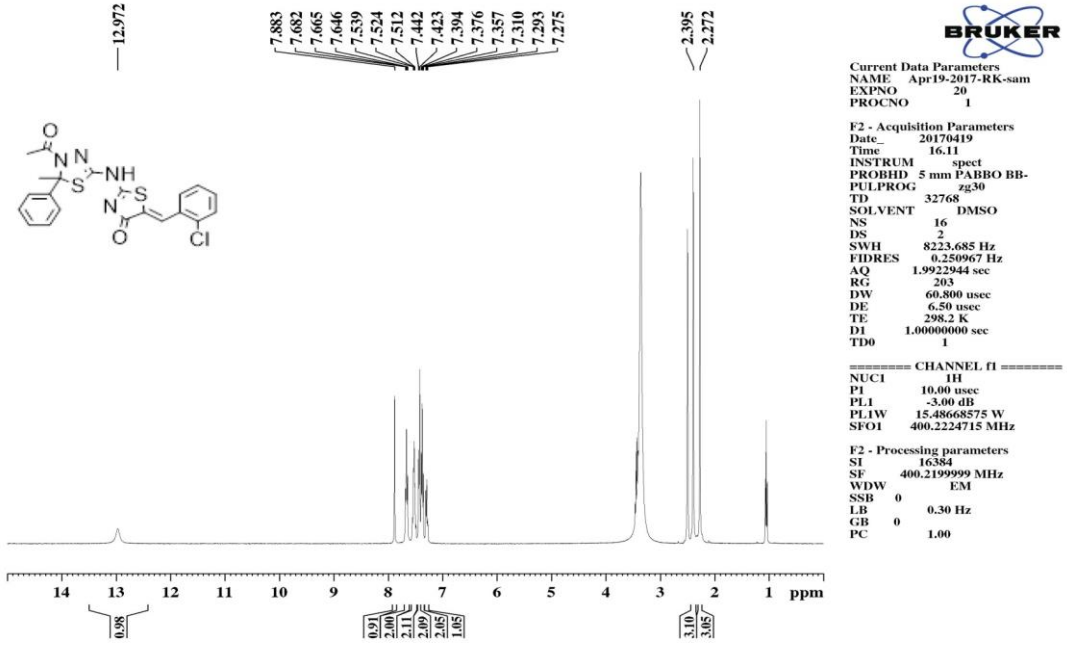

Figure S38: ^{1}H NMR of compound **8h**

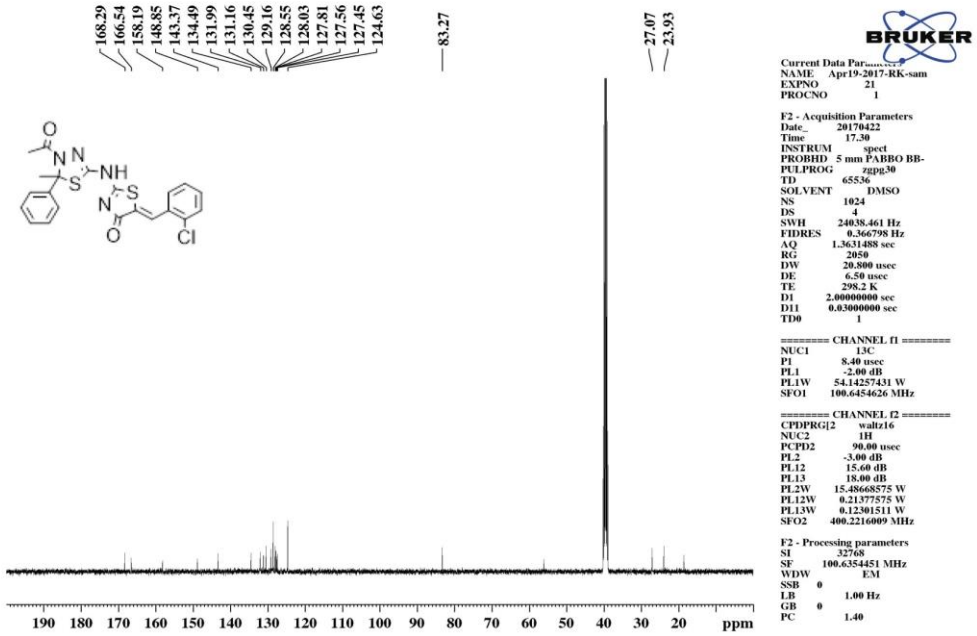

Figure S39: ^{13}C NMR of compound **8h**

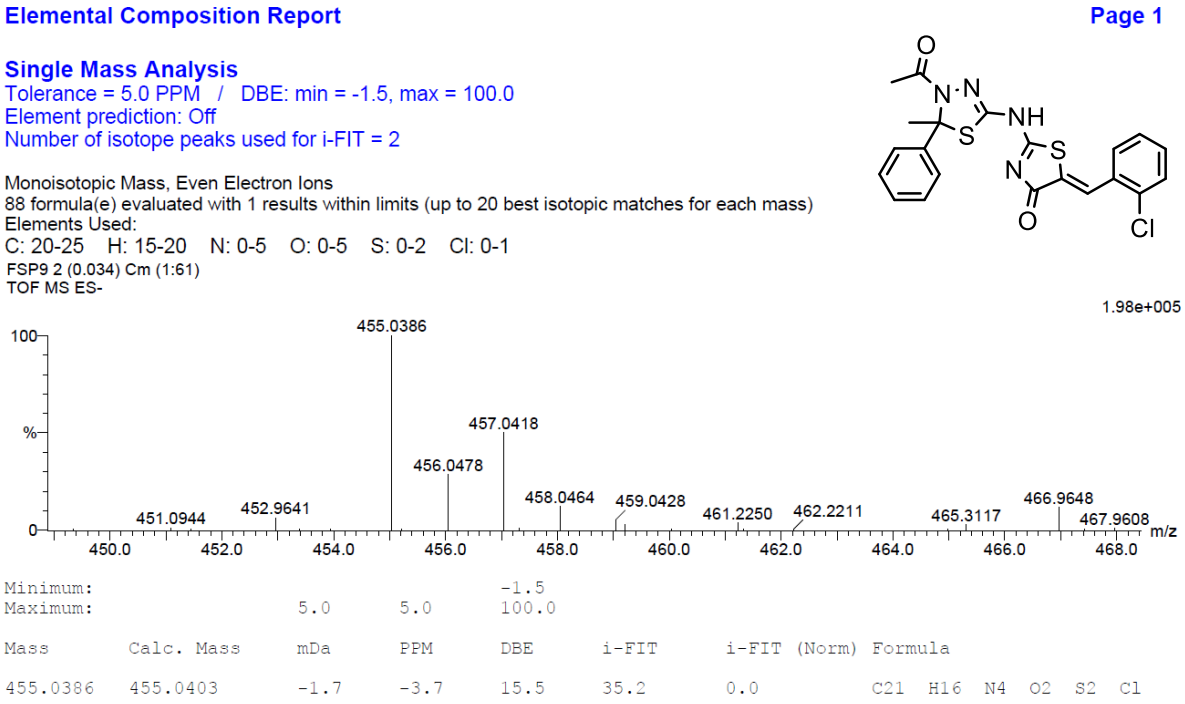

Figure S40: HR-MS of compound **8h**

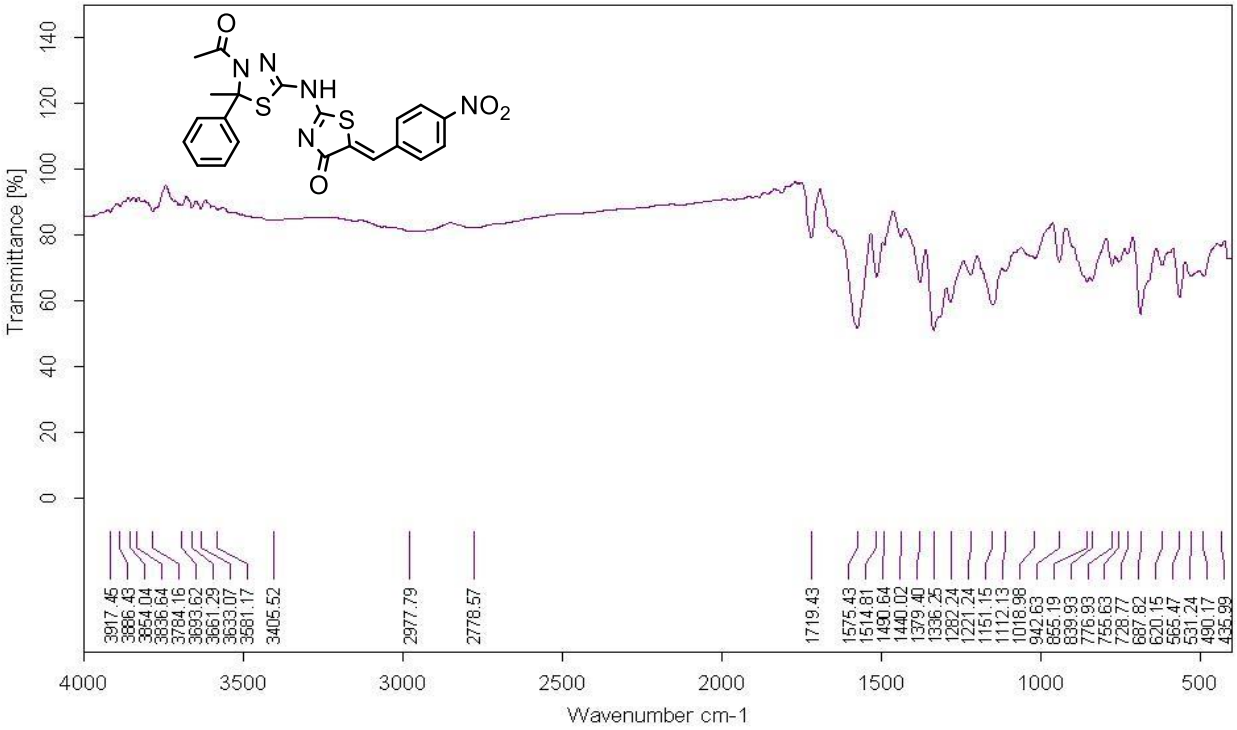

Figure S41: FT-IR of compound **8i**

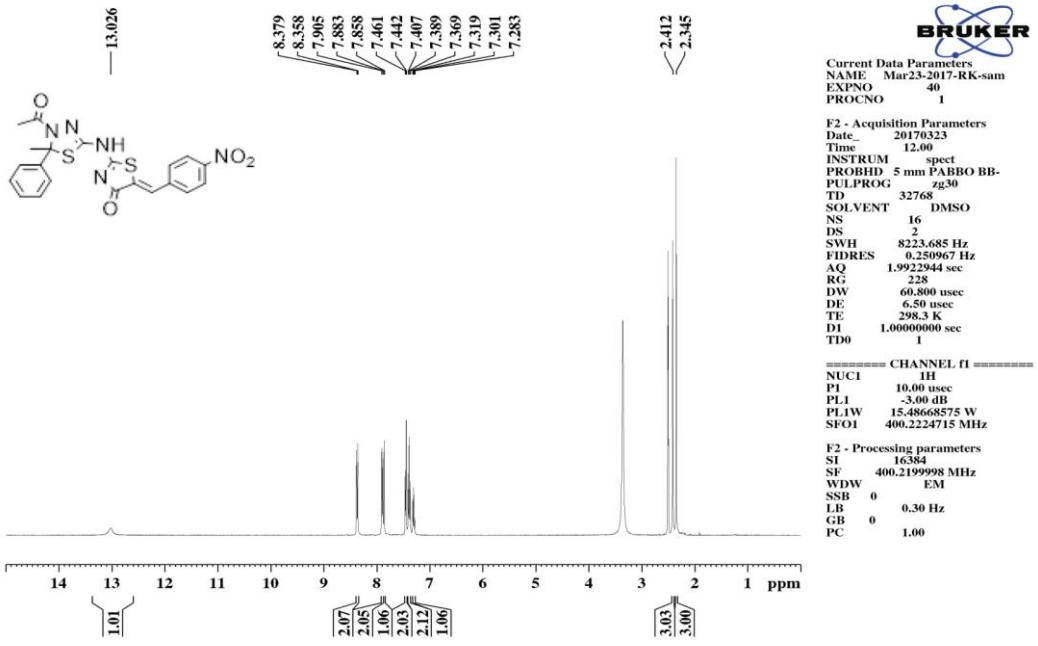

Figure S42: ^{1}H NMR of compound **8i**

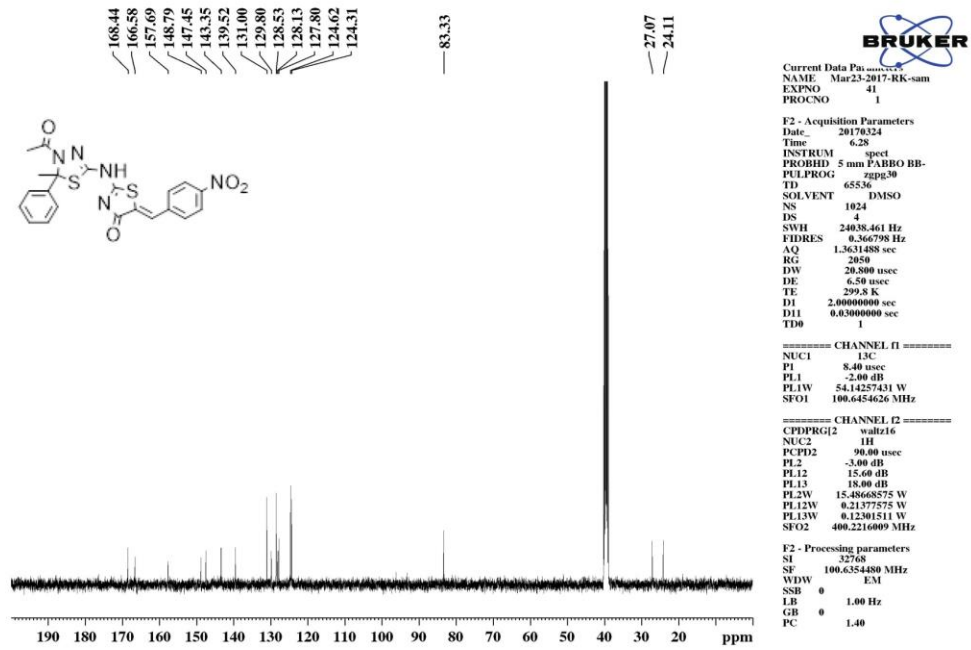

Figure S43: ^{13}C NMR of compound **8i**

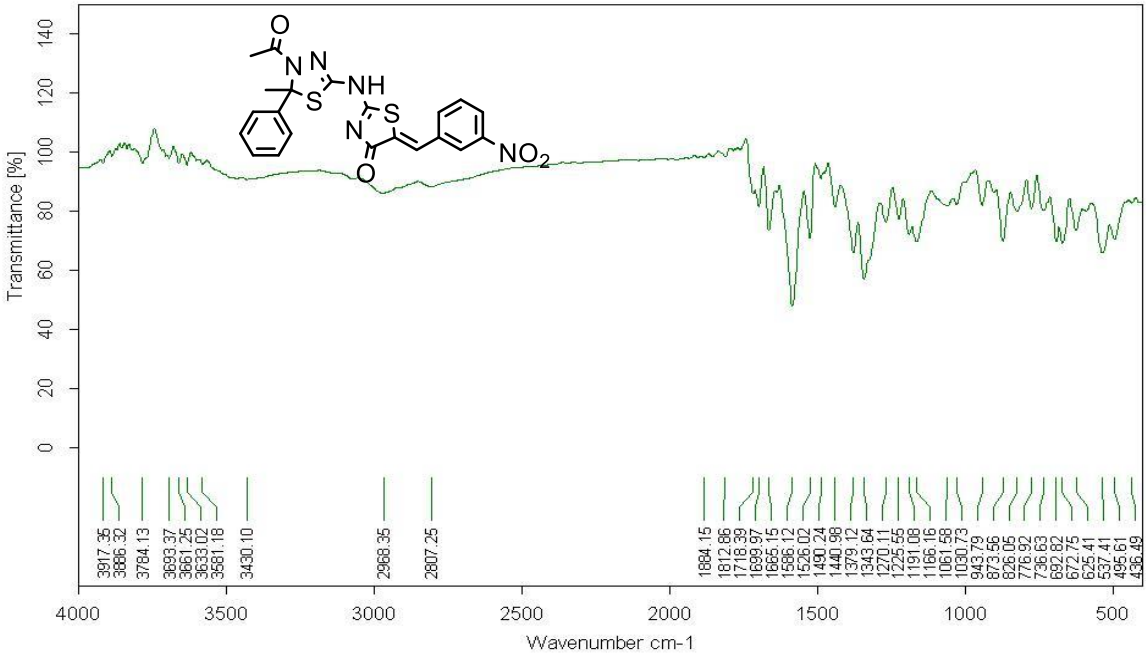

Figure S44: FT-IR of compound **8j**

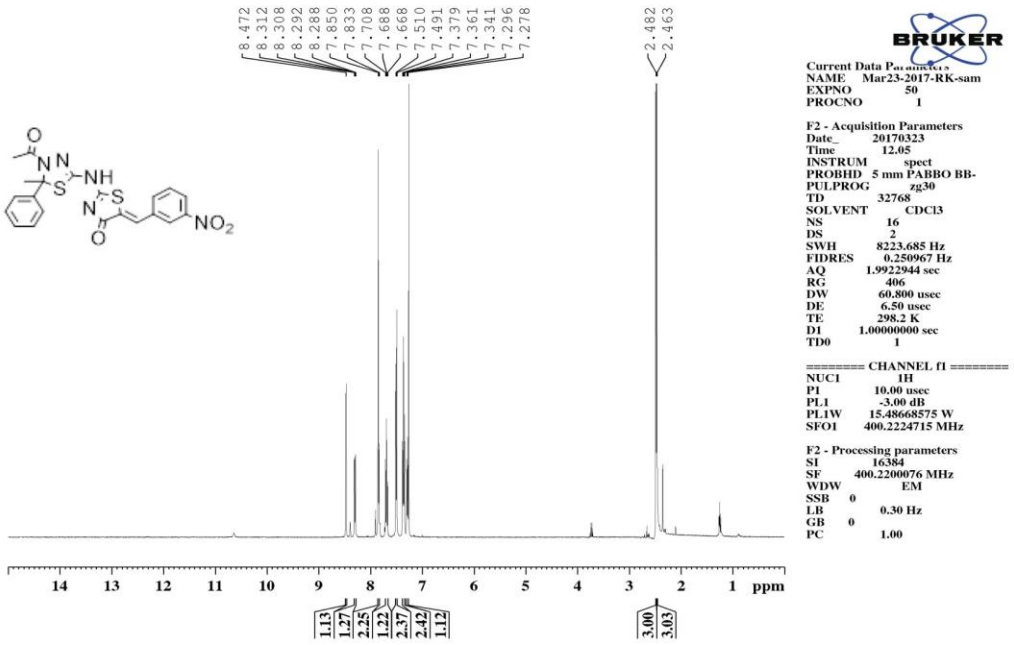

Figure S45: ^{1}H NMR of compound **8j**

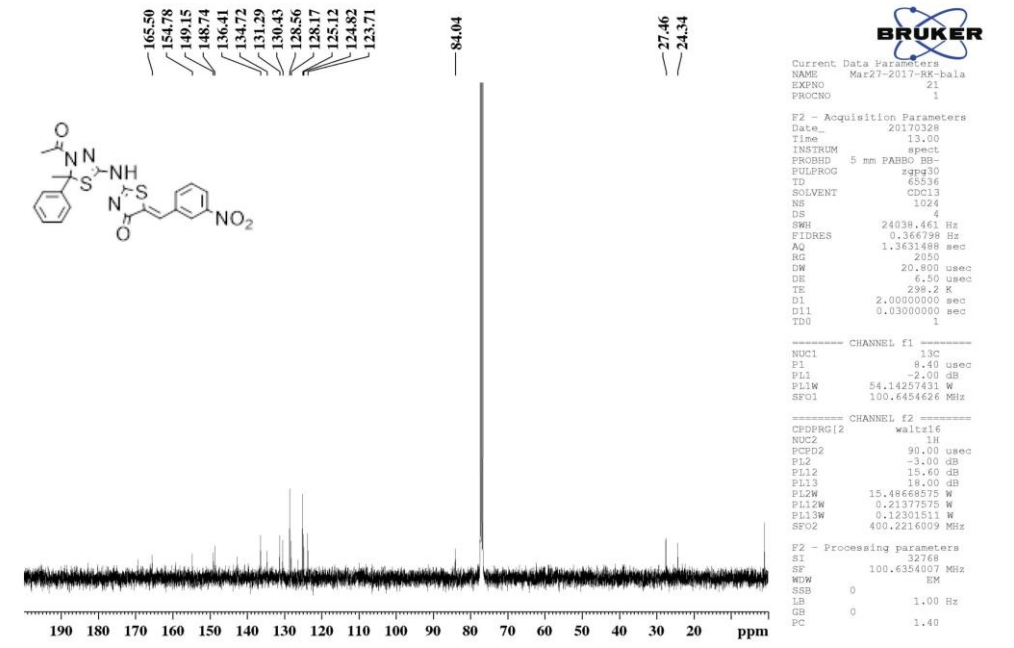

Figure S46: ^{13}C NMR of compound **8j**

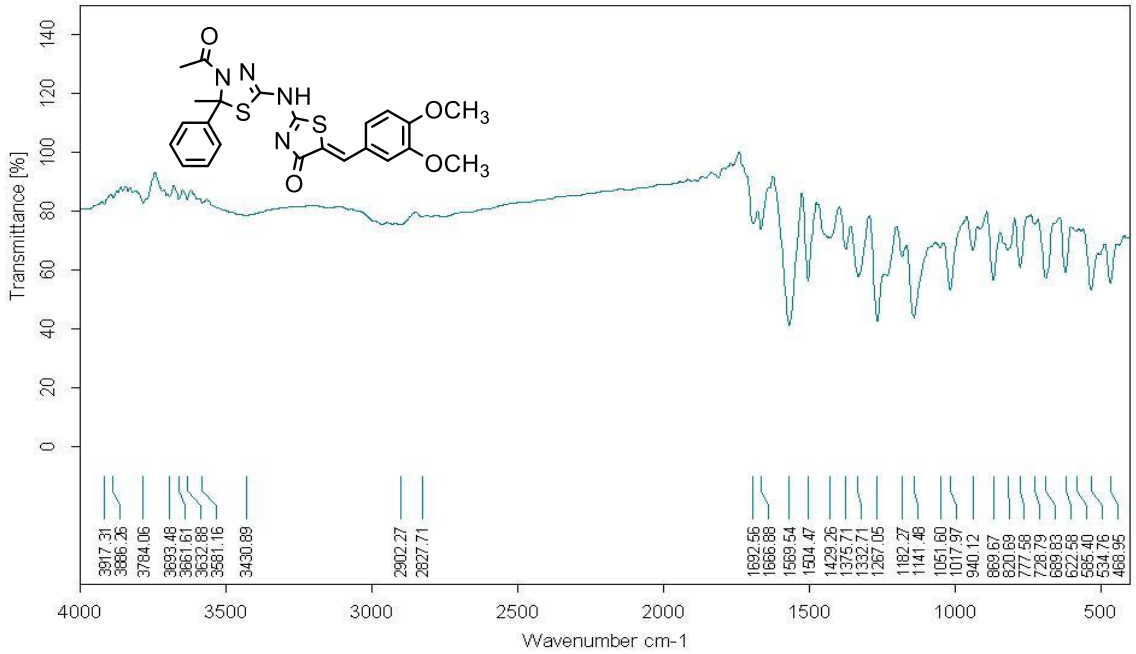

Figure S47: FT-IR of compound **8k**

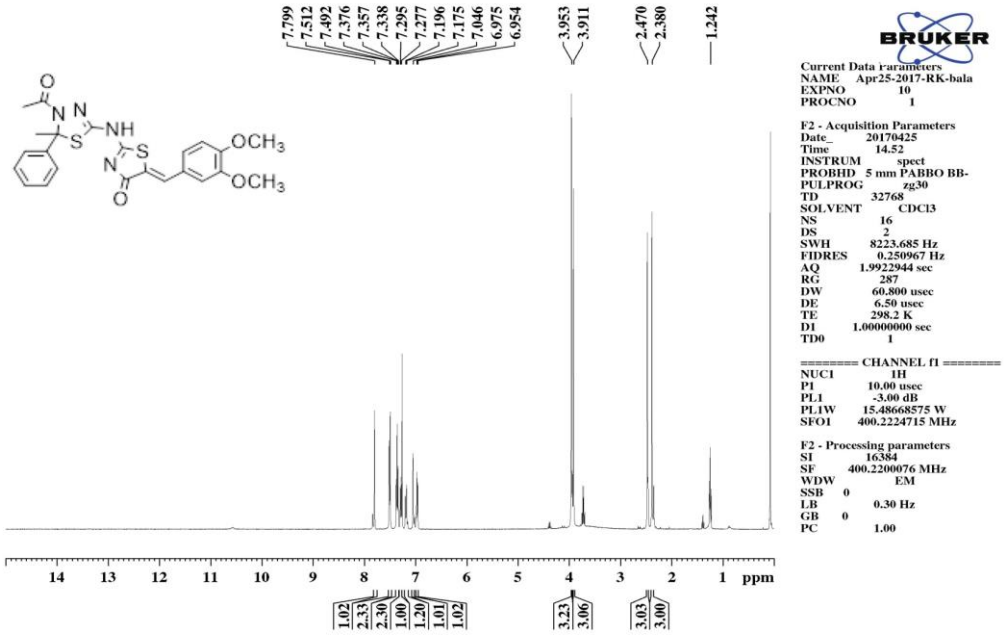

Figure S48: ^{1}H NMR of compound **8k**

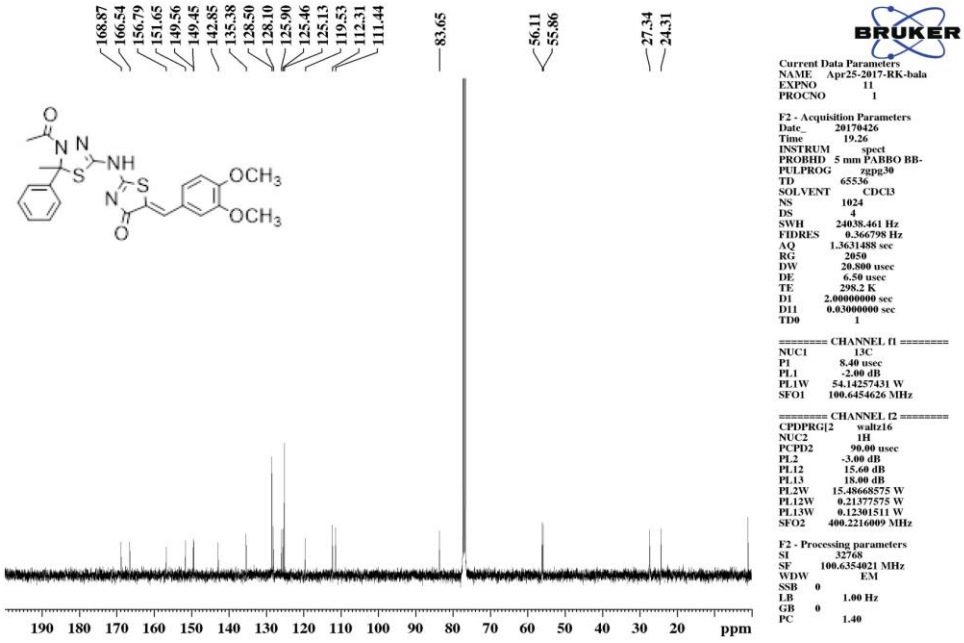

Figure S49: ^{13}C NMR of compound **8k**

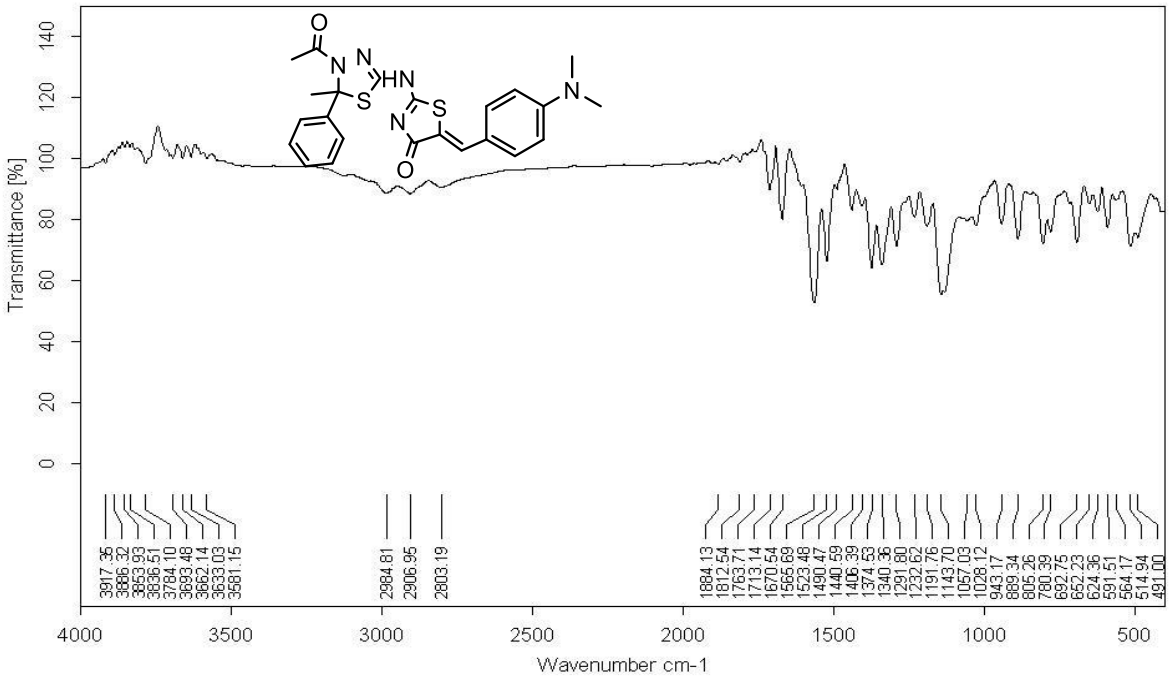

Figure S50: FT-IR of compound **8l**

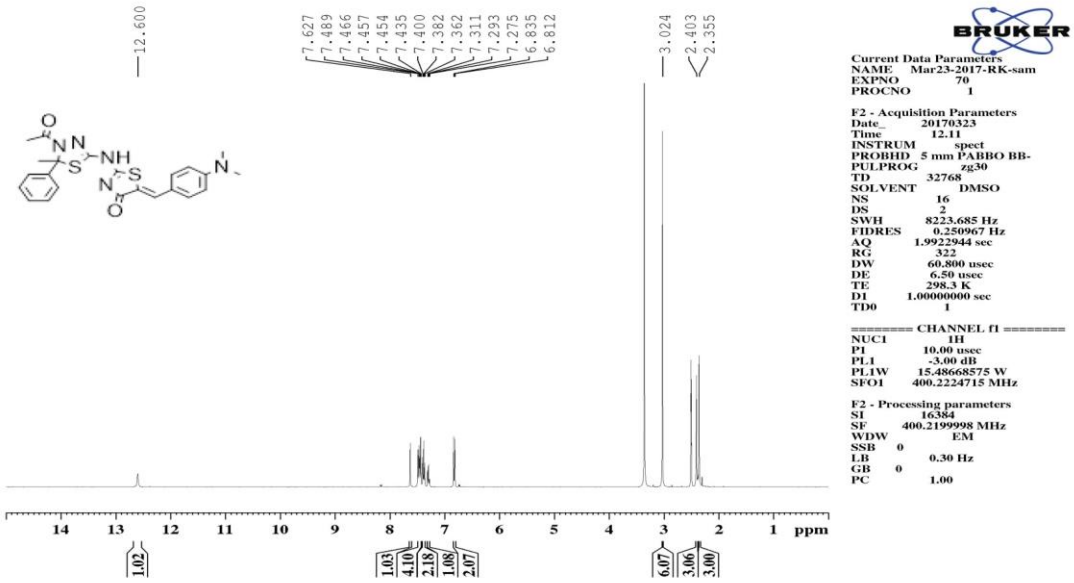

Figure S51: ^{1}H NMR of compound **8l**

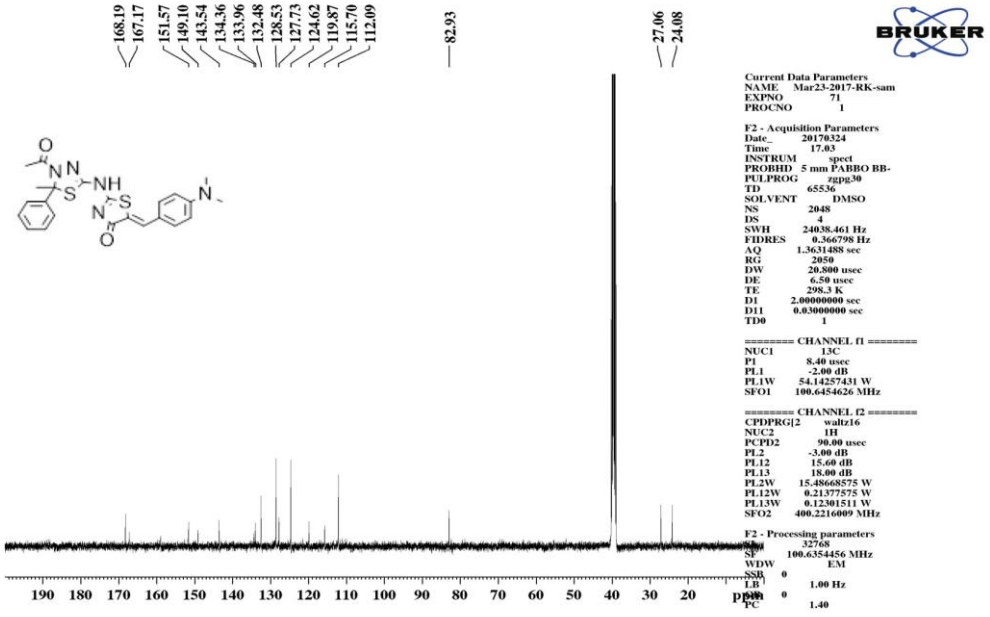

Figure S52: ^{13}C NMR of compound **8l**

Elemental Composition Report **Page 1**

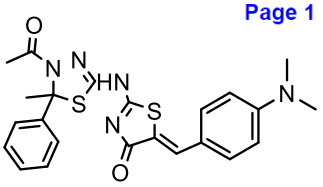

Single Mass Analysis
Tolerance = 5.0 PPM / DBE: min = -1.5, max = 100.0
Element prediction: Off
Number of isotope peaks used for i-FIT = 2

Monoisotopic Mass, Even Electron Ions
49 formula(e) evaluated with 1 results within limits (up to 20 best isotopic matches for each mass)
Elements Used:
C: 20-25 H: 20-25 N: 0-5 O: 0-5 S: 0-2
FSP13 61 (2.023) Cm (1:61)
TOF MS ES-

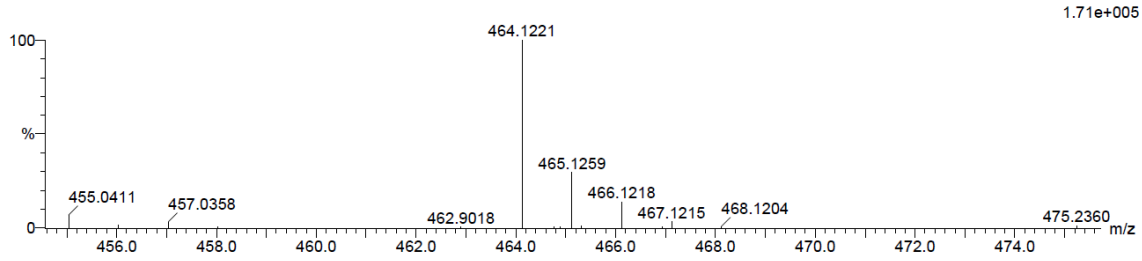

Minimum:				-1.5			
Maximum:		5.0	5.0	100.0			
Mass	Calc. Mass	mDa	PPM	DBE	i-FIT	i-FIT (Norm)	Formula
464.1221	464.1215	0.6	1.3	15.5	50.0	0.0	C23 H22 N5 O2 S2

Figure S53: HR-MS of compound **8l**

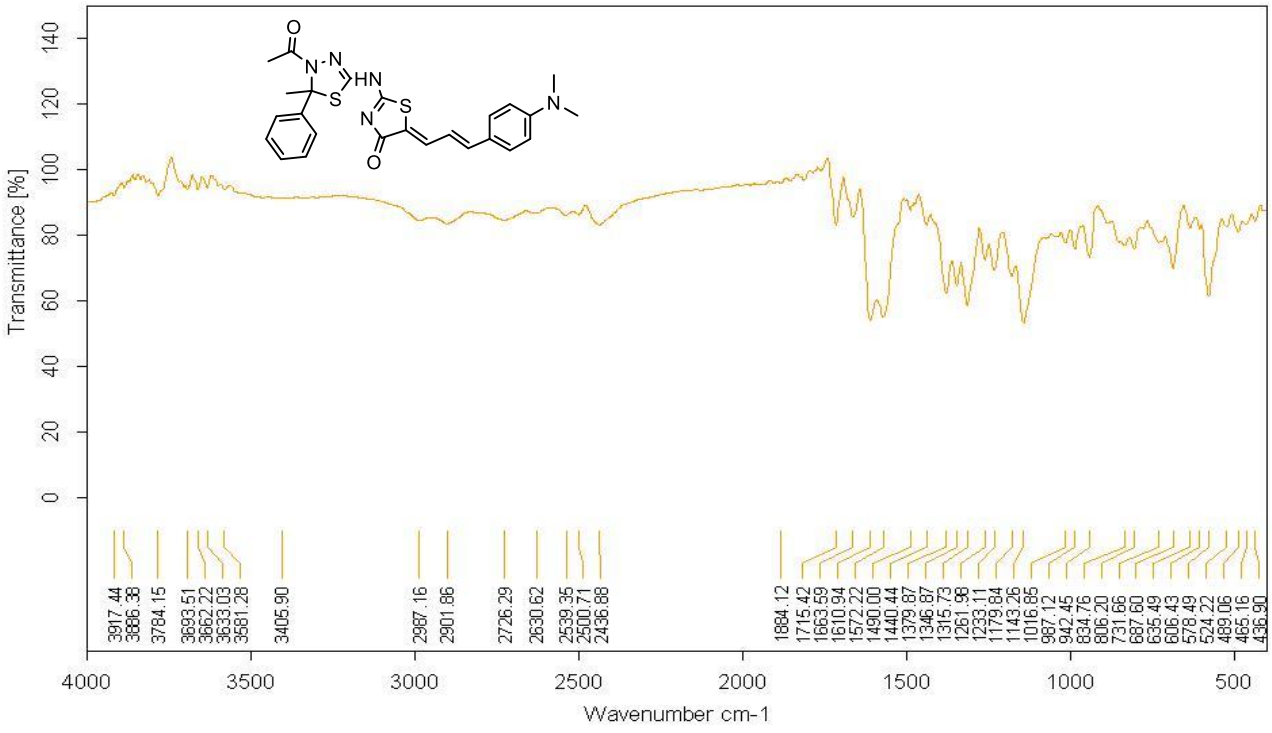

Figure S54: FT-IR of compound **8m**

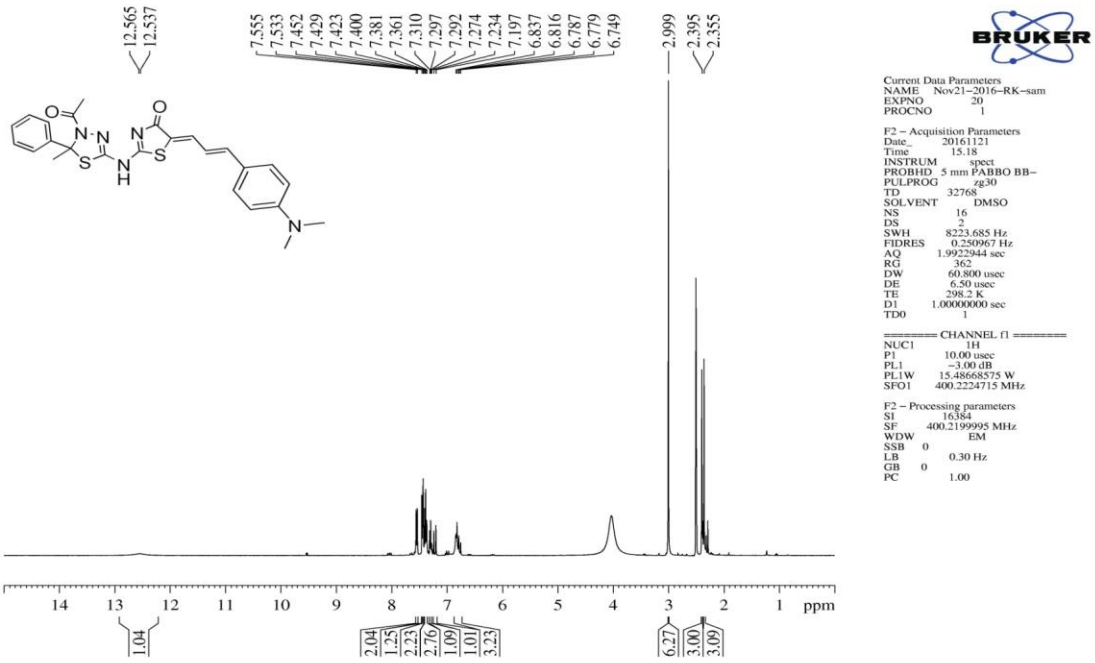

Figure S55: ^{1}H NMR of compound **8m**

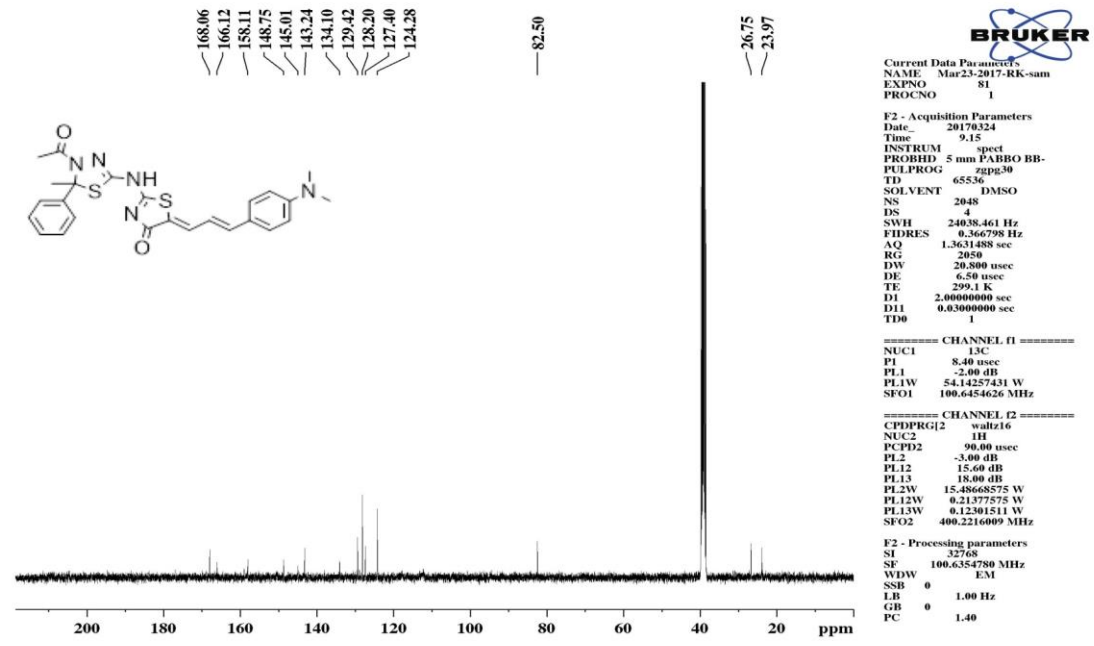

Figure S56: ^{13}C NMR of compound **8m**

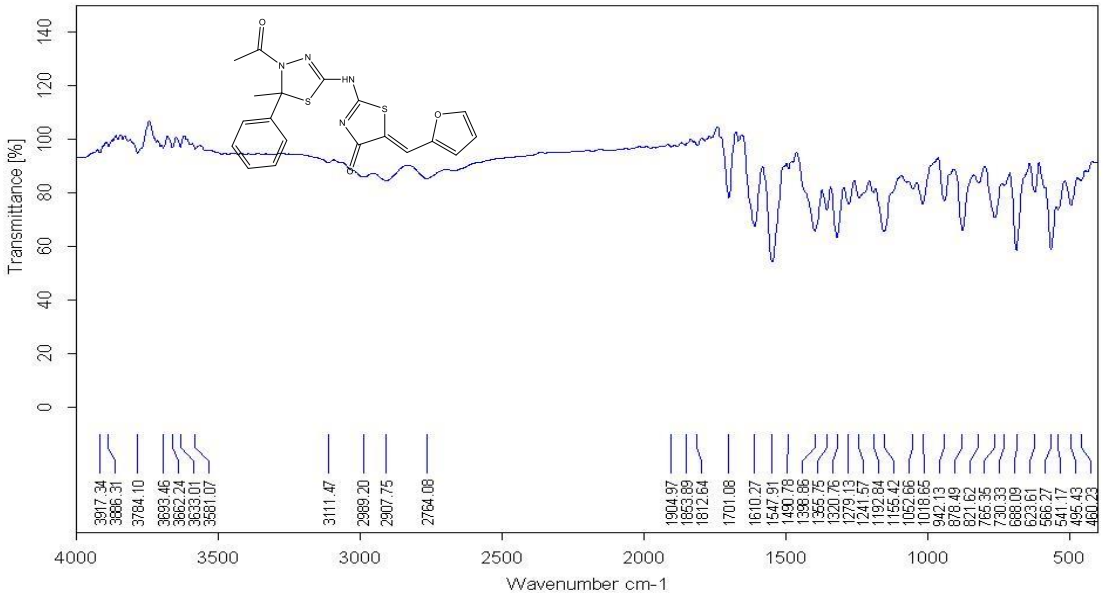

Figure S57: FT-IR of compound **8n**

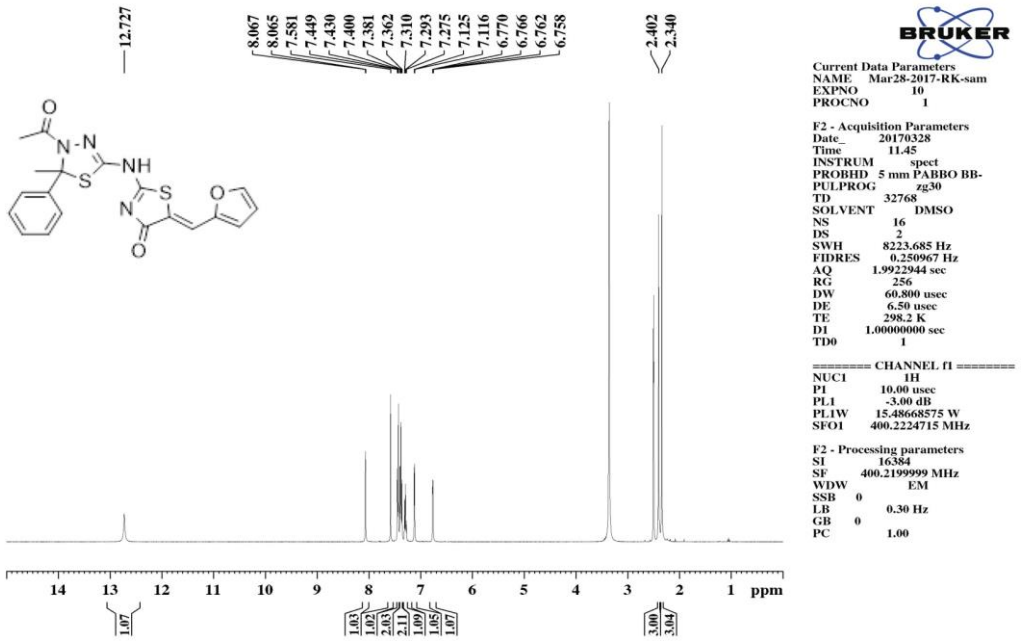

Figure S58: ^{1}H NMR of compound **8n**

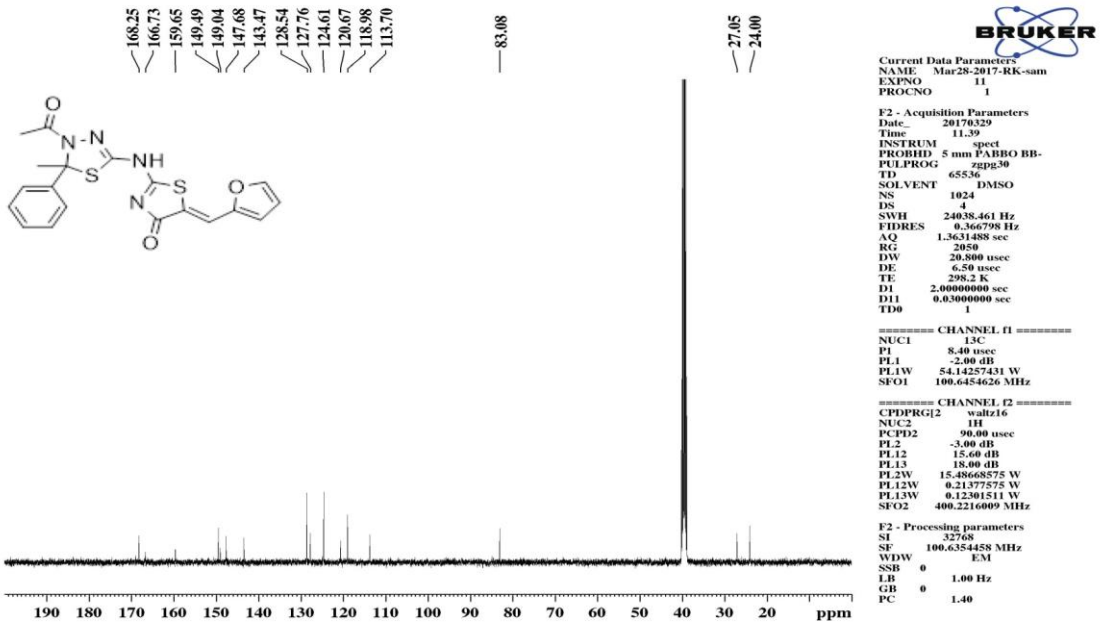

Figure S59: ^{13}C NMR of compound **8n**

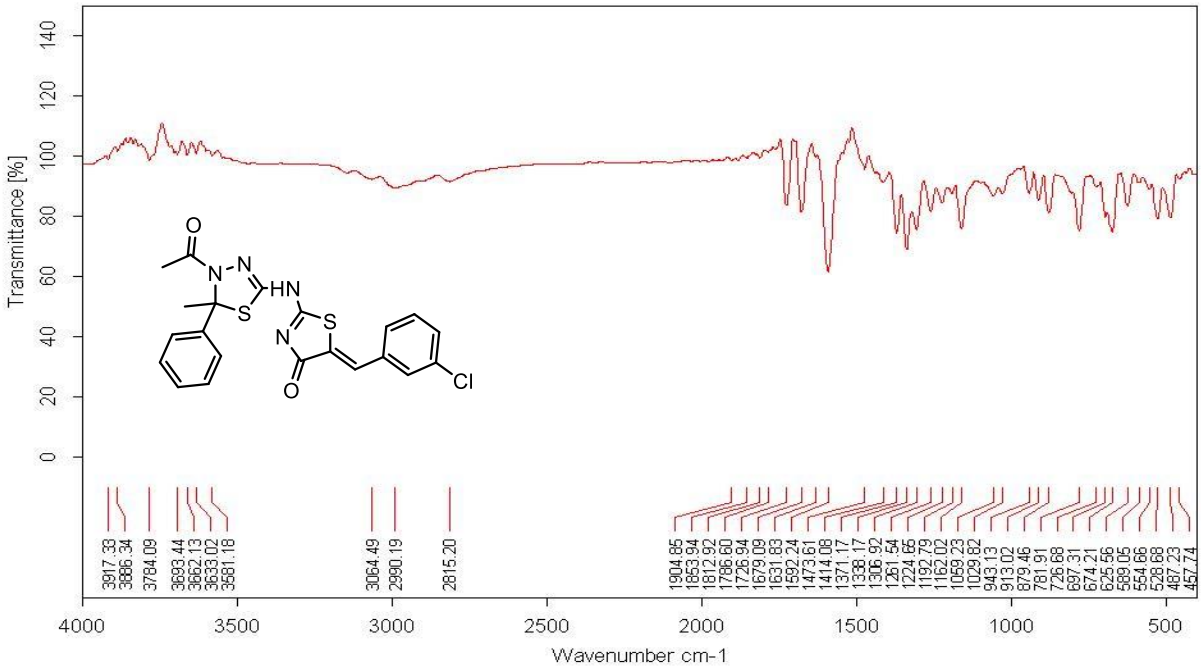

Figure S60: FT-IR of compound **8o**

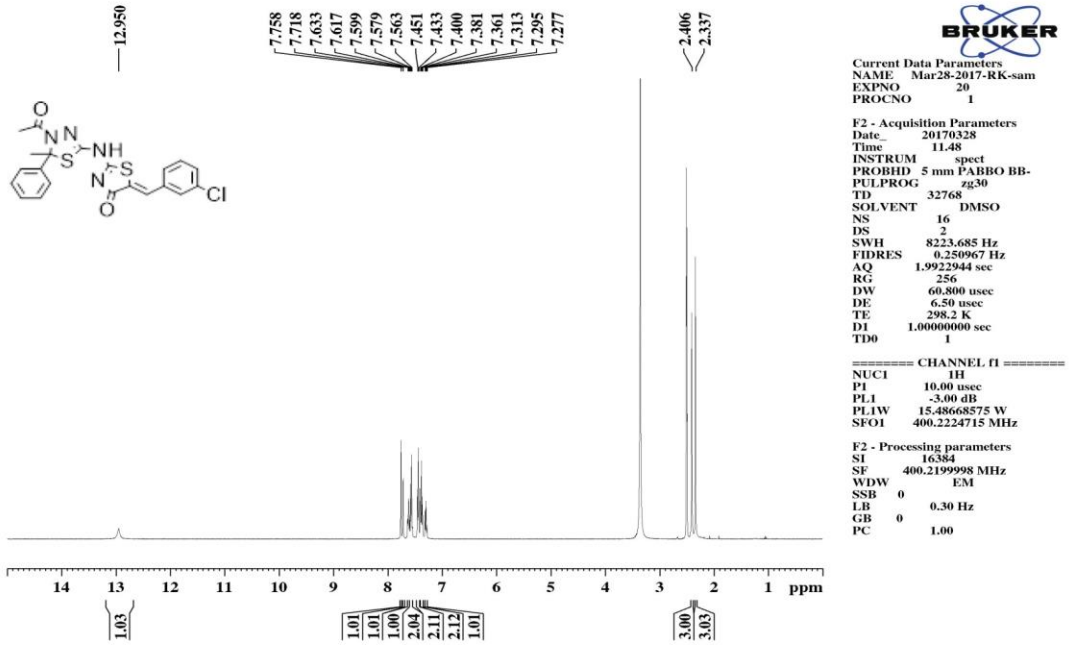

Figure S61: ^{1}H NMR of compound **8o**

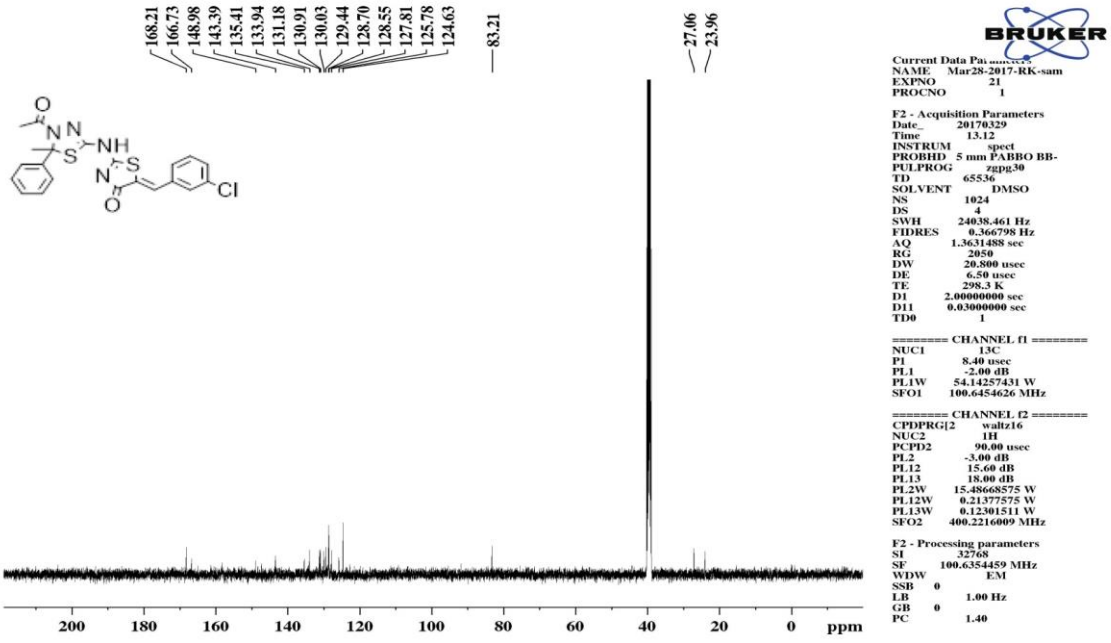

Figure S62: ^{13}C NMR of compound **8o**

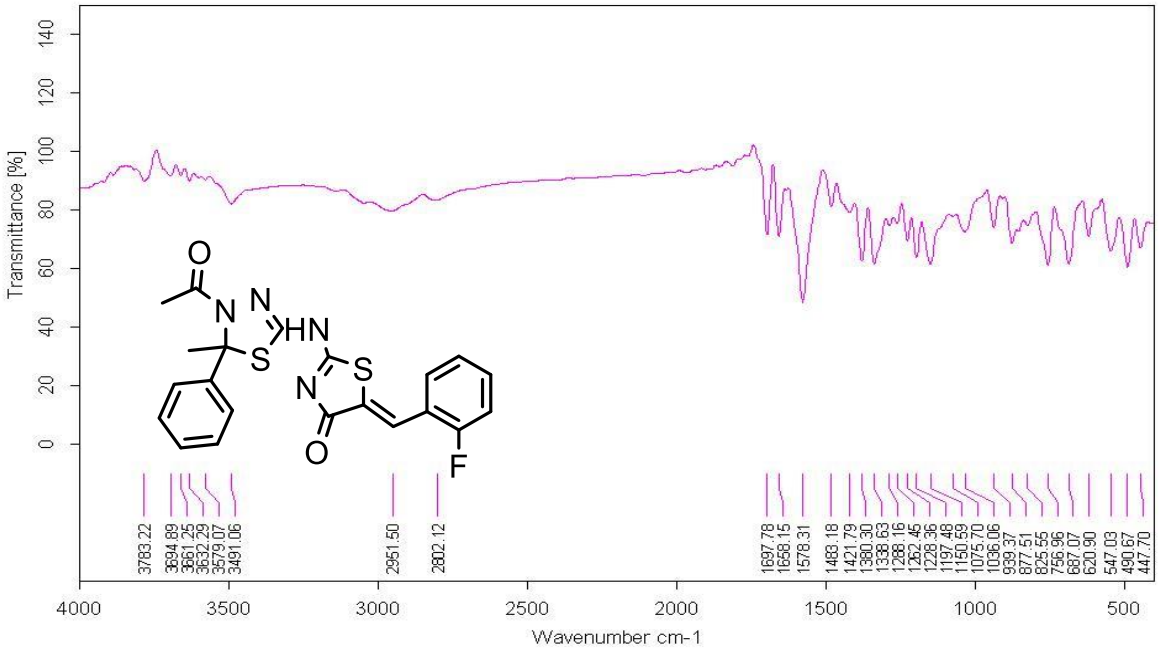

Figure S63: FT-IR of compound **8p**

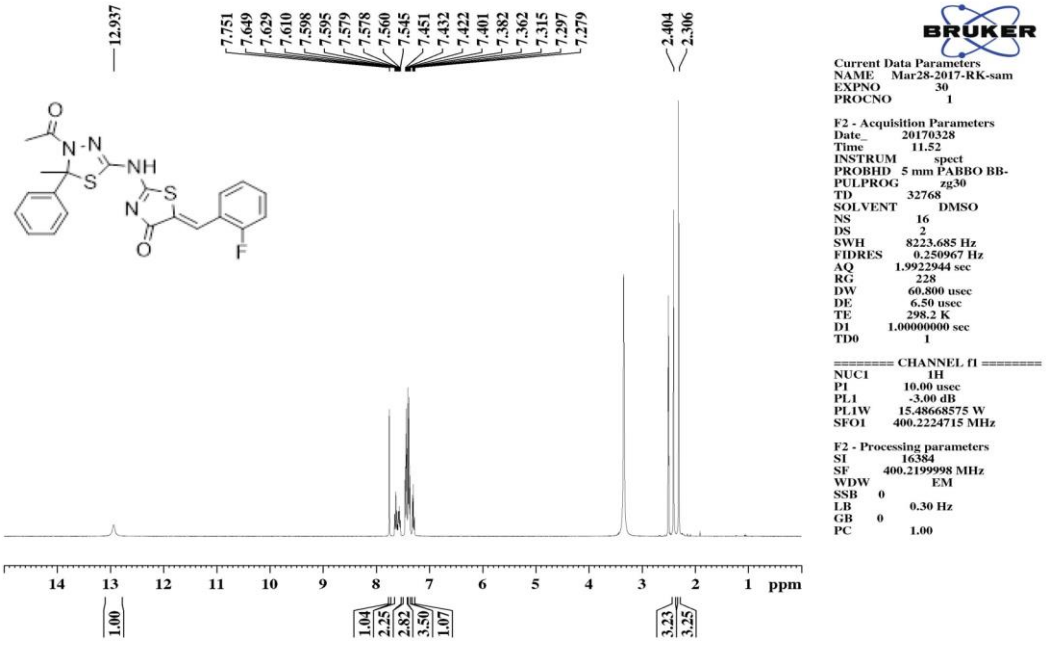

Figure S64: ^{1}H NMR of compound **8p**

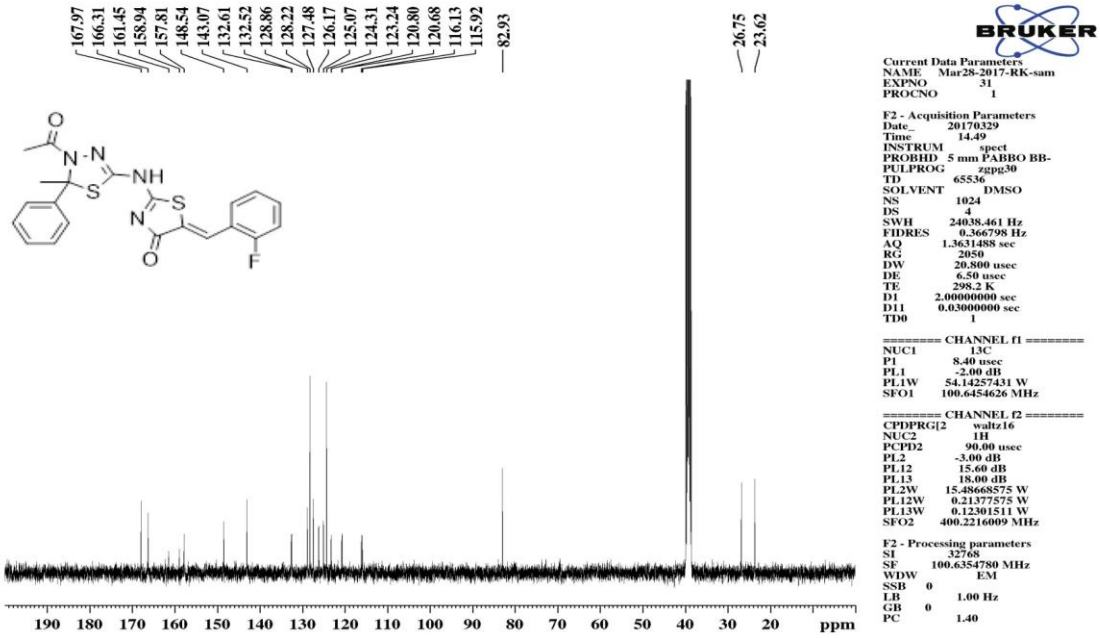

Figure S65: ^{13}C NMR of compound **8p**

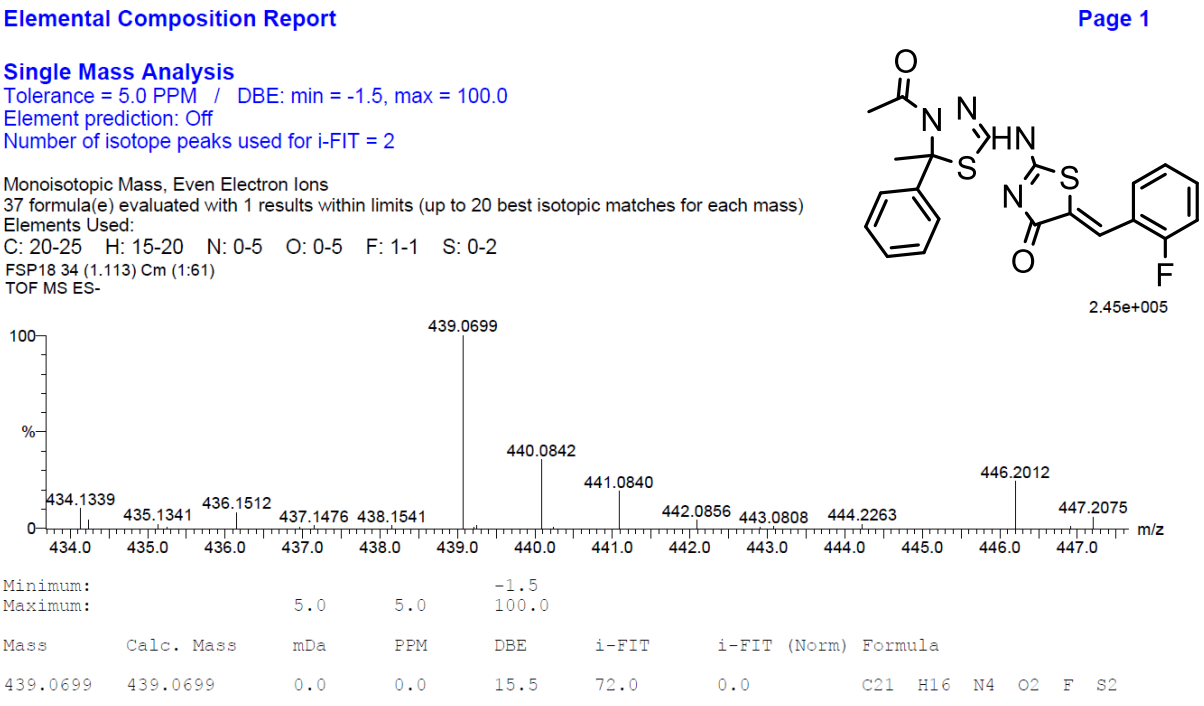

Figure S66: HR-MS of compound **8p**

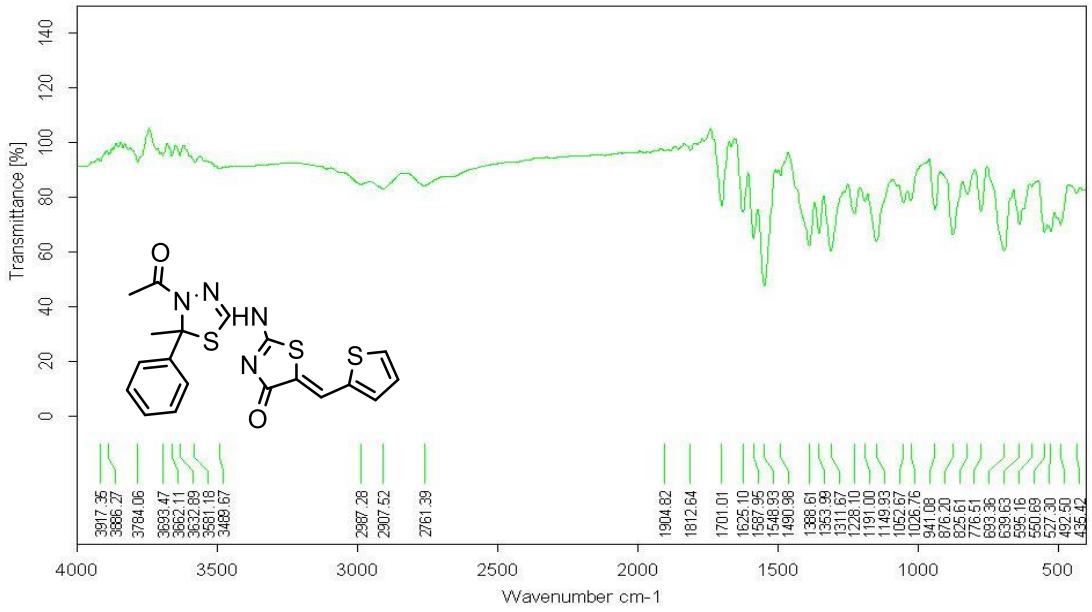

Figure S67: FT-IR of compound **8q**

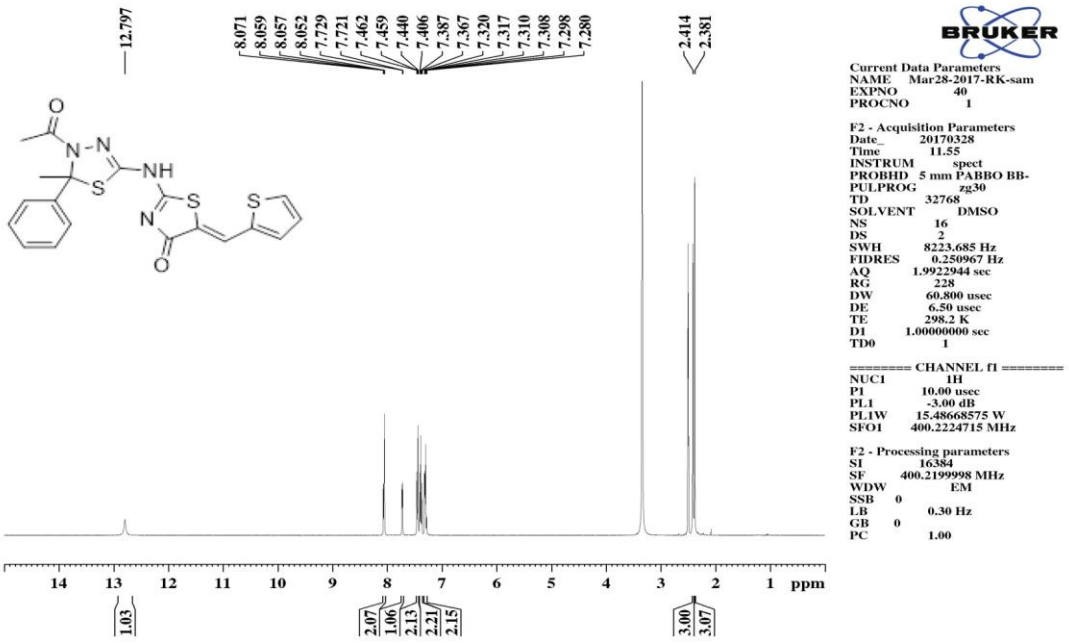

Figure S68: ^{1}H NMR of compound **8q**

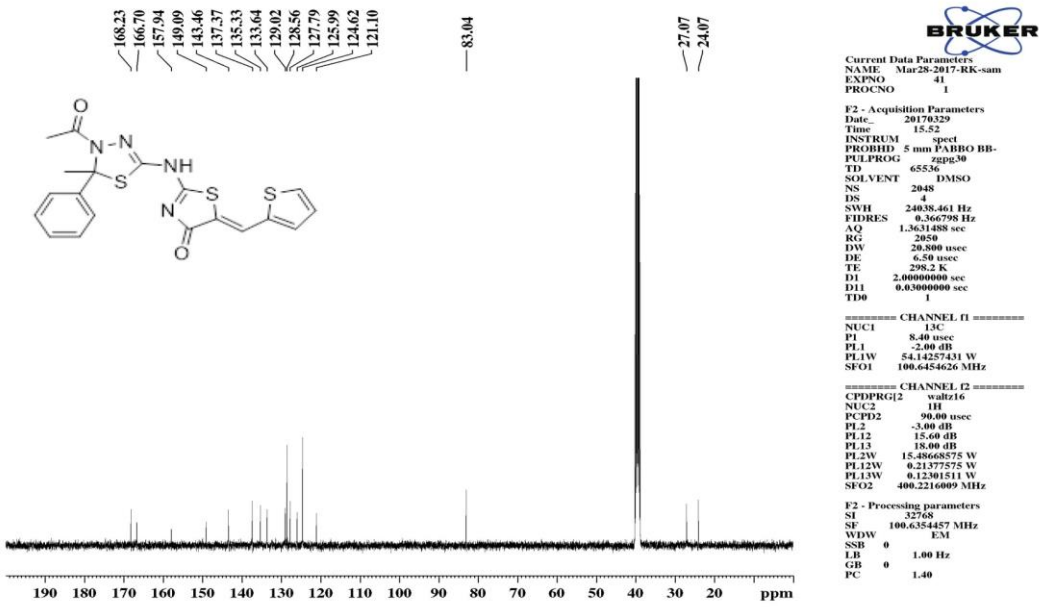

Figure S69: ^{13}C NMR of compound **8q**

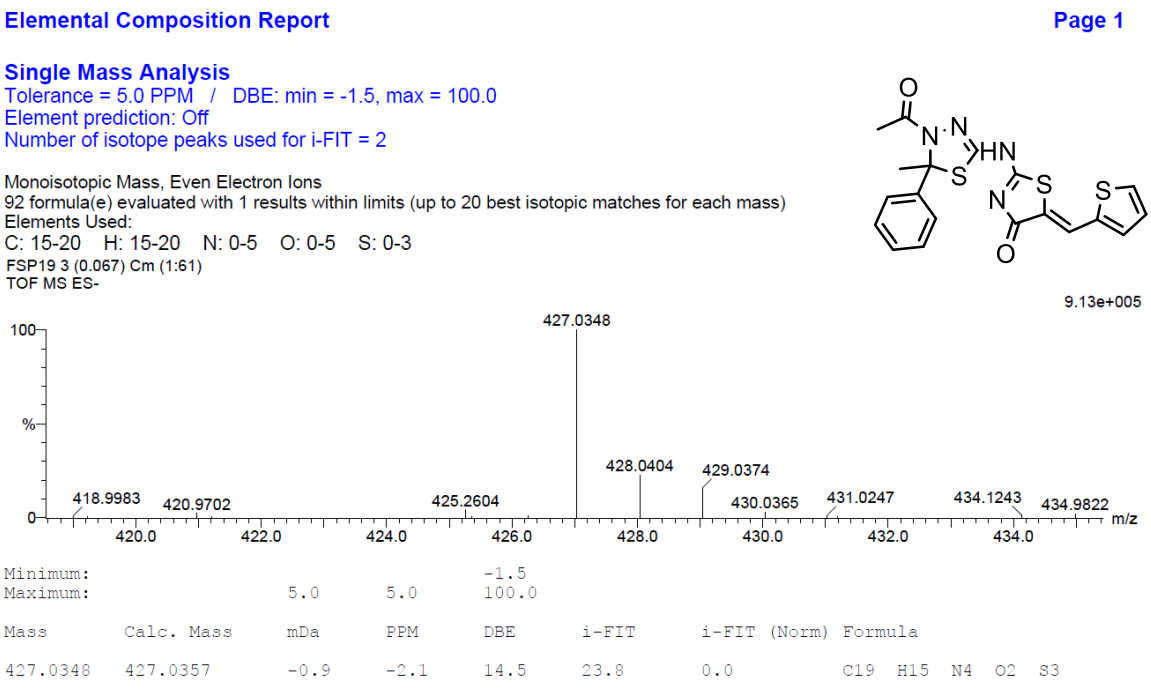

Figure S70: HR-MS of compound **8q**

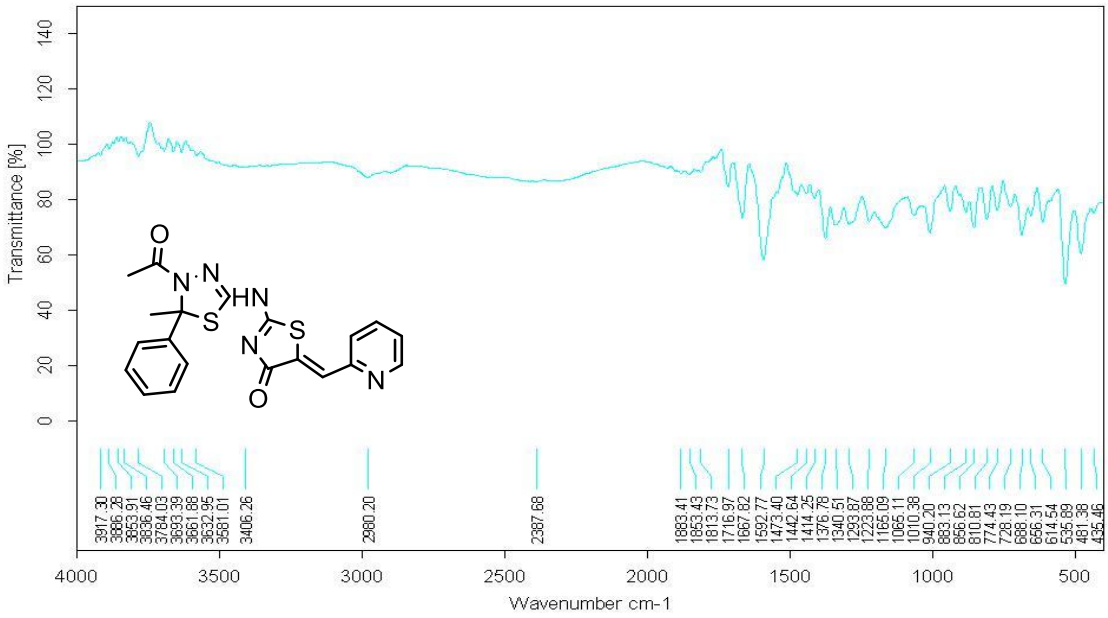

Figure S71: FT-IR of compound **8r**

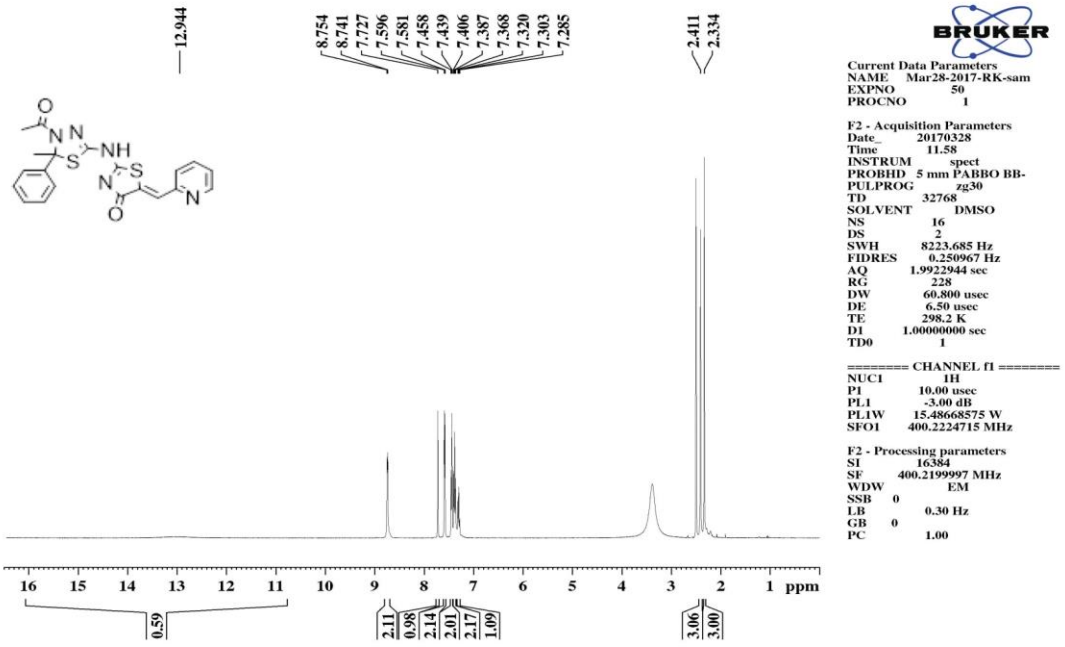

Figure S72: ^{1}H NMR of compound **8r**

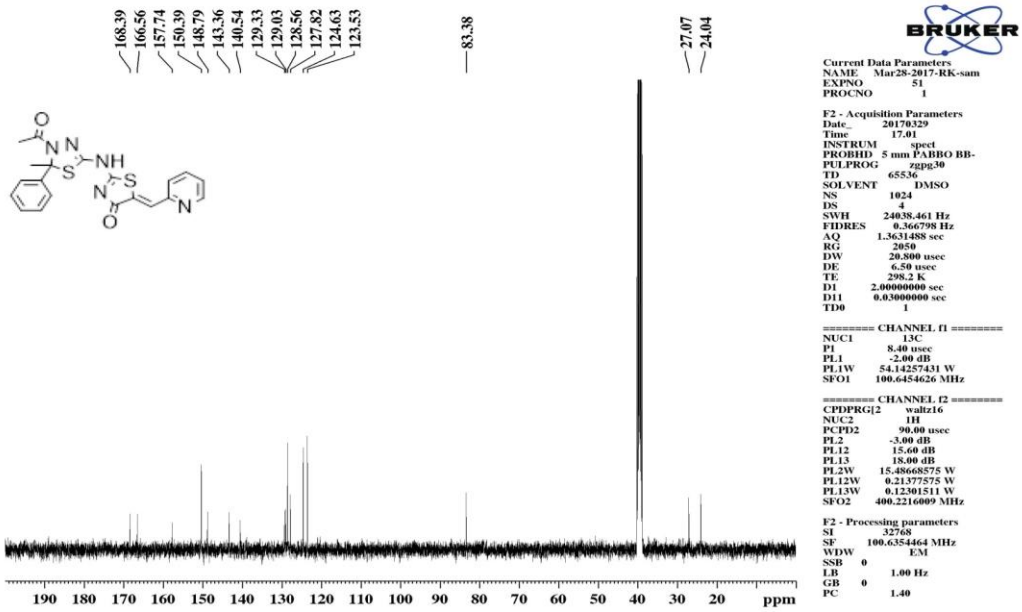

Figure S73: ^{13}C NMR of compound **8r**

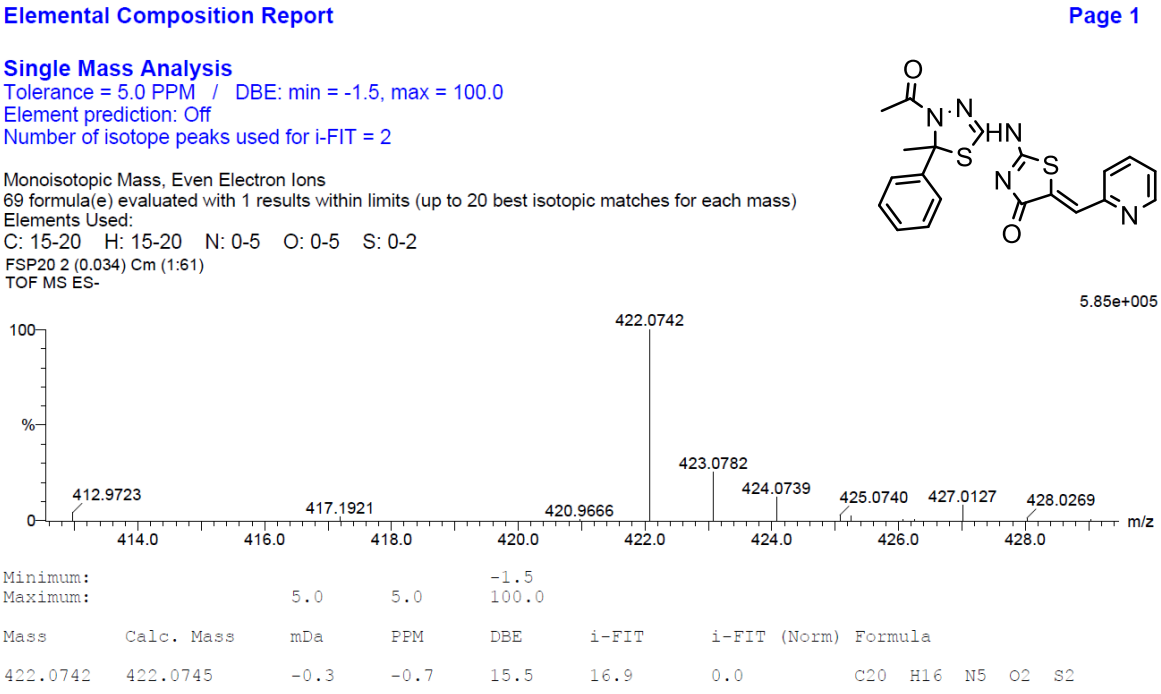

Figure S74: HR-MS of compound **8r**

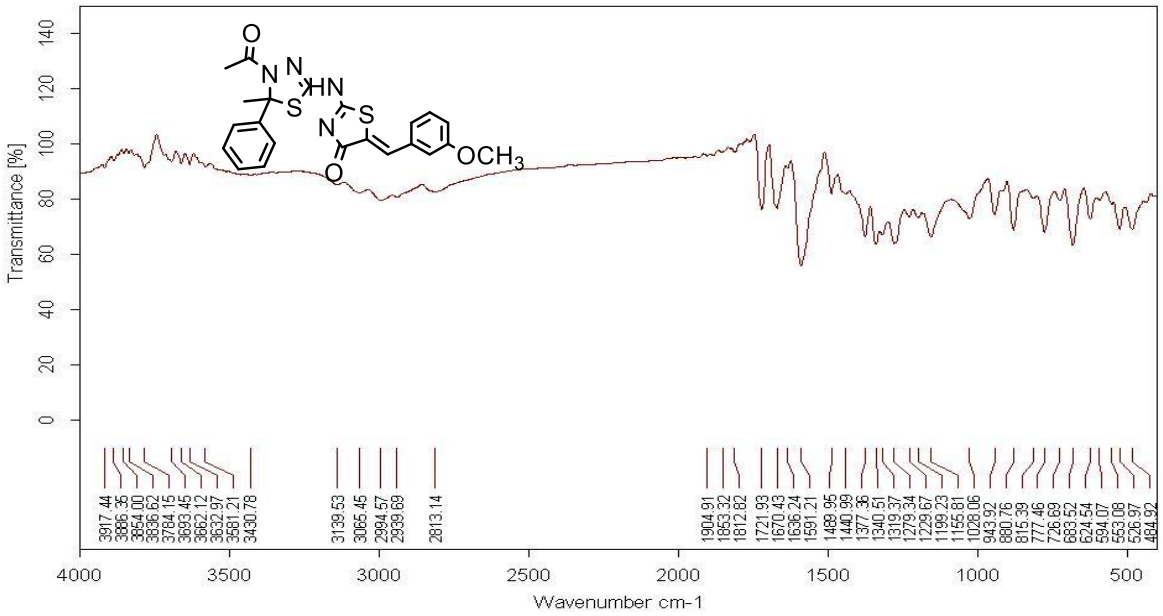

Figure S75: FT-IR of compound **8s**

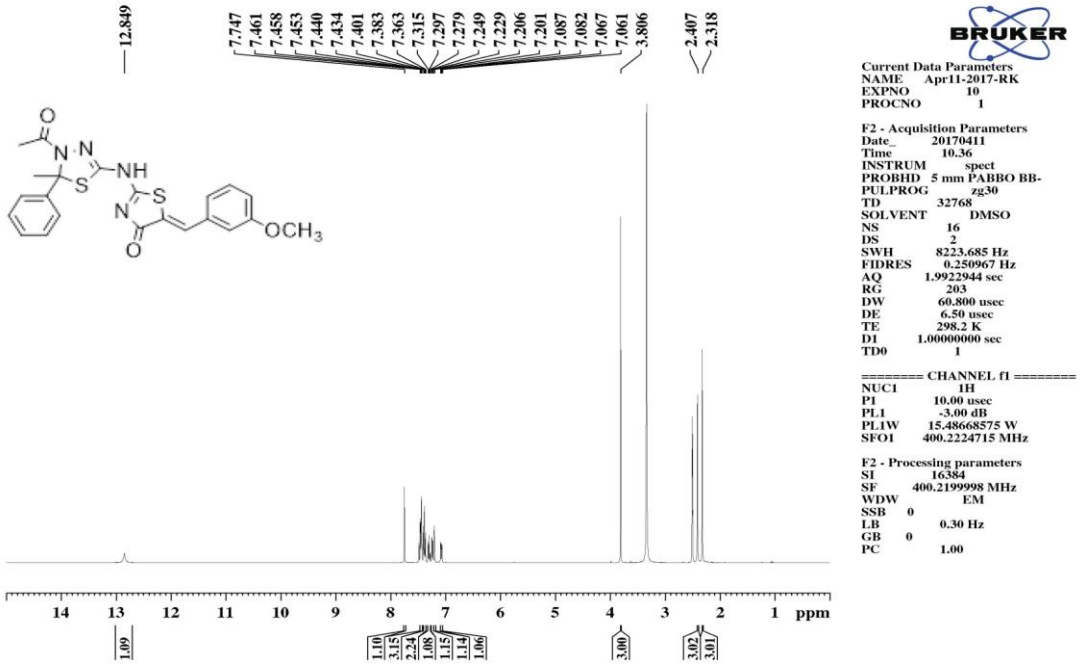

Figure S76: ^{1}H NMR of compound **8s**

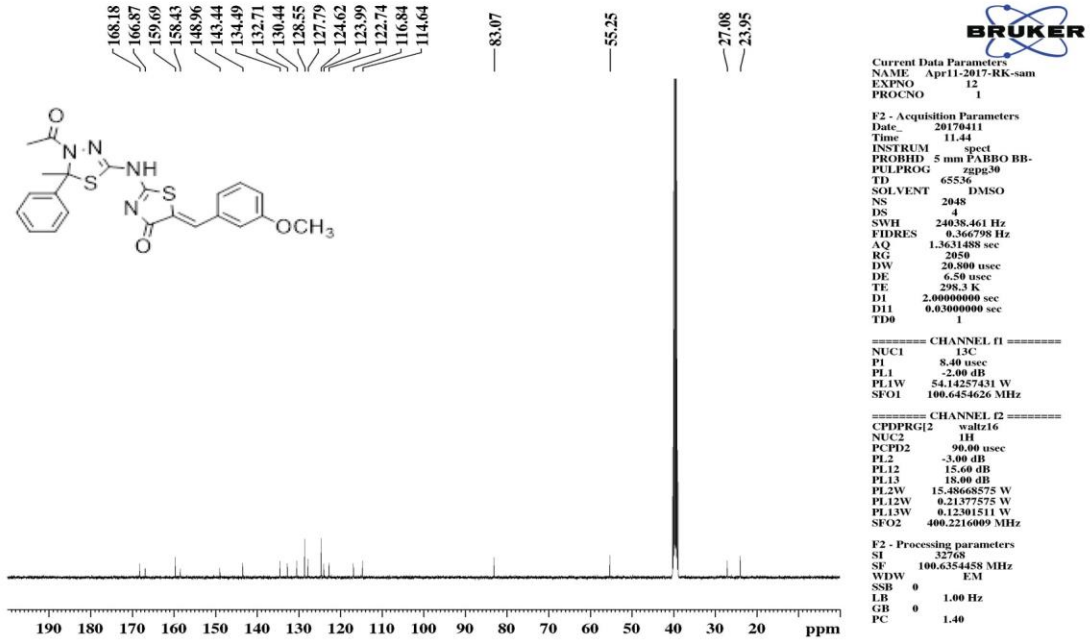

Figure S77: ^{13}C NMR of compound **8s**

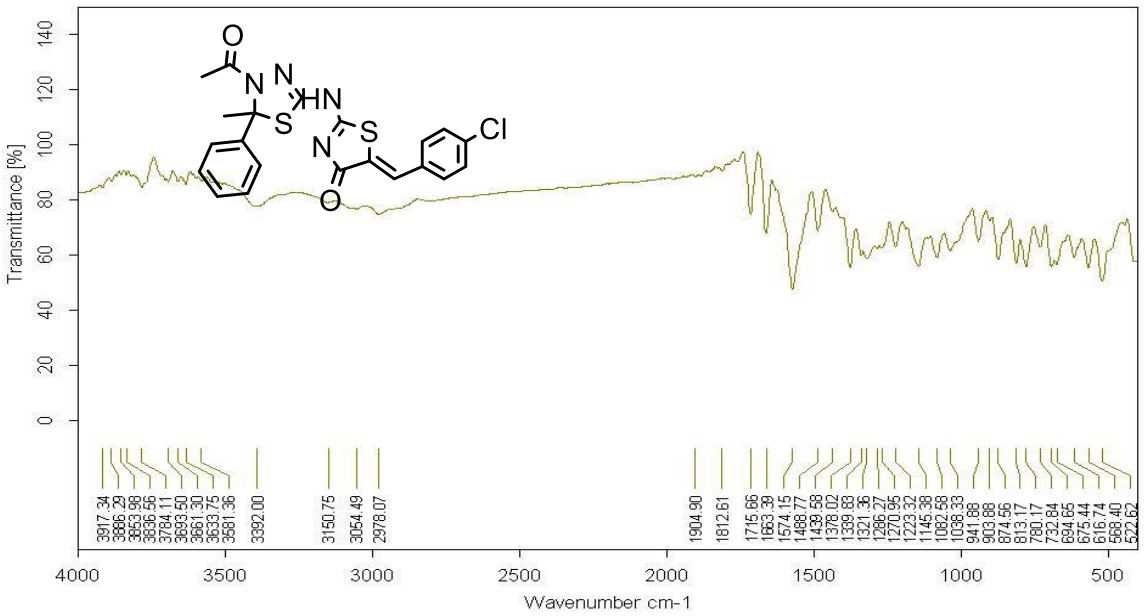

Figure S78: FT-IR of compound **8t**

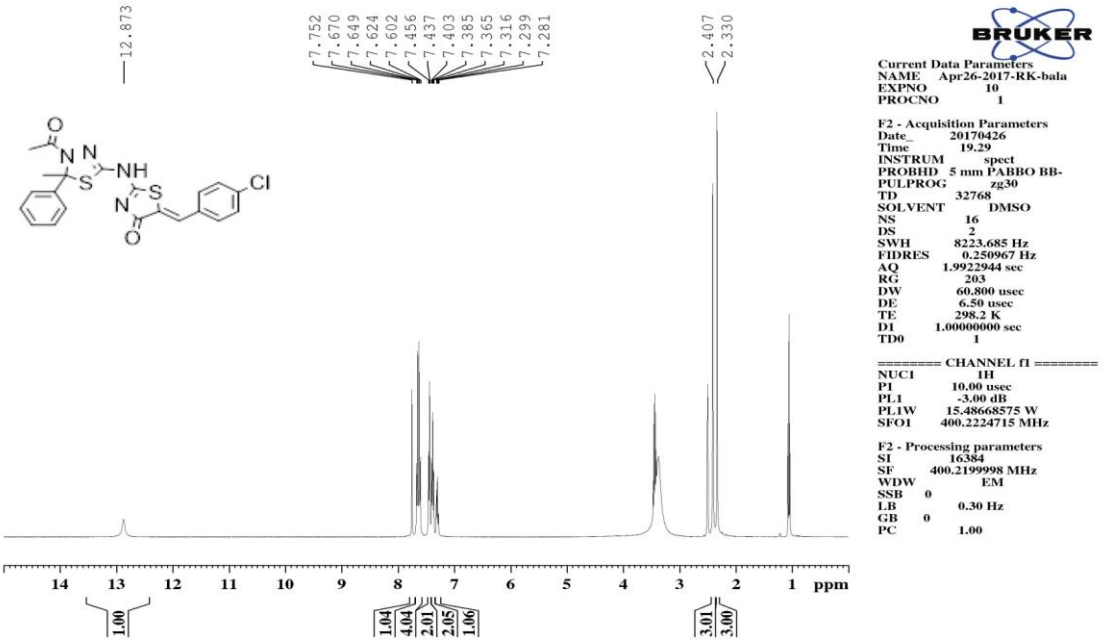

Figure S79: ^{1}H NMR of compound **8t**

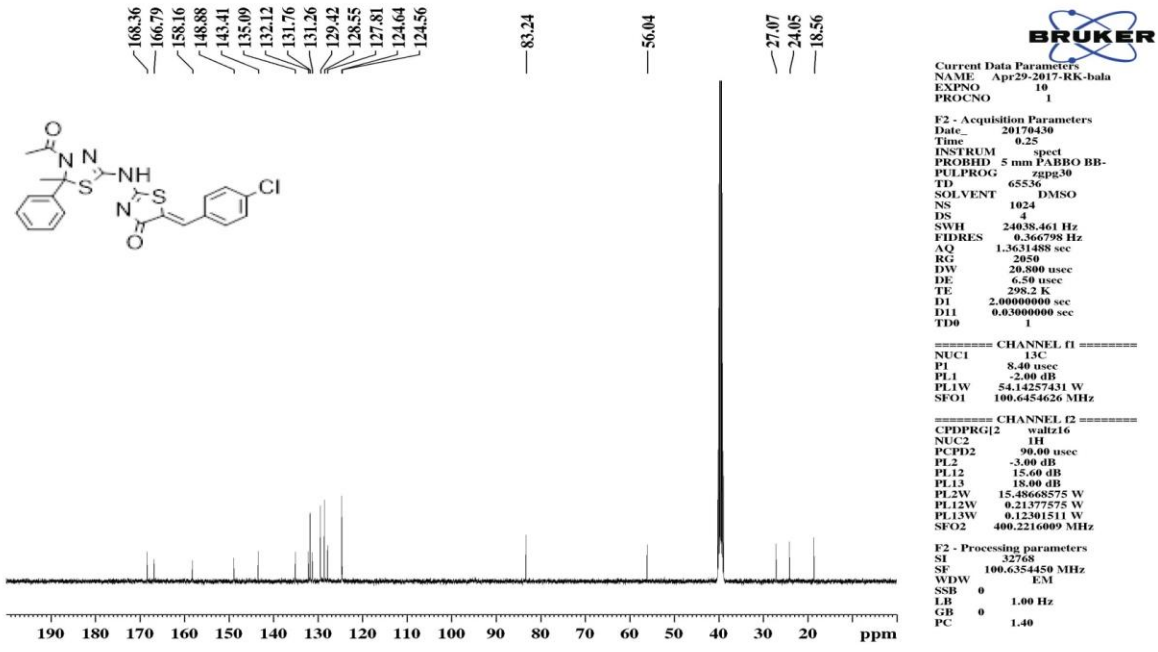

Figure S80: ^{13}C NMR of compound **8t**

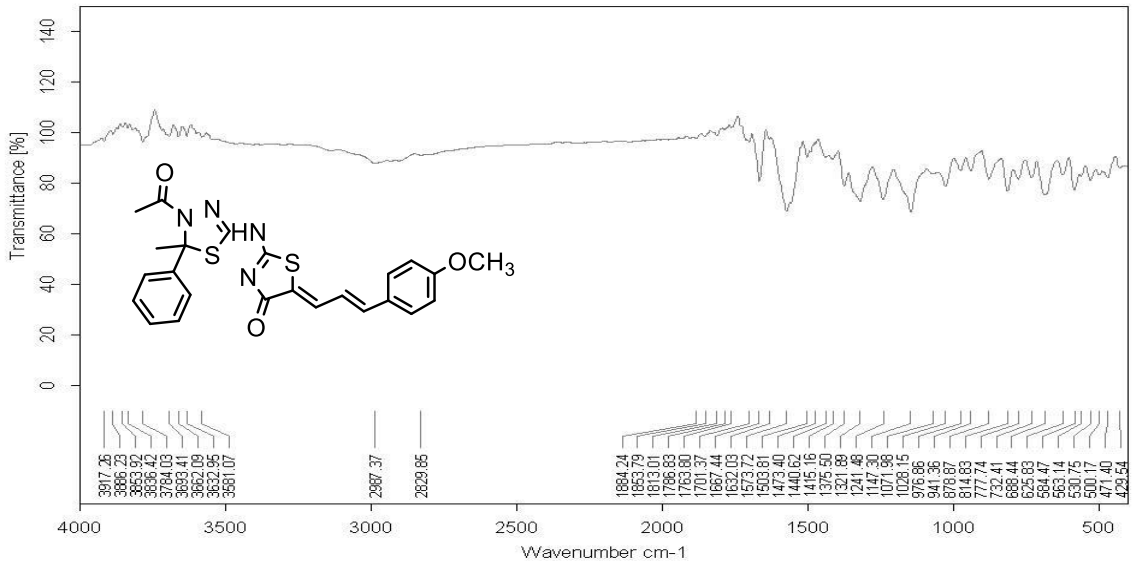

Figure S81: FT-IR of compound **8u**

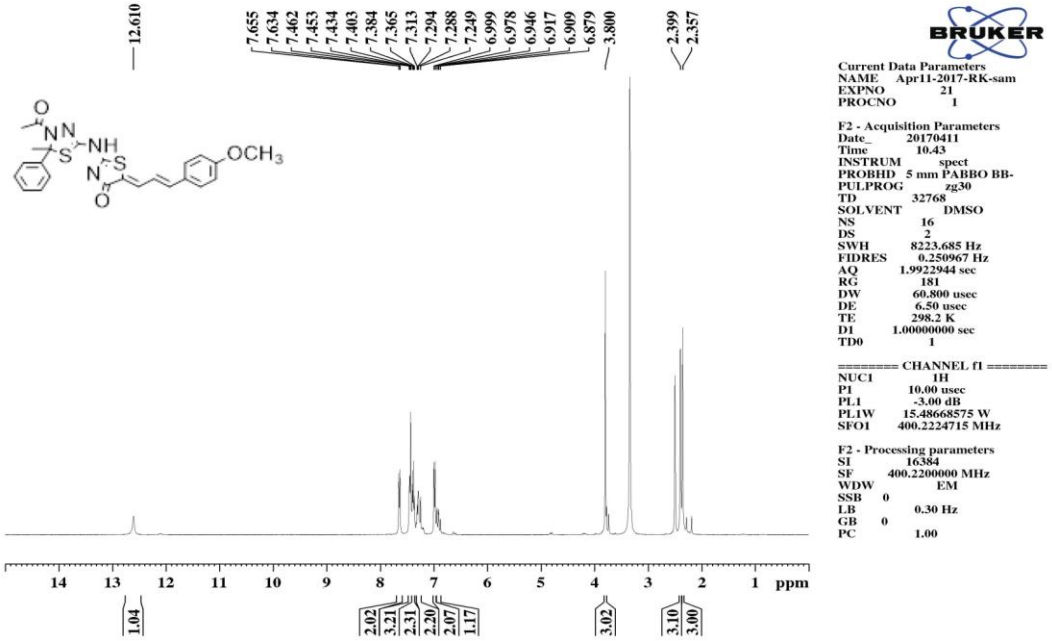

Figure S82: ^{1}H NMR of compound **8u**

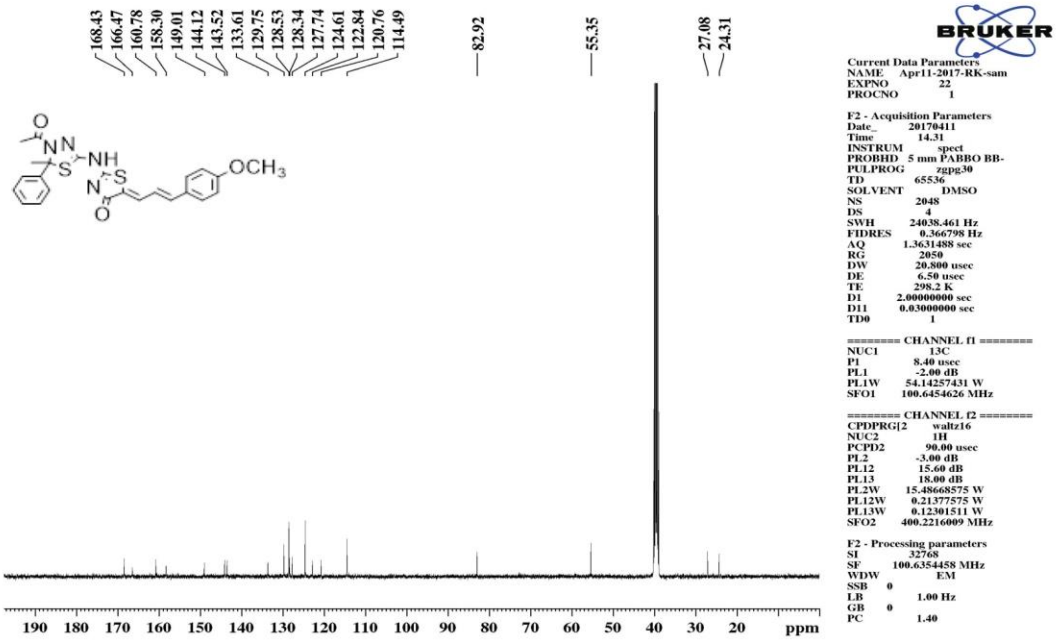

Figure S83: ^{13}C NMR of compound **8u**

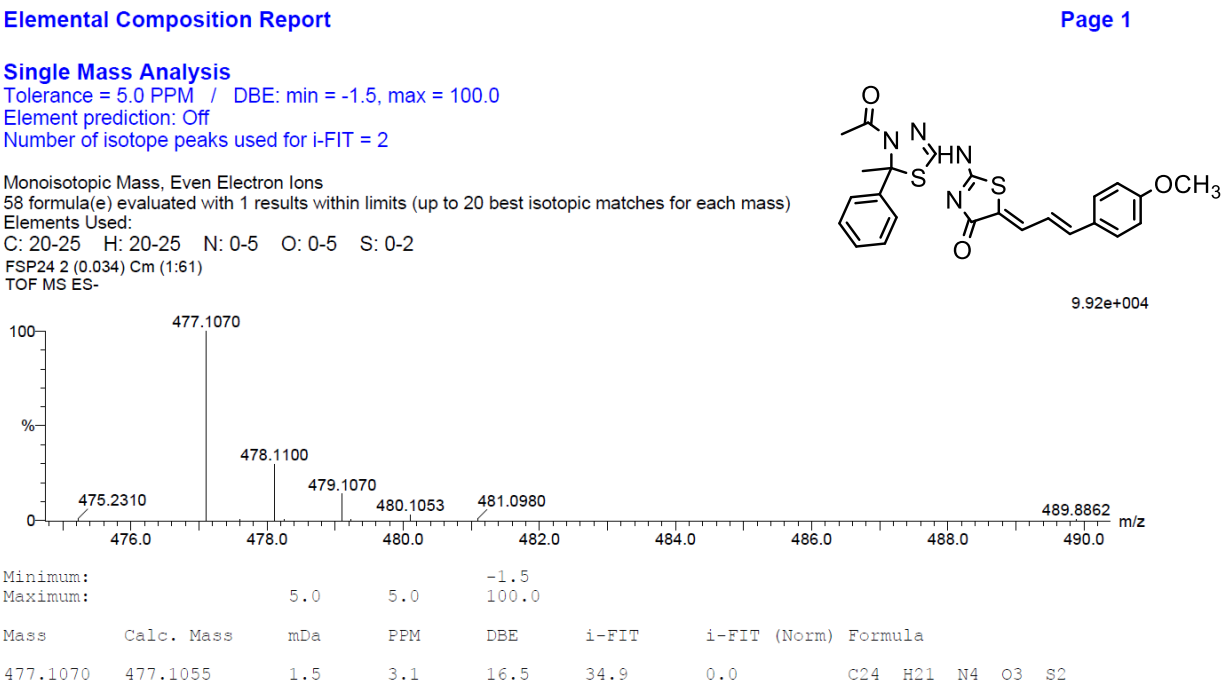

Minimum:				-1.5			
Maximum:		5.0	5.0	100.0			
Mass	Calc. Mass	mDa	PPM	DBE	i-FIT	i-FIT (Norm)	Formula
477.1070	477.1055	1.5	3.1	16.5	34.9	0.0	C24 H21 N4 O3 S2

Figure S84: HR-MS of compound **8u**

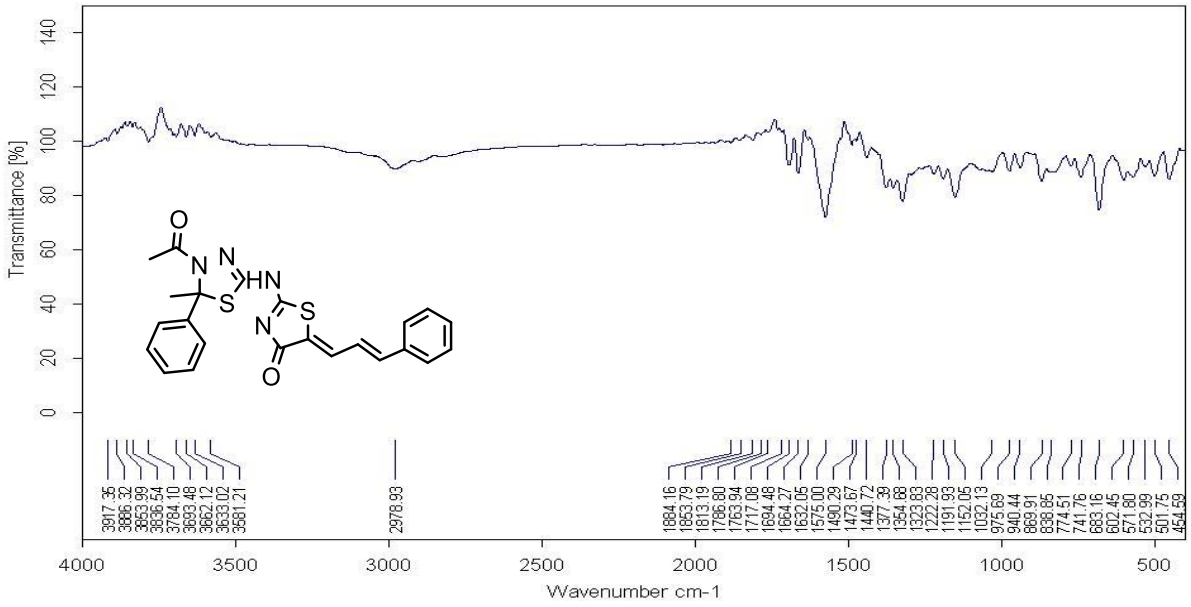

Figure S85: FT-IR of compound **8v**

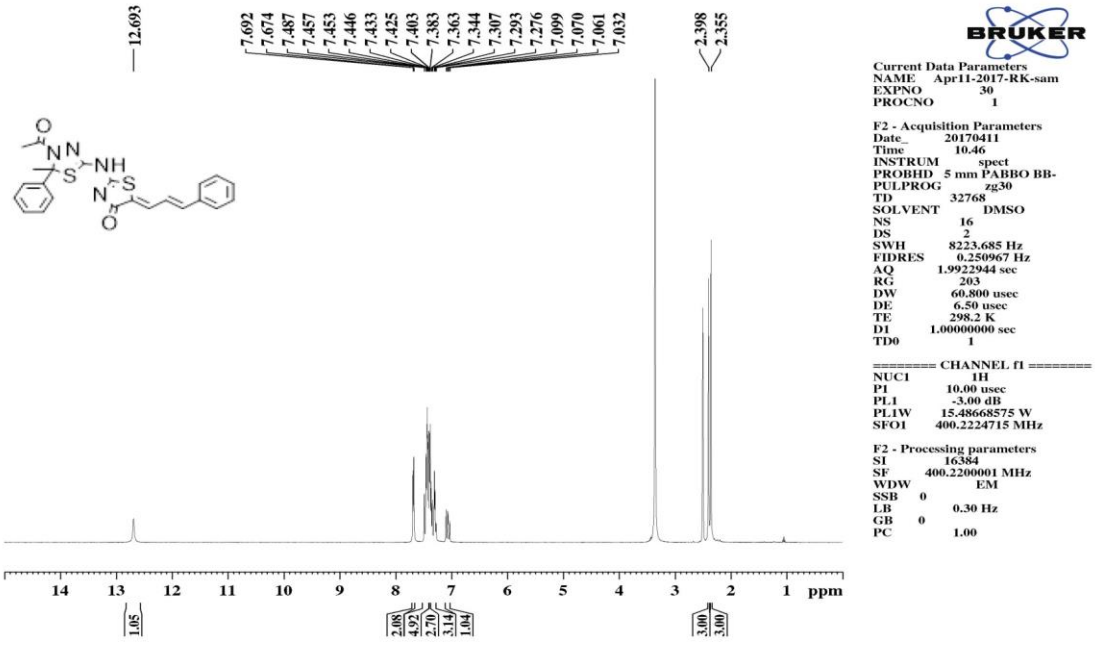

Figure S86: ^{1}H NMR of compound **8v**

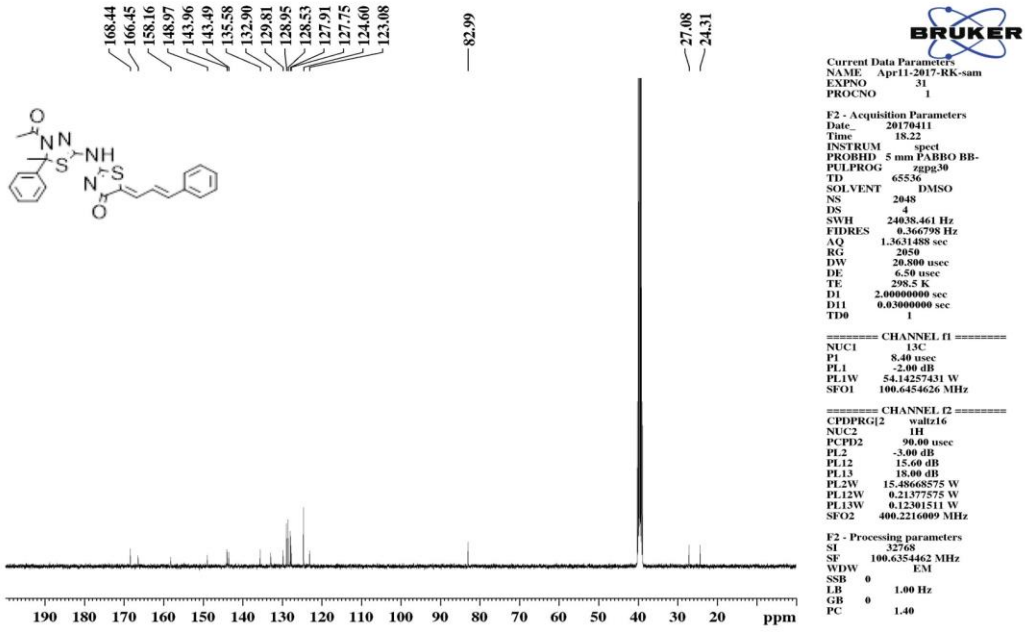

Figure S87: ^{13}C NMR of compound **8v**

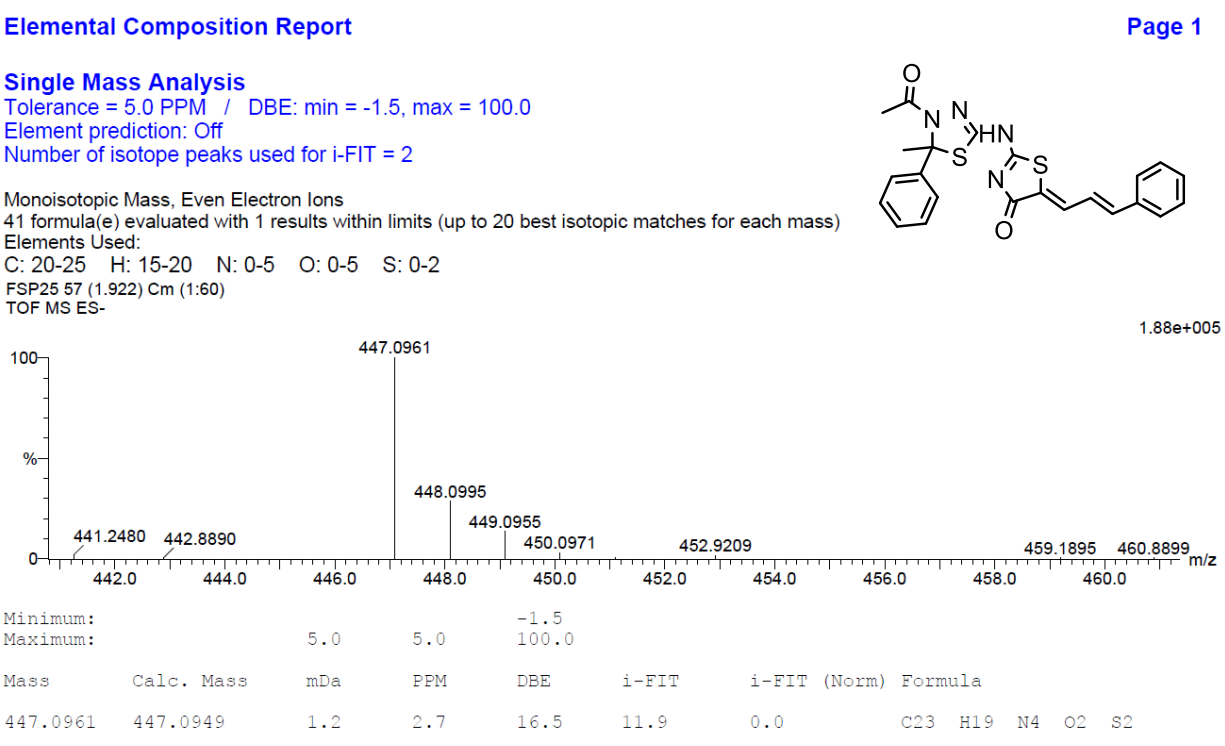

Figure S88: HR-MS of compound **8v**

7.2. Inhibition of MT-stimulated KSP ATPase activity profiles

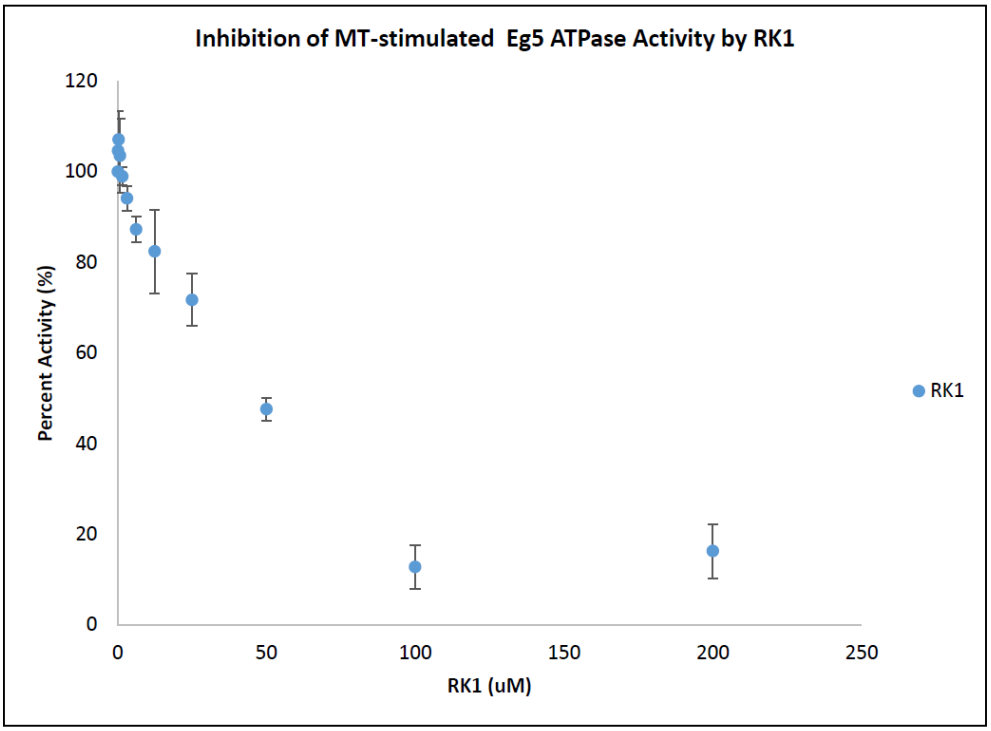

Figure S89: Inhibition of MT-stimulated KSP ATPase activity by **8a**

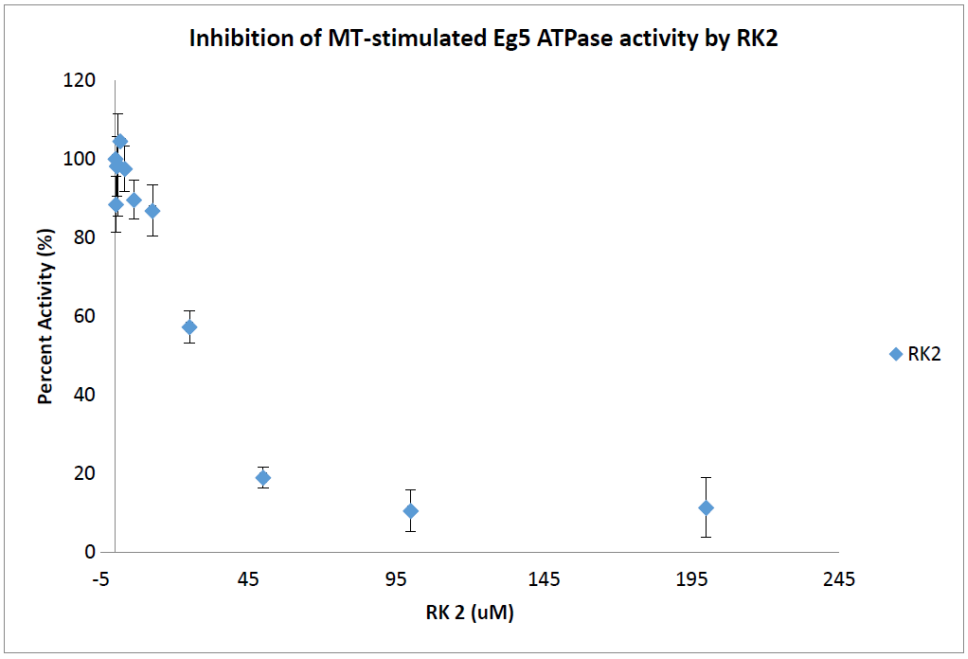

Figure S90: Inhibition of MT-stimulated KSP ATPase activity by **8b**

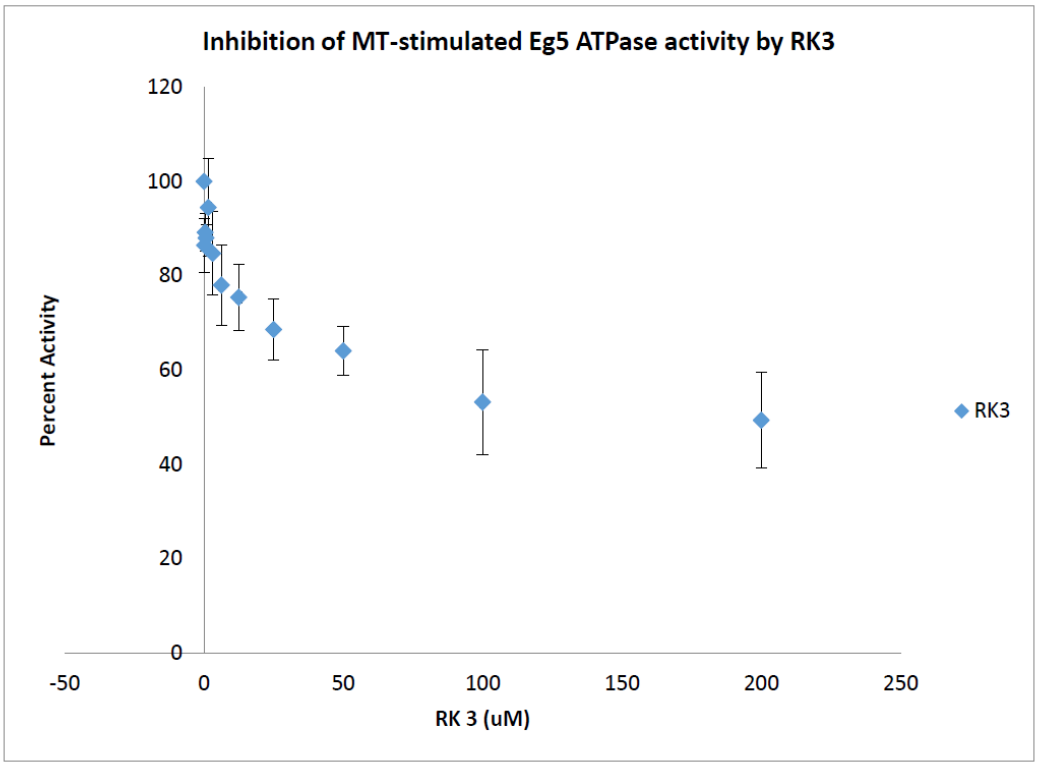

Figure S91: Inhibition of MT-stimulated KSP ATPase activity by **8c**

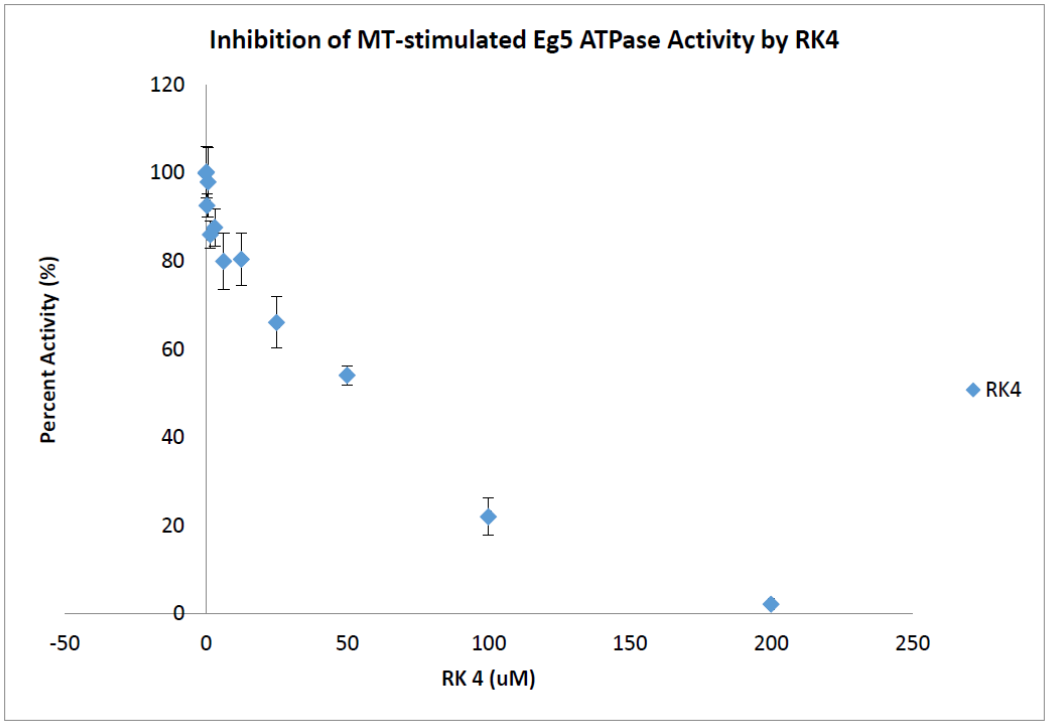

Figure S92: Inhibition of MT-stimulated KSP ATPase activity by **8d**

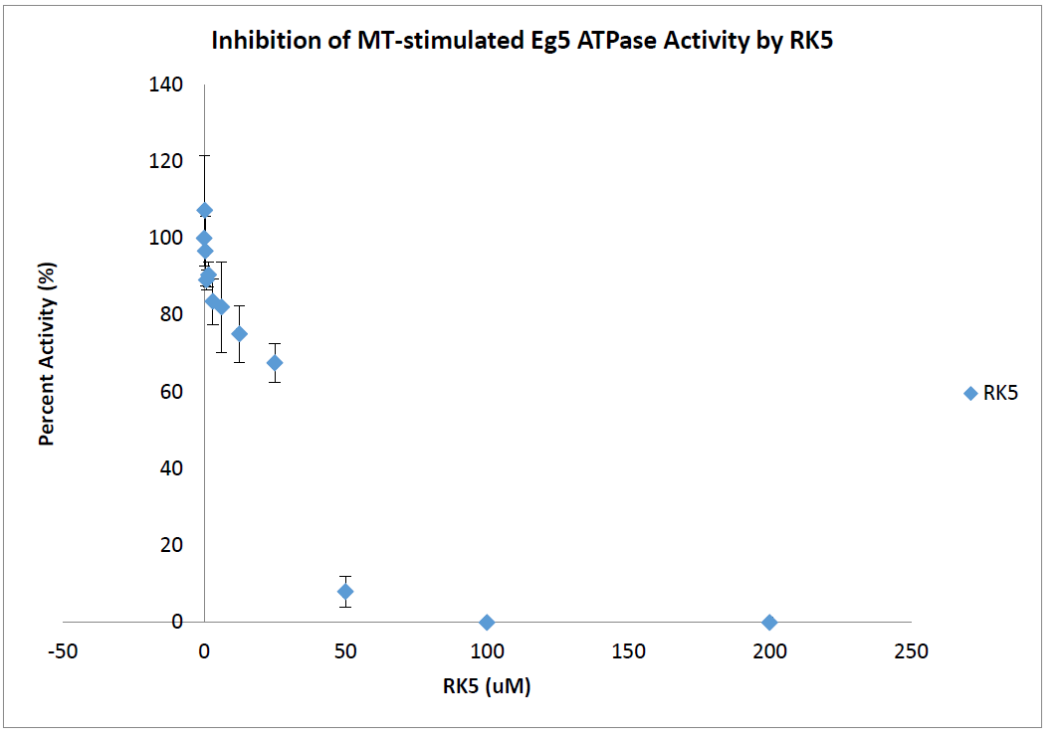

Figure S93: Inhibition of MT-stimulated KSP ATPase activity by **8e**

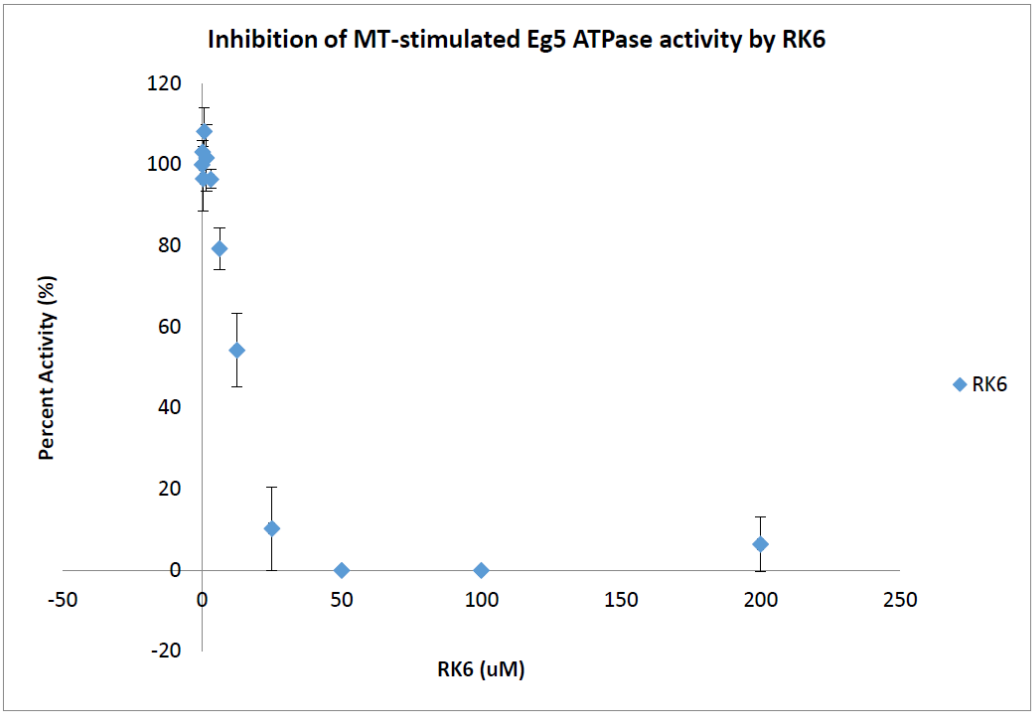

Figure S94: Inhibition of MT-stimulated KSP ATPase activity by **8f**

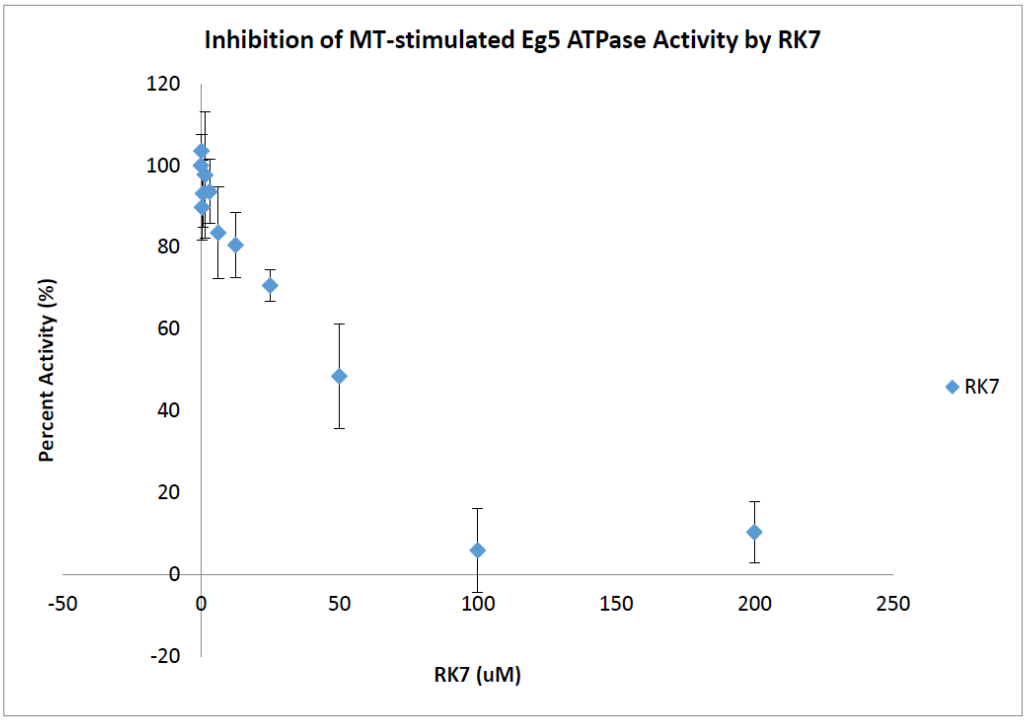

Figure S95: Inhibition of MT-stimulated KSP ATPase activity by **8g**

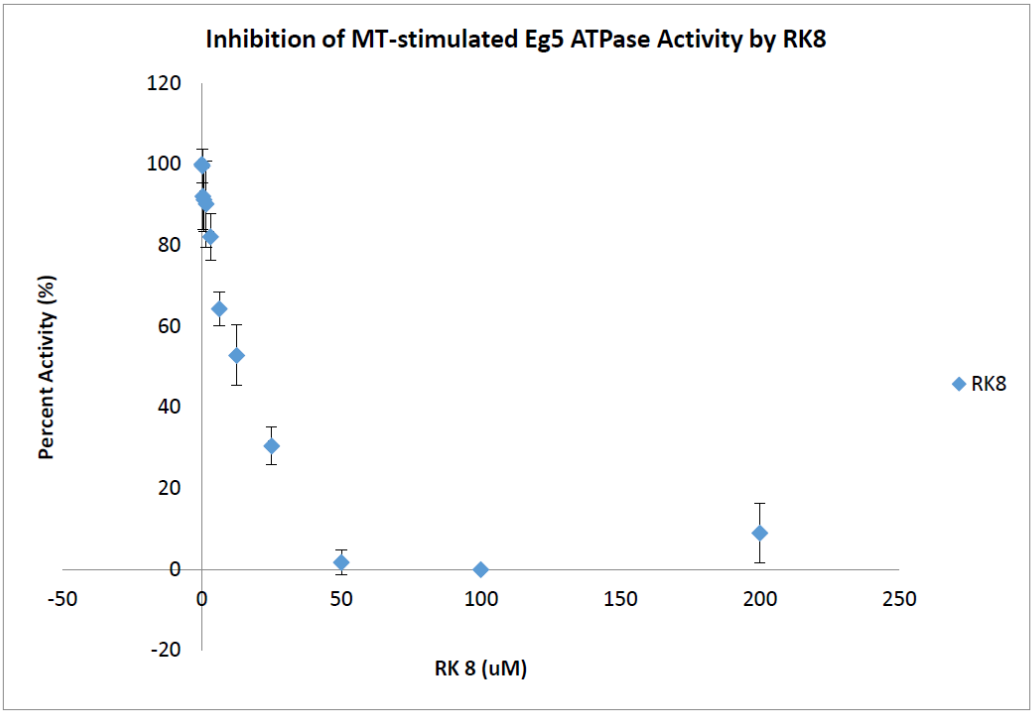

Figure S96: Inhibition of MT-stimulated KSP ATPase activity by **8h**

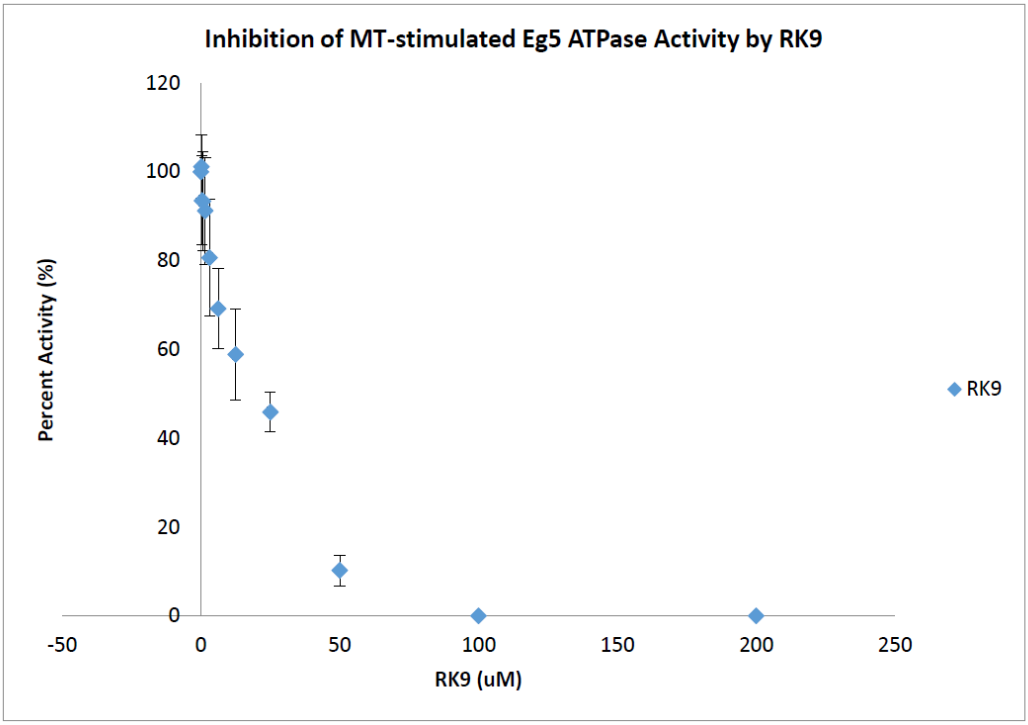

Figure S97: Inhibition of MT-stimulated KSP ATPase activity by **8i**

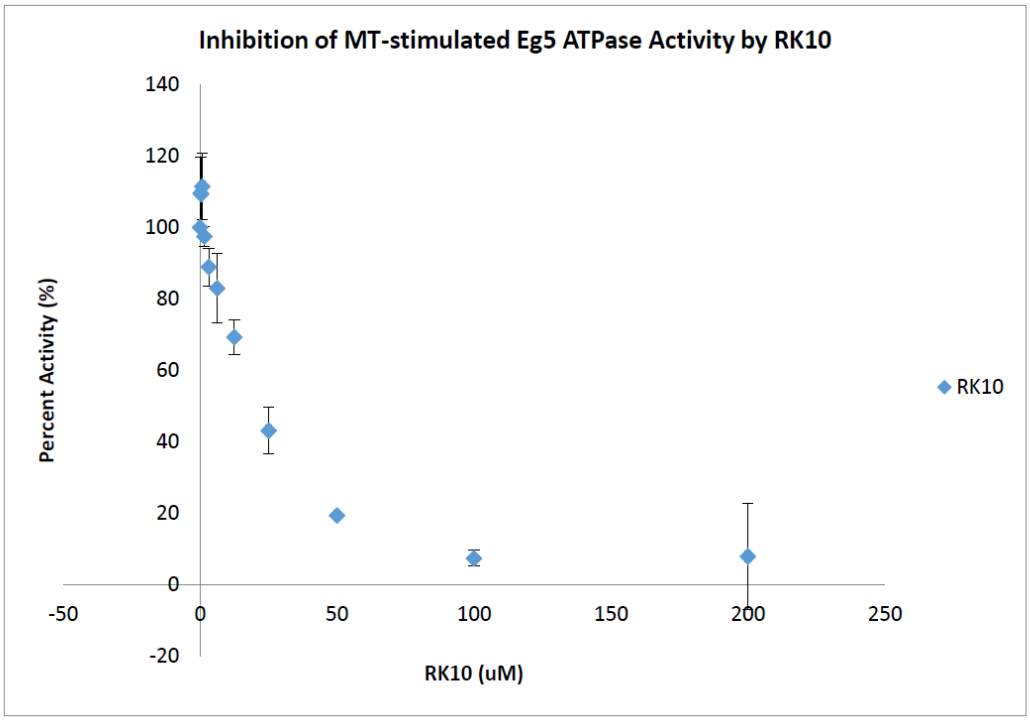

Figure S98: Inhibition of MT-stimulated KSP ATPase activity by **8j**

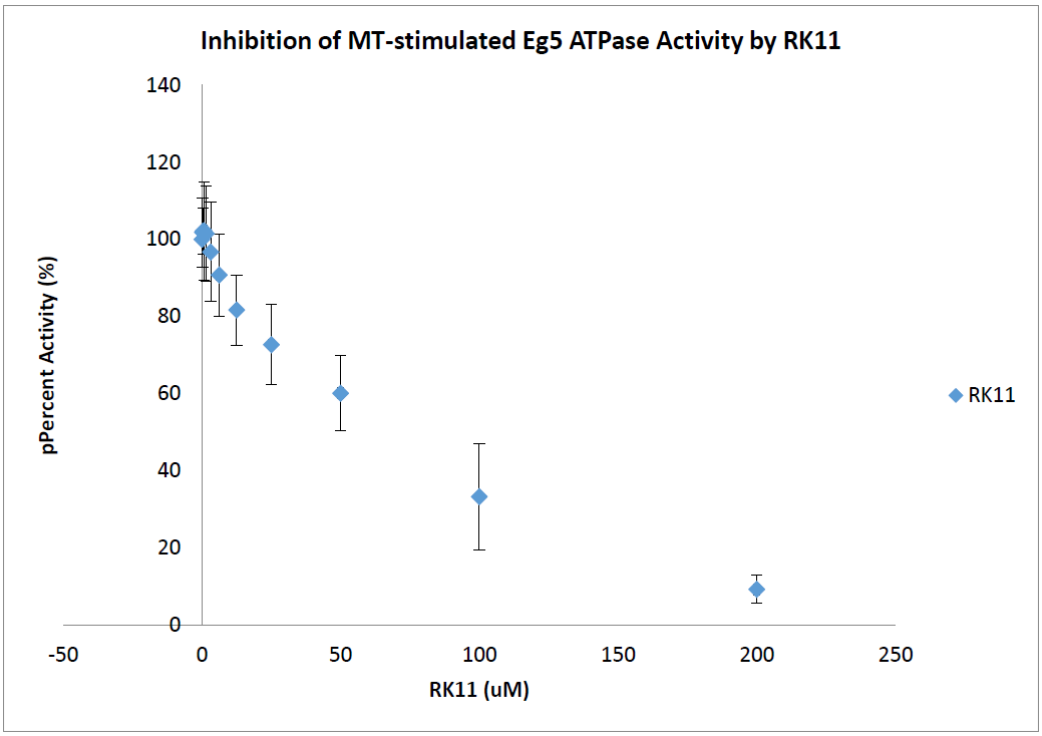

Figure S99: Inhibition of MT-stimulated KSP ATPase activity by **8k**

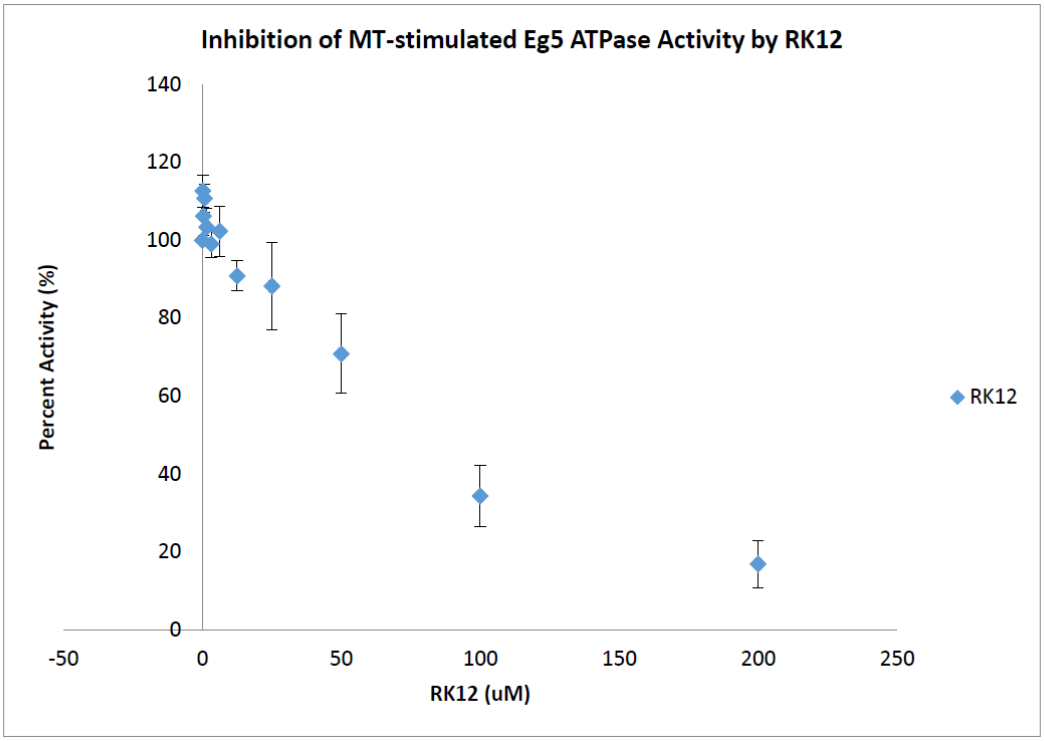

Figure S100: Inhibition of MT-stimulated KSP ATPase activity by **8l**

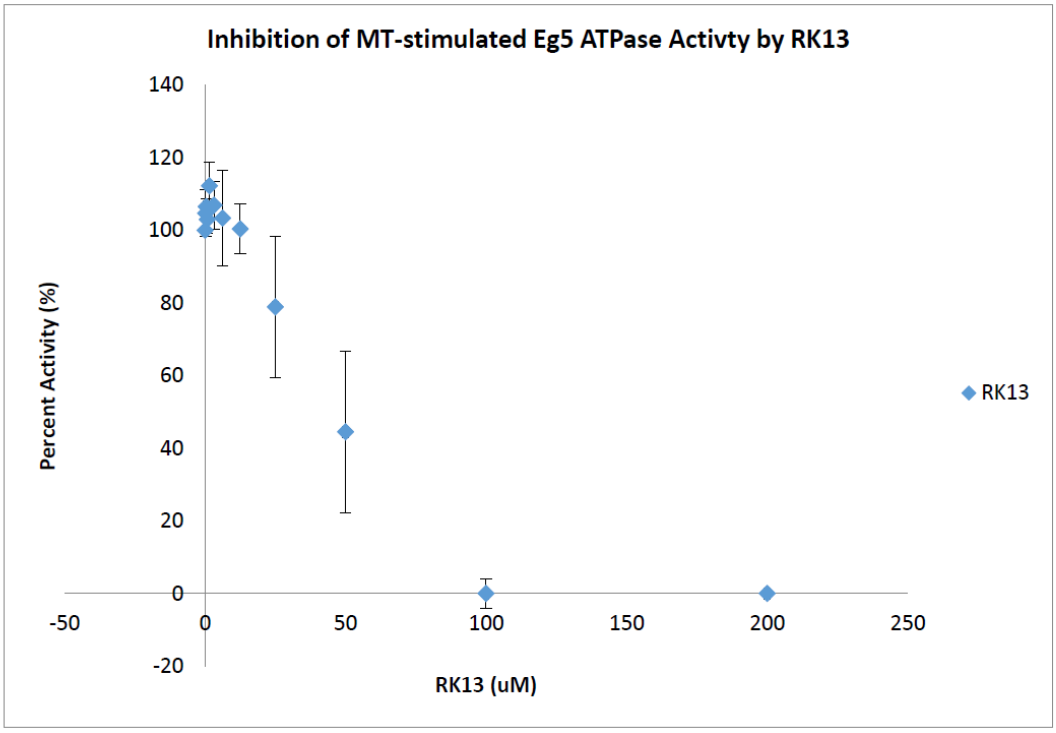

Figure S101: Inhibition of MT-stimulated KSP ATPase activity by **8m**

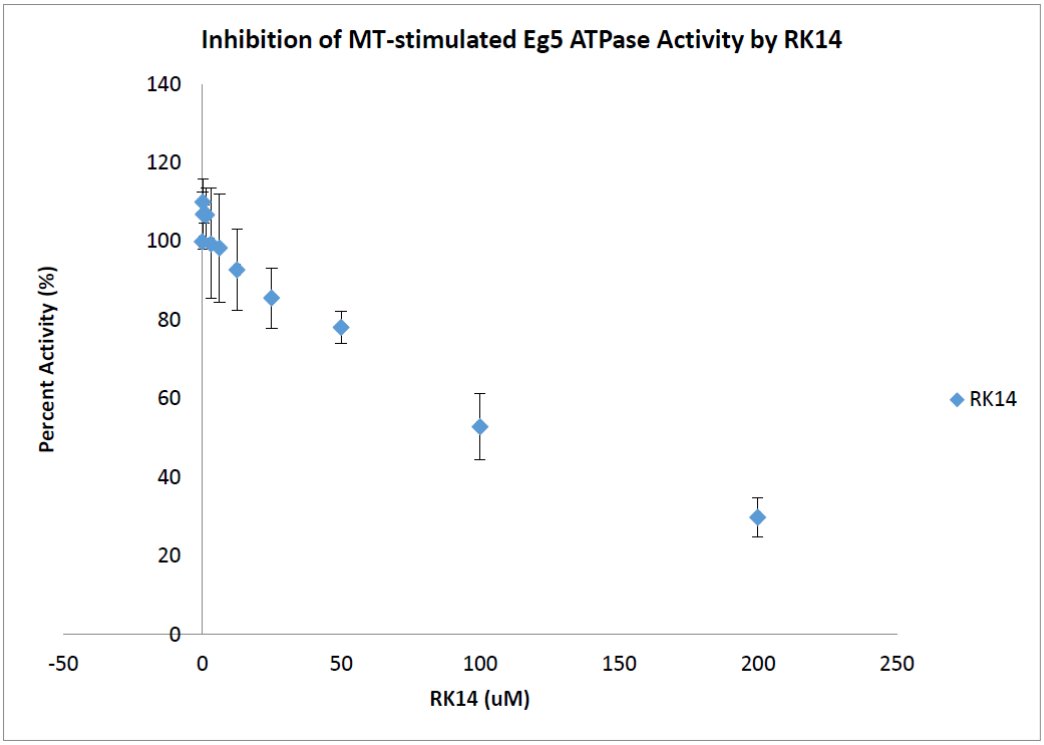

Figure S102: Inhibition of MT-stimulated KSP ATPase activity by **8n**

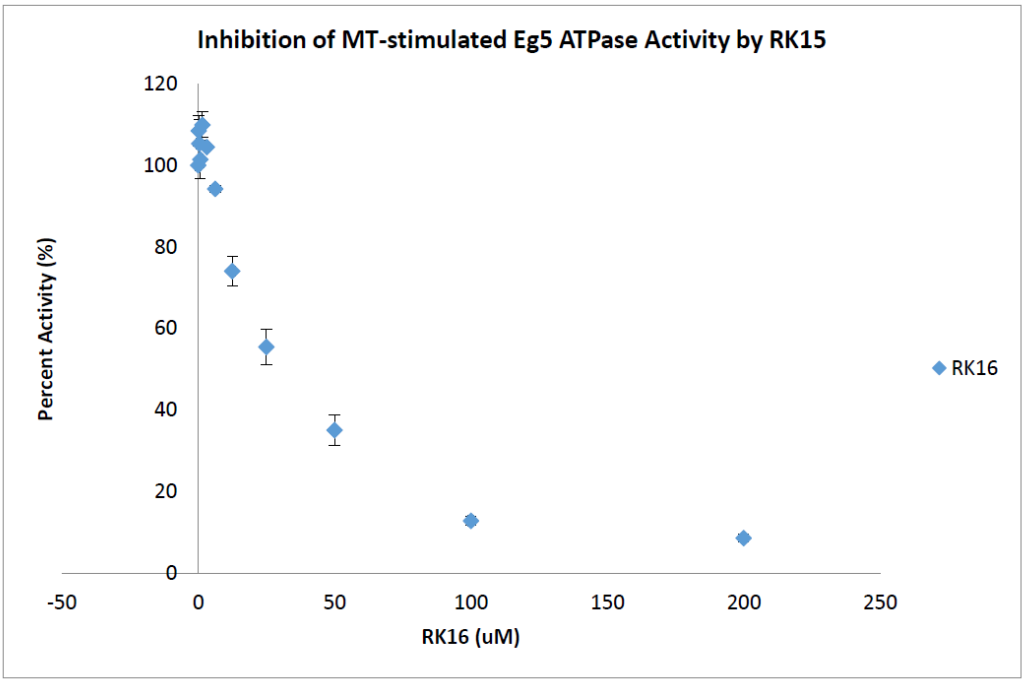

Figure S103: Inhibition of MT-stimulated KSP ATPase activity by **8o**

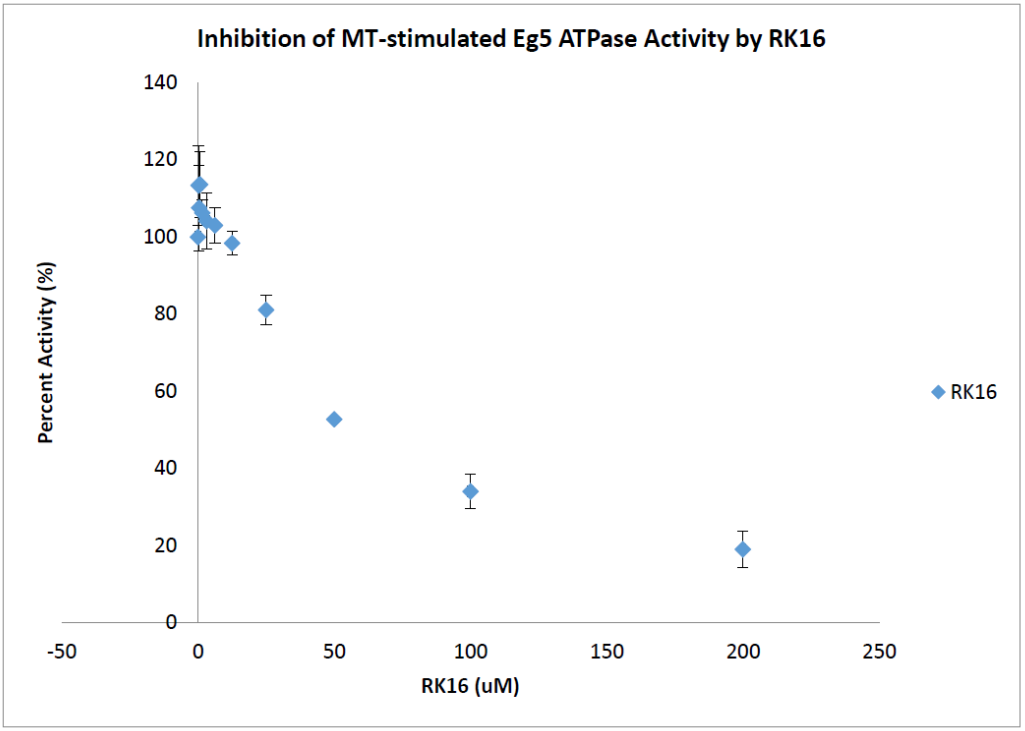

Figure S104: Inhibition of MT-stimulated KSP ATPase activity by **8p**

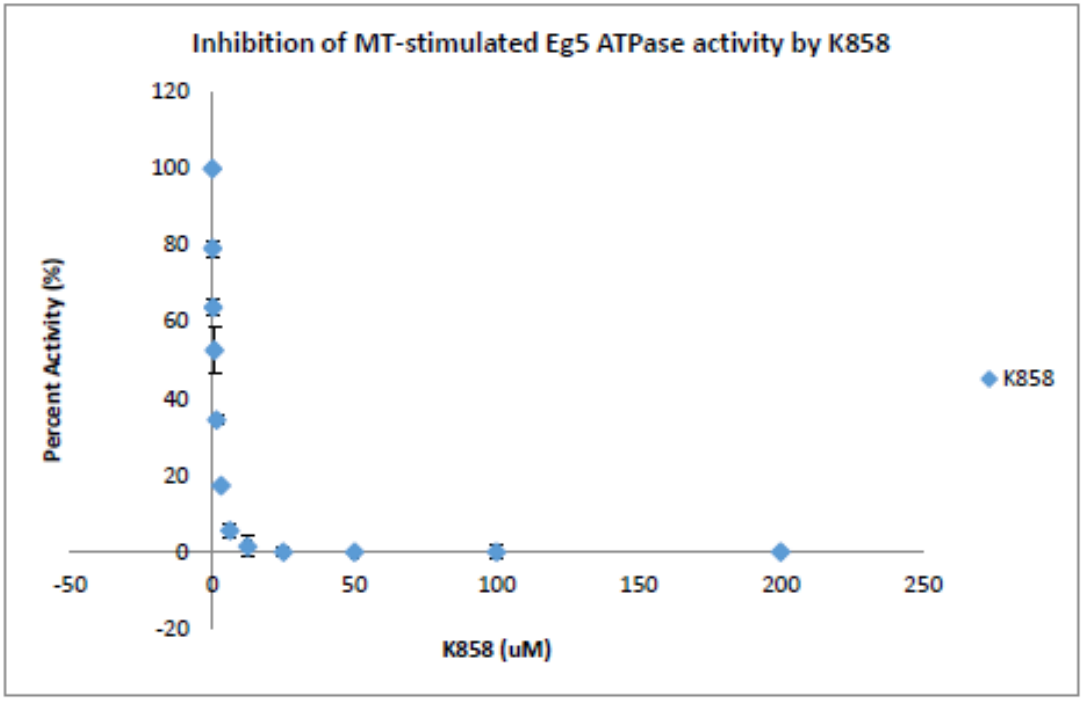

Figure S105: Inhibition of MT-stimulated KSP ATPase activity by **K858**